

**Ruthenium and Copper Complexes for Anti-cancer and Catalytic
Applications**

Cecilia Rutendo Madzivire

Submitted in accordance with the requirements for the degree of
Doctor of Philosophy

The University of Leeds
School of Chemistry

April, 2018

The candidate confirms that the work submitted is her own and that appropriate credit has been given where reference has been made to the work of others.

This copy has been supplied on the understanding that it is copyright material and that no quotation from the thesis may be published without proper acknowledgement.

The right of Cecilia Rutendo Madzivire as Author of this work has been asserted by her in accordance with the Copyright, Designs and Patents Act 1988.

© 2018 The University of Leeds and Cecilia Rutendo Madzivire

Acknowledgements

I would like to begin by saying a huge thank you to my supervisor Paddy for allowing me to pursue this project. Coming to this “lovely country”, with its grey gloomy skies, snow, rain and icy negative temperatures, as a heavily pregnant (which you literally over looked) international research student, I did not think I would survive, let alone get out of the house. However, your warm welcome, words of wisdom, encouragement and support have helped me get through some of the toughest times in my life.

I would also like to thank our collaborators, Professor Roger Phillips at the University of Huddersfield and Pablo Caramés-Mendéz for the biological studies. The Community for Open Antimicrobial Drug Discovery (CO-ADD) for the anti-bacterial and anti-fungal investigations. Professor Andrew Nelson, his researcher Shezi and Danielle (MChem) for the artificial biomembrane studies, Ms. Tanya Marinko-Covell and Mr. Stephen Boyer (London Metropolitan University) for the microanalyses, and Dr Chris Pask for assistance with X-ray crystallography. Thank you to The Schlumberger Foundation-Faculty for the Future for funding.

To Dr Chris, a very special and heart-felt thank you. In life I have met nice and kind people, but you are the epitome of kindness. You have been an ever present help from the 1st day of my PhD till now. I genuinely would not have completed this project without you.

Team McGowan, past (Carlo) and present, thank you for a wonderful time at the University of Leeds. You guys are simply the best. Thank you for understanding me, in my diverse way, getting that being a mum meant that conference nights are strictly for catching up on sleep and nothing else. To Laura (shame on you!!), thank you for helping me adjust to the lab and the dynamics of the office, particularly accepting Matt and Pablo and their lost ways (lol). Above all, thank you for being my prototype for reports and presentations. During my PhD journey, Matt you have been my Sam to Frodo, a Chandler to Joey, and the milk in my black tea (lol). Thank you for everything, from the strangest coffee morning banter to your annoying calculator skits during demonstrating. You have been my writing buddy, understanding and sharing in the thesis writing related stresses, you really

are a great friend. Pablo, the craziest of them all, I am glad to call you a friend. Thank you for being you, the crazy full of life and too much love person that you are. There was never a dull moment with you in the office. Thank you to the rest of office 1.25, Raf, for having all the chemistry answers, Sam G, for introducing me to cyclic voltammetry even though it never worked for me, Kay for reminding me that I am a super mum, even when I did not feel like one, Namrah for “getting me”, Izar, for annoying me all the time, Iurii, for the cool birthday gifts, and Ahmed for the “black” support. A special thank you to Anjo, you started off as my lunch buddy but now you are a treasured friend, thank you for everything. To my wonderful friends, my inner circle, Sandra R., Thembakazi, Sandra V. Pumeza, Rufaro and Kue, thank you for your support and encouragement. Your enthusiasm about my doctorate kept me going when I wanted to quit. To Apostle B. Ndlovu, here are the fruits of your prayers, we made it!

To my family, Collet, Mercy, Sandra, Dee, Huggins, Moises, Stewart, Evelyn and my wonderful babies Kairos, Elim, Kiera and Karis, I thank God for you. Thank you for your love, support and encouragement. You guys have been my biggest fans from day 1. To my parents, Whitimos and Simbisai Madzivire, words fail me. Thank you for believing in me even when I did not believe in myself and for standing by me, through thick and thin. Your sacrifices, love and support for me has really stood the test of time. I love you so much and I hope I have made you proud.

Lastly, I dedicate this thesis to my amazing husband Emmanuel and our joy Emmani. To my daughter Emmani, I apologise for being an absent mum, however, after a long day in the lab it was always a delight to take off my lab coat and put on my mother coat. You understood that “mama is doing important work”, thank you for that. To Emmanuel, you are my all, thank you for standing in and being a mother to our daughter in my absence. Thank you for loving, supporting, encouraging and standing by me always, you are my pillar of strength. I wouldn't have done and completed this PhD had it not been of you.

Where would I be had it not been for your grace and favour God? *Ephesians 3:20*
Now to Him who is able to do exceedingly, abundantly, above all that we can think or imagine according to His power that is at work within us.

Abstract

This thesis details the synthesis, characterisation and evaluation of novel β -bis-ketoiminate ruthenium(II) and β -bis-ketoiminate copper(II) complexes for their biological and chemical applications. The anti-cancer, anti-bacterial and anti-fungal and catalytic activity of these complexes was investigated, with lead complexes undergoing further mechanistic investigations.

Chapter 1 contains the background introduction to the project, through literature research of similar work as well as the aims of this project.

Chapter 2 presents the synthesis and characterisation of novel β -bis-ketoiminate ruthenium(II) dicarbonyl complexes. ^1H NMR, ^{13}C $\{^1\text{H}\}$ NMR and detailed X-ray crystallographic data are given for this series of complexes.

Chapter 3 introduces novel β -bis-ketoiminate copper(II) complexes, their synthesis and characterisation, with X-ray crystallographic data discussed.

Chapter 4 introduces the MTT technique for assessing cytotoxicity, and discusses the anti-cancer activities of the series of complexes synthesised in **Chapters 2** and **3**. In addition, the chapter gives a brief literature review to anti-bacterial and anti-microbial studies, and the results of anti-bacterial and anti-fungal investigations on the β -bis-ketoiminate ruthenium(II) and copper(II) complexes.

Chapter 5 presents the results of chemical investigations, hydrolysis and biomembrane, conducted on the two libraries of complexes.

Chapter 6 contains a brief literature review on catalysis, and the results for transfer hydrogenation and Ullmann catalytic reactions on β -bis-ketoiminate ruthenium(II) complexes and β -bis-ketoiminate copper(II) complexes respectively.

Chapter 7 contains experimental details and characterisation data for all the complexes synthesised within this thesis, and protocols for all the biological and chemical studies.

Appendix presents a summary of X-ray crystallographic structure analysis for all the crystal structures reported within this thesis.

Table of Contents

Acknowledgements	iii
Abstract	v
Table of Contents	vi
List of abbreviations	xiii
Glossary	xvii
Introduction	1
1.1 Cancer	2
1.2 Metal based drugs	3
1.2.1 Cisplatin	5
1.2.2 Other platinum based anti-cancer drugs.....	9
1.2.3 Ruthenium anti-cancer drugs	11
1.2.4 Copper anti-cancer drugs	16
1.3 Carbon Monoxide Releasing Molecules	22
1.3.1 Ruthenium CORMs.....	24
1.3.2 CORMs in cancer	25
1.4 Metal ketoiminate complexes	27
1.5 Research project objectives.....	28
1.6 References	30
Synthesis and Characterisation of Functionalised β-bis-Ketoiminate	
Ruthenium(II) Dicarbonyl Complexes	48
2.1 Synthesis of Biaryl- β -Ketoiminate Ligands.....	49
2.2 Synthesis of Ruthenium(II) Dicarbonyl complexes.....	50
2.3 Characterisation of Ruthenium(II) Dicarbonyl Complexes.....	54
2.4 Infrared Spectroscopy of Ruthenium(II) Dicarbonyl Complexes.....	54
2.5 NMR Data of Ruthenium(II) Dicarbonyl Complexes.....	56
2.6 X-ray Crystallography of Ruthenium(II) Dicarbonyl complexes.....	58

2.6.1	X-ray characterisation for C1	59
2.6.2	X-ray characterisation for C2	61
2.6.3	X-ray characterisation for C3	63
2.6.4	X-ray characterisation for C4	65
2.6.5	X-ray characterisation for C5	67
2.6.6	X-ray characterisation for C6	70
2.6.7	X-ray characterisation for C8	72
2.6.8	X-ray characterisation for C9	74
2.6.9	X-ray characterisation for C11	77
2.6.10	X-ray characterisation for C12	79
2.6.11	X-ray characterisation for C14	81
2.6.12	X-ray characterisation for C15	84
2.7	Conclusion	86
2.8	References	87
Synthesis and Characterisation of Functionalised β-bis-Ketoiminate Copper(II) Complexes		
89		
3.1	Introduction to β -bis-Ketoiminate Copper(II) Complexes	90
3.2	Synthesis of β -bis-Ketoiminate Copper(II) Complexes	91
3.3	Characterisation of β -bis-Ketoiminate Copper(II) Complexes	92
3.3.1	X-Ray crystallography β -bis-ketoiminate Copper(II) complexes ...	92
3.4	Conclusion	104
3.5	References	105
Biological investigations on β-bis-Ketoiminate analogue Complexes of Ruthenium and Copper		
107		
4.1	Introduction to biological studies	108
4.2	Cytotoxicity	108
4.2.1	MTT Assay	108

4.3	Results and Discussion	109
4.3.1	Cytotoxicity of β -bis-Ketoiminate Ru(II) Dicarbonyl Complexes	109
4.3.2	Hypoxia	114
4.3.3	Cytotoxicity of β -bis-Ketoiminate Copper(II) Complexes.....	118
4.4	Anti-bacterial Studies.....	121
4.4.1	Ruthenium CORMs in anti-bacterial studies.....	122
4.4.2	Copper complexes in anti-bacterial studies	126
4.5	Anti-fungal Studies	128
4.5.1	Ruthenium complexes in anti-fungal studies.....	129
4.5.2	Copper complexes in anti-fungal studies.....	131
4.6	Conclusions.....	133
4.7	References.....	134
	Biological Relevance Studies on β-bis-Ketoiminate Complexes of Ruthenium and Copper.....	141
5.1	Introduction to biological relevance	142
5.2	Hydrolysis Studies	142
5.2.1	Introduction to hydrolysis	142
5.2.2	Hydrolysis of β -bis-Ketoiminate Ru(II) Dicarbonyl Complexes.....	143
5.2.3	Hydrolysis of β -bis-Ketoiminate Cu(II) Complexes.....	150
5.3	Biomembrane Studies	152
5.3.1	Introduction to biomembrane studies.....	152
5.3.2	Biomembrane Studies of β -bis-Ketoiminate Ru(II) Dicarbonyl Complexes.....	155
5.4	Conclusion	159
5.5	References.....	160

Catalytic Investigations on β-bis-Ketoiminate Complexes of Ruthenium and Copper	164
6.1 Transition metals in catalysis.....	165
6.2 Catalytic transfer hydrogenation.....	166
6.2.1 Introduction to transfer hydrogenation	166
6.2.2 Catalytic mechanisms	170
6.2.3 Catalytic viability of β -bis-Ketoiminate Ru(II) Dicarbonyl Complexes .	172
6.3 Catalytic Ullmann reactions.....	175
6.3.1 Copper in catalysis.....	175
6.3.2 Introduction to Ullmann reaction.....	176
6.3.3 The mechanism of the Ullmann reaction.....	179
6.3.4 Catalytic viability of β -bis-Ketoiminate Copper(II) Complexes	180
6.4 Conclusion	185
6.5 References.....	187
Experimental.....	193
7.1 General Experimental Procedure	194
7.2 Instrumentation	194
7.3 X-Ray crystallography	195
7.4 Synthesis of functionalised β -diketonate ligands.....	195
7.4.1 General synthetic procedure for β -diketonate ligands	195
7.5 Synthesis of functionalised β -bis-ketoiminate ligands	196
7.5.1 General synthetic procedure for β -bis-ketoiminate ligands.....	196
7.5.2 Synthesis of L2	197
7.6 Synthesis of β -bis-ketoiminate Ru(II) dicarbonyl complexes	197
7.6.1 Synthesis of C1 (C ₃₄ H ₂₈ N ₂ O ₄ Ru)	197
7.6.2 Synthesis of C2 (C ₃₄ H ₂₆ Br ₂ N ₂ O ₄ Ru).....	198

7.6.3 Synthesis of C3 (C ₃₄ H ₂₆ Cl ₂ N ₂ O ₄ Ru)	199
7.6.4 Synthesis of C4 (C ₃₄ H ₂₆ F ₂ N ₂ O ₄ Ru).....	199
7.6.5 Synthesis of C5 (C ₃₄ H ₂₆ F ₂ N ₂ O ₄ Ru).....	200
7.6.6 Synthesis of C6 (C ₃₄ H ₂₆ Br ₂ N ₂ O ₄ Ru).....	201
7.6.7 Synthesis of C7 (C ₃₄ H ₂₄ Cl ₄ N ₂ O ₄ Ru)	201
7.6.8 Synthesis of C8 (C ₃₆ H ₃₂ N ₂ O ₄ Ru)	202
7.6.9 Synthesis of C9 (C ₃₆ H ₃₂ N ₂ O ₄ Ru)	203
7.6.10 Synthesis of C10 (C ₃₄ H ₂₆ F ₂ N ₂ O ₄ Ru).....	203
7.6.11 Synthesis of C11 (C ₃₄ H ₂₆ Cl ₂ N ₂ O ₄ Ru)	204
7.6.12 Synthesis of C12 (C ₃₄ H ₂₆ F ₂ N ₂ O ₄ Ru).....	205
7.6.13 Synthesis of C13 (C ₃₄ H ₂₆ Br ₂ N ₂ O ₄ Ru).....	205
7.6.14 Synthesis of C14 (C ₃₄ H ₂₄ Cl ₄ N ₂ O ₄ Ru)	206
7.6.15 Synthesis of C15 (C ₃₄ H ₂₄ F ₄ N ₂ O ₄ Ru).....	206
7.6.16 Synthesis of C16 (C ₃₈ H ₃₆ N ₂ O ₄ Ru)	207
7.7 Synthesis of β -bis-ketoiminate copper(II) complexes	209
7.7.1 Synthesis of C17 (C ₃₂ H ₂₈ N ₂ O ₂ Cu)	201
7.7.2 Synthesis of C18 (C ₃₂ H ₂₆ N ₂ O ₂ Br ₂ Cu).....	210
7.7.3 Synthesis of C19 (C ₃₂ H ₂₆ N ₂ O ₂ Cl ₂ Cu)	210
7.7.4 Synthesis of C20 (C ₃₂ H ₂₆ N ₂ O ₂ Br ₂ Cu).....	211
7.7.5 Synthesis of C21 (C ₃₂ H ₂₆ N ₂ O ₂ Cl ₂ Cu).....	211
7.7.6 Synthesis of C22 (C ₃₂ H ₂₆ N ₂ O ₂ F ₂ Cu).....	211
7.7.7 Synthesis of C23 (C ₃₂ H ₂₆ N ₂ O ₂ I ₂ Cu).....	212
7.7.8 Synthesis of C24 (C ₃₄ H ₃₂ N ₂ O ₂ Cu)	212
7.7.9 Synthesis of C25 (C ₃₄ H ₃₂ N ₂ O ₄ Cu)	212
7.7.10 Synthesis of C26 (C ₃₆ H ₃₆ N ₂ O ₄ Cu)	213
7.7.11 Synthesis of C27 (C ₃₄ H ₂₆ N ₂ O ₂ F ₆ Cu).....	213

7.7.12 Synthesis of C28 (C ₃₆ H ₃₆ N ₂ O ₂ Cu)	214
7.7.13 Synthesis of C29 (C ₃₈ H ₄₀ N ₂ O ₂ Cu)	214
7.7.14 Synthesis of C30 (C ₃₂ H ₂₄ N ₂ O ₂ Cl ₄ Cu)	214
7.7.15 Synthesis of C31 (C ₃₄ H ₃₂ N ₂ O ₆ Cu)	215
7.7.16 Synthesis of C32 (C ₃₂ H ₂₄ N ₂ O ₂ F ₂ Br ₂ Cu).....	215
7.7.17 Synthesis of C33 (C ₃₄ H ₃₂ N ₂ O ₄ Cu)	215
7.7.18 Synthesis of C34 (C ₃₂ H ₂₆ CuF ₂ N ₂ O ₂).....	216
7.7.19 Synthesis of C35 (C ₃₆ H ₃₄ N ₂ O ₄ F ₂ Cu).....	216
7.7.20 Synthesis of C36 (C ₃₂ H ₂₆ N ₂ O ₂ Br ₂ Cu).....	216
7.7.21 Synthesis of C37 (C ₃₂ H ₂₆ N ₂ O ₂ F ₂ Cu).....	216
7.7.22 Synthesis of C38 (C ₃₂ H ₂₆ N ₂ O ₂ Br ₂ Cu)	217
7.7.23 Synthesis of C39 (C ₃₂ H ₂₆ N ₂ O ₂ Cl ₂ Cu)	217
7.7.24 Synthesis of C40 (C ₃₂ H ₂₆ N ₂ O ₂ Cl ₂ Cu)	218
7.7.25 Synthesis of C41 (C ₃₂ H ₂₄ N ₂ O ₂ F ₄ Cu).....	218
7.7.26 Synthesis of C42 (C ₃₂ H ₂₄ N ₂ O ₂ F ₄ Cu).....	218
7.8 Cytotoxicity Evaluation	219
7.8.1 General	219
7.8.2 Conducting the 5-Day MTT Assay (Normoxia).....	220
7.8.3 Conducting the 5-Day MTT Assay (Hypoxia)	221
7.9 Anti-bacterial Evaluation	221
7.9.1 Anti-bacterial screening procedure	221
7.10 Anti-fungal Evaluation.....	222
7.10.1 Anti-fungal screening procedure.....	222
7.11 Hydrolysis	223
7.12 Biomembrane studies.....	223
7.13 Catalysis	224

7.14 References.....	225
Appendix: Crystallographic data	228

List of abbreviations

$> / \geq$	greater than / greater than or equal to
$< / \leq$	less than / less than or equal to
$^{\circ}$	degrees
δ	chemical shift
η	hapticity
λ	wavelength
μg	microgram
μL	microlitre
μM	micromolar
μm	micrometre
\AA	Angstrom
A	adenine
acac	acetylacetonate
acnac	β - ketoiminate ligand
ADR	adverse drug reaction
ARPE-19	human retinal pigment epithelial cell line
BE	human colon carcinoma cell line
br. s / d / m / t	broad singlet / doublet / multiplet / triplet
$^{\circ}\text{C}$	degrees Celsius
CC_{50}	concentration for 50 % cell death
CFU	colony-forming units
cm	centimetre
CO-ADD	Community for Open Antimicrobial Drug Discovery
CORM	carbon monoxide releasing molecule
<i>d</i>	deuterated
d	doublet
dt	doublet of triplet
D.....A	donor to acceptor distance

Da	Dalton
DCM	dichloromethane
DMSO	dimethyl sulphoxide
DNA	deoxyridonucleic acid
DOPC	dioleoyl phosphatidylcholine
EDTA	ethylenediaminetetraacetic acid
e.g.	<i>exempli gratia</i> , for example
en	ethylenediamine
ESI	electrospray
<i>et al.</i>	and others
Et ₃ N	triethylamine
ETOH	ethanol
FBS	foetal bovine serum
FDA	Food and Drug Administration
g	gram
G	Gauss
G	guanine
h	hours
¹ H	proton coupled
{ ¹ H}	proton decoupled
HBSS	Hank's balanced salt solution
HEK	human embryonic kidney cell line
HIF-1	hypoxia inducible factor-1
HPV	Human papilloma virus
HRE	hypoxia responsive element
IC ₅₀	concentration for 50 % growth inhibition
i.e.	<i>id est</i> , that is
IGF	insulin-like growth factor
IR	infrared

<i>in vacuo</i>	under vacuum
<i>in vitro</i>	in glass
<i>in vivo</i>	in a living organism
<i>J</i>	coupling constant
K	degrees Kelvin
kG	kilo Gauss
log <i>P</i>	partition coefficient
m	multiplet
MHz	mega Hertz
MIA PaCAa-2	human pancreatic carcinoma cell line
MIC	minimum inhibitory concentration
min	minute
mL	millilitre
mM	millimolar
mm	millimetre
mmol	millimole
MMP	matrix metalloproteinase
MS	mass spectrometry
MTT	3-(4,5-dimethylthiazol-2-yl)-2,5-diphenyltetrazolium bromide
mV	millivolt
NAD(H)	nicotinamide adenine dinucleotide
NADP(H)	nicotinamide adenine dinucleotide phosphate
NBS	non-binding surface
NHS	National Health Service
NIR	near infrared
nm	nanometre
NMR	nuclear magnetic resonance
NSAID	nonsteroidal anti-inflammatory drug
NSCLC	non-small cell lung cancer

PBS	phosphate buffered saline
pK _a	acid dissociation constant
PKC	protein kinase C
ppm	parts per million
pta	1,3,5-triaza-7-phosphaadamantane
RCV	rapid cyclic voltgram
RNA	ribonucleic acid
ROS	reactive oxygen species
s	singlet (for NMR), strong (for IR)
SAR	structure activity relationship
sh	shoulder
t	triplet
td	triplet of doublets
TLC	thin layer chromatography
tpa	<i>tris</i> (2-methylpyridyl)amine
U87	human glioblastoma cell line
UK	United Kingdom
UV	ultraviolet
UV/vis	ultraviolet-visible
V	volt
VEGF	vascular endothelial growth factor
<i>via</i>	by way of

Glossary

Anaemia: decrease in the total amount of red blood cells or haemoglobin in the blood

Angiogenesis: the formation of new blood vessels

Apoptosis: the process of programmed cell death

Carcinogenesis: the initiation of cancer formation

Carcinoma: a cancer arising in the epithelial tissue of the skin or of the lining of the internal organs

Cytosol: the aqueous component of the cytoplasm of a cell

Emesis: the action or process of vomiting

Eukaryote: an organism with a complex cell or cells, in which the genetic material is organised into a clearly defined membrane-bound nucleus

Genome: the genetic material of an organism

Homeostasis: the tendency towards a relatively stable equilibrium between interdependent elements, especially as maintained by physiological processes

Hydropic degeneration: one of the early signs of cellular degeneration in response to injury

Hypoxia: deficiency in the amount of oxygen reaching the tissues

Intercalation: insertion of a molecule into DNA between the bases

Lesion: region in an organ or tissue which has suffered damage through injury or disease

Lymphoma: a cancer of the lymphatic system

Metastasis: the spread of a cancer or other disease from one organ or part of the body to another

Mitochondria: an organelle in which the biochemical processes of respiration and energy production occur

Mitosis: a part of the cell cycle when replicated chromosomes are separated into two new nuclei

Morbidity: the condition of being diseased

Mutation: a change that occurs in the DNA sequence

Neoplasia: abnormal and excessive growth of tissues

Nephrotoxicity: toxicity to the kidneys

Neurotoxicity: toxicity to the nervous system

Normoxia: normal levels of oxygen reaching the tissues

Oncogene: a gene that has the potential to cause cancer

Ototoxicity: toxicity to the ear leading to hearing loss

Paresthesia: an abnormal sensation such as tingling, tickling, pricking, numbness or burning of the skin with no apparent physical cause

Protease: any enzyme that performs proteolysis by hydrolysis of peptide bonds

Proteasome: protein complexes which degrade unneeded or damaged proteins by proteolysis

Replication: the biological process of producing two identical replicas of DNA from one original DNA molecule

Transcription: the first step of gene expression, in which a particular segment of DNA is copied into RNA

Vasculature: the vascular system of a part of the body and its arrangement

Chapter 1

Introduction

1.1 Cancer

Cancer remains one of the main causes of morbidity and mortality worldwide; an estimated 8.8 million people died from cancer worldwide in 2015. The incidence and mortality rates of cancer continue to increase globally, more so in developing countries.¹ In the UK, statistics for 2015 indicate that every two minutes someone was diagnosed with cancer, accounting for 359 960 new cases in that year.² Cancer risk is factual and an estimated 1 in 2 people born in the UK after 1960 will be diagnosed with some form of cancer during their lifetime.

There are over 100 different types of known cancers, however, nearly half (46%) of the new cases reported in 2014, in the UK, were accounted for by lung, breast, prostate and colorectal cancers.³ Cancer also has significant economic impacts, with the NHS spending over £5 billion annually on cancer care,⁴ a figure that is set to increase with growth and aging of the population.

Cancer is an umbrella term given to a heterogenic group of complex diseases characterised by cellular malfunctions. Healthy or normal cells are programmed to know “what to do” and “when to do it”. Cancerous cells do not have this programming and therefore grow and replicate out of control, eventually invading and spreading from the site of origin (primary site) to other parts in the body.^{5, 6} Mitosis is the process through which cells divide and is controlled by two cancer genes known as oncogenes and tumour gene suppressors. If one or usually more of the genes have a mutation the cell can uncontrollably divide causing a lump of abnormal tissue known as a tumour to develop.

Activated oncogenes can cause the abnormal cell to avert programmed cell death (apoptosis), survive and cell proliferate.⁷ This can result in one of the two types of tumours, benign or malignant. A benign tumour cannot metastasize, is rarely life threatening and can be treated. However, a malignant tumour can invade surrounding tissues, spread throughout the body, is usually life threatening and difficult to treat.⁸

Tumours are not simply isolated masses, but are complex tissues with distinct originality, cell type and molecular mechanisms, participating in heterotypic interactions with each other.⁶ Despite the complexity and diversity, Hanahan and Weinberg have proposed six essential alterations in normal cell physiology that

facilitate the evolution of normal cells to a neoplastic state, allowing them to survive, proliferate and disseminate. The six hallmarks, common for nearly all cancer types (>100) are; autonomous growth signals, evasion of growth inhibitory signals, evasion of apoptosis, infinite replicative potential, sustained formation of new blood vessels (angiogenesis) and tissue invasion and metastasis.^{6, 9} The hallmarks above are made possible by two enabling characteristics: genomic instability and tumour promoting instability, the former being the most prominent.¹⁰

The number of cancer survivors has increased over the years due to positive advances in preventive measures (changes associated with diet and lifestyle), early detection and prognosis, better treatment and (or) patient care as well as universal access to health care.^{11, 12} Treatment options for cancer include but are not limited to, surgery, chemo-, radiation-, immune- and targeted therapy. In many cases a combination of therapies are used for enhanced effects.¹¹

1.2 Metal based drugs

The pharmaceutical industry is largely made up of organic, biological and (or) natural based drugs.¹³ However, metal based medicines and remedies have been known and used since the ancient days of civilisation of Egypt, India, Mesopotamia and China. The ancient Egyptians used copper in the sterilisation of water and the Chinese used gold for medical applications.¹³⁻¹⁵ Perhaps the birth of modern chemotherapy was through one of the first known metal based drugs salvarsan (**Figure 1.2.1**), an arsenic-based antimicrobial agent used for the effective treatment of syphilis, until it was replaced by penicillin after World War II.^{13, 16}

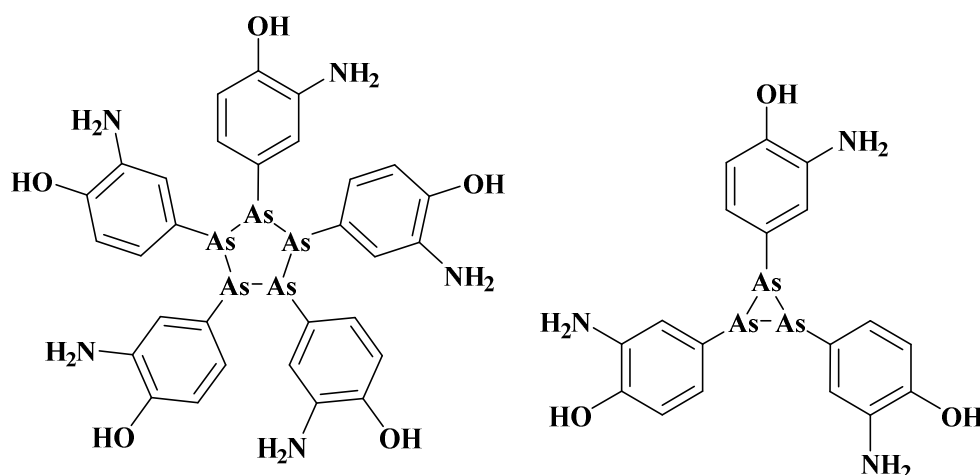


Figure 1.2.1: Cyclic pentamers and trimers of Salvarsan

Natural evolution has also incorporated a number of metal ions in vital and essential roles in living systems, for example iron in oxygen transportation, calcium and zinc for structural framework, zinc in insulin for regulation of sugar metabolism as well as copper and zinc as metallo-enzymes for biological catalytic reactions.^{14, 17} Such diverse applications are possible due to the interaction between the positively charged, electron deficient metal ions and the electron rich biological molecules such as proteins and DNA.¹⁴

Interest in the application, importance and reputation of metal based drugs, particularly organometallic compounds has gradually increased in the last two decades. Organometallic compounds have unique and remarkable physiochemical properties, an added advantage over purely organic based compounds. These properties include diverse structure and stereochemistry, variable accessible oxidation states, possibility of ligand exchange as well as redox and catalytic activities.^{16, 18}

In greater detail, compared to carbon based chemistry, organometallic compounds are able to form linear to octahedral. Metal ions are known to readily coordinate to a diverse range of ligands. This allows for chemical modifications and the tailoring of the resultant organometallic compound to recognise and specifically interact with biological targets. The variable accessible oxidation states facilitate the participation of the compound in biological redox reactions. Additionally, ligand exchange reactions give the possibility of interaction and coordination of organometallic compounds with cellular components such as enzymes, proteins and DNA. Most of

these compounds are kinetically stable, lipophilic and neutral, with the metal atom in a low oxidation state making them susceptible to chemical reactions.^{16, 18} Perhaps of all these advantages the most significant is the control that the medicinal chemist has over all these properties through rational ligand design and synthesis.

To date, a number of metals including antimony, bismuth, copper, cobalt, gallium, gold, iridium, iron, osmium, palladium, rhodium, ruthenium, silver, tin, titanium, vanadium and zirconium have been investigated for therapeutic applications.¹⁹⁻²⁷ Arguably the landmark discovery of the therapeutic activity and subsequent clinical success of cisplatin (**Figure 1.2.2**) by Rosenberg *et al.* was the turning point for medicinal inorganic chemistry, particularly anti-cancer research.²⁸

1.2.1 Cisplatin

Platinum based drugs form a distinct class of highly regarded and successful chemotherapeutic compounds with anti-tumour and anti-viral clinical applications.²⁹ Known as Peyrone's chloride, cisplatin was first synthesised by Peyrone in 1844 and its structure documented by Alfred Werner in 1893.³⁰ However, the compound did not gain any scientific significance until the serendipitous discovery of its therapeutic properties by Rosenberg *et al.* in 1965. In his experiment Rosenberg observed cell division inhibition in *Escherichia coli* when using platinum mesh electrodes. Further investigations identified *cis*-diamminedichloroplatinum(II) as the species responsible for this activity, thus initiating exploration of possible medical applications.³¹

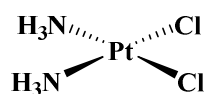
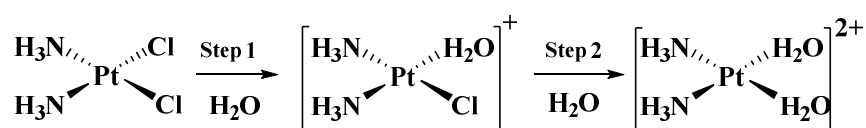


Figure 1.2.2: Cisplatin

Cisplatin (**Figure 1.2.2**) entered clinical phase trials in 1971 and was approved by the United States Food and Drug Administration (FDA) for pharmaceutical use in 1978.^{32, 33} Since then cisplatin has become the world's leading anti-cancer drug and is highly successful in the treatment of different types of neoplasms such as lung, ovarian, bladder, testicular, head and neck, esophageal, colon, gastric, breast, melanoma and prostate cancer. More than half a century after its clinical approval, cisplatin, used as a first-line treatment or in combination with other drugs remains

the “gold standard” against which potential platinum and non-platinum metal based anti-cancer drugs are compared.³⁴

The inherent anti-cancer properties of cisplatin are as a result of its interaction with DNA leading to induction of apoptosis. Once administered, through injection or infusion, the neutral cisplatin enters the bloodstream where the high chloride concentration (~100 mM) prevents exchange of labile *cis*-chloro ligands with water molecules.³⁵ Cisplatin becomes activated once it enters the cytoplasm through a combination of passive diffusion and facilitated active transport mechanisms. Passive diffusion is highly dependent on the concentration of the drug inside and outside the cell and the overall charge on the platinum species. Transporter proteins responsible for copper cell regulation, copper influx protein CTR1 and two copper efflux proteins, ATP7A and APT7B have been implicated in the facilitated and active uptake of cisplatin.³⁶⁻³⁸ Inside the cytoplasm, the chloride ion concentration is low (~10mM) allowing the labile *cis*-chloro ligands of cisplatin to dissociate and be replaced by water molecules (**Scheme 1.2.1**).^{35, 39}



Scheme 1.2.1: Hydrolysis of cisplatin

The mono- or di- aquated hydrolysis products are potent electrophiles that potentially react with any nucleophile, including the sulfhydryl groups on proteins and nitrogen donor atoms on nucleic acids. The cytotoxicity of cisplatin is due to its preferential interaction with the N-7 reactive centre of guanine and adenine in DNA forming DNA adducts (**Figure 1.2.3**). The DNA adducts can be DNA-protein, DNA-DNA interstrand and intrastrand crosslinks (**Figure 1.2.3**), with DNA-DNA intrastrand adducts being the most favoured.^{30, 40} Such cisplatin–DNA adducts, together with cellular pathways (including those involving p53, p73, ATR and MAPK) activated in response to cisplatin lead to cell division blockage, transcription inhibition, cell-cycle arrests, oxidative stress, failure to repair Pt-DNA adducts and ultimately apoptosis.^{13, 30, 41} Transplatin, the *trans* stereoisomer of cisplatin is known to be less cytotoxic than cisplatin and inactive against tumours. This is primarily because of its inability to form intrastrand DNA adducts and the ease with which

trans adducts are easily repaired compared to their *cis* analogues. The toxicity of the diaquo intermediate in the *cis* configuration is 30 times more than that of the *trans* diaquo intermediate.⁴²

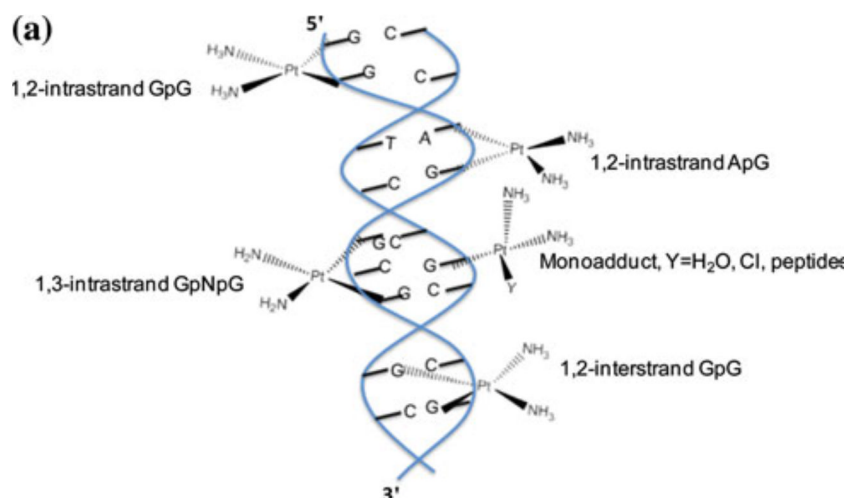


Figure 1.2.3: Cisplatin intra- and interstrand DNA cross linking⁴³

Despite the impressive success of cisplatin in clinical use, a number of drawbacks and side-effects associated with its narrow therapeutic window limit its application. Cisplatin is intravenously administered, cytotoxic to a limited spectrum of cancers and like many antineoplastic agents is not selective between healthy and cancerous cells. Of major concern is systemic toxicity as a result of cisplatin binding to other biomolecules other than the primary target DNA.⁴⁴ A known fact is that only 1% of the intravenously administered drug reaches DNA, this is because platinum has high affinity for thiol- and selenium-containing proteins in the cytoplasm. Thiol- and selenium-containing proteins are abundant both extra- and intracellularly, platinum subsequently interacts with them leading to disruption of various protein and enzyme functions. This limits the bioavailability and efficacy of the drug leading to drug inactivation⁴⁵ and adverse drug reactions (ADRs). ADRs related to clinical use of cisplatin are not limited to but include, nephro-,⁴⁶ neuro-, cardio- oto-, gastro- and hepatotoxicity,⁴⁷ hair loss, anaemia, and bone marrow suppression.^{44, 46, 48, 49} Nephrotoxicity is among the most severe ADRs and occurs in approximately a third of patients. The kidneys absorb cisplatin more than other body organs and are the main route for its excretion.³⁰ The exact mechanism of cisplatin-induced nephrotoxicity has not yet been fully clarified. However, cisplatin is known to induce degenerative renal lesions characterised by hydropic degeneration, necrosis and

tubular atrophy which in some cases can lead to severe kidney failure.⁴⁸ Although to a lesser extent, cisplatin is also known to induce immunological side effects such as anaphylactic shock and asthma. Some of the allergic reactions can include abdominal discomfort (diarrhoea and cramps), rashes (swelling, pruritus and urticaria) and respiratory dysfunction (for example wheezing).⁴⁸

Another drawback associated with the clinical use of cisplatin is the development of resistance, defined as the failure to undergo programmed cell death at clinically relevant drug concentrations. Resistance can be natural (intrinsic resistance) as seen in colon cancer or through prolonged drug exposure (acquired resistance) as seen in non-small cell lung cancer.²⁹ Resistance mechanisms although still under debate are a combination of insufficient formation of cisplatin-DNA adducts due to changes in the uptake and efflux of the drug, cellular survival of cisplatin-DNA adducts through DNA repair or removal or by tolerance mechanisms and increased inactivation of the drug through interaction with thiol containing molecules such as glutathione (GSH).^{33, 44, 50} **Figure 1.2.4** shows the different mechanisms involved in inhibiting the apoptotic signal in cisplatin resistant tumour cells.⁴⁰ Better understanding of mechanisms of action and tumour resistance have led to four strategies being proposed to bypass cisplatin resistance:

1. Improved delivery of platinum to tumours; targeted delivery using delivery vehicles
2. Co-administration of cisplatin with pharmacological modulators of resistance mechanisms
3. Combination of cisplatin with molecularly targeted drugs
4. New, improved platinum drugs.³³

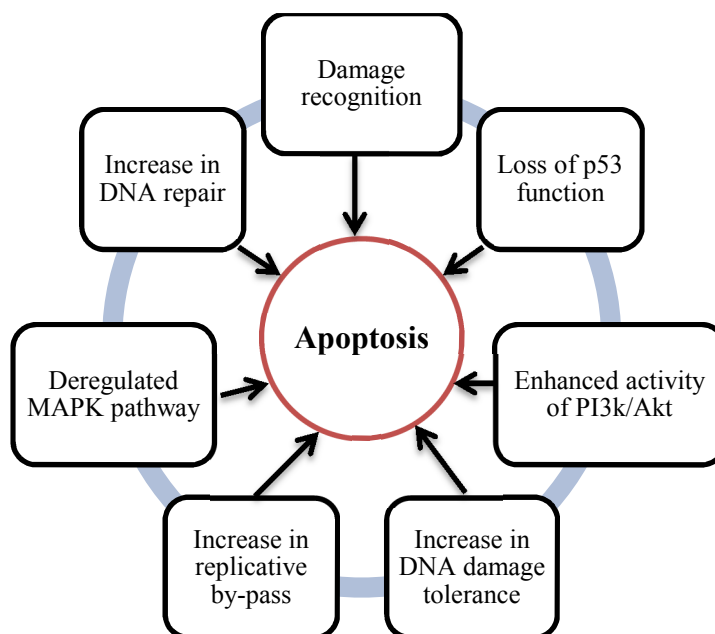


Figure 1.2.4: Mechanisms involved in apoptotic signal inhibition in cisplatin resistant tumours

1.2.2 Other platinum based anti-cancer drugs

The limitations and drawbacks associated with the clinical use of cisplatin, particularly toxicity and drug resistance have prompted research into alternative platinum anti-cancer agents. Various cisplatin analogues have been synthesised and evaluated over the years with 13 of these going into clinical trials.³⁰ However only two other platinum anti-cancer drugs have so far gained FDA approval; carboplatin in 1989 and oxaliplatin in 2002 (European approval in 1999).¹³ **Figure 1.2.5** shows the platinum based drugs currently in clinical use trials.

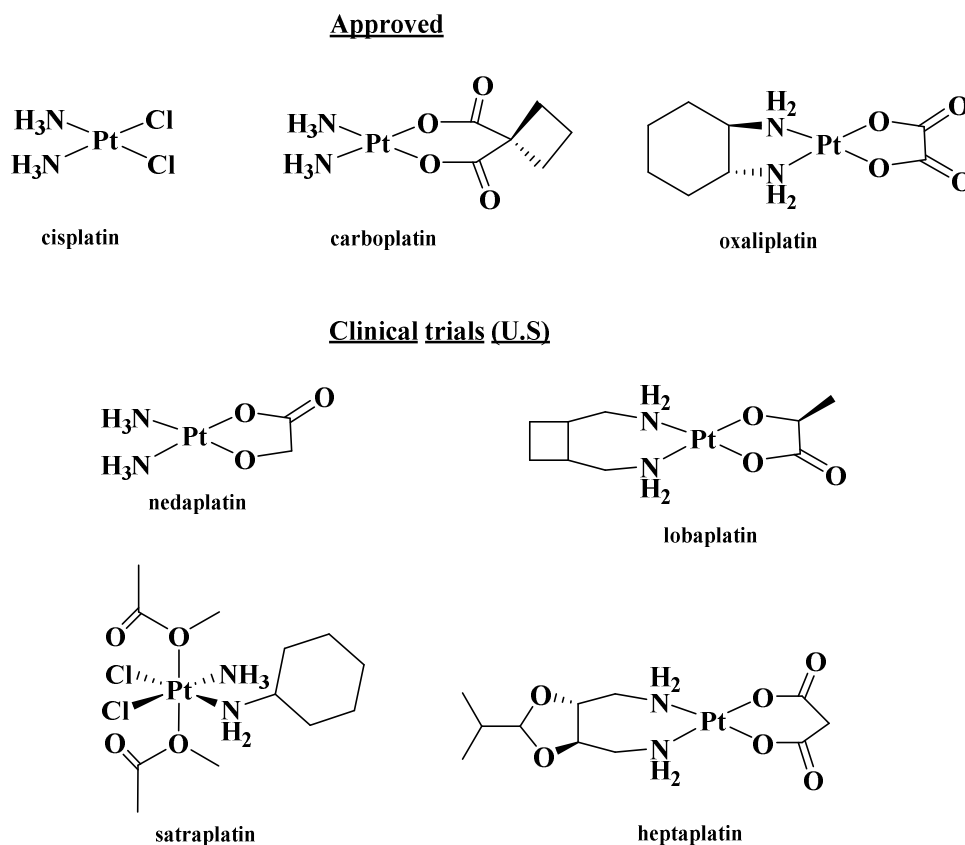


Figure 1.2.5: Platinum drugs in clinical use and trials¹³

Cisplatin, carboplatin and oxaliplatin (**Figure 1.2.5**) are structurally similar with a square planar geometry around the central platinum(II) ion. The amine ligands are strongly bound to the platinum ion, and as such the carboxylate ligand acts as a leaving group, allowing the platinum to interact with DNA bases.⁵¹

Carboplatin, [*cis*-diammine(1,1-cyclobutanedicarboxylato)platinum(II)], is an intravenously administered chemotherapeutic drug for the treatment of ovarian, lung, head and neck cancer. The chelate effect of the carboxylate ligand makes it less labile than the chloride leaving groups in cisplatin as such carboplatin is less reactive than cisplatin, showing slower DNA binding kinetics.²⁹ The inherent stability of carboplatin leads to less carboplatin-protein adducts being formed and excreted. The lower excretion rate increases the retention half life of carboplatin, a significant advantage over cisplatin.³⁰ Similar to cisplatin, the mechanism of action of carboplatin is through binding to DNA and proteins although carboplatin may be susceptible to alternative mechanisms. The greatest advantage of carboplatin over cisplatin is the reduced side effects such as nephro-, oto- and neurotoxicity.^{13, 33} A major drawback associated with carboplatin is myelo suppression which leads to

blood white cell reduction evidently exposing the patient to infection by various organisms.³⁴

Colorectal cancer was previously known to be insensitive to platinum based neoplastic agents.³³ Oxaliplatin, [(1R,2R)-diaminocyclohexane oxalatoplatinum(II)], is currently the only platinum based drug to show any activity against colorectal cancer, especially when used in combination with 5-fluorouracil and leucovorin.⁵² Oxaliplatin shows activity against cisplatin-resistant tumours, and is less myelo suppressive than carboplatin. A limitation of oxaliplatin is that the drug induces peripheral neuropathy (nerve damage).^{53, 54} Interestingly the intracellular accumulation of oxaliplatin is less dependent on the copper transporter CTR1, a feature quite different from cisplatin and carboplatin.³³

Heptaplatin, lobaplatin and nedaplatin (**Figure 1.2.5**) are other cisplatin analogues that have gained regional clinical use approval but are still under clinical trials in the United States.¹³ Hepta-, loba- and nedaplatin are licensed in Korea, China and Japan respectively.³⁴ A number of platinum based drugs are also under investigation in either pre-clinical or clinical trials, all in attempt to improve or eliminate the adverse side effects of the present drugs while maintaining or improving the efficacy of the drug.

1.2.3 Ruthenium anti-cancer drugs

The last four decades have witnessed a surge in the search for bioorganometallic anti-cancer drugs based on metals other than platinum. Among these, ruthenium (Ru^{II} and Ru^{III}), gold (Au^I and Au^{III})⁵⁵⁻⁵⁷ and titanium (Ti^{IV})^{58, 59} complexes are among the most studied.⁶⁰ The following sections discuss some key complexes currently being investigated for application in the anti-cancer field, with particular focus on ruthenium (**1.2.3**) and copper (**1.2.4**) complexes.

Ruthenium based complexes have emerged as promising anti-tumour and anti-metastatic agents with potential anti-cancer applications against platinum-resistant tumours.⁶¹ Ruthenium complexes theoretically possess a number of unique properties that can justify their potential use as alternative therapeutic agents to platinum based drugs:

- i. The rich synthetic chemistry of ruthenium is well investigated and known, with most complexes being stable both in solid and solution state.⁶² Ruthenium is known to form strong chemical bonds and can bind to a variety of biomolecules with differing electronic properties and hardness.⁶³ The octahedral geometry around the ruthenium centre offers more diversity in terms of ligand coordination, substitution and in turn ligand exchange kinetics, implying a reactivity and mode of action different from cisplatin.⁶¹
- ii. The ruthenium centre can easily access oxidation states II, III and IV under physiological conditions. The energy barrier for interconversion between these oxidation states is relatively small allowing Ru(III) and Ru(IV) complexes to act as inert prodrugs, being reduced under hypoxic conditions inside the tumour to the active Ru(II) species. This activation by reduction phenomenon results in ruthenium complexes being more selective towards cancerous cells and more importantly hypoxic tumours, known to be resistant to chemotherapy and radiation.^{61, 64-66}
- iii. Ruthenium can mimic iron in binding to serum transferrin and albumin for transportation into cells.⁶⁷ In addition to higher membrane permeability, rapidly dividing cancer cells have a presumed higher need for iron leading to an over-expression of transferrin receptors on the cancerous cell surface. As such ruthenium based drugs are able to preferentially accumulate in neoplastic cells compared to normal cells, a feature which reduces their systemic toxicity and side effects.^{61, 64, 68, 69}

The discovery in the 1970s of “ruthenium red”, a cytological dye which exhibits anti-cancer properties through inhibiting mitochondrial calcium transport marked the first systematic investigation of ruthenium complexes for therapeutic applications.⁷⁰⁻⁷² This preceded the discovery by Clarke *et al.* that chloro-ammine-Ru(III) compounds that could be regarded as Ru analogues of chloro-ammine-Pt compounds showed promising therapeutic properties.^{62, 73} Poor solubility was the major obstacle with these complexes leading to termination of further investigations.^{74, 75} However, further synthetic investigations into more soluble complexes led to the discovery of NAMI-A and KP1019, the first ruthenium based anti-cancer drugs to progress to clinical trials.

1.2.3.1 NAMI-A

NAMI-A, imidazolium- $[trans\text{-imidazole-DMSO-tetrachlororuthenate(III)}]$ (**Figure 1.2.6(a)**), a Ru(III) coordination compound discovered by Sava *et al.* is perhaps the most investigated in the ruthenium family and the first to enter phase I clinical trials.⁷⁶ NAMI-A was originally synthesised as NAMI (**Figure 1.2.6(b)**) in which the imidazolium counter-ion is replaced by sodium. Due to reproducibility issues in the synthetic procedure and poor stability and solubility, NAMI was replaced by NAMI-A in pre-clinical experiments.^{73,76}

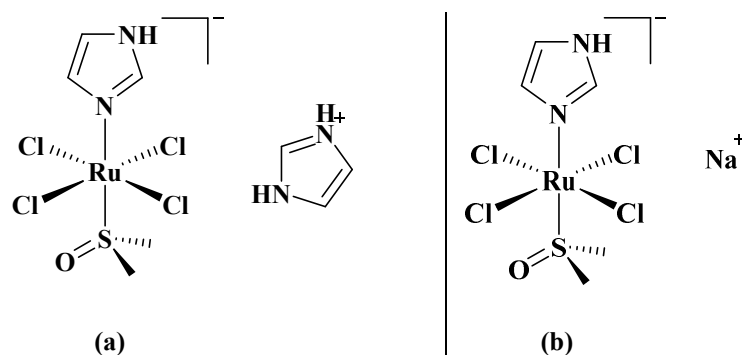


Figure 1.2.6: (a) NAMI-A, (b) NAMI

Similar to cisplatin, hydrolytic decomposition of NAMI-A is highly dependent on pH. NAMI-A undergoes both chloride and DMSO hydrolysis to form a mixture of poly-oxo Ru species, that to date have not been fully characterised. According to Alessio,⁷⁷ NAMI-A can be considered as the “ultimate prodrug” that gradually loses all its original (supporting and leaving) ligands, with only the Ru metal ion eventually reaching the target site. In this scenario once administered there is no control over the rate and location of ligand release.⁷⁷

Interestingly NAMI-A has negligible cytotoxicity towards the primary tumour, rather exhibits anti-metastatic and growth inhibition properties independent of the type of primary tumour and stage of growth against lung metastases for various solid tumours.⁶⁴ The substantial lack of cisplatin-like cytotoxicity against solid tumour cell lines is related to the rather low cellular internalisation of NAMI-A and its metabolites. This is as a result of the rapid extracellular transformations that NAMI-A undergoes and the ability of its metabolites to primarily interact with cell walls rather than DNA as in cisplatin.^{78,79}

Although still under extensive investigation, NAMI-A is thought to inhibit metastasis through non-traditional cell cytotoxicity mechanisms *via* multiple interactions outside and inside the cells. NAMI-A has been shown to temporarily block cell cycle progression⁸⁰ leading to DNA and RNA binding^{81, 82} and the inhibition of matrix metalloproteinase (MMP-2 and MMP-9) release.⁸³ However, these intracellular effects are related to cellular uptake and are only feasible at physiologically non-relevant concentrations (>100 μ M) of NAMI-A and thus cannot explain the anti-metastatic activity of NAMI-A.⁷⁷ Other properties that occur at lower, physiologically relevant drug concentrations such as the inhibition of key steps in angiogenesis (for example cell proliferation) are more likely involved in the mechanism of action.⁸⁴ In addition factors unrelated to the penetration of the compound inside cells such as increased cell adhesion, reduced cell mobility, and decreased ability of cells to penetrate into collagen gels better explain the anti-metastatic property of NAMI-A.⁸⁵

Phase I dose escalation and pharmacokinetics studies for NAMI-A on several solid tumours gave promising results with fairly moderate toxicity prompting phase II clinical trials.⁸⁶ In support of the proposed mechanisms of action described above, no ruthenium-DNA adducts were detected in DNA extracted from white blood cells even at high drug concentrations. However, to a larger extent NAMI-A was found bound to plasma proteins.⁷⁷ Based on phase I results NAMI-A was given in combination with gemcitabine to patients with non-small cell lung cancer (NSCLC) in phase II clinical trials. However, NAMI-A did not progress beyond phase II clinical trials as the overall efficacy was lower compared to gemcitabine alone.^{77, 87}

1.2.3.2 KP1019 and NKP1339

KP418, imidazolium *trans*-[tetrachloro-bis(1H-imidazole)-ruthenate(III)] (**Figure 1.2.7(a)**) discovered by Keppler *et al.* display tumour reduction activity against B16 melanoma cell lines⁸⁸ and rat colorectal carcinoma models.⁸⁹ Further investigations on this class of complexes led to the discovery of KP1019, indazolium [*trans*-tetrachloro-bis(indazole)-ruthenate(III)] (**Figure 1.2.7(b)**), the indazole analogue of KP418.⁹⁰ Pre-clinical studies with KP1019 showed higher activity against rat colon cancer models. Interestingly KP1019 also showed higher activity than 5-fluorouracil, the standard licensed agent against colorectal cancer.⁹¹

NKP1339 (**Figure 1.2.7(c)**), the sodium salt analogue of KP1019 was prepared as a precursor in the synthesis of KP1019.⁹² However, due to its high water solubility has become the representative of this class of compounds and lead candidate for further clinical development.⁹³

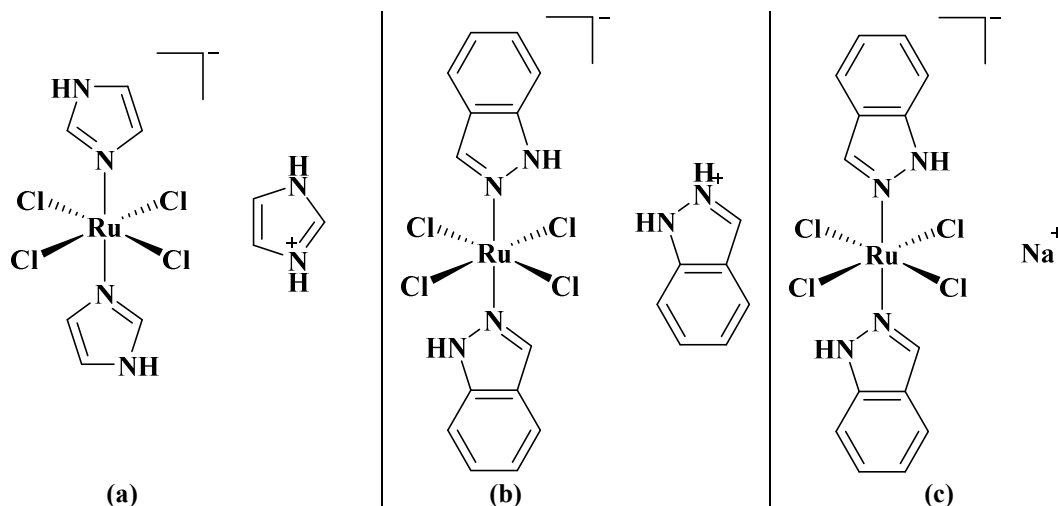


Figure 1.2.7: Structures of (a) KP418 (b) KP1019 (c) NKP1339

Despite being structurally similar to NAMI-A, KP1019 shows no anti-metastatic effects, rather showing classical characteristics of conventional cytotoxicity against primary cisplatin-resistant colorectal tumours with negligible occurrence of acquired resistance.^{62, 94} Both KP1019 and NKP1339 are intravenously administered and undergo rapid cellular uptake through interactions with plasma proteins, in particular albumin and transferrin.^{95, 96} These proteins transport and deliver the Ru compounds inside the cell, with KP1019 preferentially binding to albumin. The preferential tumour accumulation of KP1019 can be explained by the “enhanced permeability and retention effect” (EPR) in which albumin accumulates in malignant tissues due to adverse structural changes such as porous capillary tubes.⁹⁷

NK1019 and NKP1339 are hypothesised to undergo activation by reduction in which Ru(III) compounds serve as prodrugs, being reduced under hypoxic conditions to the active Ru(II) species which are in turn more reactive towards biomolecules. Notably activation by reduction takes place after intracellular release of the compound from the plasma proteins.^{75, 93, 98} Thus the mechanism of action of KP1019 and NKP1339 is highly dependent on their redox chemistry and through induction of G₂M cell cycle arrest, blockage of DNA synthesis and initiation of apoptosis *via* the mitochondrial pathway.⁶² Additionally, NKP1339 serves as a direct nitric oxide

scavenger, possibly inducing effects in cell migration and angiogenesis.⁸⁴ Taken in combination, KP1019 and NKP1339 are potential potent drug candidates with limited side effects as observed so far in clinical phase I trials.⁹³

1.2.4 Copper anti-cancer drugs

In the ongoing search for non-platinum based anti-cancer agents, copper complexes have received considerable attention.⁹⁹ Copper is an essential element involved in many biological pathways such as the function of several enzymes and proteins involved in energy metabolism, respiration, and DNA synthesis.^{100, 101} The concentration of copper in the body is tightly regulated; although rare disruptions in copper homeostatic balance can result in disorders such as Menkes' disease¹⁰² (copper deficiency) or Wilson's disease¹⁰³ (copper overload).¹⁰⁴

Facilitated by the hypothesis that copper being an endogenous trace element found in virtually all living things will be less toxic to healthy cells than non-essential ones, investigating therapeutic applications for copper based complexes is a logical advancement.¹⁰⁵ The use of multiple copper transporters in the uptake, intracellular transport and efflux of platinum drugs such as cisplatin offers the possibility of overcoming cisplatin resistance and improving selectivity towards neoplastic tumours.¹⁰⁶ *Ex vivo* experiments have shown that in comparison to healthy tissues cancerous tissues (breast, prostate, brain and lung) have increased copper concentrations.¹⁰⁷ A seemingly appropriate explanation for this is the participation of copper as a crucial cofactor in angiogenesis,¹⁰⁸ a critical factor in tumour growth, invasion and metastasis.¹⁰⁹ Thus, copper based anti-cancer drugs have the ability to selectively induce cytotoxicity in tumours. In addition, intensive research has gone into the chemistry and biochemistry of copper,^{110, 111} its mechanisms of absorption,¹¹²⁻¹¹⁴ distribution,¹¹⁵⁻¹¹⁷ metabolism and excretion^{107, 118} as well as its role in development of cancer and other diseases.^{100, 104, 119, 120}

Copper can easily access oxidation states I and II under physiological conditions. As such most common coordination and organometallic complexes of copper in the literature have the central ion in the +1 and +2 oxidation states, and only a few examples with +3.^{121, 122} These copper (III) complexes are labile and can preferentially adopt distorted coordination geometries.¹⁰⁰ These factors are highly

dependent on the donor atoms (N, O, S and halides) bound to the metal ion and the choice and nature of the ligand(s) (chelation, electronic and steric properties).¹²³

1.2.4.1 Copper complexes with thiosemicarbazone ligands

Thiosemicarbazones (TSCs) (**Figure 1.2.8**) are a class of diverse ligands that have found applications as pharmacophores due to their ability to form stable complexes with transition metal ions.¹²⁴ Interest in their potential medical application as anti-viral, anti-fungal, anti-bacterial and anti-cancer agents has been intensively explored.¹²⁵

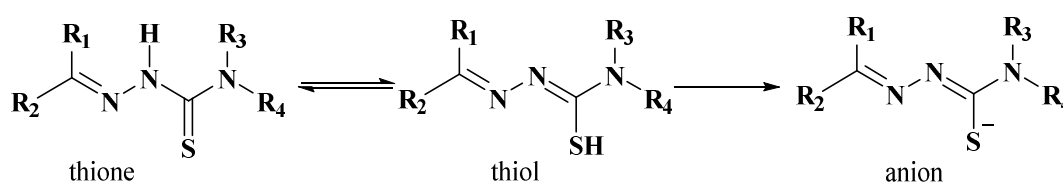


Figure 1.2.8: Thiosemicarbazone frameworks

The anti-neoplastic effects of copper-thiosemicarbazone complexes have been explored as far back as the 1960s^{126, 127} and are still ongoing, with promising results.¹²⁸⁻¹³⁰ The major obstacle observed with the various analogues of copper-thiosemicarbazone complexes synthesised over the years is poor water solubility and high *in vivo* toxicity.^{131, 132} As with other transition metals current research is primarily focused on improving the solubility and toxicity of these complexes through modification of the TSC ligand framework.¹³³⁻¹³⁵

Despite the evident therapeutic efficacy of TSC ligands, chelation to metal complexes such as copper has been shown to greatly enhance the efficacy and solubility of the resultant complex.^{128, 136} Currently many mono and dimeric copper(II) thiosemicarbazone complexes have been synthesised and investigated as anti-tumour agents in various *in vivo* and *in vitro* experiments.^{124, 137, 138} A significant number of these complexes have displayed activity in the nano-molar range against a broad spectrum of cancers.^{100, 133, 139} Interest in copper complexes has been fuelled by the hypothesis that, in addition to lower toxicity copper complexes are able to overcome cisplatin resistance in tumours. The possibility of different mechanism(s) of action to that of covalent DNA binding observed in cisplatin and analogues is possible and supports this hypothesis.¹⁰⁰ The mechanisms of action of copper

thiosemicarbazone complexes, although still under investigation, involve cell proliferation inhibition, cell cycle arrest and initiation of apoptosis.¹⁰⁵

To date, the most successful therapeutic agents in the thiosemicarbazone family are triapine, (3-aminopyridine-2-carboxaldehyde TSC) (**Figure 1.2.9(a)**) and di-2-pyridylketone-4,4-dimethyl-3-TSC (Dp44mT) (**Figure 1.2.9(c)**), with triapine (3-AP) having reached phase II clinical trials against several cancer types.^{100, 140, 141}

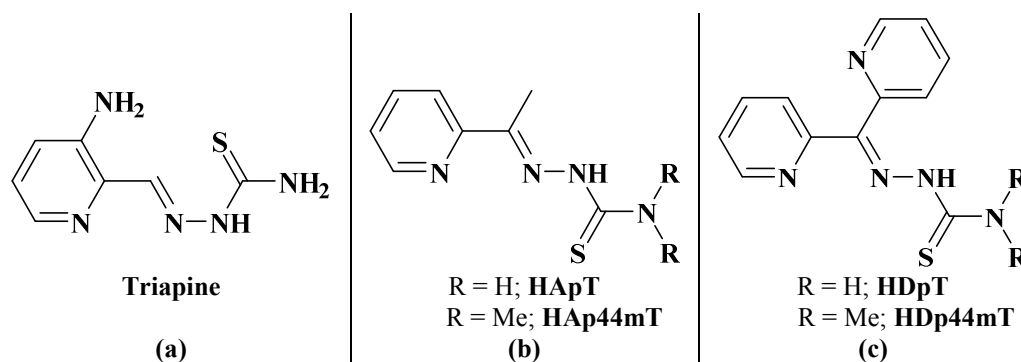


Figure 1.2.9: Structures of copper TSCs

Copper(II)-3-AP complexes of the type shown in **Figure 1.2.10** have been synthesised for studies aimed at comparing their inhibitory activity relative to that of metal free 3-AP. The efficacy of copper(II)-3-AP complexes were in contrast to the popular hypothesis that coordination to metal ions leads to higher cytotoxic activity. The complexes displayed similar or decreased biological activity to the free ligand. Their anti-proliferative activities were likely due to the complexes acting as intracellular transporters of the ligand that in turn dissociate initiating biological activity. In addition, the decrease in biological activity may be due to the high stability of the Cu(II) complexes.¹⁴²⁻¹⁴⁵

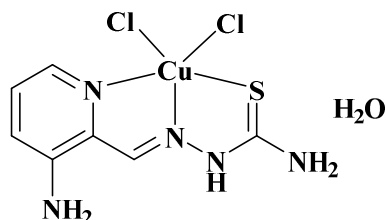


Figure 1.2.10: Copper(II)-3-AP complexes

In further attempts to improve the activity of 3-AP and Dp44mT, copper complexes with their analogues, ApT (**Figure 1.2.9(b)**) and DpT (**Figure 1.2.9(c)**), have been synthesised and their anti-cancer activities evaluated. Santini¹⁰⁰ and other research

groups¹⁴⁶⁻¹⁴⁸ have shown that the monovalent species $[\text{Cu}(\text{TSC})]^+$ are the active potent species *in vivo* and *in vitro* and resulted in significant increases in anti-tumour activity. They have hypothesised that instead of the dissociated ligands, the copper complexes were responsible for the biological activity. In addition, copper(DpT) complexes showed higher anti-proliferative effects compared to the copper(ApT) complexes.¹⁴⁶

1.2.4.2 Copper complexes with mixed chelate ligands

Ruiz-Azuara *et al.* have developed a series of copper based drugs registered under the trade name Casiopeinas® (Cas) (**Figure 1.2.11**).¹⁴⁹ These mixed-chelate cationic copper(II) complexes have the general formula $(\text{Cu}(\text{N-N})(\text{X-X}))\text{NO}_3$ where N-N represents diamine donor type ligands (phen, bipy and analogues) and X-X represents (N,O) or (O,O) donor ligands (acetylacetonate (acac) or salicylaldehyde (alal)).¹⁵⁰⁻¹⁵² In successive investigations the nature of the X-X ligand was found to have negligible influence on the biological activity of the complexes. However, the presence of the fused aromatic ring in the phen-containing complexes was necessary for biological activity, as such phen-containing complexes had higher activity than their bipy-analogues.^{100, 153} *In vivo* and *in vitro* assays on HeLa, MCF-7 and HCT-15 cells showed cytotoxic,^{149, 154} genotoxic¹⁴⁹ and anti-tumour activity.^{152, 155}

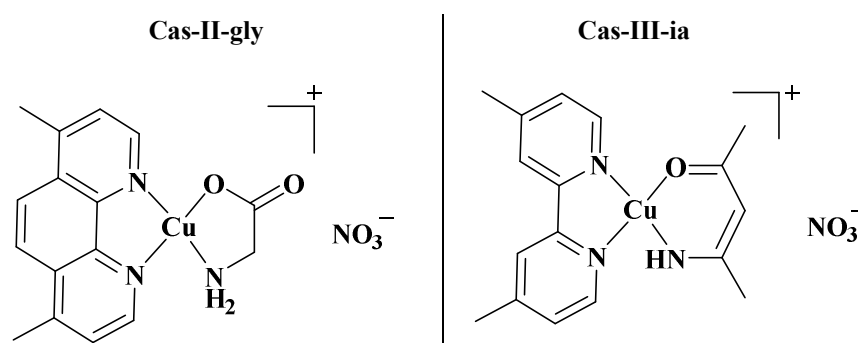


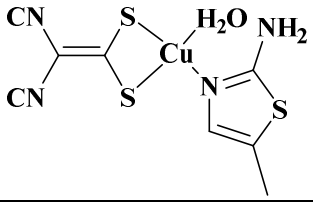
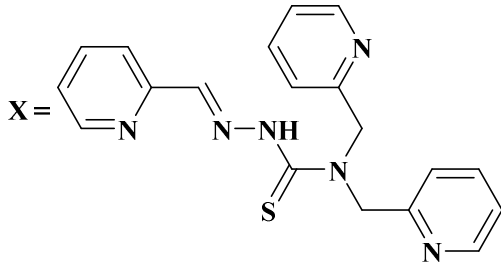
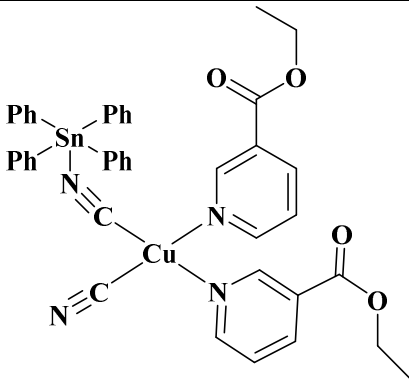
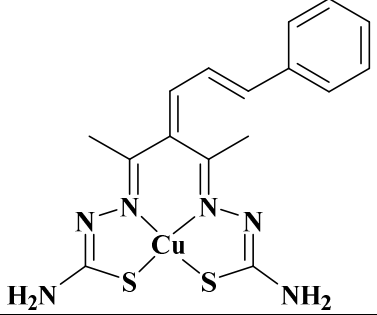
Figure 1.2.11: Structures of representative Casiopeinas family of complexes

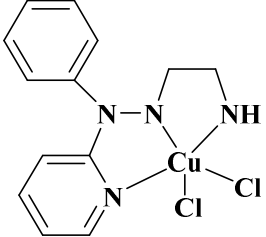
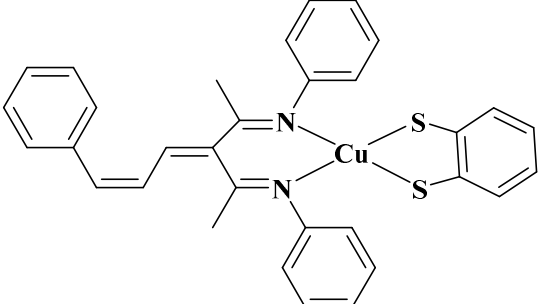
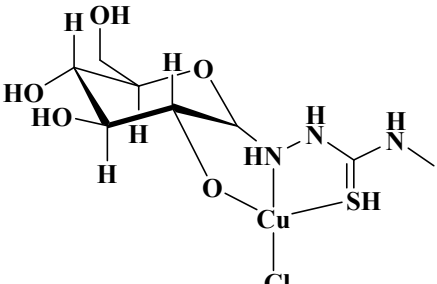
Figure 1.2.11 shows the two most investigated within this broad and diverse family of complexes. Cas-II-gly is the most successful having reached clinical trials in Mexico.¹⁰⁵ The mechanism of action of the casiopeinas family of complexes is still under intense investigations although preliminary results suggest a number of biological targets leading to a complex mechanism of action. Cytotoxic activity is as a result of activation of pro-apoptotic pathways (through generation of reactive

oxygen species (ROS), mitochondrial toxicity or dysfunction and cell cycle arrest), DNA intercalation (and fragmentation), cell migration and cell proliferation inhibition.^{100, 156-158}

The chemistry of copper based anti-cancer drugs is broad and diverse; further compounds with promising therapeutic applications that have not been covered by the author in this review are summarised in **Table 1.2.1**¹⁰⁰

Table 1.2.1: Summary of other copper based compound with therapeutic applications

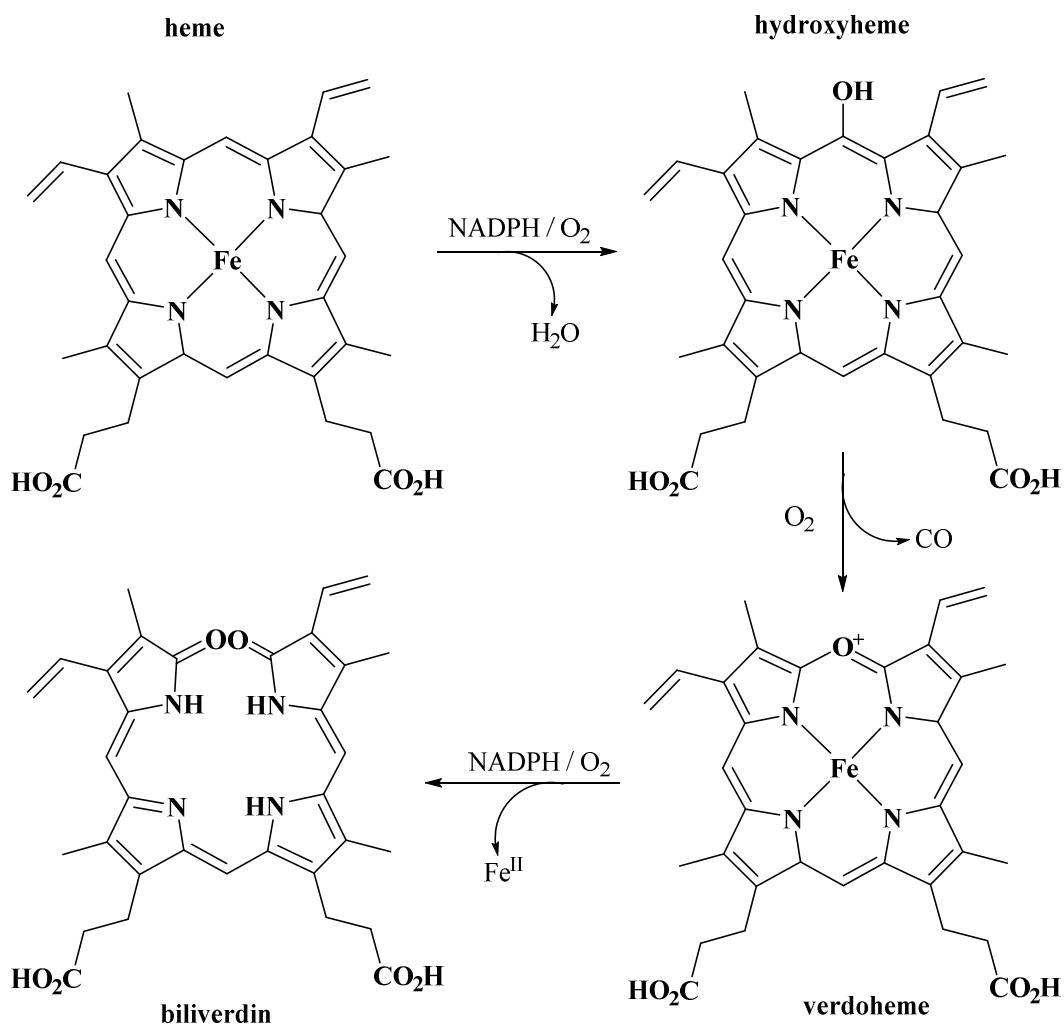
Compound	Tumour type	Ref
	Leukemia P380	159
<p>CuX</p> 	HL60 human xenografts	160
	MNU induced rat mammary carcinoma	161
	Erlich ascites carcinoma	162

Compound	Tumour type	Ref
 <p>The structure shows a central copper atom coordinated to two chlorine atoms, a pyridine ring, and a 1,2-diphenylhydrazine ligand.</p>	MNU induced rat breast cancer	163, 164
 <p>The structure shows a central copper atom coordinated to two imine nitrogen atoms of a bis-imine ligand, a phenyl ring, and a benzothiazole ring.</p>	Erlich ascites carcinoma	165
 <p>The structure shows a central copper atom coordinated to a chlorine atom, a thiosemicarbazide ligand, and a sugar moiety (likely a pyranose ring).</p>	Erlich ascites carcinoma	166

1.3 Carbon Monoxide Releasing Molecules

Carbon monoxide (CO) was first discovered in 1849 as a naturally occurring metabolite in the exhaled air of healthy human beings.¹⁶⁷ Despite its natural occurrence and role as an endogenous small signalling molecule in the human body, carbon monoxide is also known to be relatively toxic and dangerous to mammals at high concentrations. Commonly referred to as the “silent killer” due to its ability to rise, undetected, to toxic concentration; the toxicity of this gas partially arises from increased concentration in the tissues as a result of inhalation, which in turn interferes with normal mitochondrial function. CO bound to iron centres in haemoglobin [carboxyhaemoglobin (HbCO)] is also known to reduce the oxygen carrying capacity of blood, resulting in inhibition of oxygen delivery and release to tissues eventually leading to hypoxia.¹⁶⁸⁻¹⁷²

However, endogenous carbon monoxide produced in mammals by the catabolism of heme by heme oxygenase enzymes (inducible (HO-1) and constitutive (HO-2)) (**Scheme 1.3.1**) has been shown to have therapeutic and immunomodulatory applications. Lack of, or excess production of, carbon monoxide has been linked to the development of conditions such as tissue cellular apoptosis¹⁷³, diabetes^{173, 174}, inflammation¹⁷⁵⁻¹⁷⁷, cystic fibrosis^{178, 179}, bronchiectasis¹⁸⁰, rhinitis¹⁸¹ and asthma.^{182, 183} On the other hand, medical evidence¹⁷⁰ has shown that CO can assuage or prevent some conditions such as cell proliferation¹⁷³, hepatic ischemia¹⁸⁴, cardiovascular inflammation^{173, 185, 186}, anti-atherogenesis¹⁸⁷ and cyto-protective effects.^{173, 188}



Scheme 1.3.1: Production of CO through catabolism of heme

The therapeutic properties and applications of CO present an interesting and intriguing area of research in drug discovery. The challenge however has been the strictly-controlled delivery, localisation and selectivity of carbon monoxide administered in its gaseous form, in order to avoid toxic side effects and tissue hypoxia. Carbon monoxide releasing molecules, also known as CORMS, have emerged as a possible and alternative delivery system. These organometallic compounds, containing at least one carbonyl ligand bound to a transition metal can act as a prodrug and upon triggering or activation release the bound CO, which then acts as endogenously generated CO.^{168-170, 172, 189} Thus, in principle CORMs act as prodrugs allow for the controlled, targeted and specific delivery of carbon monoxide to cellular and tissue targets. To date, different stimuli have been explored in promoting CO release including photochemical,^{190, 191} thermodynamic^{192, 193} and enzymatic triggers.^{170, 194, 195}

Over the years a number of metal carbonyl complexes have been prepared and their medicinal properties investigated, examples include cobalt¹⁹⁶, ruthenium¹⁹⁷, iron¹⁹⁸, chromium^{199, 200} and manganese.¹⁹² Of particular interest to the author are ruthenium carbon monoxide releasing molecules, thus a brief overview of these is provided herein.

1.3.1 Ruthenium CORMs

The commercially available $[\text{RuCl}_2(\text{CO})_3]_2$, tri-carbonyldichlororuthenium(II) dimer (**Figure 1.3.1(a)**) also known as CORM-2 is one of the first reported CORMs, and has attracted considerable attention as a control substance. Extensive research has gone into the investigation of therapeutic and biological application of CORM-2, as shown by the large number of publications available.²⁰¹

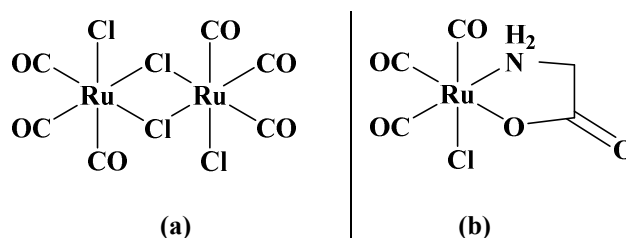


Figure 1.3.1: (a) CORM-2 and (b) CORM-3

Tricarbonylchloro(glycinato)ruthenium(II) (CORM-3) [**Figure 1.3.1(b)**] is possibly the most commonly used CORM to date due to its solubility in water. With more than 100 publications this compound has become the standard CORM for the investigation of different therapeutic applications of carbon monoxide releasing molecules on a wide range of biological systems.¹⁶⁹ Interestingly CORM-3 has low toxicity, can act as a vasodilator and greatly increases the survival rate of mice after heart transplants.²⁰²

To date *in vivo* and *in vitro* tests on ruthenium CORMs has shown a variety of good therapeutic properties. Examples include protection against cisplatin-induced nephrotoxicity,²⁰³ suppression of the inflammatory response^{204, 205} and prevention of cardiac graft rejection and positive inotropic effects of the heart.^{202, 206}

Despite their therapeutic advantages, factors controlling the release of CO from these complexes are not yet fully understood. However, it is thought that factors such as

solubility in water, electron density, type of ligand and oxidation state of the metal centre play an important role.²⁰⁷

1.3.2 CORMs in cancer

The immense interest in biological applications of CO and CORMs in inflammatory and vascular diseases, microbial infections, and organ transplants has led to a large number of scientific publications on the subject.²⁰⁸⁻²¹² In contrast, little interest has been shown in pursuit of the potential application of CO and CORMs as anti-cancer agents. The effects of carbon monoxide releasing molecules on specific cancer processes involved in cancer initiation and progression, such as angiogenesis and apoptosis, have been studied. Results obtained are as variable as they are cell-type specific, highlighting a major obstacle in the potential application of CO and CORMs in cancer therapy. Controversy on the molecular targets and specific signalling pathways affected by CO remain unclear, often leading to contradicting reports; affecting research interest in their application as anti-cancer agents.^{167, 213, 214}

The effects of CORM-2 (**Figure 1.3.1 (a)**) on human pancreatic cancer cell lines have been investigated by Vitek *et al.*²¹⁵ CORM-2 in clinically relevant and applicable doses was a potent inhibitor of pancreatic carcinogenesis. Prevention of Akt protein phosphorylation, a key process in pancreatic cancer initiation,²¹⁶ led to cell proliferation inhibition and apoptosis. In addition, *in vivo* treatment of pancreatic cancer models with CORM-2 led to significant decrease in tumour volume and increase in survival rate. Further investigations with CO gas confirmed that the anti-cancer properties were as a result of carbon monoxide release from CORM-2.²¹⁵

Carrington *et al.*²¹⁷ have synthesised azopyridine derived Mn(I) carbonyl complexes (**Figure 1.3.2**) and investigated their activity as anti-cancer agents against malignant cell lines, HeLa (cervical cancer) and MDA-MB-231 (breast cancer). In addition to favourable visible light dependant CO release, MnBr(azpy)CO₃ [**Figure 1.3.2(a)**] showed dose-dependent eradication of the cancer cells. On exposure to CO, morphological changes such as cell shrinkage and bulging, co-factors in apoptosis were observed. Control reactions in the absence of light showed no cell viability supporting the potential application of these complexes as photo-activated anti-cancer drugs.^{213, 217}

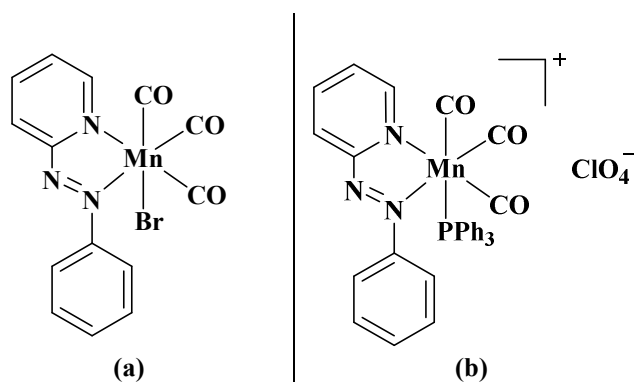


Figure 1.3.2: Azopyridine derived Mn(I) carbonyl complexes

In a later study, aimed at tracking the photoCORMs in biological targets, the same group synthesised a fluorescent manganese carbonyl complex that acts as a “turn-on” photoCORM. This complex, *fac*-[MnBr(CO)₃(pbt)] (**Figure 1.3.3**), is visible light sensitive coupled with heightened fluorescence upon CO release to cellular targets. MTT assays showed trackable CO delivery within cells and dose-dependent inhibition of breast cancer cells through rapid CO-induced apoptosis.²¹⁸

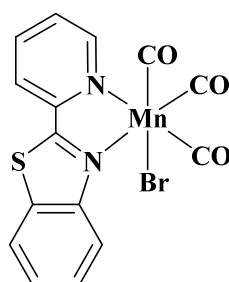


Figure 1.3.3: PhotoCORM MnBr(CO)₃(pbt)

A series of N-substituted heterocyclic carbonyl complexes with manganese, molybdenum or tungsten metal centres have been synthesised by Hu and co-workers. The various growth inhibitory effects observed on HeLa cells were a result of the in solution slow release of CO and the heterocyclic ligands from the complexes.²¹⁹ Similarly, proliferation inhibition effects on HeLa cells were observed by Gong *et al.*²²⁰ with slow CO releasing hexacarbonylcobalt complex esters (**Figure 1.3.4**). The mechanism of action is a combination of cell cycle arrest, generation and increase of ROS, cell division and proliferation inhibition leading to apoptosis.²¹³

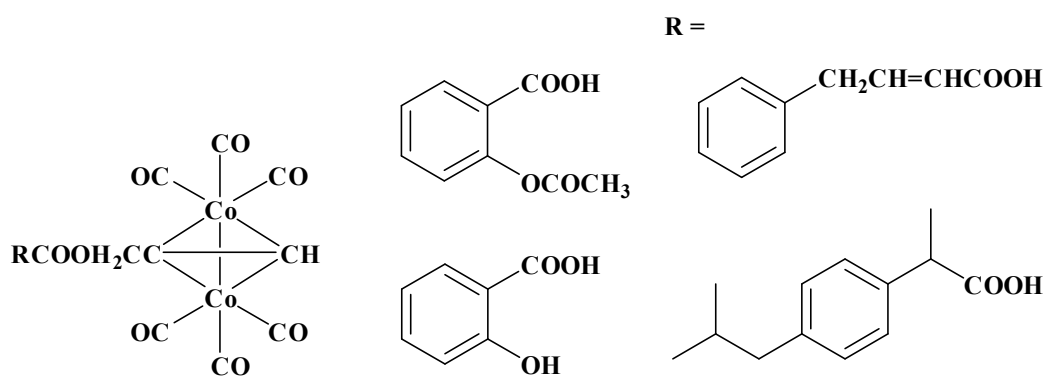


Figure 1.3.4: Hexacarbonylcobalt complex esters by Gong *et al.*

1.4 Metal ketoiminate complexes

β -Ketoiminate (acnac) ligands are analogues of β -diketonate (acac) ligands in which one keto group is replaced by an imine group (**Figure 1.4.1**). β -ketoiminate ligands have been widely investigated and applied as chelating systems in main group and transition metal chemistry. This is mainly due to their ease of preparation and modification of both steric and/or electronic properties.²²¹ Transition metal complexes such as copper, cobalt, nickel, palladium, ruthenium, titanium, platinum, iridium, zinc and zirconium, stabilised by various forms of β -ketoiminate ligands have been synthesised and reported with the main applications being in catalysis.²²²⁻

234

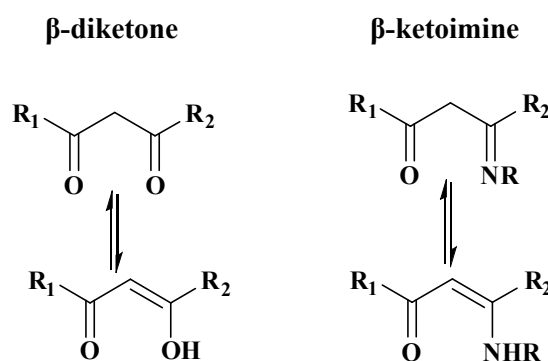


Figure 1.4.1: Diketonate and Ketoiminate ligands

The McGowan research group has extensively researched β -ketoiminate complexes of ruthenium, iridium and titanium.²³⁵ A series of ruthenium-arene and iridium-Cp* complexes with acnac ligands (**Figure 1.4.2**) have been investigated for their anti-cancer activity. The complexes have shown high activity against MCF-7, HT-29, A2780, and A2780cis cell lines, with some complexes being significantly more

active than cisplatin against the A2780cis cell line. In addition, the complexes were hypoxia-sensitive, showing enhanced activity under hypoxic conditions. The proposed mechanism of action is thought to include inhibition of the enzyme thioredoxin reductase and apoptosis.^{235, 236}

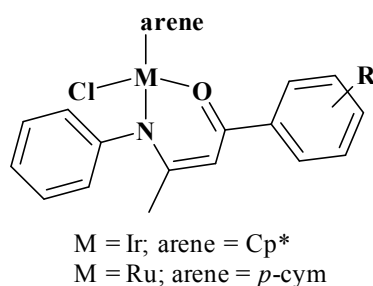


Figure 1.4.2: Ru-arene and Ir-Cp* acnac complexes studied within the McGowan research group

1.5 Research project objectives

The objective of this research project was to synthesise, characterise and explore the biological and catalytic activities of a range of ruthenium and copper complexes with β -ketoiminate (acnac) ligands (**Figure 1.5.1**). Electronic and steric properties of the complexes will be varied through functionalisation of the acnac ligands with various substituents in order to gain structural activity relationships (SARs) and their effect on potential biological and chemical applications. Results from previous studies of metal complexes with β -ketoiminate ligands and those of their precursors, namely β -diketonate (acac) ligands, have shown that complexes with acnac ligands have higher anti-cancer activity compared to their acac ligand analogues.²³⁷ In line with these findings only the anti-cancer activity of acnac metal complexes will be evaluated.

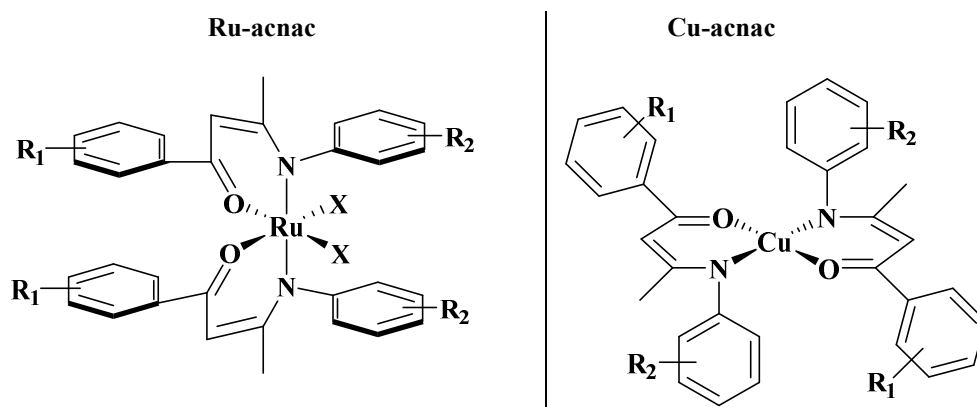


Figure 1.5.1: Target complexes within this thesis

The metal ketoiminate complexes synthesised (**Figure 1.5.1**) will contain several fragments which have been shown to be important for anti-cancer activity. The planar aryl rings of the ketoiminate ligand provide a potential site for π - π stacking interactions with nucleobases within the DNA chain. Varying the substituents (R_1 and R_2) on the ketoiminate aryl rings can alter the solubility and hydrophobicity of the complex, influencing cellular uptake and in turn the corresponding anti-cancer activity of the complexes. In the case of ruthenium(acnac)₂ complexes, the presence of a labile group X [**Figure 1.5.1 (a)**] (halide or pseudohalide ligand) allows the possibility of activation through hydrolysis and ligand exchange forming more reactive species which may then interact with target biomolecules.

In addition to investigations on potential therapeutic applications, the catalytic activities of the metal complexes will be evaluated. The proposed catalytic reactions are transfer hydrogenation and Ullmann reactions for ruthenium- and copper ketoiminate complexes respectively.

1.6 References

1. World Health Organisation, *Cancer*, <http://www.who.int/mediacentre/factsheets/fs297/en/>, Accessed 19.02.2018.
2. Cancer Research UK, *Cancer Statistics for the UK*, <http://www.cancerresearchuk.org/health-professional/cancer-statistics-for-the-uk#heading-Zero>, Accessed 19.02.2018.
3. Cancer Research UK, *Statistics for UK*, <http://www.cancerresearchuk.org/health-professional/cancer-statistics-for-the-uk#heading-One>, Accessed 19.02.2018.
4. A. Aggarwal and R. Sullivan, *Journal of Cancer Policy*, 2014, **2**, 31-39.
5. J. Gabriel, *Biology of Cancer*, John & Wiley Sons. Ltd, Chichester, 2007.
6. L. Pecorino, *Molecular Biology of Cancer: Mechanisms, Targets, and Therapeutics*, Oxford university press, 2012.
7. V. J. N. Bykov and K. G. Wiman, *Annals of Medicine*, 2003, **35**, 458-465.
8. B. D. Voet and J. G. Voet, 2 edn., John Wiley & Sons Inc., 1995.
9. D. Hanahan and R. A. Weinberg, *Cell*, 2000, **100**, 57-70.
10. D. Hanahan and R. A. Weinberg, *Cell*, 2011, **144**, 646-674.
11. A. Urruticoechea, R. Alemany, J. Balart, A. Villanueva, F. Vinals and G. Capella, *Current Pharmaceutical Design*, 2010, **16**, 3-10.
12. C. E. DeSantis, C. C. Lin, A. B. Mariotto, R. L. Siegel, K. D. Stein, J. L. Kramer, R. Alteri, A. S. Robbins and A. Jemal, *CA: A Cancer Journal for Clinicians*, 2014, **64**, 252-271.
13. K. D. Mjos and C. Orvig, *Chemical Reviews*, 2014, **114**, 4540-4563.
14. C. Orvig and M. J. Abrams, *Chemical Reviews*, 1999, **99**, 2201-2204.
15. P. J. Sadler, in *Advances in Inorganic Chemistry*, Elsevier, Editon edn., 1991, vol. 36, pp. 1-48.

16. S. P. Fricker, *Dalton Transactions*, 2007, 4903-4917.
17. R. H. Holm, P. Kennepohl and E. I. Solomon, *Chemical Reviews*, 1996, **96**, 2239-2314.
18. G. Gasser and N. Metzler-Nolte, *Current Opinion in Chemical Biology*, 2012, **16**, 84-91.
19. O. R. Allen, R. J. Knox and P. C. McGowan, *Dalton Transactions*, 2008, 1293-1295.
20. A. Cuin, A. C. Massabni, G. A. Pereira, C. Q. Fujimura Leite, F. R. Pavan, R. Sesti-Costa, T. A. Heinrich and C. M. Costa-Neto, *Biomedicine & Pharmacotherapy*, 2011, **65**, 334-338.
21. B. Desoize, *Anticancer Research*, 2004, **24**, 1529-1544.
22. Z. Liu, A. Habtemariam, A. M. Pizarro, S. A. Fletcher, A. Kisova, O. Vrana, L. Salassa, P. C. A. Bruijninx, G. J. Clarkson, V. Brabec and P. J. Sadler, *Journal of Medicinal Chemistry*, 2011, **54**, 3011-3026.
23. I. Ott and R. Gust, *Archiv Der Pharmazie*, 2007, **340**, 117-126.
24. C. Santini, M. Pellei, V. Gandin, M. Porchia, F. Tisato and M. Marzano, *Chemical Reviews*, 2014, **114**, 815-862.
25. S. H. van Rijt, A. F. A. Peacock, R. D. L. Johnstone, S. Parsons and P. J. Sadler, *Inorganic Chemistry*, 2009, **48**, 1753-1762.
26. A. R. Kapdi and I. J. S. Fairlamb, *Chemical Society Reviews*, 2014, **43**, 4751-4777.
27. M. Nath, M. Vats and P. Roy, *European Journal of Medicinal Chemistry*, 2013, **59**, 310-321.
28. B. Rosenberg, L. Vancamp, J. E. Trosko and V. H. Mansour, *Nature*, 1969, **222**, 385.
29. M. Gielen and E. R. Tiekink, *Metallotherapeutic Drugs and Metal-based Diagnostic Agents: The Use of Metals in Medicine*, John Wiley & Sons, 2005.

30. S. Dasari and P. B. Tchounwou, *European Journal of Pharmacology*, 2014, **740**, 364-378.
31. B. Rosenberg, L. Van Camp and T. Krigas, *Nature*, 1965, **205**, 698-699.
32. C. Moucheron, *New Journal of Chemistry*, 2009, **33**, 235-245.
33. L. Kelland, *Nature Reviews Cancer*, 2007, **7**, 573.
34. J. C. Dabrowiak, *Metals in Medicine*, John Wiley & Sons, 2017.
35. M. S. Davies, S. J. Berners-Price and T. W. Hambley, *Journal of Inorganic Biochemistry*, 2000, **79**, 167-172.
36. D. Gately and S. Howell, *British Journal of Cancer*, 1993, **67**, 1171.
37. M. D. Hall, M. Okabe, D.-W. Shen, X.-J. Liang and M. M. Gottesman, *Annu. Rev. Pharmacol. Toxicol.*, 2008, **48**, 495-535.
38. J. Zisowsky, S. Koegel, S. Leyers, K. Devarakonda, M. U. Kassack, M. Osmak and U. Jaehde, *Biochemical Pharmacology*, 2007, **73**, 298-307.
39. A. M. J. Fichtinger-Schepman, J. L. Van der Veer, J. H. Den Hartog, P. H. Lohman and J. Reedijk, *Biochemistry*, 1985, **24**, 707-713.
40. Z. H. Siddik, *Oncogene*, 2003, **22**, 7265.
41. J. Reedijk, *Chemical Reviews*, 1999, **99**, 2499-2510.
42. J. A. Mello, S. J. Lippard and J. M. Essigmann, *Biochemistry*, 1995, **34**, 14783-14791.
43. M. H. Shamsi and H.-B. Kraatz, *Journal of Inorganic and Organometallic Polymers and Materials*, 2013, **23**, 4-23.
44. S. Medici, M. Peana, V. M. Nurchi, J. I. Lachowicz, G. Crisponi and M. A. Zoroddu, *Coordination Chemistry Reviews*, 2015, **284**, 329-350.
45. R. C. Dolman, G. B. Deacon and T. W. Hambley, *Journal of Inorganic Biochemistry*, 2002, **88**, 260-267.

46. F. De Jongh, R. Van Veen, S. Veltman, R. De Wit, M. Van der Burg and M. Van den Bent, *British Journal of Cancer*, 2003, **88**, 1196-1206.
47. A. A. Al-Majed, *Basic & Clinical Pharmacology & Toxicology*, 2007, **100**, 145-150.
48. J. T. Hartmann and H.-P. Lipp, *Expert Opinion on Pharmacotherapy*, 2003, **4**, 889-901.
49. J. T. Hartmann, L. M. Fels, S. Knop, H. Stolte, L. Kanz and C. Bokemeyer, *Investigational New Drugs*, 2000, **18**, 281-289.
50. B. Stordal and M. Davey, *IUBMB Life*, 2007, **59**, 696-699.
51. D. S. Goodsell, *The Oncologist*, 2006, **11**, 316-317.
52. F. Lévi, J. L. Misset, S. Brienza, R. Adam, G. Metzger, M. Itzakhi, J. P. Caussanel, F. Kunstlinger, S. Lecouturier and A. Descorps-Declère, *Cancer*, 1992, **69**, 893-900.
53. A. A. Argyriou, P. Polychronopoulos, G. Iconomou, E. Chroni and H. P. Kalofonos, *Cancer Treatment Reviews*, 2008, **34**, 368-377.
54. R. J. Cersosimo, *Annals of Pharmacotherapy*, 2005, **39**, 128-135.
55. B. Bhuyan, B. Loughman, T. Fraser and K. Day, *Experimental Cell Research*, 1976, **97**, 275-280.
56. T. M. Simon, D. H. Kunishima, G. J. Vibert and A. Lorber, *Cancer*, 1979, **44**, 1965-1975.
57. C. K. Mirabelli, R. K. Johnson, C. M. Sung, L. Faucette, K. Muirhead and S. T. Crooke, *Cancer Research*, 1985, **45**, 32-39.
58. F. Caruso and M. Rossi, *Mini Reviews in Medicinal Chemistry*, 2004, **4**, 49-60.
59. M. M. Harding and G. Mokdsi, *Current Medicinal Chemistry*, 2000, **7**, 1289-1303.

60. N. Muhammad and Z. Guo, *Current Opinion in Chemical Biology*, 2014, **19**, 144-153.
61. E. S. Antonarakis and A. Emadi, *Cancer Chemotherapy and Pharmacology*, 2010, **66**, 1-9.
62. C. G. Hartinger, S. Zorbas-Seifried, M. A. Jakupec, B. Kynast, H. Zorbas and B. K. Keppler, *Journal of Inorganic Biochemistry*, 2006, **100**, 891-904.
63. M. Abid, F. Shamsi and A. Azam, *Mini Reviews in Medicinal Chemistry*, 2016, **16**, 772-786.
64. A. Bergamo, C. Gaiddon, J. Schellens, J. Beijnen and G. Sava, *Journal of Inorganic Biochemistry*, 2012, **106**, 90-99.
65. P. Schluga, C. G. Hartinger, A. Egger, E. Reisner, M. Galanski, M. A. Jakupec and B. K. Keppler, *Dalton Transactions*, 2006, 1796-1802.
66. S. Rockwell, I. T. Dobrucki, E. Y. Kim, S. T. Marrison and V. T. Vu, *Current Molecular Medicine*, 2009, **9**, 442-458.
67. F. Kratz and L. Messori, *Journal of Inorganic Biochemistry*, 1993, **49**, 79-82.
68. G. Sava, S. Zorzet, T. Giraldi, G. Mestroni and G. Zassinovich, *European Journal of Cancer*, 1984, **20**, 841-847.
69. M. A. Jakupec, M. Galanski, V. B. Arion, C. G. Hartinger and B. K. Keppler, *Dalton Transactions*, 2008, 183-194.
70. L. J. Anghileri, *Zeitschrift für Krebsforschung und Klinische Onkologie*, 1975, **83**, 213-217.
71. R. Rudolph, *Archiv für Experimentelle Veterinärmedizin*, 1971, **25**, 925.
72. M. G. Somermeyer, T. C. Knauss, J. M. Weinberg and H. D. Humes, *Biochemical Journal*, 1983, **214**, 37.
73. I. Bratsos, S. Jedner, T. Gianferrara and E. Alessio, *CHIMIA International Journal for Chemistry*, 2007, **61**, 692-697.

74. M. J. Clarke, F. Zhu and D. R. Frasca, *Chemical Reviews*, 1999, **99**, 2511-2534.
75. M. J. Clarke, *Coordination Chemistry Reviews*, 2002, **232**, 69-93.
76. G. Sava, I. Capozzi, K. Clerici, G. Gagliardi, E. Alessio and G. Mestroni, *Clinical & Experimental Metastasis*, 1998, **16**, 371-379.
77. E. Alessio, *European Journal of Inorganic Chemistry*, 2017, **2017**, 1549-1560.
78. A. Levina, A. Mitra and P. A. Lay, *Metallomics*, 2009, **1**, 458-470.
79. M. I. Webb and C. J. Walsby, *Metallomics*, 2013, **5**, 1624-1633.
80. F. Frausin, V. Scarcia, M. Cocchietto, A. Furlani, B. Serli, E. Alessio and G. Sava, *Journal of Pharmacology and Experimental Therapeutics*, 2005, **313**, 227-233.
81. D. Pluim, R. C. van Waardenburg, J. H. Beijnen and J. H. Schellens, *Cancer Chemotherapy and Pharmacology*, 2004, **54**, 71-78.
82. A. A. Hostetter, M. L. Miranda, V. J. DeRose and K. L. M. Holman, *JBIC Journal of Biological Inorganic Chemistry*, 2011, **16**, 1177-1185.
83. L. Masiero, M. Onisto, G. M. Enzo Alessio and S. Garbisa, *International Journal of Cancer*, 1996, **68**, 60-66.
84. L. Morbidelli, S. Donnini, S. Filippi, L. Messori, F. Piccioli, P. Orioli, G. Sava and M. Ziche, *British Journal of Cancer*, 2003, **88**, 1484.
85. G. Sava, S. Zorzet, C. Turrin, F. Vita, M. Soranzo, G. Zabucchi, M. Cocchietto, A. Bergamo, S. DiGiovine and G. Pezzoni, *Clinical Cancer Research*, 2003, **9**, 1898-1905.
86. J. M. Rademaker-Lakhai, D. van den Bongard, D. Pluim, J. H. Beijnen and J. H. Schellens, *Clinical Cancer Research*, 2004, **10**, 3717-3727.

87. S. Leijen, S. A. Burgers, P. Baas, D. Pluim, M. Tibben, E. van Werkhoven, E. Alessio, G. Sava, J. H. Beijnen and J. H. Schellens, *Investigational New Drugs*, 2015, **33**, 201-214.
88. B. Keppler and W. Rupp, *Journal of Cancer Research and Clinical Oncology*, 1986, **111**, 166-168.
89. F. Garzon, M. Berger, B. Keppler and D. Schmähl, *Cancer Chemotherapy and Pharmacology*, 1987, **19**, 347-349.
90. A. Galeano, M. Berger and B. Keppler, *Arzneimittel-Forschung*, 1992, **42**, 821-824.
91. B. Keppler, M. Henn, U. Juhl, M. Berger, R. Niebl and F. Wagner, in *Ruthenium and Other Non-Platinum Metal Complexes in Cancer Chemotherapy*, Springer, Editon edn., 1989, pp. 41-69.
92. W. Peti, T. Pieper, M. Sommer, B. K. Keppler and G. Giester, *European Journal of Inorganic Chemistry*, 1999, **1999**, 1551-1555.
93. R. Trondl, P. Heffeter, C. R. Kowol, M. A. Jakupec, W. Berger and B. K. Keppler, *Chemical Science*, 2014, **5**, 2925-2932.
94. E. Reisner, V. B. Arion, B. K. Keppler and A. J. Pombeiro, *Inorganica Chimica Acta*, 2008, **361**, 1569-1583.
95. F. Kratz, B. Keppler, M. Hartmann, L. Messori and M. Berger, *Metal-Based Drugs*, 1996, **3**, 15-23.
96. M. Sulyok, S. Hann, C. Hartinger, B. Keppler, G. Stingeder and G. Koellensperger, *Journal of Analytical Atomic Spectrometry*, 2005, **20**, 856-863.
97. H. Maeda, J. Wu, T. Sawa, Y. Matsumura and K. Hori, *Journal of Controlled Release*, 2000, **65**, 271-284.
98. A. Kelman, M. Clarke, S. Edmonds and H. Peresie, *Journal of Clinical Hematology and Oncology*, 1977, **7**, 2.

99. C. Acilan, B. Cevatemre, Z. Adiguzel, D. Karakas, E. Ulukaya, N. Ribeiro, I. Correia and J. C. Pessoa, *Biochimica et Biophysica Acta (BBA)-General Subjects*, 2017, **1861**, 218-234.
100. C. Santini, M. Pellei, V. Gandin, M. Porchia, F. Tisato and C. Marzano, *Chemical Reviews*, 2013, **114**, 815-862.
101. L. Ruiz-Azuara and M. E Bravo-Gomez, *Current Medicinal Chemistry*, 2010, **17**, 3606-3615.
102. P. C. Bull, G. R. Thomas, J. M. Rommens, J. R. Forbes and D. W. Cox, *Nature Genetics*, 1993, **5**, 327.
103. G. J. Brewer and V. Yuzbasiyan-Gurkan, *Medicine*, 1992, **71**, 139-164.
104. V. Goodman, G. Brewer and S. Merajver, *Endocrine-related Cancer*, 2004, **11**, 255-263.
105. I. Esteban Leon, J. Fernando Cadavid-Vargas, A. Laura Di Virgilio and S. Beatriz Etcheverry, *Current Medicinal Chemistry*, 2017, **24**, 112-148.
106. K. Benjamin Garbutcheon-Singh, M. P Grant, B. W Harper, A. M Krause-Heuer, M. Manohar, N. Orkey and J. R Aldrich-Wright, *Current Topics in Medicinal Chemistry*, 2011, **11**, 521-542.
107. A. Gupte and R. J. Mumper, *Cancer Treatment Reviews*, 2009, **35**, 32-46.
108. B. McAuslan and W. Reilly, *Experimental Cell Research*, 1980, **130**, 147-157.
109. D. Chen, V. Milacic, M. Frezza and Q. P. Dou, *Current Pharmaceutical Design*, 2009, **15**, 777-791.
110. A. K. Boal and A. C. Rosenzweig, *Chemical Reviews*, 2009, **109**, 4760-4779.
111. R. A. Festa and D. J. Thiele, *Current Biology*, 2011, **21**, R877-R883.
112. T. Wang and Z. Guo, *Current Medicinal Chemistry*, 2006, **13**, 525-537.
113. B. Lönnerdal, *The American Journal of Clinical Nutrition*, 1996, **63**, 821S-829S.

114. M. Valko, H. Morris and M. Cronin, *Current Medicinal Chemistry*, 2005, **12**, 1161-1208.
115. H. Tapiero, D. Townsend and K. Tew, *Biomedicine & Pharmacotherapy*, 2003, **57**, 386-398.
116. N. E. Hellman and J. D. Gitlin, *Annual Review of Nutrition*, 2002, **22**, 439-458.
117. M. C. Linder, L. Wooten, P. Cerveza, S. Cotton, R. Shulze and N. Lomeli, *The American Journal of Clinical Nutrition*, 1998, **67**, 965S-971S.
118. M. Arredondo and M. T. Núñez, *Molecular Aspects of Medicine*, 2005, **26**, 313-327.
119. G. J. Brewer, *Drug discovery Today*, 2005, **10**, 1103-1109.
120. F. Tisato, C. Marzano, M. Porchia, M. Pellei and C. Santini, *Medicinal Research Reviews*, 2010, **30**, 708-749.
121. C. Pettinari, C. Santini, J. McCleverty and T. Meyer, *Comprehensive Coordination Chemistry II*, Elsevier: New York, 2004.
122. M. Melník and M. Kabešová, *Journal of Coordination Chemistry*, 2000, **50**, 323-338.
123. N. Kitajima and Y. Moro-oka, *Chemical Reviews*, 1994, **94**, 737-757.
124. D. X. West, A. E. Liberta, S. B. Padhye, R. C. Chikate, P. B. Sonawane, A. S. Kumbhar and R. G. Yerande, *Coordination Chemistry Reviews*, 1993, **123**, 49-71.
125. H. Beraldo and D. Gambino, *Mini Reviews in Medicinal Chemistry*, 2004, **4**, 31-39.
126. J. A. Crim and H. G. Petering, *Cancer Research*, 1967, **27**, 1278-1285.
127. M. R. Taylor, E. J. Gabe, J. P. Glusker, J. A. Minkin and A. Patterson, *Journal of the American Chemical Society*, 1966, **88**, 1845-1846.
128. H. Zhang, R. Thomas, D. Oupicky and F. Peng, *JBIC Journal of Biological Inorganic Chemistry*, 2008, **13**, 47-55.

129. D. S. Kalinowski, P. Quach and D. R. Richardson, *Future Medicinal Chemistry*, 2009, **1**, 1143-1151.
130. Y. Yu, D. S. Kalinowski, Z. Kovacevic, A. R. Siafakas, P. J. Jansson, C. Stefani, D. B. Lovejoy, P. C. Sharpe, P. V. Bernhardt and D. R. Richardson, *Journal of Medicinal Chemistry*, 2009, **52**, 5271-5294.
131. B. A. Booth, K. C. Agrawal, E. C. Moore and A. C. Sartorelli, *Cancer Research*, 1974, **34**, 1308-1314.
132. R. W. Brockman, J. R. Thomson, M. J. Bell and H. E. Skipper, *Cancer Research*, 1956, **16**, 167-170.
133. C. Marzano, M. Pellei, F. Tisato and C. Santini, *Anti-Cancer Agents in Medicinal Chemistry (Formerly Current Medicinal Chemistry-Anti-Cancer Agents)*, 2009, **9**, 185-211.
134. J. Easmon, G. Heinisch, W. Holzer and B. Rosenwirth, *Arzneimittel-Forschung*, 1989, **39**, 1196-1201.
135. A. Sîrbu, O. Palamarciuc, M. V. Babak, J. M. Lim, K. Ohui, E. A. Enyedy, S. Shova, D. Darvasiová, P. Rapta and W. H. Ang, *Dalton Transactions*, 2017, **46**, 3833-3847.
136. L. A. Saryan, E. Ankel, C. Krishnamurti, D. H. Petering and H. Elford, *Journal of Medicinal Chemistry*, 1979, **22**, 1218-1221.
137. J. García-Tojal, A. García-Orad, J. L. Serra, J. L. Pizarro, L. Lezama, M. I. Arriortua and T. Rojo, *Journal of Inorganic Biochemistry*, 1999, **75**, 45-54.
138. J. García-Tojal, J. L. Pizarro, A. García-Orad, A. R. o. Pérez-Sanz, M. a. Ugalde, A. A. Díaz, J. L. Serra, M. a. I. Arriortua and T. Rojo, *Journal of Inorganic Biochemistry*, 2001, **86**, 627-633.
139. J. Easmon, G. Pürstinger, G. Heinisch, T. Roth, H. H. Fiebig, W. Holzer, W. Jäger, M. Jenny and J. Hofmann, *Journal of Medicinal Chemistry*, 2001, **44**, 2164-2171.
140. J. Yuan, D. B. Lovejoy and D. R. Richardson, *Blood*, 2004, **104**, 1450-1458.

141. G. Pelosi, *The Open Crystallography Journal*, 2010, **3**.
142. A. Popović-Bijelić, C. R. Kowol, M. E. Lind, J. Luo, F. Himo, É. A. Enyedy, V. B. Arion and A. Gräslund, *Journal of Inorganic Biochemistry*, 2011, **105**, 1422-1431.
143. P. V. Bernhardt, P. C. Sharpe, M. Islam, D. B. Lovejoy, D. S. Kalinowski and D. R. Richardson, *Journal of Medicinal Chemistry*, 2008, **52**, 407-415.
144. R. A. Finch, M.-C. Liu, A. H. Cory, J. G. Cory and A. C. Sartorelli, *Advances in Enzyme Regulation*, 1999, **39**, 3-12.
145. K. Ishiguro, Z. P. Lin, P. G. Penketh, K. Shyam, R. Zhu, R. P. Baumann, Y.-L. Zhu, A. C. Sartorelli, T. J. Rutherford and E. S. Ratner, *Biochemical Pharmacology*, 2014, **91**, 312-322.
146. P. J. Jansson, P. C. Sharpe, P. V. Bernhardt and D. R. Richardson, *Journal of Medicinal Chemistry*, 2010, **53**, 5759-5769.
147. C. Stineman, J. Vance, D. West and I. Hall, *Anticancer Research*, 1998, **18**, 4131-4139.
148. M. Miller, C. Stineman, J. Vance, D. West and I. Hall, *Applied Organometallic Chemistry*, 1999, **13**, 9-19.
149. R. Alemón-Medina, M. Breña-Valle, J. L. Muñoz-Sánchez, M. I. Gracia-Mora and L. Ruiz-Azuara, *Cancer Chemotherapy and Pharmacology*, 2007, **60**, 219-228.
150. L. Hernández-Esquivel, A. Marín-Hernández, N. Pavón, K. Carvajal and R. Moreno-Sánchez, *Toxicology and Applied Pharmacology*, 2006, **212**, 79-88.
151. A. Rivero-Müller, A. De Vizcaya-Ruiz, N. Plant, L. Ruiz and M. Dobrota, *Chemico-biological Interactions*, 2007, **165**, 189-199.
152. C. Trejo-Solís, G. Palencia, S. Zúniga, A. Rodríguez-Ropon, L. Osorio-Rico, S. T. Luvia, I. Gracia-Mora, L. Marquez-Rosado, A. Sánchez and M. E. Moreno-García, *Neoplasia*, 2005, **7**, 563-574.

153. M. E. Bravo-Gómez, J. C. García-Ramos, I. Gracia-Mora and L. Ruiz-Azuara, *Journal of Inorganic Biochemistry*, 2009, **103**, 299-309.
154. I. Gracia-Mora, L. Ruiz-Ramírez, C. Gómez-Ruiz, M. Tinoco-Méndez, A. Márquez-Quiñones, L. R.-D. Lira, Á. Marín-Hernández, L. Macías-Rosales and M. Bravo-Gómez, *Metal-based Drugs*, 2001, **8**, 19-28.
155. F. Carvallo-Chaigneau, C. Trejo-Solís, C. Gómez-Ruiz, E. Rodríguez-Aguilera, L. Macías-Rosales, E. Cortés-Barberena, C. Cedillo-Peláez, I. Gracia-Mora, L. Ruiz-Azuara and V. Madrid-Marina, *Biometals*, 2008, **21**, 17-28.
156. A. I. Valencia-Cruz, L. I. Uribe-Figueroa, R. Galindo-Murillo, K. Baca-López, A. G. Gutiérrez, A. Vázquez-Aguirre, L. Ruiz-Azuara, E. Hernández-Lemus and C. Mejía, *PLoS One*, 2013, **8**, e54664.
157. J. Espinal-Enríquez, E. Hernández-Lemus, C. Mejía and L. Ruiz-Azuara, *Frontiers in Physiology*, 2016, **6**, 406.
158. L. Álvarez-Barrera, J. J. Rodríguez-Mercado, M. López-Chaparro and M. A. Altamirano-Lozano, *Drug and Chemical Toxicology*, 2017, **40**, 333-338.
159. C. Bolos, A. Chaviara, D. Mourelatos, Z. Iakovidou, E. Mioglou, E. Chrysogelou and A. Papageorgiou, *Bioorganic & Medicinal Chemistry*, 2009, **17**, 3142-3151.
160. C. N. Hancock, L. H. Stockwin, B. Han, R. D. Divelbiss, J. H. Jun, S. V. Malhotra, M. G. Hollingshead and D. L. Newton, *Free Radical Biology and Medicine*, 2011, **50**, 110-121.
161. S. E.-d. H. Etaiw, A. S. Sultan and M. M. El-Bendary, *Journal of Organometallic Chemistry*, 2011, **696**, 1668-1676.
162. N. Raman, R. Jeyamurugan, B. Raj Kapoor and V. Magesh, *Applied Organometallic Chemistry*, 2009, **23**, 283-290.
163. K. Ghosh, P. Kumar, N. Tyagi, U. P. Singh, N. Goel, A. Chakraborty, P. Roy and M. C. Baratto, *Polyhedron*, 2011, **30**, 2667-2677.

164. A. Chakraborty, P. Kumar, K. Ghosh and P. Roy, *European Journal of Pharmacology*, 2010, **647**, 1-12.
165. N. Raman, R. Jeyamurugan, R. Senthilkumar, B. Raj Kapoor and S. G. Franzblau, *European Journal of Medicinal Chemistry*, 2010, **45**, 5438-5451.
166. M. Sathisha, S. Budagumpi, N. V. Kulkarni, G. S. Kurdekar, V. Revankar and K. Pai, *European Journal of Medicinal Chemistry*, 2010, **45**, 106-113.
167. C. C. Romão and H. L. Vieira, *Bioorganometallic Chemistry: Applications in Drug Discovery Biocatalysis, and Imaging*, 2014, 165-202.
168. U. Schatzschneider, *British Journal of Pharmacology*, 2015, **172**, 1638-1650.
169. B. E. Mann, *Organometallics*, 2012, **31**, 5728-5735.
170. E. Kottelat and Z. Fabio, *Inorganics*, 2017, **5**, 24.
171. B. Widdop, *Annals of Clinical Biochemistry*, 2002, **39**, 378-391.
172. C. C. Romao, W. A. Blattler, J. D. Seixas and G. J. L. Bernardes, *Chemical Society Reviews*, 2012, **41**, 3571-3583.
173. R. Motterlini and L. E. Otterbein, 2010, **9**, 728.
174. P. Paredi, W. Biernacki, G. Invernizzi, S. A. Kharitonov and P. J. Barnes, *Chest*, 1999, **116**, 1007-1011.
175. A. Halilovic, K. A. Patil, L. Bellner, G. Marrazzo, K. Castellano, G. Cullaro, M. W. Dunn and M. L. Schwartzman, *Journal of Cellular Physiology*, 2011, **226**, 1732-1740.
176. R. Motterlini, A. Gonzales, R. Foresti, J. E. Clark, C. J. Green and R. M. Winslow, *Circulation Research*, 1998, **83**, 568-577.
177. L. E. Otterbein, *Antioxidants & Redox Signaling*, 2002, **4**, 309-319.
178. J. D. Antuni, S. A. Kharitonov, D. Hughes, M. E. Hodson and P. J. Barnes, *Thorax*, 2000, **55**, 138-142.

179. P. Paredi, S. A. Kharitonov, D. Leak, P. L. Shah, D. Cramer, M. E. Hodson and P. J. Barnes, *American Journal of Respiratory and Critical Care Medicine*, 2000, **161**, 1247-1251.
180. I. Horvath, S. Loukides, T. Wodehouse, S. A. Kharitonov, P. J. Cole and P. J. Barnes, *Thorax*, 1998, **53**, 867-870.
181. Monma, Yamaya, Sekizawa, Ikeda, Suzuki, Kikuchi, Takasaka and Sasaki, *Clinical & Experimental Allergy*, 1999, **29**, 1537-1541.
182. K. Zayasu, K. Sekizawa, S. Okinaga, M. Yamaya, T. Ohruai and H. Sasaki, *American Journal of Respiratory and Critical Care Medicine*, 1997, **156**, 1140-1143.
183. I. Horváth, L. E. Donnelly, A. Kiss, P. Paredi, S. A. Kharitonov and P. J. Barnes, *Thorax*, 1998, **53**, 668-672.
184. J. S. Neto, A. Nakao, K. Kimizuka, A. J. Romanosky, D. B. Stolz, T. Uchiyama, M. A. Nalesnik, L. E. Otterbein and N. Murase, *American Journal of Physiology - Renal Physiology*, 2004, **287**, F979-F989.
185. L. E. Otterbein, F. H. Bach, J. Alam, M. Soares, H. Tao Lu, M. Wysk, R. J. Davis, R. A. Flavell and A. M. K. Choi, *Natural Medicine*, 2000, **6**, 422-428.
186. M.-L. Wu, Y.-C. Ho and S.-F. Yet, *Antioxidants & Redox Signaling*, 2010, **15**, 1835-1846.
187. L. E. Otterbein, B. S. Zuckerbraun, M. Haga, F. Liu, R. Song, A. Usheva, C. Stachulak, N. Bodyak, R. N. Smith, E. Csizmadia, S. Tyagi, Y. Akamatsu, R. J. Flavell, T. R. Billiar, E. Tzeng, F. H. Bach, A. M. K. Choi and M. P. Soares, *Natural Medicine*, 2003, **9**, 183-190.
188. M. Katori, R. W. Busuttil and J. W. Kupiec-Weglinski, *Transplantation*, 2002, **74**, 905-912.
189. B. J. Aucott, J. S. Ward, S. G. Andrew, J. Milani, A. C. Whitwood, J. M. Lynam, A. Parkin and I. J. Fairlamb, *Inorganic Chemistry*, 2017, **56**, 5431-5440.

190. M. A. Gonzales and P. K. Mascharak, *Journal of Inorganic Biochemistry*, 2014, **133**, 127-135.
191. M. A. Wright and J. A. Wright, *Dalton Transactions*, 2016, **45**, 6801-6811.
192. R. Motterlini, J. E. Clark, R. Foresti, P. Sarathchandra, B. E. Mann and C. J. Green, *Characterization of Biochemical and Vascular Activities*, 2002, **90**, e17-e24.
193. L. Hewison, S. H. Crook, B. E. Mann, A. J. H. M. Meijer, H. Adams, P. Sawle and R. A. Motterlini, *Organometallics*, 2012, **31**, 5823-5834.
194. S. Romanski, B. Kraus, M. Guttentag, W. Schlundt, H. Rucker, A. Adler, J.-M. Neudorfl, R. Alberto, S. Amslinger and H.-G. Schmalz, *Dalton Transactions*, 2012, **41**, 13862-13875.
195. S. Romanski, B. Kraus, U. Schatzschneider, J.-M. Neudörfl, S. Amslinger and H.-G. Schmalz, *Angewandte Chemie International Edition*, 2011, **50**, 2392-2396.
196. I. Ott, B. Kircher, R. Dembinski and R. Gust, *Expert Opinion on Therapeutic Patents*, 2008, **18**, 327-337.
197. V. D. Reddy, D. Dayal, S. C. Cosenza, M. V. R. Reddy, W. C. Pearl, Jr. and R. D. Adams, *Journal of Organometallic Chemistry*, 2009, **694**, 959-967.
198. D. Schlawe, A. Majdalani, J. Velcicky, E. Hessler, T. Wieder, A. Prokop and H. G. Schmalz, *Angewandte Chemie-International Edition*, 2004, **43**, 1731-1734.
199. G. B. Jones and J. E. Mathews, *Bioorganic & Medicinal Chemistry Letters*, 1995, **5**, 93-96.
200. M. Patra, G. Gasser, A. Pinto, K. Merz, I. Ott, J. E. Bandow and N. Metzler-Nolte, *Chemmedchem*, 2009, **4**, 1930-1938.
201. B. E. Mann, in *Medicinal Organometallic Chemistry*, eds. G. Jaouen and N. Metzler-Nolte, Springer Berlin Heidelberg, Berlin, Heidelberg, Editon edn., 2010, pp. 247-285.
202. J. E. Clark, P. Naughton, S. Shurey, C. J. Green, T. R. Johnson, B. E. Mann, R. Foresti and R. Motterlini, *Circulation Research*, 2003, **93**, E2-E8.

203. A. Sandouka, B. J. Fuller, B. E. Mann, C. J. Green, R. Foresti and R. Motterlini, *Kidney International*, 2006, **69**, 239-247.
204. P. Sawle, R. Foresti, B. E. Mann, T. R. Johnson, C. J. Green and R. Motterlini, *British Journal of Pharmacology*, 2005, **145**, 800-810.
205. M. G. Bani-Hani, D. Greenstein, B. E. Mann, C. J. Green and R. Motterlini, *Journal of Pharmacology and Experimental Therapeutics*, 2006, **318**, 1315-1322.
206. A. B. Stein, Y. R. Guo, W. Tan, W. J. Wu, X. P. Zhu, Q. H. Li, C. Luo, B. Dawn, T. R. Johnson, R. Motterlini and R. Bolli, *Journal of Molecular and Cellular Cardiology*, 2005, **38**, 127-134.
207. W.-Q. Zhang, A. J. Atkin, R. J. Thatcher, A. C. Whitwood, I. J. S. Fairlamb and J. M. Lynam, *Dalton Transactions*, 2009, 4351-4358.
208. R. Motterlini and L. E. Otterbein, *Nature Reviews Drug Discovery*, 2010, **9**, 728.
209. C. C. Romão, W. A. Blättler, J. D. Seixas and G. J. Bernardes, *Chemical Society Reviews*, 2012, **41**, 3571-3583.
210. R. Motterlini, B. E. Mann and R. Foresti, *Expert Opinion on Investigational Drugs*, 2005, **14**, 1305-1318.
211. F. Gullotta, A. d. Masi and P. Ascenzi, *IUBMB life*, 2012, **64**, 378-386.
212. R. Foresti, M. G. Bani-Hani and R. Motterlini, *Intensive Care Medicine*, 2008, **34**, 649-658.
213. M. Kourti, W. G. Jiang and J. Cai, *Oxidative Medicine and Cellular Longevity*, 2017, **2017**.
214. A. Loboda, A. Jozkowicz and J. Dulak, *Vascular pharmacology*, 2015, **74**, 11-22.
215. L. Vitek, H. Gbelcová, L. Muchová, K. Váňová, J. Zelenka, R. Koníčková, J. Šuk, M. Zadinova, Z. Knejzlík and S. Ahmad, *Digestive and Liver Disease*, 2014, **46**, 369-375.

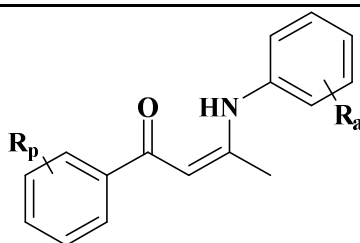
216. C. M. Parsons, D. Muilenburg, T. L. Bowles, S. Virudachalam and R. J. Bold, *Anticancer Research*, 2010, **30**, 3279-3289.
217. S. J. Carrington, I. Chakraborty and P. K. Mascharak, *Chemical Communications*, 2013, **49**, 11254-11256.
218. S. J. Carrington, I. Chakraborty, J. M. Bernard and P. K. Mascharak, *ACS Medicinal Chemistry Letters*, 2014, **5**, 1324-1328.
219. S. Hu, X. Cui, W. He, X. Chen, Z. Gu, J. Zhao, G. Zeng, Z. Shi, L. Zhu and H. Nie, *Zeitschrift für anorganische und allgemeine Chemie*, 2015, **641**, 2452-2459.
220. Y. Gong, T. Zhang, H. Liu, Y. Zheng, N. Li, Q. Zhao, Y. Chen and B. Liu, *Transition Metal Chemistry*, 2015, **40**, 413-426.
221. I. Lee, *Focus on Organometallic Chemistry Research*, 2005, 133-145.
222. G. Zharkova, P. Stabnikov, I. Baidina, A. Smolentsev and S. Tkachev, *Polyhedron*, 2009, **28**, 2307-2312.
223. J. Kim, J.-W. Hwang, Y. Kim, M. H. Lee, Y. Han and Y. Do, *Journal of Organometallic Chemistry*, 2001, **620**, 1-7.
224. G. Xie, Y. Li, J. Sun and C. Qian, *Inorganic Chemistry Communications*, 2009, **12**, 796-799.
225. G. Sánchez, J. L. Serrano, J. Pérez and G. López, *Journal of Fluorine Chemistry*, 1997, **86**, 143-147.
226. H. Leopold and T. Strassner, *Organometallics*, 2016, **35**, 4050-4059.
227. B. Chimitov, K. Zherikova, A. Mikheev, G. Zharkova, N. Morozova, I. Igumenov, A. Arzhannikov and M. Tumm, *Russian Chemical Bulletin*, 2012, **61**, 2236-2242.
228. R. O'Donoghue, D. Peeters, D. Rogalla, H.-W. Becker, J. Rechmann, S. Henke, M. Winter and A. Devi, *Dalton Transactions*, 2016, **45**, 19012-19023.
229. R. A. Maya, A. Maity and T. S. Teets, *Organometallics*, 2016, **35**, 2890-2899.

230. P. Stabnikov, I. Baidina, S. Sysoev, N. Vanina, N. Morozova and I. Igumenov, *Journal of Structural Chemistry*, 2003, **44**, 1054-1061.
231. H. Hao, B. Zhu and J. Yi, *Acta Crystallographica Section E: Structure Reports Online*, 2012, **68**, m351-m352.
232. S. K. KS, Y. Li, Y. Gnanou, U. Baisch, Y. Champouret, R. Poli, K. C. Robson and W. S. McNeil, *Chemistry—An Asian Journal*, 2009, **4**, 1257-1265.
233. K. C. Robson, C. D. Phillips, B. O. Patrick and W. S. McNeil, *Dalton Transactions*, 2010, **39**, 2573-2578.
234. D. González-Flores, S. A. Patil, P. A. Medina, S. Dever, C. Uthaisar, L. W. Pineda, M. L. Montero, J. W. Ziller and B. D. Fahlman, *Inorganica Chimica Acta*, 2013, **396**, 60-65.
235. R. M. Lord, University of Leeds, 2014.
236. S. J. Lucas, R. M. Lord, R. L. Wilson, R. M. Phillips, V. Sridharan and P. C. McGowan, *Dalton Transactions*, 2012, **41**, 13800-13802.
237. R. M. Lord, A. J. Hebden, C. M. Pask, I. R. Henderson, S. J. Allison, S. L. Shepherd, R. M. Phillips and P. C. McGowan, *Journal of Medicinal Chemistry*, 2015, **58**, 4940-4953.

Chapter 2
Synthesis and Characterisation of Functionalised
 β -*bis*-Ketoiminate Ruthenium(II) Dicarbonyl
Complexes

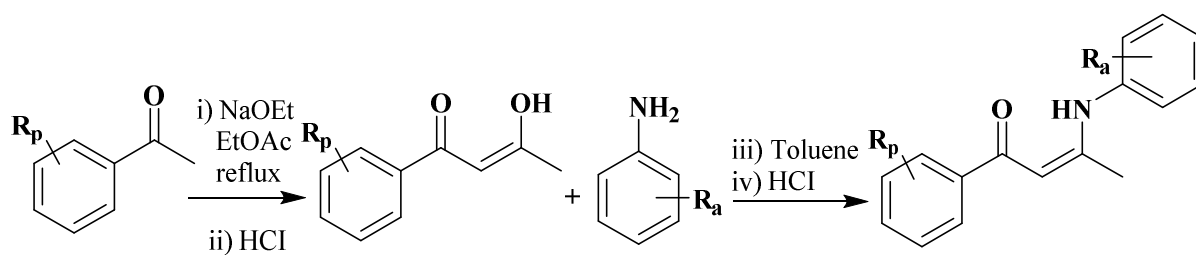
2.1 Synthesis of Biaryl- β -Ketoiminate Ligands

This section expands on the library of phenyl-3(phenylamino)-2-buten-1-one (β -ketoiminate) ligands, previously synthesised and reported within our research group.¹ A range of 1,3- β -diketonate ligands were synthesised *via* a Claisen condensation by reaction of a substituted acetophenone with ethyl acetate in the presence of sodium ethoxide.³ The functionalised 1,3- β -ketoiminate ligands (**Figure 2.1.1**) were subsequently synthesised according to an adaptation of a method by Tang *et al.*, in which the β -diketonate ligand is reacted with aniline in the presence of toluene and HCl to give the resulting 1,3-ketoiminate ligand (**Scheme 2.1.1**).⁴



$R_a = H, R_p = H$	L1	$R_p = H, R_a = 4'Cl$	L21
4'F	L2	4'F	L22
4'Cl	L3	4'Me	L23
4'Br	L4	3'Br	L24
3'F	L5	3'Me	L25
3'Br	L6	2'F	L26
4'I	L7	2',4' diCl	L27
4'Me	L8	2',4' diF	L28
2'Cl	L9	2',3' diMe	L29
2'Br	L10	2'Br	L30
4'OMe	L11	3'Cl	L31
4'CF ₃	L12	2',5' diF	L32
4'OEt	L13		
2'OMe	L14		
3',4' diCl	L15		
2',4',6' triMe	L16		
3',4' methylene	L17		
3'Br, 4'F	L18		

Figure 2.1.1: β -Bis-ketoiminate ligands reported within this thesis



Scheme 2.1.1: General synthetic route for β -bis-ketoiminate ligands

The β -bis-ketoiminate ligands show similar ^1H NMR spectra, with characteristic peaks corresponding to NH proton appearing between 12.5-13.5 ppm, as well as the methine hydrogen peak (H7 in **Figure 2.1.2**), appearing as a singlet between 5.5-6.1 ppm.

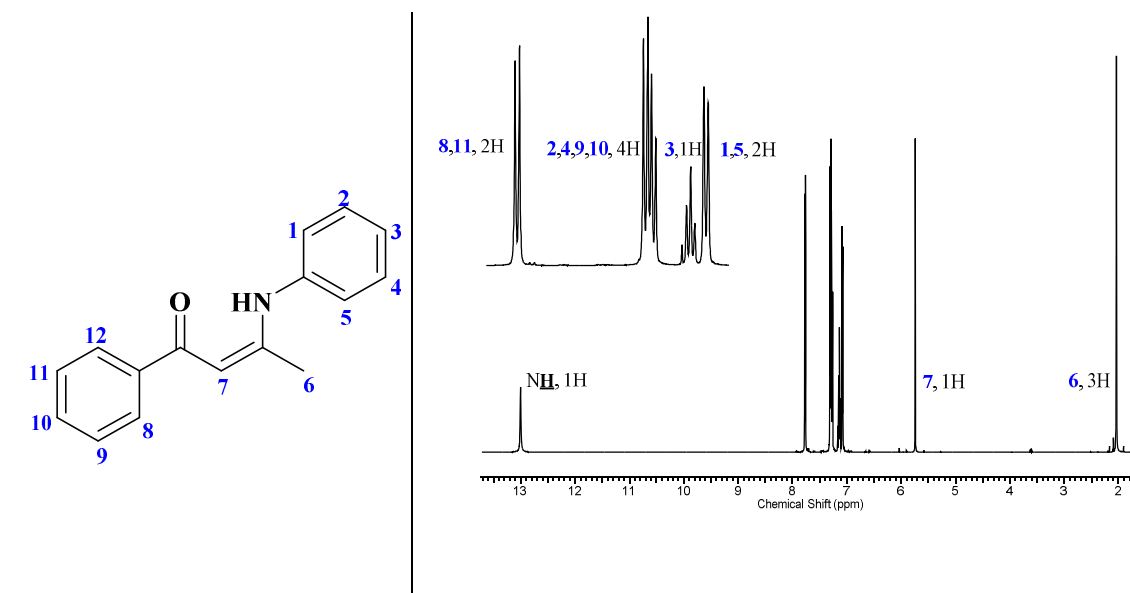


Figure 2.1.2: ^1H NMR spectrum example for ligand **L3**

2.2 Synthesis of Ruthenium(II) Dicarbonyl complexes

The β -bis-ketoiminate Ru(II) dicarbonyl complexes synthesised within this thesis are shown in **Figure 2.2.1**. All complexes (**C1–C16**) were synthesised according to **Scheme 2.2.1** by reacting two equivalents of a functionalised β -bis-ketoiminate ligand and two equivalents of the base, triethylamine, with one equivalent of ruthenium(III) salt in 2-ethoxyethanol under reflux for 6 hours.

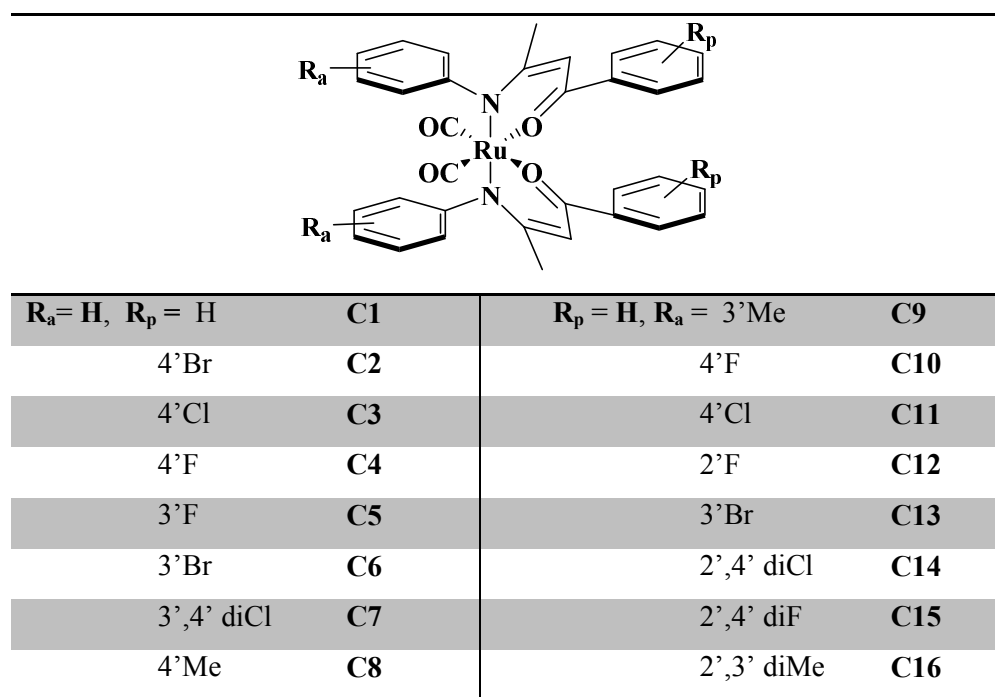
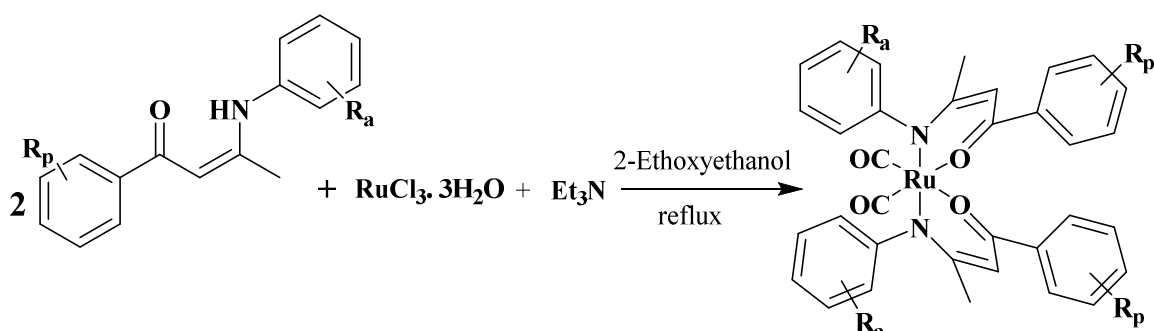


Figure 2.2.1: Ru(II) dicarbonyl complexes synthesised in this thesis



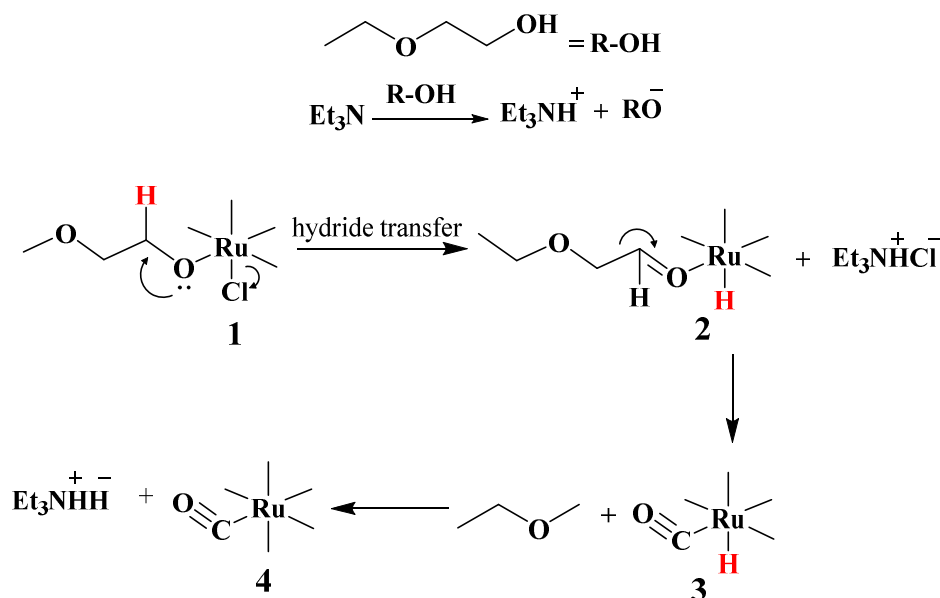
Scheme 2.2.1: Synthetic route for Ru(II) dicarbonyl complexes

This synthesis is characterised by the reduction of ruthenium in the metal precursor from Ru(III) to Ru(II). The carbonyl ligands, though initially unexpected, are thought to be a result of the decarbonylation of the primary alcohol 2-ethoxyethanol acting as the solvent. Although unusual, the possibility of the formation of hydride, carbonyl or hydridocarbonyl metal complexes when a transition metal complex is in contact with an alcoholic medium is well documented. Known alcohols such as allyl alcohol, ethanol, methanol and 2-methoxyethanol are readily decarbonylated by metal salts resulting in the formation of CO-containing complexes and a degraded fragment of the alcohol. These products are likely to be formed under vigorous and basic

conditions, although in some cases the decarbonylation of primary alcohols has been shown to occur under neutral conditions.⁵⁻⁷

This synthesis of complexes was characterised by yields within the range 30-43%. While choice of base did not result in any improvement in the yield of the final product or elimination of side products, reactions without base did not yield any isolable complexes. Investigative reactions with bases such as triethylamine, potassium hydroxide and potassium carbonate gave the carbonyl product in relatively similar yields. Triethylamine was therefore used as the base of choice for all reactions.

Chatt *et al.*⁸ have shown that ruthenium phosphine complexes can form ruthenium carbonyl complexes in alcoholic solutions of methanol and ethanol, however, in this synthesis substitution of 2-ethoxyethanol with either solvent did not result in the formation of β -bis-ketoiminate Ru(II) dicarbonyl complexes. Subsequent investigative reactions with other solvents such as dichloromethane, tetrahydrofuran, acetonitrile and toluene have led to the conclusion that, the solvent 2-ethoxyethanol facilitates the formation of the carbonyl species. In addition, reactions where the ketoiminate ligand was removed or replaced with other ligands such as picolinamides did not result in the formation of the carbonyl complex.



Scheme 2.2.2: Proposed mechanism for the formation of Ru(II) dicarbonyl complexes

Although the mechanism of the reaction has not been investigated to sufficient detail, a reaction scheme similar to that of Chatt *et al.* is proposed (**Scheme 2.2.2**) for the formation of these complexes. The mechanism is thought to go *via* the formation of a ruthenium-alkoxide complex (**1** in **Scheme 2.2.2**). Transition metal alkoxide complexes have been implicated as intermediates in alcohol dehydrogenation reactions.^{9,10} However due to the instability of the alkoxide complexes in protic solvents they decompose *via* β -hydride elimination to form ruthenium hydride species (**2** in **Scheme 2.2.2**). The hydride ligand is labile to acids, therefore is abstracted by the protonated form of triethylamine, allowing for the formation of the carbonyl complex (**4** in **Scheme 2.2.2**).

As observed by Hin Ling Lee *et al.*,⁷ incorporation of the alkyl group of the alcohol into the final complex is unusual and was not observed in this synthesis. Instead, methoxyethane was produced as a side product. Other work has highlighted the formation and isolation of either the hydride or hydridocarbonyl complexes,⁸ but in this synthesis only the dicarbonyl complexes were isolated. This could be because the β -ketoiminate Ru(II) dihydride complexes and the β -ketoiminate Ru(II) hydridocarbonyl complex are highly unstable compared to the final dicarbonyl complex.

The isolation of the Ru(II) carbonyl complexes was made difficult by the presence of an uncharged starting material and several bands in thin layer chromatography that could not be identified. In an effort to eliminate side products, reactions under inert atmosphere with dry solvents were carried out. However, this neither improved the yield of the reaction nor eliminated side reactions. Subsequently column chromatography using dichloromethane and hexane as the eluant was used to achieve pure solids of the β -*bis*-ketoiminate Ru(II) dicarbonyl complexes. Yields were improved when the base was used in excess. Use of excess ligand resulted in the isolation of the excess ligand *via* column chromatography as part of the side products. These β -*bis*-ketoiminate Ru(II) dicarbonyl complexes are air and thermal stable crystalline complexes with yellow to green colours. They are soluble in most organic solvents such as acetonitrile, dichloromethane and ethanol.

Using trimethylamine promoted alcohol decarbonylation, only the *cis*- β -ketoiminate Ru(II) dicarbonyl complexes and not the *trans*- β -ketoiminate Ru(II) dicarbonyl complexes were isolated. Carbon monoxide being a strong π -backbonding ligand prefers not to be in a *trans* position to another carbon monoxide. The ketoiminate ligand being a better σ -donor than it is a π -acceptor when compared to carbon monoxide assumes a position *trans* to the carbon monoxide.

2.3 Characterisation of Ruthenium(II) Dicarbonyl Complexes

Complexes **C1-C16** (**Figure 2.2.1**) were synthesised, purified and characterised by infrared spectroscopy, ^1H NMR, ^1H - ^1H COSY, $^{13}\text{C}\{^1\text{H}\}$ NMR, ^1H - $^{13}\text{C}\{^1\text{H}\}$ HMQC spectroscopy, mass spectrometry, elemental analysis and single crystal X-ray crystallography.

2.4 Infrared Spectroscopy of Ruthenium(II) Dicarbonyl Complexes

The IR spectra of complexes **C1** to **C16** are very similar, with several bands of different intensities due to C=C bonds observed in the 400-1600 cm^{-1} region. A comparison of the spectra of the uncoordinated ligand and the corresponding complex, (**Figure 2.4.1**)Error! Reference source not found., shows a strong stretch due to the terminal CO ligands bonded to the metal centre. These stretches are observed in the region 1900-2100 cm^{-1} and are consistent for all the Ru(II) dicarbonyl complexes (**Table 2.4.1**).

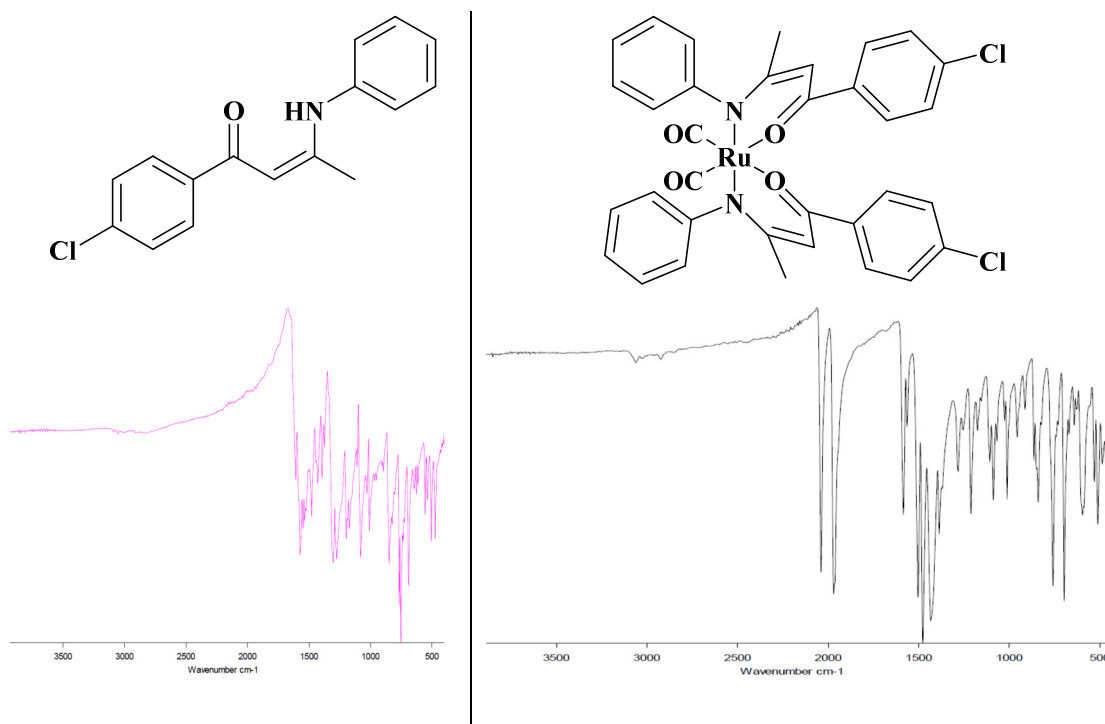


Figure 2.4.1: Example of infrared spectra of free ligand and complex

Table 2.4.1: Infrared spectroscopy data for complexes C1-C16

Complex	Substituent	$\bar{\nu}(\text{C}=\text{O})$	Complex	Substituent	$\bar{\nu}(\text{C}=\text{O})$
C1	H(p)	2039, 1964	C9	3'Me(a)	2037, 1964
C2	4'Br(p)	2037, 1963	C10	4'F(a)	2036, 1963
C3	4'Cl(p)	2039, 1969	C11	4'Cl(a)	2041, 1971
C4	4'F(p)	2033, 1963	C12	2'F(a)	2047, 1972
C5	3'F(p)	2039, 1963	C13	3'Br(a)	2045, 1973
C6	3'Br(p)	2039, 1962	C14	2',4' diCl(a)	2045, 1978
C7	3',4' diCl(p)	2043, 1975	C15	2',4' diF(a)	2047, 1971
C8	4'Me(p)	2033, 1964	C16	2',3' diMe(a)	2036, 1961

(p) = substituent on *phenolate* ring; (a) = substituent on *aniline* ring

The results shown in **Table 2.4.1** indicate that the electronic nature of the substituent and the position of the substituent on either of the phenyl rings (*phenolate* or *aniline*) have little or no significant effect on the resulting wavenumbers of the carbonyl ligands. This can be seen by a lack of trend when moving from the least to the most electronegative complexes, for example, **C2**, **C3** and **C4**.

2.5 NMR Data of Ruthenium(II) Dicarbonyl Complexes

A comparison of the ^1H NMR of the uncoordinated ligand and the complex shows the disappearance of the broad singlet due to the NH peak at around 13 ppm indicating the deprotonation and coordination of N^- . A slight upfield chemical shift upon complexation is observed for all the protons, with the exception of the *aniline* ring protons **2** and **6** [Figure 2.5.1 (b)]. In the uncoordinated ligand, *aniline* ring protons **2** and **6** are seen as a doublet (for example at $\delta \sim 7.09$ ppm for ligand L3 (Figure 2.1.2)), but upon complexation split into two doublets with significantly different chemical shifts (for example two doublets at $\delta \sim 7.25$ and $\delta \sim 6.85$ (Figure 2.5.1(b))). This is attributed to the geometry of the ligands around the metal centre, and the steric clash with the carbonyl ligand which blocks the free rotation of the *aniline* ring. The CO ligands are *cis* to each other thereby causing a slight difference in the chemical environments experienced by protons **2** and **6**.

The $^{13}\text{C}\{^1\text{H}\}$ NMR spectra for the β -ketoiminate Ru(II) dicarbonyl complexes, given in Figure 2.5.1(c), shows a characteristic peak in the region 196-198 ppm due to the terminal carbon monoxide ligands, **17**. Quaternary carbons, **1**, **8**, **10**, **11** and **14** have higher chemical shifts in the range 130-170 ppm. The aromatic carbon peaks for the ketoinimate ligand are in the range 120-130 ppm, while the methine carbon (**9**) is observed at lower chemical shifts 94-96 ppm. The methyl carbon (**7**) is in the range 23-25 ppm. Similar $^{13}\text{C}\{^1\text{H}\}$ NMR spectra trends are observed for all the β -ketoiminate Ru(II) dicarbonyl complexes.

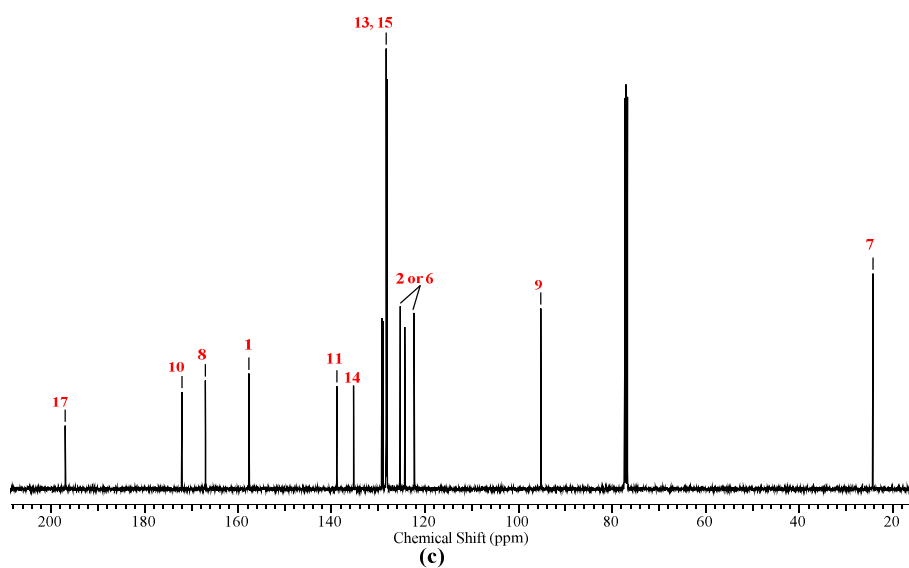
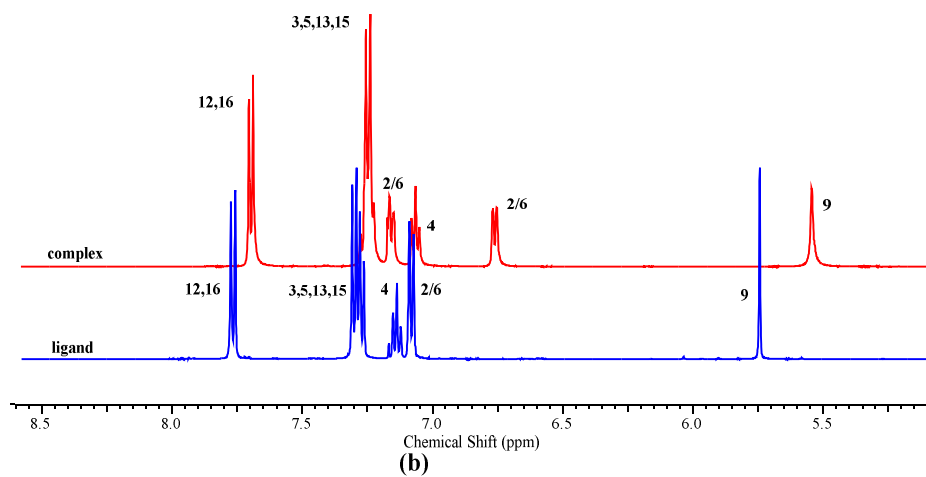
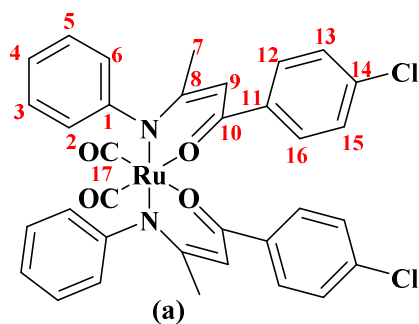


Figure 2.5.1: Example of a typical (b) ^1H NMR (c) ^{13}C $\{^1\text{H}\}$ NMR for Ru(II) dicarbonyl complexes (part of the spectra omitted for clarity)

2.6 X-Ray Crystallography of Ruthenium(II) Dicarbonyl complexes

After column chromatography, single crystals suitable for X-ray crystallography were obtained either by slow vapour diffusion of pentane or hexane into a saturated dichloromethane solution of the complex, or by slow cooling of a saturated solution of the complex in acetonitrile.

A consistent *pseudo* octahedral geometry around the Ru(II) centre is observed for this series of complexes. In the molecular structures of these complexes four coordination sites are occupied by the bidentate ketoiminate ligands, in a *trans* configuration to each other, and the two remaining sites are occupied by the carbonyl ligands, in a *cis* configuration to each other (Figure 2.6.1).

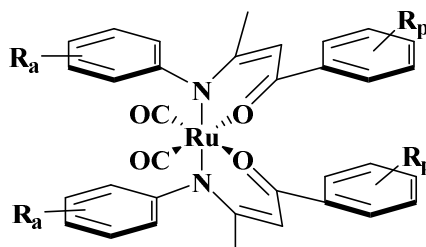


Figure 2.6.1: General structure of β -bis-ruthenium(II) dicarbonyl complexes

As expected for *pseudo* octahedral structures, the molecular structures are characterised by unequal bond lengths and angles around the Ru(II) centre. The angles between the metal centre and the ligands are in the ranges, 83–96° and 170–185°, deviating from the expected 90° and 180° respectively. The Ru-N and Ru-O bond lengths, are within the ranges 2.08–2.10 Å and 2.04–2.10 Å respectively. These are consistent with ketoiminate Ru(II) complexes reported in the literature.¹ The Ru-carbonyl (Ru-C≡O) bond lengths, in the range 1.86–1.88 Å, are considerably shorter than typical Ru-C bonds (ca. 2.1 Å)¹², and shorter than most Ru-carbonyl bonds (1.92–1.93 Å) reported within the literature.¹³ Characteristic short bond lengths, in the range 1.13–1.14 Å are observed for C≡O in all complexes and are within reported literature values.^{14–16}

2.6.1 X-Ray characterisation for C1

Complex **C1** crystallised as yellow plates from slow vapour diffusion of hexane into a concentrated solution of the complex in dichloromethane. The complex crystallised in a monoclinic cell with a single molecule per asymmetric unit cell. Structural solution was performed in the $C2/c$ space group. The molecular structure of **C1** is shown in **Figure 2.6.2**, and selected bond lengths and angles are given in **Table 2.6.1**.

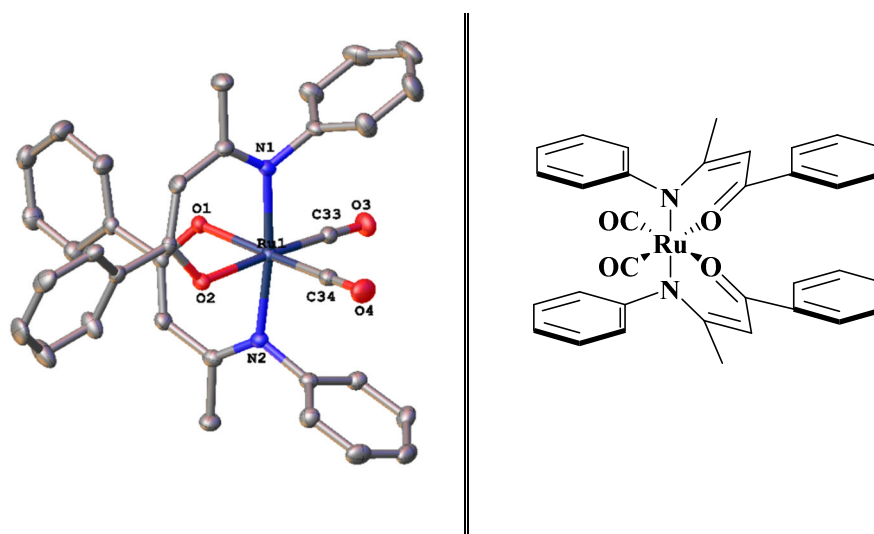


Figure 2.6.2: Molecular structure of **C1**, displacement ellipsoids are at the 50% probability level and hydrogen atoms are omitted for clarity

Table 2.6.1: Selected bond lengths and angles for **C1**

Bond	Distance / Å	Bond	Angle/ °
Ru(1)–O(1)	2.0605(16)	O(1)–Ru(1)–N(1)	89.39(7)
Ru(1)–O(2)	2.0555(16)	O(2)–Ru(1)–N(2)	91.26(7)
Ru(1)–N(1)	2.0824(19)	O(1)–Ru(1)–O(2)	83.98(7)
Ru(1)–N(2)	2.0863(19)	N(1)–Ru(1)–N(2)	172.93(8)
Ru(1)–C(33)	1.869(3)	N(1)–Ru(1)–C(33)	91.22(9)
Ru(1)–C(34)	1.876(3)	N(2)–Ru(1)–C(34)	90.80(9)
C(33)≡O	1.141(3)	C(33)–Ru(1)–C(34)	89.76(11)
C(34)≡O	1.137(3)		

The molecules pack through intermolecular hydrogen bonding in a head to tail arrangement as seen in **Figure 2.6.3**, with no evidence of π - π interactions. There is evidence of weak intramolecular hydrogen bonds between the oxygen atom of $C\equiv O$

and the *phenolate* phenyl ring hydrogen atoms (**Figure 2.6.4(a)**). Several intermolecular hydrogen bonds contributing to the packing of the molecule are observed and shown in **Figure 2.6.4(b)**. **Table 2.6.1** gives the bond length of the respective hydrogen bonds.

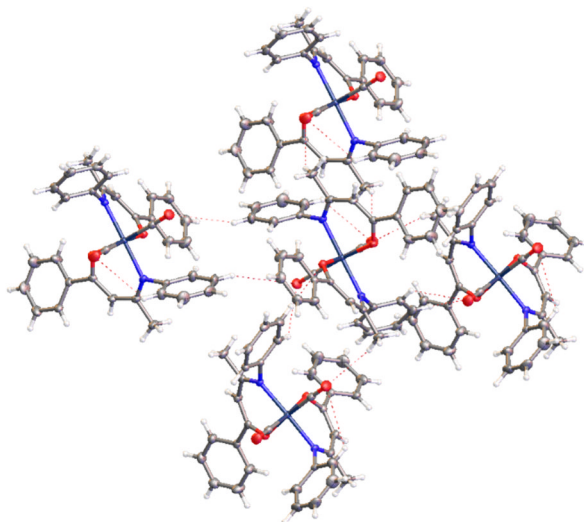


Figure 2.6.3: Molecular packing seen in complex C1

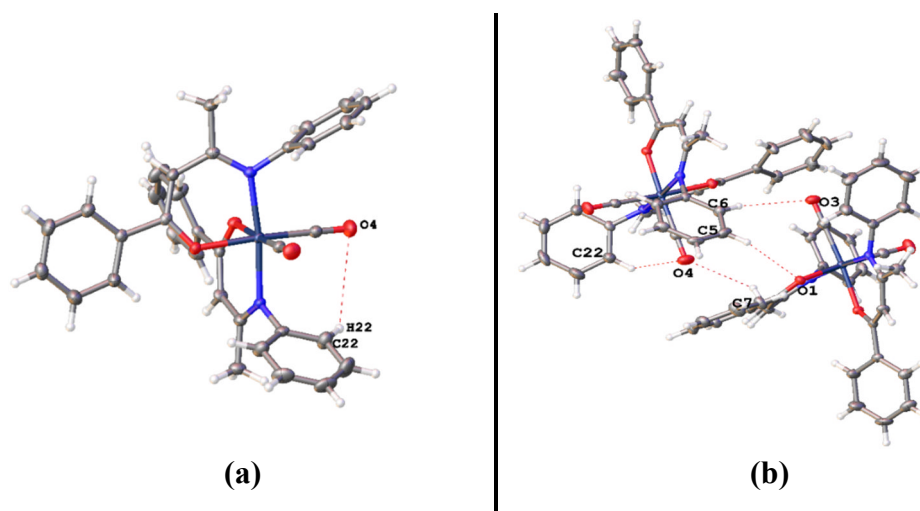


Figure 2.6.4: (a) Intramolecular hydrogen bonds and (b) intermolecular hydrogen bonds in complex, C1

Table 2.6.2: Bond lengths for intra- and intermolecular hydrogen bonds in complex C1

Interaction	Atoms (A....D)	Bond length / Å
Intramolecular	C(22)-H.....O(4)	3.773(3)
Intermolecular	C(5)-H.....O(1)	3.526(3)
	C(6)-H.....O(3)	3.468(3)
	C(7)-H.....O(4)	3.498(4)

C(22)-H.....O(4)	3.773(3)
------------------	----------

2.6.2 X-Ray characterisation for C2

Complex **C2** crystallised as pale green plates, from vapour diffusion of hexane into a dichloromethane solution of the complex.. The complex crystallised in a triclinic cell and was solved in the $P\bar{1}$ space group, with one complex molecule and a disordered molecule of dichloromethane in the asymmetric unit. The molecular structure of **C2** is given in **Figure 2.6.5** and selected bond lengths and angles are given in **Table 2.6.3**.

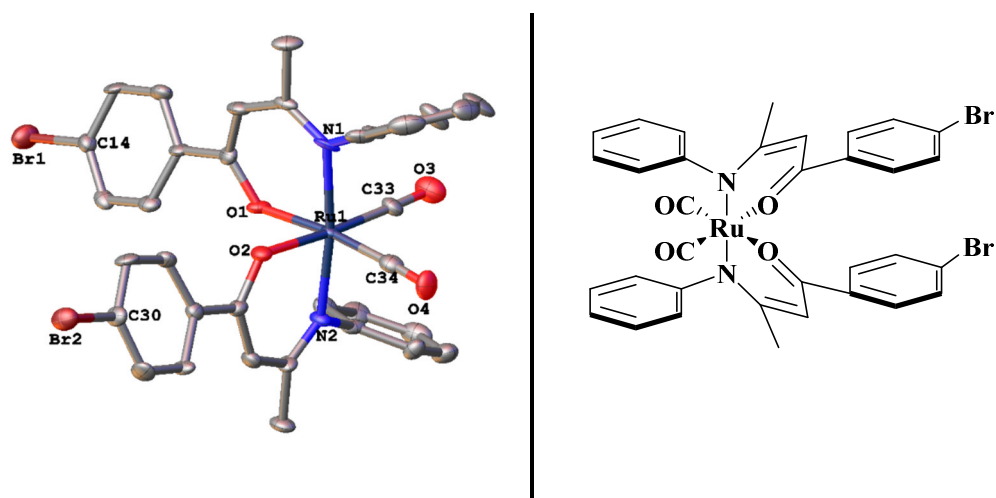


Figure 2.6.5: Molecular structure of **C2**, displacement ellipsoids are at the 50% probability level and hydrogen atoms and disordered solvent are omitted for clarity

Table 2.6.3: Selected bond lengths and angles for **C2**

Bond	Distance	Bond	Angle / °
Ru(1)–O(1)	2.063(3)	O(1)-Ru(1)-N(1)	90.62(14)
Ru(1)–O(2)	2.061(3)	O(2)-Ru(1)-N(2)	90.56(15)
Ru(1)–N(1)	2.093(4)	O(1)-Ru(1)-O(2)	85.44(14)
Ru(1)–N(2)	2.079(4)	N(1)-Ru(1)-N(2)	172.85(16)
Ru(1)-C(33)	1.881(5)	N(1)-Ru(1)-C(33)	94.61(19)
Ru(1)-C(34)	1.872(6)	N(2)-Ru(1)-C(34)	93.71(19)
C(33)≡O	1.132(6)	C(33)-Ru(1)-C(34)	89.7(2)
C(34)≡O	1.141(6)		
C-Br	1.889(5)		

The molecules pack in sheets with π - π interactions evident between the *phenolate* and *aniline* phenyl rings as shown in **Figure 2.6.6**.

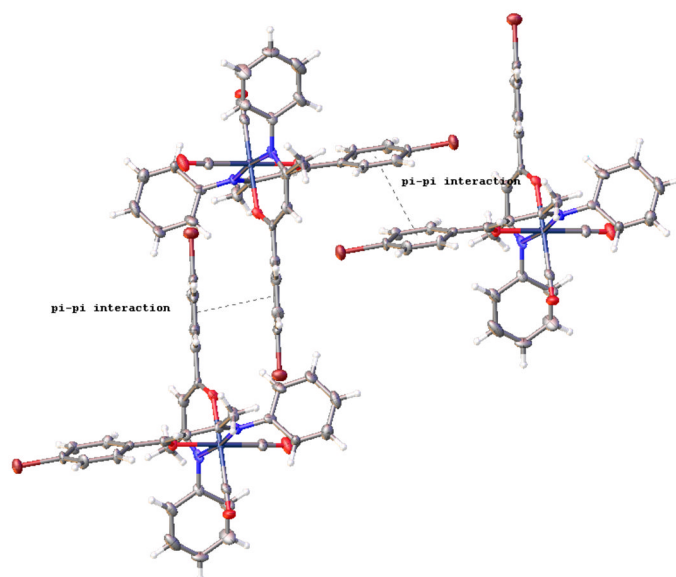


Figure 2.6.6: Molecular packing of **C2** with evident π - π interactions (solvent molecules omitted for clarity)

Figure 2.6.7 shows additional interactions such as intra- and intermolecular hydrogen bonds, participating in the packing of the molecules. Selected bond lengths of these interactions are given in **Table 2.6.4**.

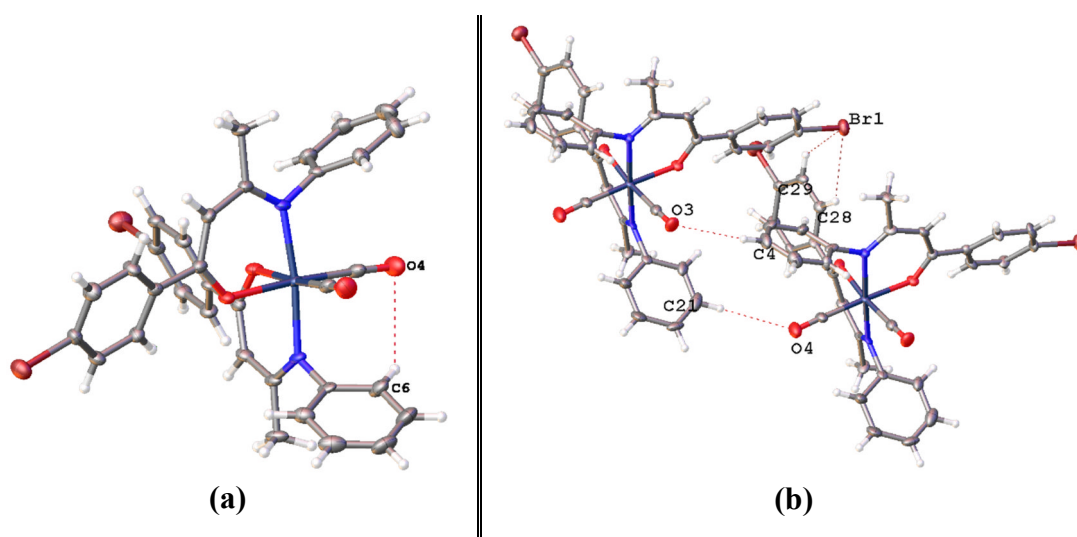


Figure 2.6.7: Selected (a) Intramolecular hydrogen bonds and (b) intermolecular hydrogen bonds in complex, **C2**

Table 2.6.4: Bond lengths for intra- and intermolecular hydrogen bonds in complex **C2**

Interaction	Atoms(A.....D)	Bond length / Å
Intramolecular	C(6)-H.....O(4)	3.763(6)
Intermolecular	C(4)-H.....O(3)	3.838(6)
	C(21)-H.....O(4)	3.882(8)
	C(28)-H.....Br(1)	3.839(3)
	C(29)-H.....Br(1)	3.865(3)
	π - π interactions (<i>phenolate</i> phenyl rings)	3.819
	π - π interactions (<i>aniline</i> phenyl rings)	3.793

2.6.3 X-Ray characterisation for C3

Recrystallisation of complex **C3** from slow vapour diffusion of hexane into a solution of the complex in dichloromethane afforded yellow plates suitable for X-ray crystallography. The molecular structure is shown in **Figure 2.6.8**, with selected bond angles given in **Table 2.6.5**. The compound crystallised in a triclinic cell and was solved in the $P\bar{1}$ space group, with two complex molecules, and disordered solvent in the asymmetric unit.

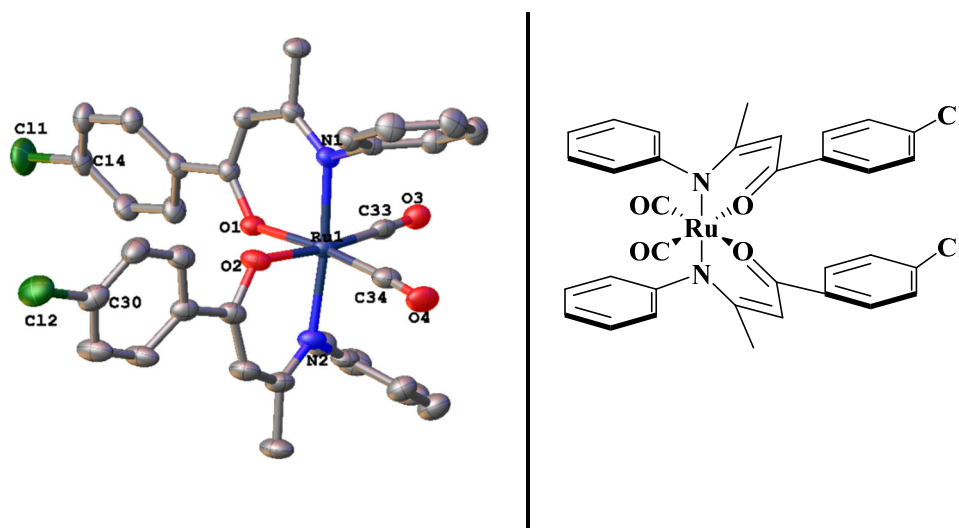
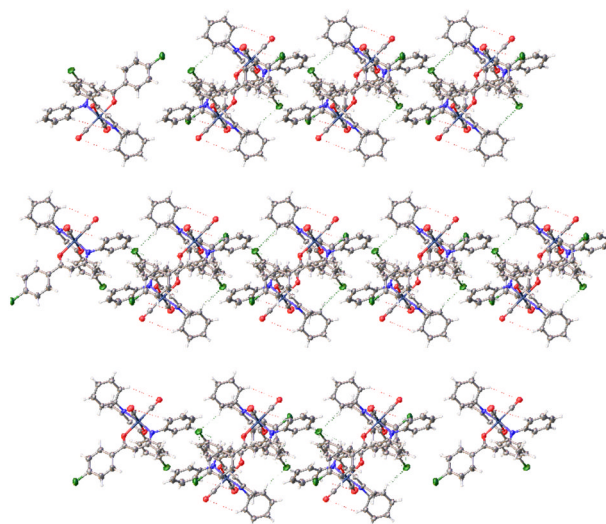


Figure 2.6.8: Molecular structure of **C3**, displacement ellipsoids are at the 50% probability level and hydrogen atoms and disordered solvents are omitted for clarity

Table 2.6.5: Selected bond lengths and angles for **C3**

Bond	Distance	Bond	Angle / Å
Ru(1)–O(1)	2.059(2)	O(1)-Ru(1)-N(1)	90.40(10)
Ru(1)–O(2)	2.063(2)	O(2)-Ru(1)-N(2)	91.24(9)
Ru(1)–N(1)	2.084(3)	O(1)-Ru(1)-O(2)	85.33(9)
Ru(1)–N(2)	2.087(3)	N(1)-Ru(1)-N(2)	174.03(11)
Ru(1)–C(33)	1.872(4)	N(1)-Ru(1)-C(33)	88.38(13)
Ru(1)–C(34)	1.872(3)	N(2)-Ru(1)-C(34)	91.50(12)
C(33)≡O	1.134(4)	C(33)-Ru(1)-C(34)	92.39(14)
C(34)≡O	1.138(4)		
C-Cl	1.731(4)		

A packing diagram of complex **C3** viewed along the *b* axis is given in **Figure 2.6.9** and shows no evidence of π - π interactions as seen with some of the complexes in this family. Instead, the molecules are held together by intra- and intermolecular hydrogen bonding. These bonds are shown in **Figure 2.6.10** and the respective bond lengths are given in **Table 2.6.6**.

**Figure 2.6.9:** Packing in complex **C3**, viewed along the *b* axis (solvent omitted for clarity)

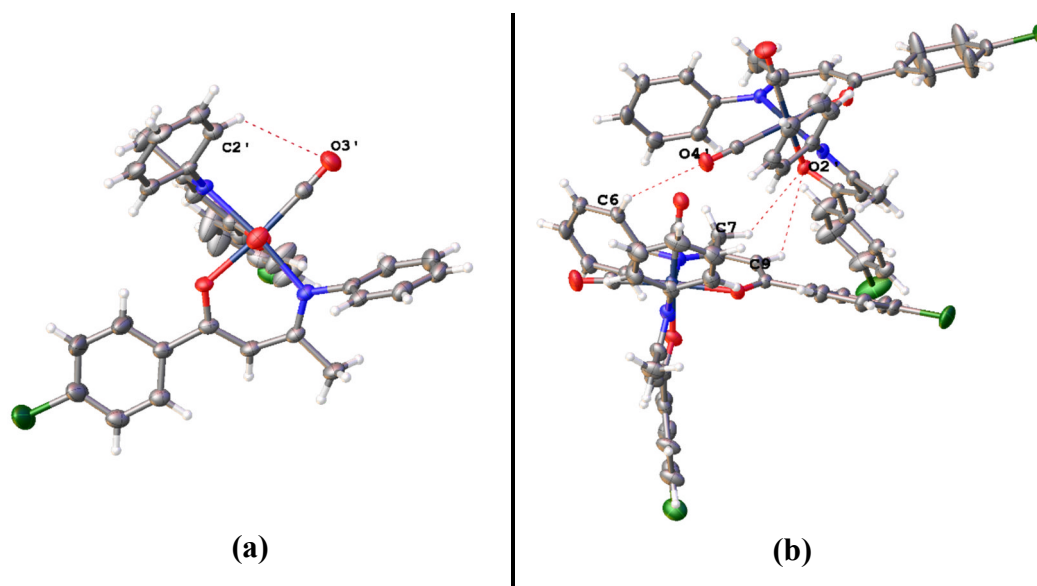


Figure 2.6.10: Selected (a) Intramolecular hydrogen bonds and (b) intermolecular hydrogen bonds in complex, **C3**

Table 2.6.6: Bond lengths for intra- and intermolecular hydrogen bonds in complex **C3**

Interaction	Atoms(A.....D)	Bond length / Å
Intramolecular	C(2')-H.....O(3')	3.843(8)
Intermolecular	C(9)-H.....O(2')	3.864(7)
	C(7)-H.....O(2')	3.537(8)
	C(6)-H.....O(4')	3.406(7)

2.6.4 X-Ray characterisation for **C4**

Single crystals suitable for X-ray crystallography for complex **C4**, were obtained from slow vapour diffusion of hexane into a solution of the complex in dichloromethane. The complex crystallised as yellow needles, in a triclinic cell and the structural solution performed in $P\bar{1}$ space group with two molecules of **C4** and a molecule of water per asymmetric unit

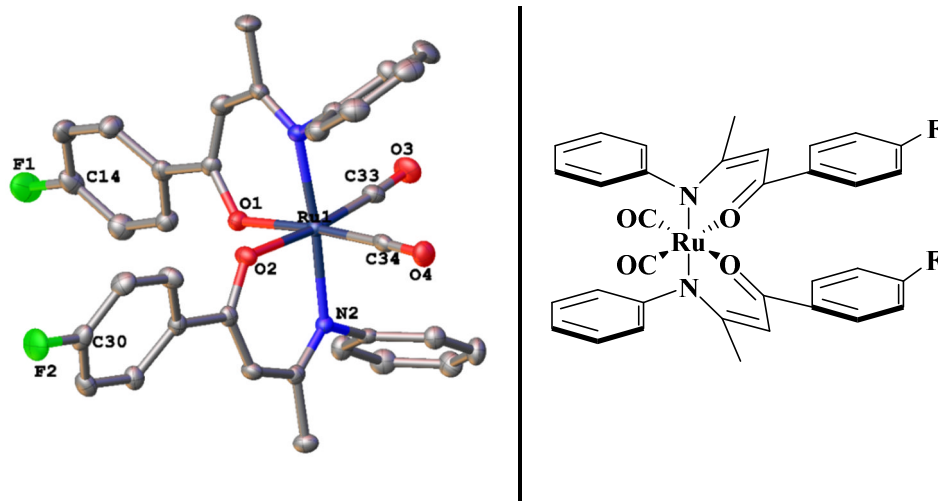


Figure 2.6.11: Molecular structure of **C4**, displacement ellipsoids are at the 50% probability level. Hydrogen atoms, disordered solvent and 2nd molecule are omitted for clarity

Table 2.6.7: Selected bond lengths and angles for **C4**

Bond	Distance	Bond	Angle / Å
Ru(1)–O(1)	2.080(4)	O(1)–Ru(1)–N(1)	90.50(18)
Ru(1)–O(2)	2.072(4)	O(2)–Ru(1)–N(2)	85.80(17)
Ru(1)–N(1)	2.087(5)	O(1)–Ru(1)–O(2)	86.27(16)
Ru(1)–N(2)	2.092(5)	N(1)–Ru(1)–N(2)	175.09(18)
Ru(1)–C(33)	1.871(6)	N(1)–Ru(1)–C(33)	88.8(2)
Ru(1)–C(34)	1.870(6)	N(2)–Ru(1)–C(34)	89.7(2)
C(33)≡O	1.134(7)	C(33)–Ru(1)–C(34)	91.7(3)
C(34)≡O	1.144(7)		
C–F	1.361(7)		

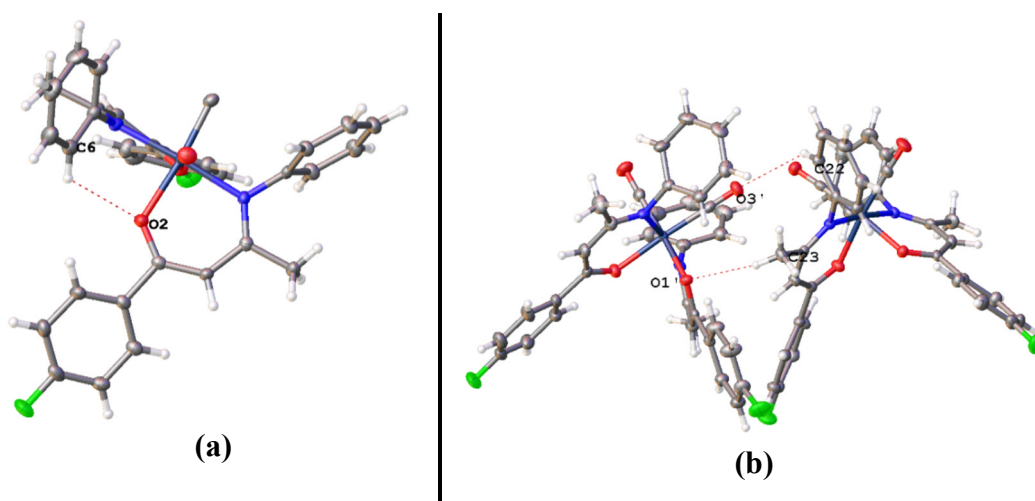
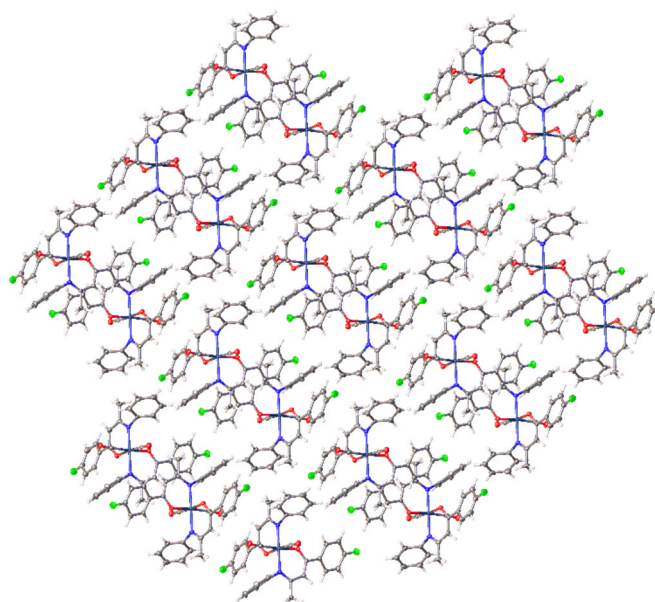


Figure 2.6.12: Selected (a) Intramolecular hydrogen bonds and (b) intermolecular hydrogen bonds in complex, **C4**

Table 2.6.8: Bond lengths for molecular interactions in complex **C4**

Interaction	Atoms(A.....D)	Bond length / Å
Intramolecular	C(6)-H.....O(2)	3.3936(8)
Intermolecular	C(23)-H.....O(1')	3.4797(6)
	C(22)-H.....O(3')	3.354(5)

The molecules pack together in layers of two molecules bound by intermolecular hydrogen bonds, with no evidence on π - π interactions between the phenyl rings. A selected view of the packing, along the *c* axis is shown in **Figure 2.6.13**.

**Figure 2.6.13:** Molecular close packing seen in complex **C4**

2.6.5 X-Ray characterisation for **C5**

Single crystals suitable for X-ray crystallography were obtained through vapour diffusion of hexane into a saturated solution of the complex in dichloromethane. Complex **C5** crystallised in a triclinic cell, the structural solution was performed in $P\bar{1}$ space group with one molecule per asymmetric unit. The molecular structure of **C5** is shown in **Figure 2.6.14**, with selected bond lengths and angles given in **Table 2.6.9**.

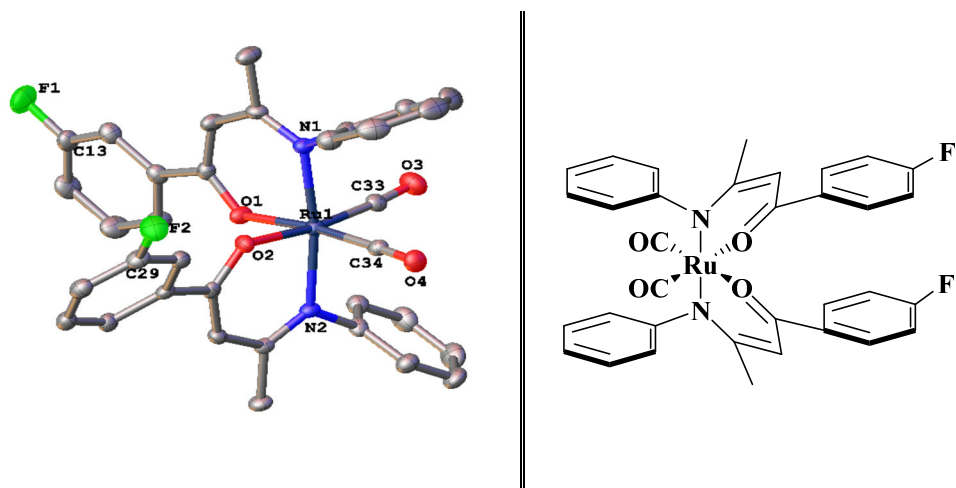


Figure 2.6.14: Molecular structure of **C5**, displacement ellipsoids are at the 50% probability level and hydrogen atoms are omitted for clarity

Table 2.6.9: Selected bond lengths and angles for **C5**

Bond	Distance	Bond	Angle / \AA
Ru(1)–O(1)	2.048(2)	O(1)–Ru(1)–N(1)	90.43(9)
Ru(1)–O(2)	2.047(2)	O(2)–Ru(1)–N(2)	82.95(9)
Ru(1)–N(1)	2.076(2)	O(1)–Ru(1)–O(2)	86.60(9)
Ru(1)–N(2)	2.087(2)	N(1)–Ru(1)–N(2)	171.10(10)
Ru(1)–C(33)	1.870(3)	N(1)–Ru(1)–C(33)	90.35(12)
Ru(1)–C(34)	1.874(3)	N(2)–Ru(1)–C(34)	91.05(11)
C(33)≡O	1.146(4)	C(33)–Ru(1)–C(34)	91.73(13)
C(34)≡O	1.139(4)		
C–F	1.363(4)		

The molecules pack in rows with π - π interactions between the *phenolate* phenyl rings as shown in **Figure 2.6.15**.

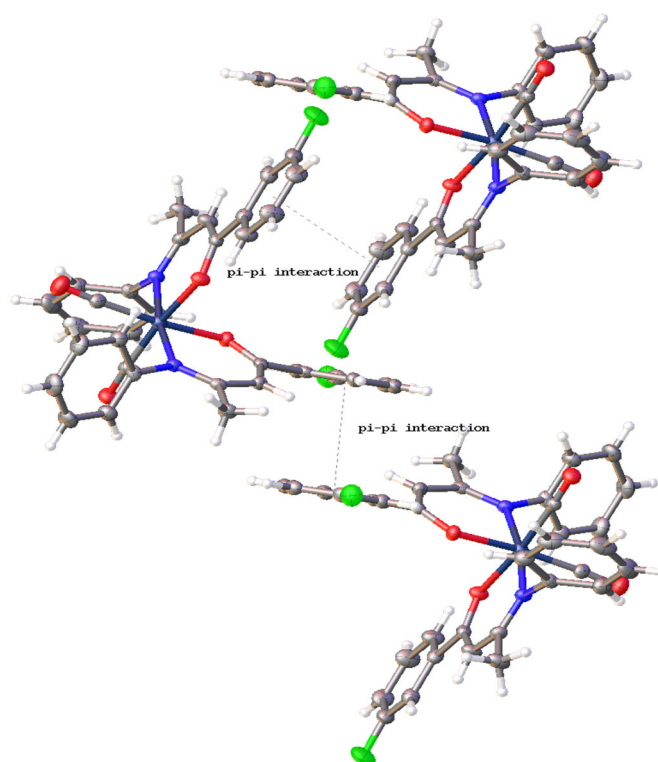


Figure 2.6.15: π - π interactions in complex C5

Figure 2.6.16 shows additional interactions such as intra- and intermolecular hydrogen bonds contributing to the packing of the molecules. The respective bond lengths of these interactions are given in **Table 2.6.10**.

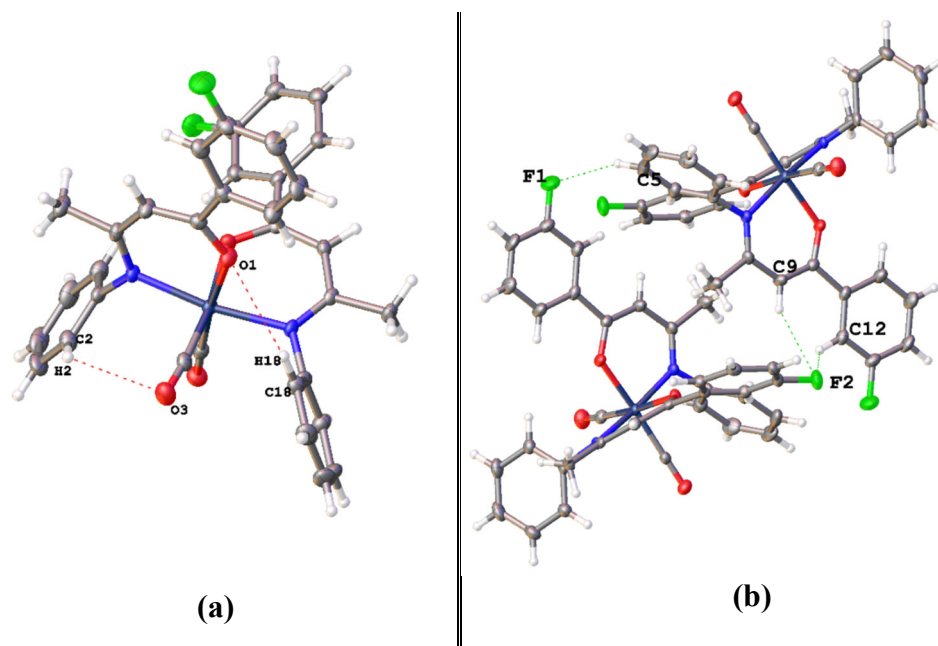


Figure 2.6.16: (a) Intramolecular hydrogen bonds and (b) intermolecular hydrogen bonds in complex, C5

Table 2.6.10: Bond lengths for molecular interactions in complex **C5**

Interaction	Atoms(A.....D)	Bond length / Å
Intramolecular	C(18)-H.....O(1)	3.603(4)
	C(2)-H.....O(3)	3.855(4)
Intermolecular	C(5)-H.....F(1)	3.391(5)
	C(9)-H.....F(2)	3.811(4)
	C(12)-H.....F(2)	3.457(4)
	π - π interactions (<i>phenolate</i> phenyl rings)	3.633
	π - π interactions (<i>phenolate</i> phenyl rings)	3.735

2.6.6 X-Ray characterisation for **C6**

Yellow blocks of **C6** suitable for X-ray crystallography were obtained from vapour diffusion of pentane into a solution of the complex in dichloromethane. The molecular structure of **C6** is shown in **Figure 2.6.17**, with selected bond lengths and angles given in **Table 2.6.11**. This complex crystallised in a triclinic cell and structural solution was performed in the $P\bar{1}$ space group with one molecule per asymmetric unit.

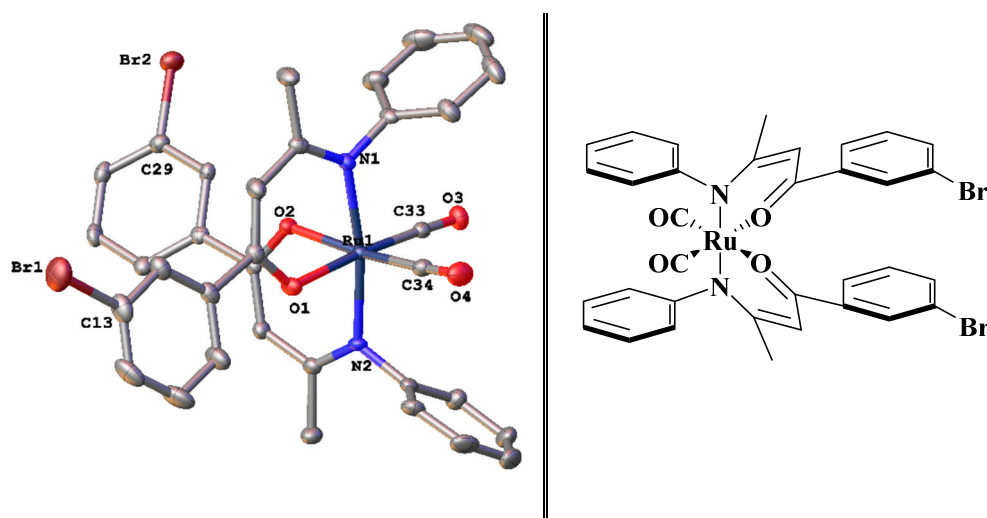
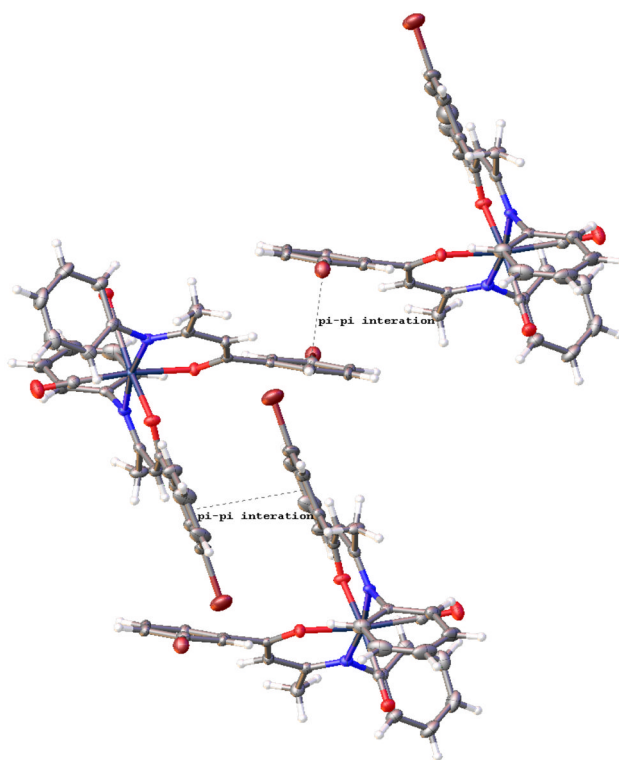


Figure 2.6.17: Molecular structure of **C6**, displacement ellipsoids are at the 50% probability level and hydrogen atoms are omitted for clarity

Table 2.6.11: Selected bond lengths and angles for **C6**

Bond	Distance	Bond	Angle / Å
Ru(1)–O(1)	2.042(3)	O(1)–Ru(1)–N(1)	90.59(12)
Ru(1)–O(2)	2.055(3)	O(2)–Ru(1)–N(2)	82.56(12)
Ru(1)–N(1)	2.085(3)	O(1)–Ru(1)–O(2)	85.90(12)
Ru(1)–N(2)	2.084(3)	N(1)–Ru(1)–N(2)	170.35(13)
Ru(1)–C(33)	1.874(4)	N(1)–Ru(1)–C(33)	95.59(15)
Ru(1)–C(34)	1.876(4)	N(2)–Ru(1)–C(34)	96.21(16)
C(33)≡O	1.137(5)	C(33)–Ru(1)–C(34)	90.98(18)
C(34)≡O	1.144(5)		
C–Br	1.875(5)		

The molecules pack in alternating rows with π - π interactions between the *phenolate* phenyl rings as shown in **Figure 2.6.18**.

**Figure 2.6.18:** π - π interactions in complex **C6**

Addition interactions in the form of intra- and intermolecular hydrogen bonds contribute to the packing of the molecules. Selected examples of these are shown in **Figure 2.6.19**, and the bond lengths given in **Table 2.6.12**.

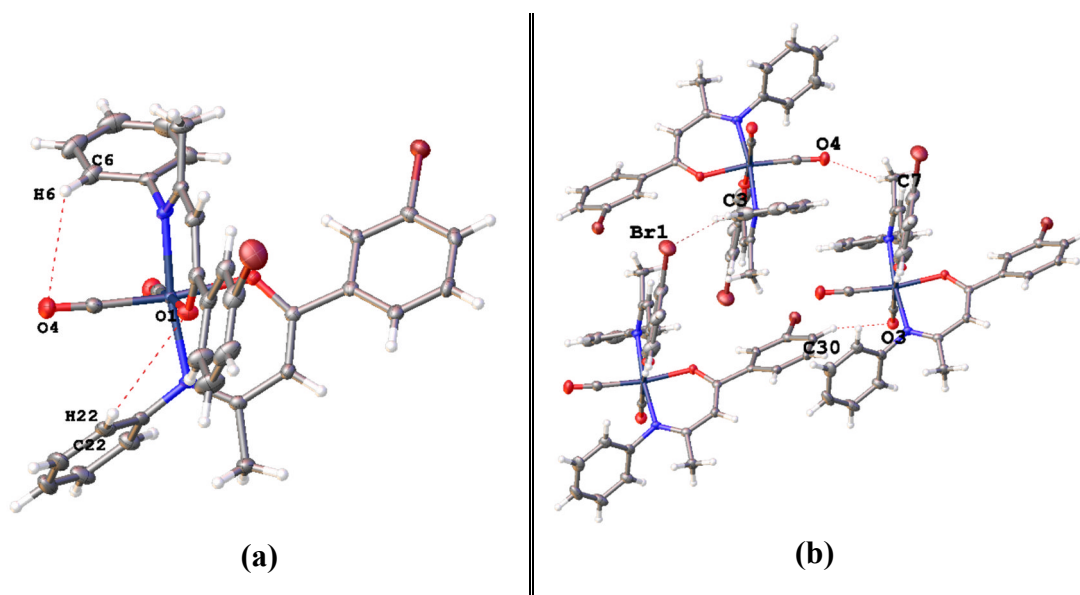


Figure 2.6.19: (a) Intramolecular hydrogen bonds and (b) intermolecular hydrogen bonds in complex, C6

Table 2.6.12: Bond lengths for molecular interactions in complex C6

Interaction	Atoms(A.....D)	Bond length / Å
Intramolecular	C(22)-H.....O(1)	3.659(5)
	C(6)-H.....O(4)	3.714(6)
Intermolecular	C(3)-H.....Br(1)	3.705(6)
	C(30)-H.....O(3)	3.326(5)
	C(7)-H.....O(4)	3.485(6)
	π - π interactions (<i>phenolate</i> phenyl rings)	3.637
	π - π interactions (<i>phenolate</i> phenyl rings)	3.766

2.6.7 X-Ray characterisation for C8

Complex **C8** crystallised as yellow blocks from slow vapour diffusion of hexane into a concentrated solution of the complex in dichloromethane. The complex crystallised in a monoclinic cell with a half molecule per asymmetric unit cell. Structural solution was performed in the $I2/c$ space group. The molecular structure of **C8** is shown in **Figure 2.6.20** and selected bond lengths and angles are given in **Table 2.6.13**.

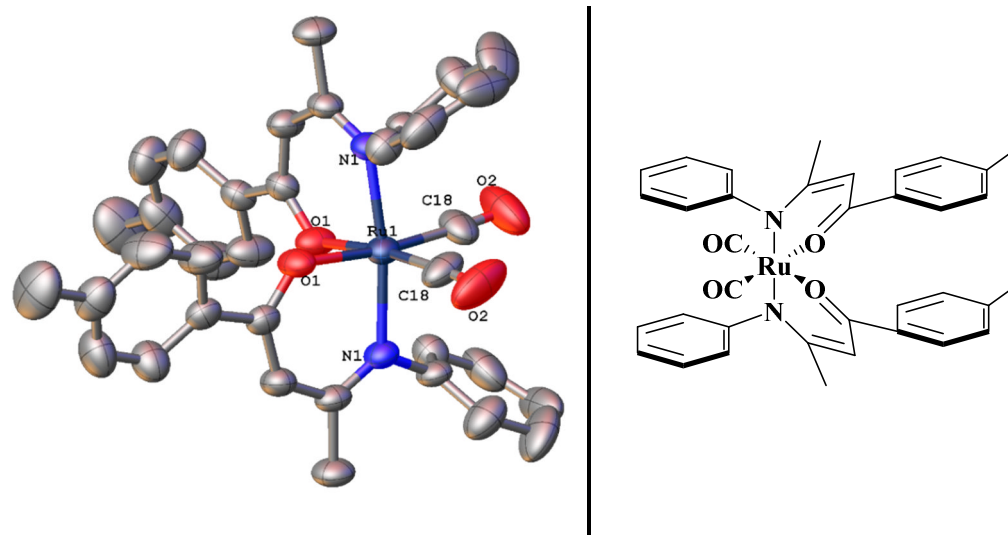


Figure 2.6.20: Molecular structure of **C8**, displacement ellipsoids are at the 50% probability level and hydrogen atoms are omitted for clarity. Only one part of the disordered *aniline* phenyl ring is shown

Table 2.6.13: Selected bond lengths and angles for **C8**

Bond	Distance	Bond	Angle / Å
Ru(1)–O(1)	2.0449(15)	O(1)–Ru(1)–N(1)	91.20(6)
Ru(1)–O(2)	2.0449(15)	O(2)–Ru(1)–N(2)	82.64(6)
Ru(1)–N(1)	2.0449(15)	O(1)–Ru(1)–O(2)	85.90(9)
Ru(1)–N(2)	2.0449(15)	N(1)–Ru(1)–N(2)	171.61(10)
Ru(1)–C(33)	1.863(3)	N(1)–Ru(1)–C(18)	90.65(9)
Ru(1)–C(34)	1.863(3)	N(2)–Ru(1)–C(18')	90.65(9)
C(18)≡O	1.138(3)	C(18)–Ru(1)–C(18')	89.74(18)

Complex **C8** only displays intramolecular hydrogen (**Figure 2.6.21**) bonding within its molecules, with no presence of intermolecular hydrogen bonding or π - π interactions. The intramolecular hydrogen bond is 3.341(10) Å and is comparable to similar bonds within this series of complexes.

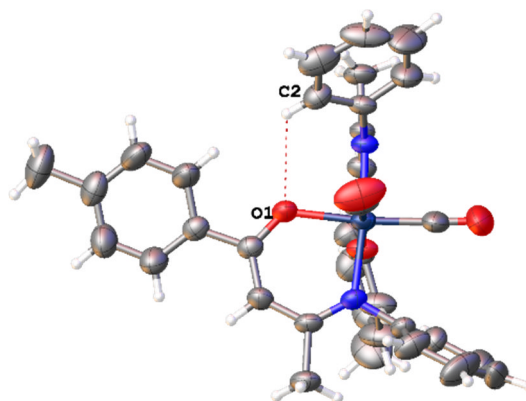


Figure 2.6.21: Intramolecular hydrogen bonding in **C8**

Figure 2.6.22 shows the herringbone type of crystal close packing seen in complex **C8**.

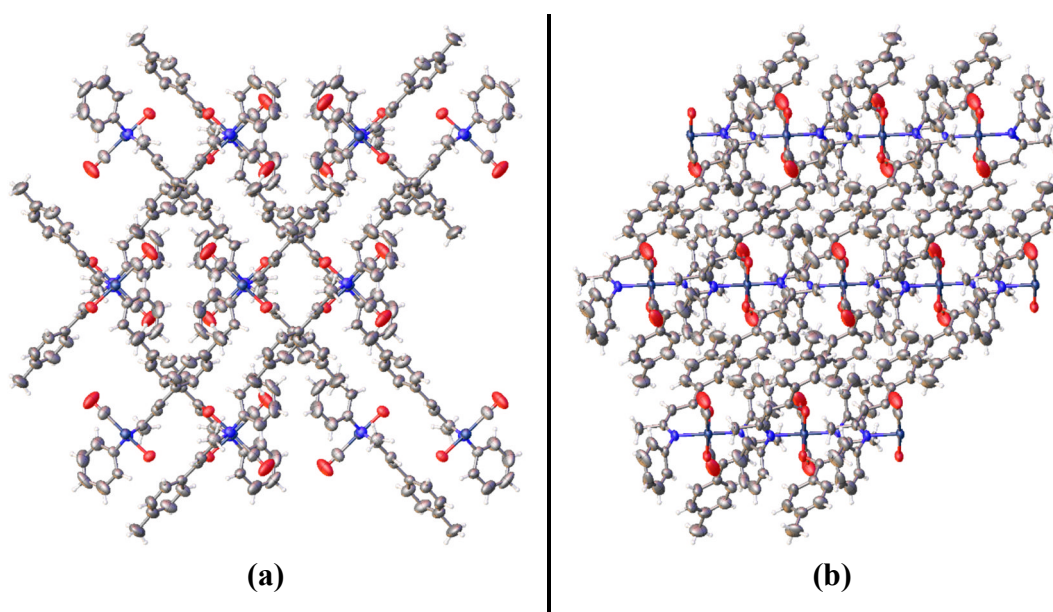


Figure 2.6.22: Herringbone arrangement in **C8** viewed along the (a) the a-axis and (b) the b-axis

2.6.8 X-Ray characterisation for **C9**

Recrystallisation of complex **C9**, from vapour diffusion of hexane into a concentrated solution of the complex in dichloromethane afforded yellow blocks suitable for crystallography. Complex **C9** crystallized in an orthorhombic cell and the structural solution performed in *Pbcn* space group with one molecule per asymmetric unit. The

molecular structure is given in **Figure 2.6.23** and selected bond lengths and bond angles are given in Table 2.6.14. The molecule shows disorder of the *aniline* phenyl ring across two positions in a 55:45 ratio.

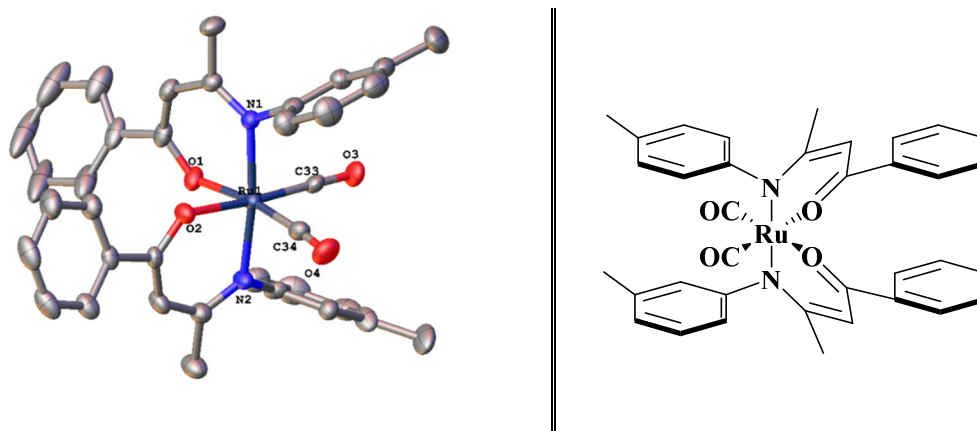


Figure 2.6.23: Molecular structure of **C9**, displacement ellipsoids are at the 50% probability level and hydrogen atoms are omitted for clarity. Only one part of disordered *aniline* phenyl ring is shown

Table 2.6.14: Selected bond lengths and angles for **C9**

Bond	Distance	Bond	Angle / Å
Ru(1)–O(1)	2.0582(19)	O(1)–Ru(1)–N(1)	89.90(8)
Ru(1)–O(2)	2.0582(19))	O(2)–Ru(1)–N(2)	91.74(8)
Ru(1)–N(1)	2.094(2)	O(1)–Ru(1)–O(2)	84.80(7)
Ru(1)–N(2)	2.083(2)	N(1)–Ru(1)–N(2)	172.37(9)
Ru(1)–C(33)	1.862(3)	N(1)–Ru(1)–C(33)	91.17(10)
Ru(1)–C(34)	1.876(3)	N(2)–Ru(1)–C(34)	90.33(11)
C(33)≡O	1.138(3)	C(33)–Ru(1)–C(34)	89.75(12)
C(34)≡O	1.136(3)		

The complex packs in a herringbone arrangement as shown in **Figure 2.6.24**, with no evidence of π - π interactions between the phenyl rings. Intra- and intermolecular hydrogen bonds participate in the packing of the complex and are shown in **Figure 2.6.25**, with selected bond lengths given in **Table 2.6.15**.

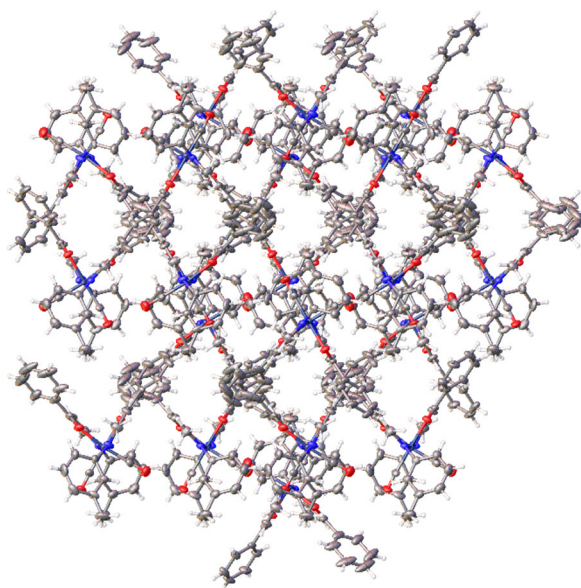


Figure 2.6.24: Herringbone close packing C9, viewed along a-axis

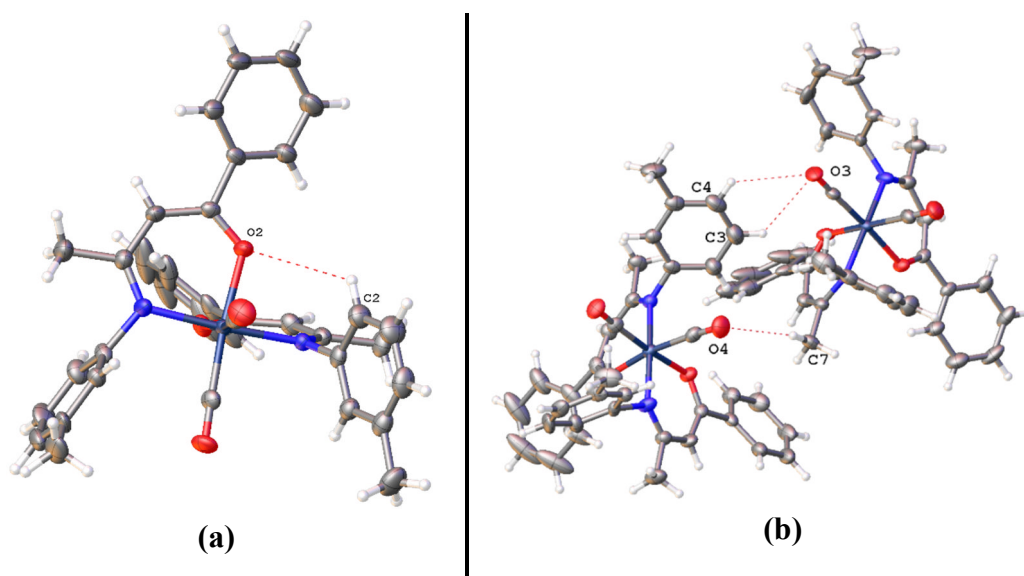


Figure 2.6.25: (a) Intramolecular hydrogen bonds and (b) intermolecular hydrogen bonds in complex, C9

Table 2.6.15: Selected bond lengths for intra- and inter-molecular interactions in complex C9

Interaction	Atoms(A.....D)	Bond length / Å
Intramolecular	C(2)-H.....O(2)	3.73002(8)
Intermolecular	C(3)-H.....O(3)	3.37081(7)
	C(4)-H.....O(3)	3.42860(9)
	C(7)-H.....O(4)	3.79207(8)

2.6.9 X-Ray characterisation for C11

Complex **C11** crystallised as yellow plates from slow vapour diffusion of hexane into a concentrated solution of the complex in dichloromethane. The complex crystallised in a monoclinic cell with a single molecule and a distorted solvent molecule per asymmetric unit cell. Structural solution was performed in the $P2_1/c$ space group. The molecular structure of **C11** is shown in **Figure 2.6.26**, and selected bond lengths and angles are given in **Table 2.6.16**.

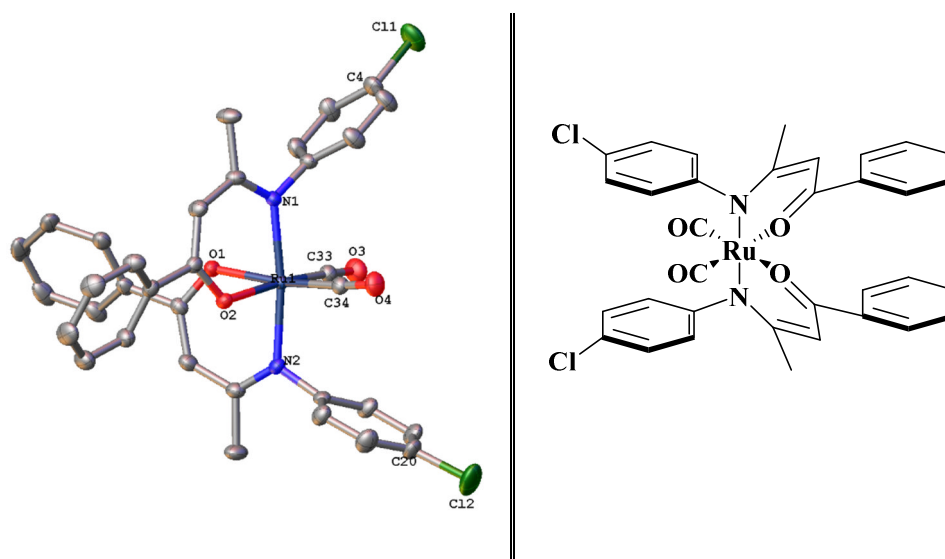


Figure 2.6.26: Molecular structure of **C11**, displacement ellipsoids are at the 50% probability level and hydrogen atoms and so disordered solvent are omitted for clarity

Table 2.6.16: Selected bond lengths and angles for **C11**

Bond	Distance	Bond	Angle / $^{\circ}$
Ru(1)–O(1)	2.0471(19)	O(1)-Ru(1)-N(1)	82.73(8)
Ru(1)–O(2)	2.0627(19)	O(2)-Ru(1)-N(2)	83.09(8)
Ru(1)–N(1)	2.079(2)	O(1)-Ru(1)-O(2)	83.17(8)
Ru(1)–N(2)	2.085(2)	N(1)-Ru(1)-N(2)	172.37(9)
Ru(1)-C(33)	1.873(3)	N(1)-Ru(1)-C(33)	95.13(10)
Ru(1)-C(34)	1.876(3)	N(2)-Ru(1)-C(34)	96.07(10)
C(33)≡O	1.137(3)	C(33)-Ru(1)-C(34)	91.52(12)
C(34)≡O	1.140(3)		
C-Cl	1.741(3)		

A packing diagram of complex **C11** viewed along the b axis is shown in **Figure 2.6.27** and shows no evidence of π - π interactions as seen with some of the complexes

in this series. Instead, the molecules pack in layers, held together by intra- and intermolecular hydrogen bonding. The intra- and intermolecular hydrogen bonds are shown in **Figure 2.6.28** and the respective bond lengths are given in **Table 2.6.16**.

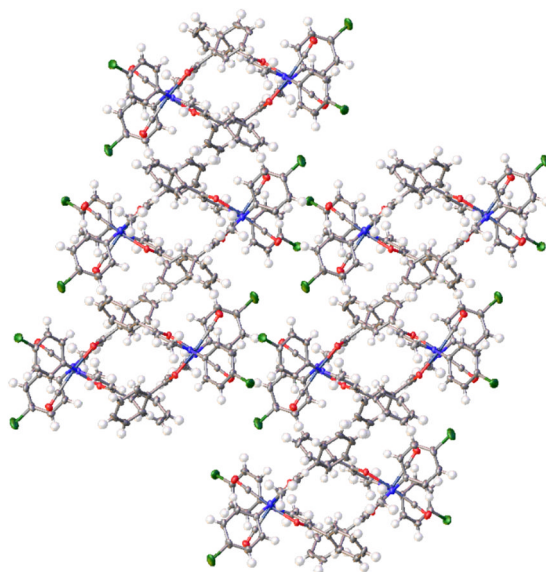


Figure 2.6.27: Packing in complex **C11**, viewed along the *b* axis (solvent omitted for clarity)

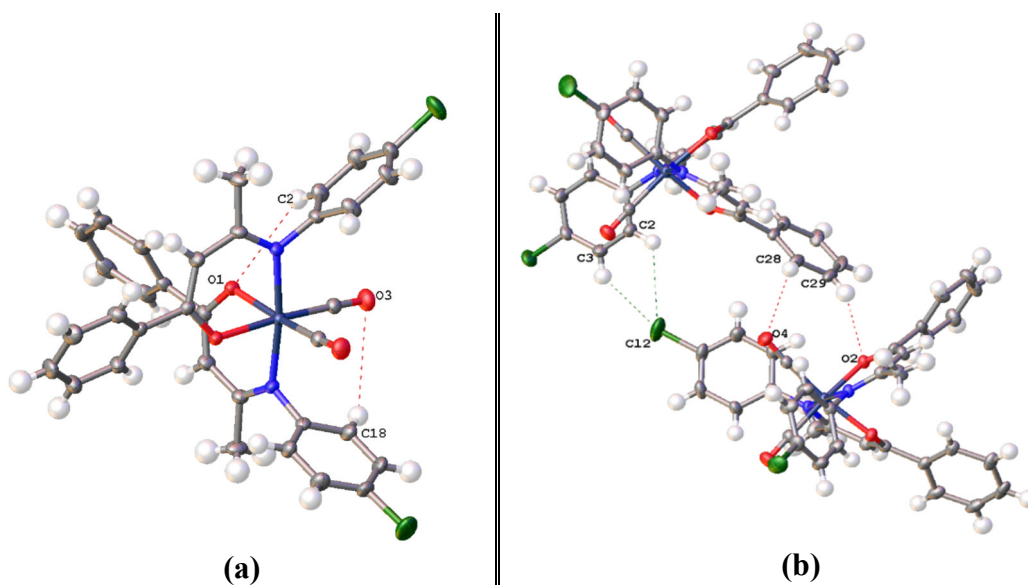


Figure 2.6.28: (a) Intramolecular hydrogen bonds and (b) intermolecular hydrogen bonds in complex, **C11**

Table 2.6.17: Selected bond lengths for intra- and intermolecular interactions in complex **C11**

Interaction	Atoms(A.....D)	Bond length / Å
Intramolecular	C(2)H.....O(1)	3.63817(7)
	C(18)-H.....O(3)	3.76571(7)
Intermolecular	C(2)-H.....Cl(2)	3.83597(13)
	C(3)-H.....Cl(2)	3.79035(9)
	C(28)-H.....O(2)	3.47027(10)
	C(29)-H.....O(4)	3.51927(14)

2.6.10 X-Ray characterisation for C12

Complex **C12** crystallised as yellow blocks from slow vapour diffusion of hexane into a concentrated solution of the complex in dichloromethane. The complex crystallised in a monoclinic cell with one molecule per asymmetric unit cell, showing distortion in the ortho position of the *aniline* ring. Structural solution was performed in the $P2_1/c$ space group. The molecular structure of **C12** is shown in **Figure 2.6.29**, and selected bond lengths and angles are given in **Table 2.6.18**.

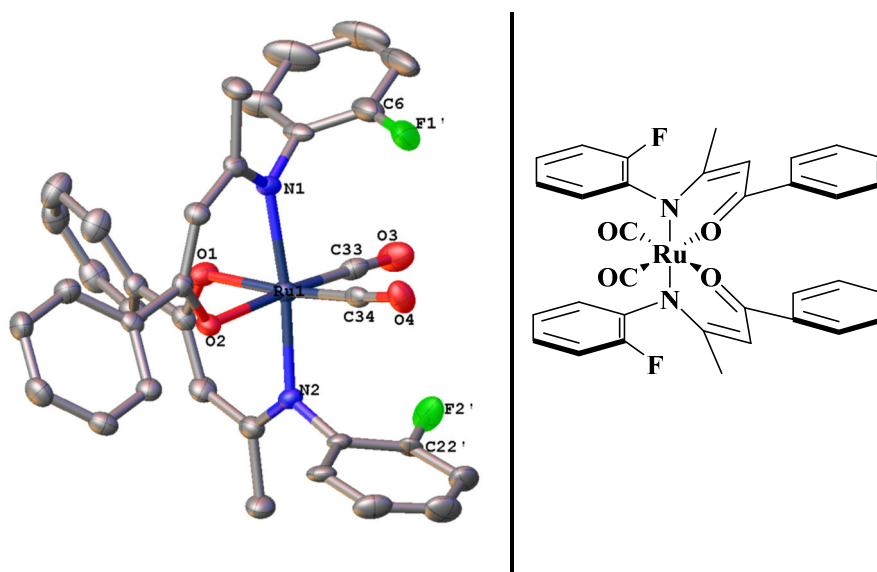
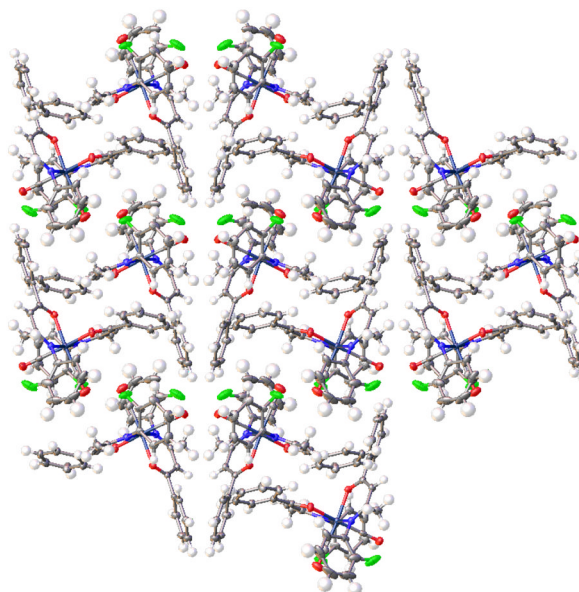
**Figure 2.6.29:** Molecular structure of **C12**, displacement ellipsoids are at the 50% probability level and hydrogen atoms and so disordered parts are omitted for clarity

Table 2.6.18: Selected bond lengths and angles for **C12**

Bond	Distance	Bond	Angle / Å
Ru(1)–O(1)	2.046(2)	O(1)-Ru(1)-N(1)	85.14(9)
Ru(1)–O(2)	2.0643(19)	O(2)-Ru(1)-N(2)	90.76(9)
Ru(1)–N(1)	2.084(2)	O(1)-Ru(1)-O(2)	86.78(8)
Ru(1)–N(2)	2.082(2)	N(1)-Ru(1)-N(2)	173.77(9)
Ru(1)-C(33)	1.870(3)	N(1)-Ru(1)-C(33)	94.62(11)
Ru(1)-C(34)	1.861(3)	N(2)-Ru(1)-C(34)	95.59(11)
C(33)≡O	1.140(3)	C(33)-Ru(1)-C(34)	90.00(13)
C(34)≡O	1.146(4)		
C-F	1.331(9)		

Complex **C12** packs in alternating layers as shown in **Figure 2.6.30**. There is no evidence of π - π interactions, instead, the molecules are held together by intra- and intermolecular hydrogen bonding. These intra- and intermolecular hydrogen bonds are shown in **Figure 2.6.31**, and the respective bond lengths are given in **Table 2.6.19**.

**Figure 2.6.30:** Packing in complex **C12**, viewed along the *c* axis (solvent and disordered parts omitted for clarity)

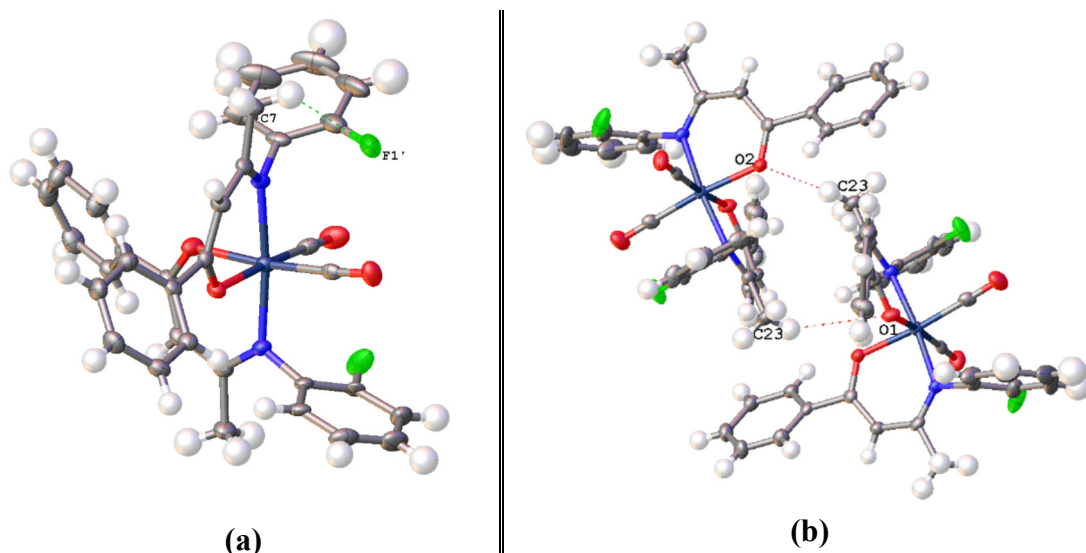


Figure 2.6.31: (a) Intramolecular hydrogen bonds and (b) intermolecular hydrogen bonds in complex, **C12**

Table 2.6.19: Selected bond lengths for intra- and intermolecular interactions in complex **C12**

Interaction	Atoms(A.....D)	Bond length / Å
Intramolecular	C(7)H.....F(1')	3.4536(3)
Intermolecular	C(23)-H.....O(1)	3.8991(4)
	C(23)-H.....O(2)	3.7390(3)

2.6.11 X-Ray characterisation for **C14**

Single crystals suitable for X-ray crystallography were obtained through vapour diffusion of hexane into a saturated solution of complex **C14** in dichloromethane. Complex **C14** crystallised in a monoclinic cell, the structural solution was performed in $P2_1/n$ space group with one molecule per asymmetric unit. The molecular structure of **C14** is shown in **Figure 2.6.32**, with selected bond lengths and angles given in **Table 2.6.20**.

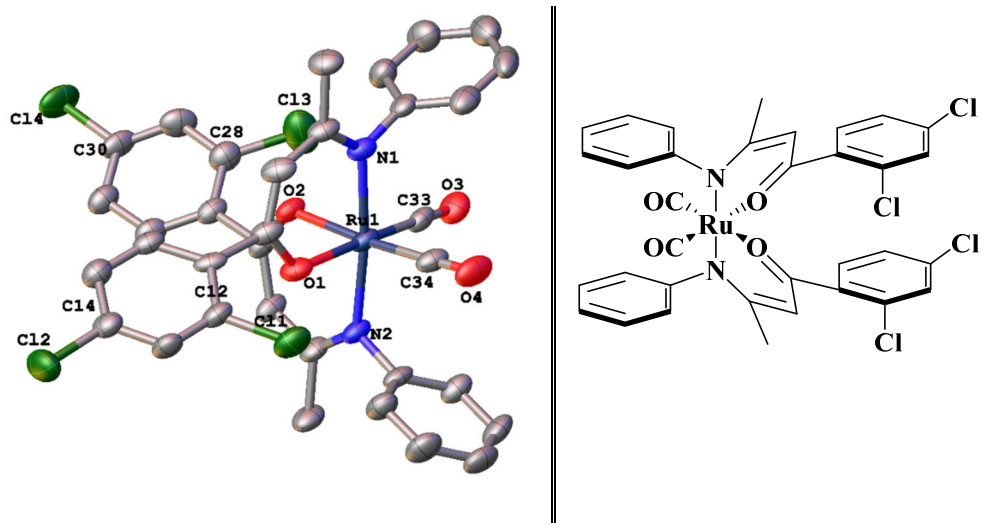


Figure 2.6.32: Molecular structure of **C14**, displacement ellipsoids are at the 50% probability level and hydrogen atoms and disordered parts are omitted for clarity.

Table 2.6.20: Selected bond lengths and angles for **C14**

Bond	Distance	Bond	Angle / $^{\circ}$
Ru(1)–O(1)	2.056(3)	O(1)–Ru(1)–N(1)	90.91(10)
Ru(1)–O(2)	2.055(2)	O(2)–Ru(1)–N(2)	91.60(10)
Ru(1)–N(1)	2.090(3)	O(1)–Ru(1)–O(2)	84.82(10)
Ru(1)–N(2)	2.084(3)	N(1)–Ru(1)–N(2)	173.35(12)
Ru(1)–C(33)	1.864(4)	N(1)–Ru(1)–C(33)	94.42(13)
Ru(1)–C(34)	1.883(4)	N(2)–Ru(1)–C(34)	93.68(13)
C(33)≡O	1.147(4)	C(33)–Ru(1)–C(34)	90.14(16)
C(34)≡O	1.127(4)		

The molecules pack through intra- and intermolecular hydrogen bonds as shown in **Figure 2.6.33**. Respective bond lengths for these interactions are given in **Table 2.6.21**.

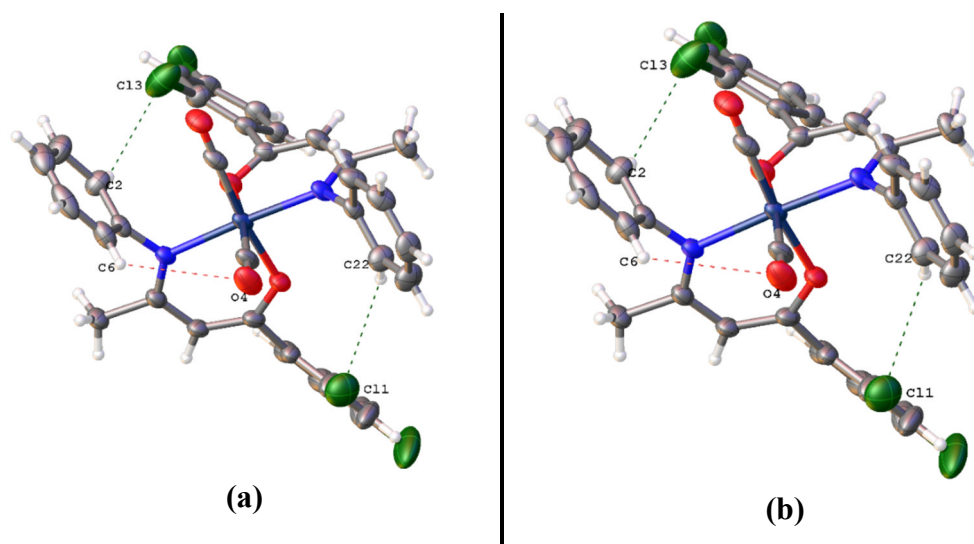


Figure 2.6.33: (a) Intramolecular hydrogen bonds and (b) intermolecular hydrogen bonds in complex, C14

Table 2.6.21: Selected bond lengths for intra- and intermolecular bonding in C14

Interaction	Atoms(A.....D)	Bond length /Å
Intramolecular	C(6)-H.....O(4)	3.833(8)
	C(22)-H.....Cl(1)	3.780(8)
	C(2)-H.....Cl(3)	3.434(8)
Intermolecular	C(31)-H.....O(1)	3.502(8)
	C(22)-H.....Cl(1)	3.781(8)
	π - π interactions (<i>phenolate</i> phenyl rings)	3.730

Additional intermolecular interactions in the form of π - π interactions between the *phenolate* phenyl rings, shown in **Figure 2.6.34**, are observed and participate in the close packing of the molecules.

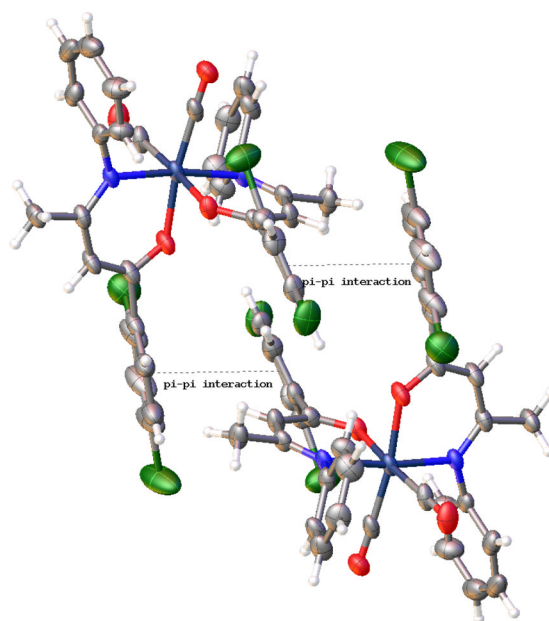


Figure 2.6.34: π - π interactions present in C14

2.6.12 X-Ray characterisation for C15

Complex **C15** crystallised as green plates from slow vapour diffusion of hexane into a concentrated solution of the complex in dichloromethane. The complex crystallised in a monoclinic cell with a single molecule per asymmetric unit cell. Structural solution was performed in the $I2/a$ space group. The molecular structure of **C15** is shown in **Figure 2.6.35**, and selected bond lengths and angles are given in **Table 2.6.22**.

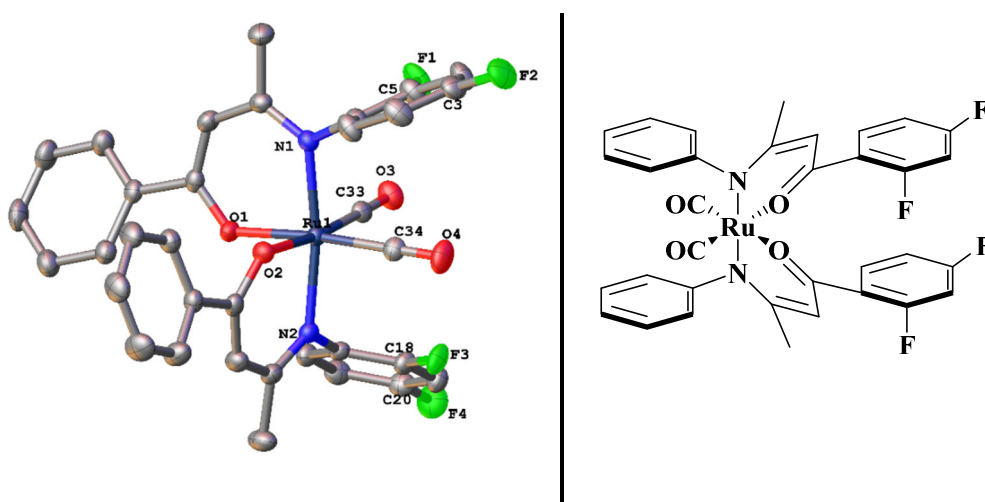
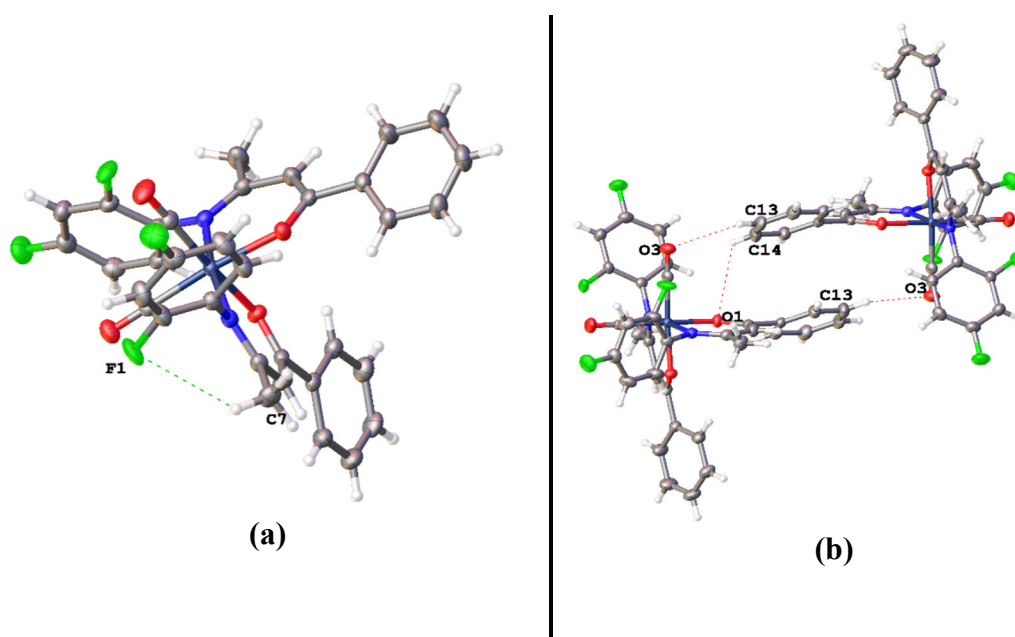


Figure 2.6.35: Molecular structure of **C15**, displacement ellipsoids are at the 50% probability level and hydrogen atoms and disordered parts are omitted for clarity

Table 2.6.22: Selected bond lengths and angles for **C15**

Bond	Distance	Bond	Angle / $^{\circ}$
Ru(1)–O(1)	2.0475(12)	O(1)–Ru(1)–N(1)	90.67(5)
Ru(1)–O(2)	2.0578(12)	O(2)–Ru(1)–N(2)	90.78(5)
Ru(1)–N(1)	2.0827(14)	O(1)–Ru(1)–O(2)	85.29(5)
Ru(1)–N(2)	2.0935(15)	N(1)–Ru(1)–N(2)	171.07(6)
Ru(1)–C(33)	1.8667(18)	N(1)–Ru(1)–C(33)	90.52(7)
Ru(1)–C(34)	1.8795(18)	N(2)–Ru(1)–C(34)	92.71(7)
C(33)≡O	1.141(2)	C(33)–Ru(1)–C(34)	88.65(7)
C(34)≡O	1.134(2)		

Figure 2.6.36 shows intra- and intermolecular hydrogen bonds participating in the close packing of the molecules. Selected bond lengths given in **Table 2.6.23**. There is no evidence of π - π interactions between the phenyl rings of the molecules.

**Figure 2.6.36:** (a) Intramolecular hydrogen bonds and (b) intermolecular hydrogen bonds in complex, **C15****Table 2.6.23:** Selected bond lengths for intra- and intermolecular bonding in **C15**

Interaction	Atoms(A.....D)	Bond length / \AA
Intramolecular	C(7)–H.....F(2)	3.56119(7)
Intermolecular	C(13)–H.....O(1)	3.72628(6)
	C(13)–H.....O(3)	3.47940(6)
	C(14)–H.....O(3)	3.52838(6)

2.7 Conclusion

A range of novel functionalised β -*bis*-ketoiminate ruthenium(II) dicarbonyl complexes, showing *pseudo* octahedral geometry around the Ru(II) centre have been synthesised and characterised, with X-ray crystallographic analysis obtained for most complexes. The synthesis is characterised by the unexpected reduction of ruthenium from Ru(III) to Ru(II) and coordination of carbon monoxide as labile ligands. The carbonyl ligands are proposed to be a result of the base promoted decarbonylation of the solvent, 2-ethoxyethanol. Investigative reactions have shown that the combination of a base (trimethylamine), high reflux temperatures, 2-thoxyethanol (as the solvent) and the ketoiminate ligand are necessary for the formation of the ruthenium(II) dicarbonyl complexes. The complexes all show similar ^1H and $^{13}\text{C}\{^1\text{H}\}$ NMR spectra, with a distinctive splitting of protons in the ortho position of the *aniline* ring (H_2 and H_6 for all complexes) to two different chemical environments. This is supported by space filling models of the crystal structures which show breaking of the symmetry around the *aniline* phenyl ring as a result of steric clash between the *aniline* phenyl ring and the carbonyl ligands. Intra- and intermolecular hydrogen bonding is observed for this series of complexes, with addition π - π stacking seen in some of the complexes. The β -ketoiminate ligands were functionalised to include electron withdrawing groups, electron donating groups and increased steric bulk. These were to allow structure activity relationships to be determined when testing for anti-cancer activity (see **Chapter 4**).

2.8 References

1. R. M. Lord, A. J. Hebden, C. M. Pask, I. R. Henderson, S. J. Allison, S. L. Shepherd, R. M. Phillips and P. C. McGowan, *Journal of Medicinal Chemistry*, 2015, **58**, 4940-4953.
2. R. M. Lord, J. J. Mannion, A. J. Hebden, A. E. Nako, B. D. Crossley, M. W. McMullon, F. D. Janeway, R. M. Phillips and P. C. McGowan, *ChemMedChem*, 2014, **9**, 1136-1139.
3. J. J. Hollick, B. T. Golding, I. R. Hardcastle, N. Martin, C. Richardson, L. J. M. Rigoreau, G. C. M. Smith and R. J. Griffin, *Bioorganic & Medicinal Chemistry Letters*, 2003, **13**, 3083-3086.
4. L. M. Tang, Y. Q. Duan, X. F. Li and Y. S. Li, *Journal of Organometallic Chemistry*, 2006, **691**, 2023-2030.
5. J. Chatt and B. Shaw, Soc Chemical Industry, Editon edn., 1961, pp. 290-290.
6. J. Chatt and B. Shaw, Soc Chemical Industry, Editon edn., 1960, pp. 931-931.
7. Y.-Z. Chen, W. C. Chan, C. P. Lau, H. S. Chu, H. L. Lee and G. Jia, *Organometallics*, 1997, **16**, 1241-1246.
8. J. Chatt, B. Shaw and A. Field, *Journal of the Chemical Society (Resumed)*, 1964, 3466-3475.
9. H. E. Bryndza and W. Tam, *Chemical Reviews*, 1988, **88**, 1163-1188.
10. O. Blum and D. Milstein, *Journal of the American Chemical Society*, 1995, **117**, 4582-4594.
11. F. A. Bassyouni, S. M. Abu-Bakr, K. H. Hegab, W. El-Eraky, A. A. El Beih and M. E. A. Rehim, *Research on Chemical Intermediates*, 2012, **38**, 1527-1550.
12. M. Bruce, R. Gardner and J. Howard, *Journal of Chemical Society, Dalton Transactions*, 1977, **621**.

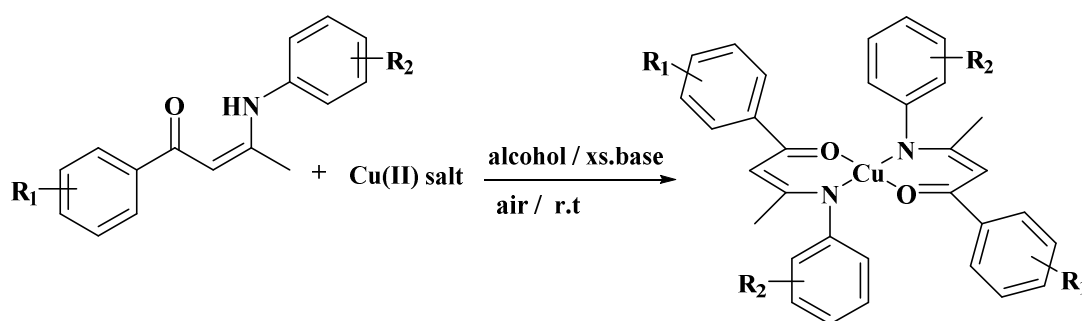
13. R. E. Cobblestick, F. W. Einstein, R. K. Pomeroy and E. R. Spetch, *Journal of Organometallic Chemistry*, 1980, **195**, 77-88.
14. J. Niesel, A. Pinto, H. W. P. N'Dongo, K. Merz, I. Ott, R. Gust and U. Schatzschneider, *Chemical Communications*, 2008, 1798-1800.
15. M. R. Churchill, R. A. Lashewycz and F. J. Rotella, *Inorganic Chemistry*, 1977, **16**, 265-271.
16. J. P. Selegue, *Organometallics*, 1982, **1**, 217-218.

Chapter 3
Synthesis and Characterisation of Functionalised
 β -*bis*-Ketoiminate Copper(II) Complexes

3.1 Introduction to β -bis-Ketoiminate Copper(II) Complexes

Ketoiminate ligands (discussed briefly in **Chapter 2**) are analogues of β -diketonates in which one of the oxygen atoms has been replaced by an amine group.¹ Despite being known in the literature for a number of years,² β -ketoiminate ligands have only received attention over the last few years. This interest is due to their simplicity, ease of preparation and ease of modification of both steric and electronic properties.³⁻⁵ Examples of ketoiminate ligands with nickel, titanium, iridium, ruthenium and cobalt have been studied and reported,⁶⁻¹⁰ however little has been reported on their complexes with copper.^{11, 12} Copper complexes with bidentate, tridentate or tetradentate (*N,O*) ligands have found wide application in many fields, particularly in catalysis and polymerisation.^{1, 11, 13-17}

Most of the *bis*-ketoiminate copper complexes reported in the literature are in the +2 oxidation state and exhibit a square planar geometry. These complexes were prepared through the reaction of a copper source, for example, $\text{Cu}(\text{NO}_3)_2 \cdot 3\text{H}_2\text{O}$ with a Schiff base ligand in a protic solvent under reflux or at room temperature.¹⁷ Alternatively, Stabnikov *et al.* have synthesised copper *bis*-ketoiminate complexes in moderate yields by reacting copper acetate with the ketoiminate ligands in aqueous alcohol in the presence of excess ammonia (**Scheme 3.1.1**).¹⁸ This procedure has since become the most popular synthetic procedure for metal ketoiminate complexes.

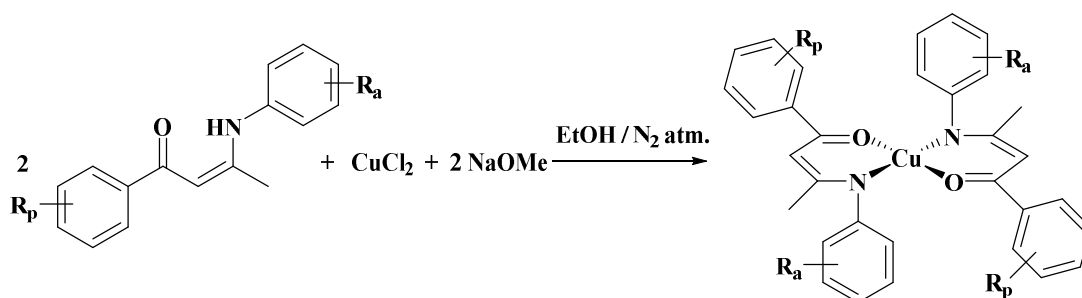


Scheme 3.1.1: General literature procedure for the synthesis of β -*bis*-ketoiminate Cu(II) complexes

Archer *et al.* have shown that the use of a base in the synthesis of these complexes is important, as reactions without base did not yield the desired product.¹⁹

3.2 Synthesis of β -bis-Ketoiminate Copper(II) Complexes

With slight modifications to the synthetic route discussed above (**Scheme 3.1.1**), novel β -bis-ketoiminate copper(II) complexes have been synthesised according to **Scheme 3.2.1**. These complexes, shown in **Figure 3.2.1**, were synthesised from the reaction of one equivalent of copper(II) chloride with two equivalents of the ketoiminate ligand and two equivalents of sodium methoxide as the base.



Scheme 3.2.1: Synthetic route for β -bis-ketoiminate copper(II) complexes in this chapter

Reactions under aerobic and anaerobic conditions both gave the desired product although reactions under anaerobic conditions gave a purer product, without need for intensive isolation and purification steps. As a result all reactions were carried out under an atmosphere of nitrogen. Reactions in the absence of a base did not result in any isolable product

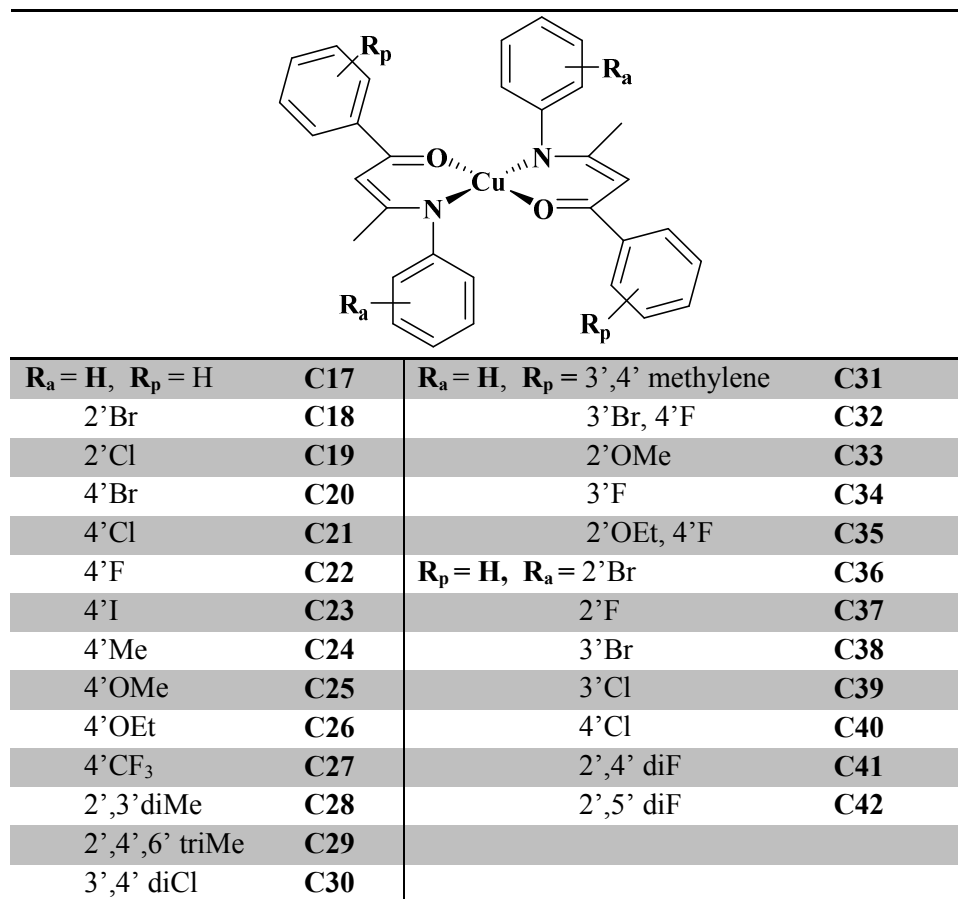


Figure 3.2.1: β -Ketoiminato copper(II) complexes synthesised by the author

Complexes **C17-C42** were obtained as brown or black solids in moderate to high yields. The complexes are air stable, soluble in chlorinated solvents and sparingly soluble in ethanol, acetonitrile and diethyl ether. They are however insoluble in water, hexane and pentane. The resulting solids were further purified by slow vapour diffusion of hexane or pentane into a solution of the complex in dichloromethane.

3.3 Characterisation of β -bis-Ketoiminato Copper(II) Complexes

With a +2 oxidation state, the copper complexes have a d^9 configuration and are paramagnetic. After purification the complexes were analysed by mass spectrometry, elemental analysis and X-ray crystallography. Paramagnetic NMR was also done, although no conclusive data was obtained.

3.3.1 X-Ray crystallography β -bis-ketoiminato Copper(II) complexes

Single crystals suitable for X-ray crystallography for all complexes were obtained by slow vapour diffusion of hexane or pentane into a concentrated solution of the

complex in dichloromethane, at room temperature. Typical shapes for these complexes were either brown/black plates/blocks, although in some cases irregular shaped crystals were obtained. The crystal structures of all the complexes show a 2:1 ligand to metal ratio.

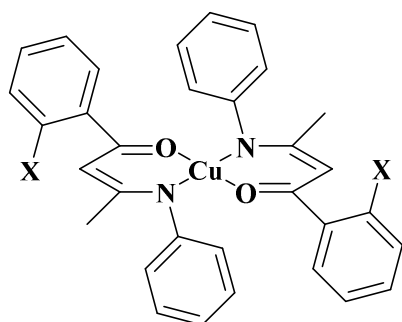
The crystallographic data for copper complexes **C17-C42** are shown in **Figure 3.3.1**. Complexes crystallised in either monoclinic, triclinic or orthorhombic cell systems, with half, one or two molecules in the asymmetric unit. A summary of the respective structural solutions and space groups is given in **Table 3.3.1**. Selected bond lengths and angles are stated in **Table 3.3.2** and **Table 3.3.3** respectively.

Table 3.3.1: X-ray crystallography data for Cu(II)(acnac)₂ complexes

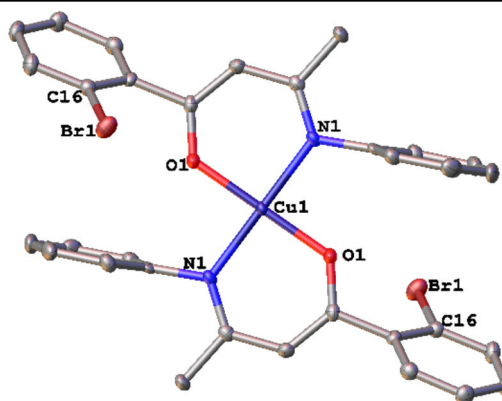
Complex	Z	Cell type	Space group
C17	4	orthorhombic	P2 ₁ 2 ₁ 2 ₁
C18	2	triclinic	P-1
C19	4	monoclinic	I2/a
C20	4	orthorhombic	P2 ₁ 2 ₁ 2 ₁
C21	4	monoclinic	I2/a
C22	2	monoclinic	P2 ₁ /n
C23	4	orthorhombic	P2 ₁ 2 ₁ 2 ₁
C24	4	monoclinic	I2/a
C25	4	orthorhombic	Pbca
C26	2	triclinic	P-1
C27	2	monoclinic	P2 ₁ /c
C28	8	orthorhombic	Pbca
C29	4	monoclinic	P2 ₁ /n
C30	4	monoclinic	C2/c
C31	2	monoclinic	P2 ₁ /n
C32	4	monoclinic	C2/c
C36	4	monoclinic	I2/a
C37	4	monoclinic	I2/a
C40	2	monoclinic	P2 ₁ /n
C41	2	monoclinic	P2 ₁ /n
C42	4	monoclinic	P2 ₁ /n

Four coordinate Cu(II) complexes are usually characterised by either square planar or distorted (flattened) tetrahedron geometry.^{11, 20} In addition, steric and electronic effects due to the substituents on the ligand may influence the planarity observed in the molecular structure. The molecular structures for this series of complexes, given

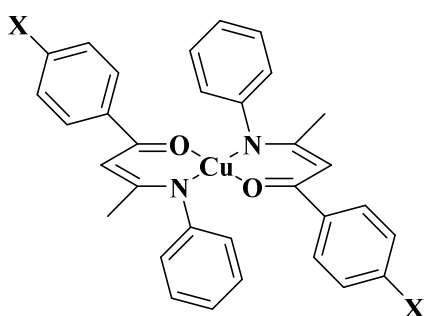
in **Figure 3.3.1**, shows that the metal centre is four-coordinated by two phenolate oxygen atoms and two imine nitrogen atoms from the ketoiminate ligands. These ketoiminate ligands coordinate to the copper(II) centre in the sterically favoured O-Cu-O and N-Cu-N *trans* geometries. A distorted square planar geometry is thus observed for all complexes as shown by the unequal metal-ligand bond distances and angles (**Table 3.3.2** and **Table 3.3.3**). The distortion can be attributed to the restrictions imposed by the chelating effects of the bidentate ketoiminate ligands.



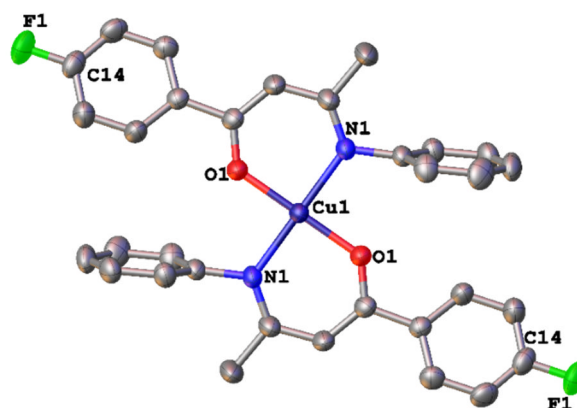
C18, X = Br; **C19**, X = Cl;
C33, X = 2'OMe



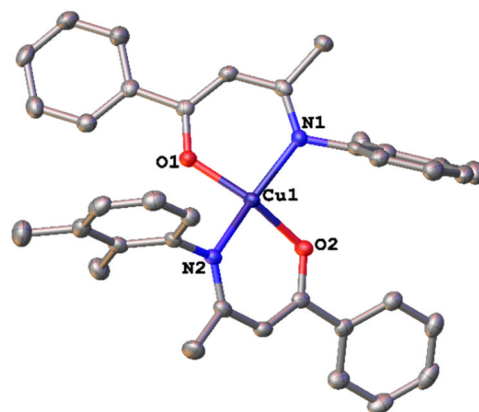
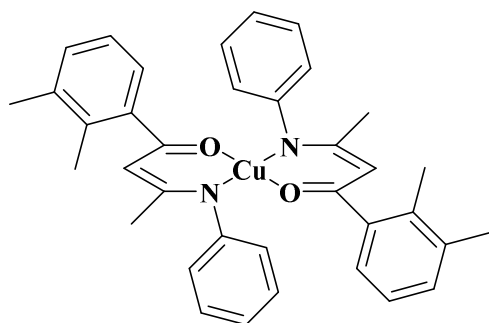
C18, X = Br



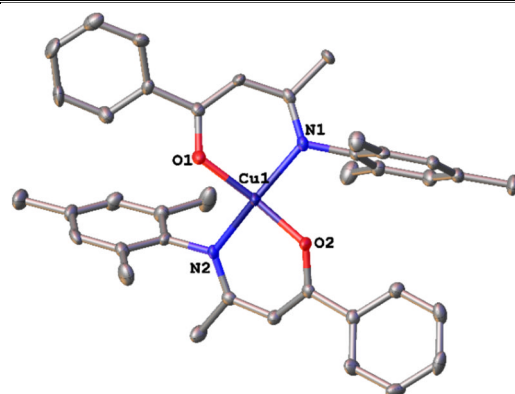
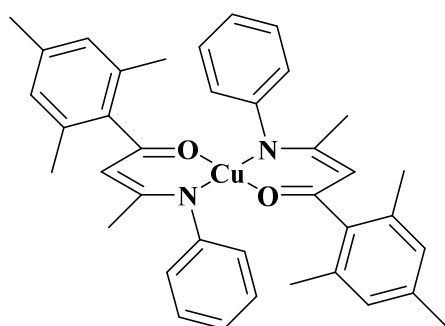
C20, X = Br; **C21**, X = Cl;
C22, X = F; **C23**, X = I;
C24, X = Me; **C25**, X = OMe;
C26, X = OEt; **C27**, X = CF₃



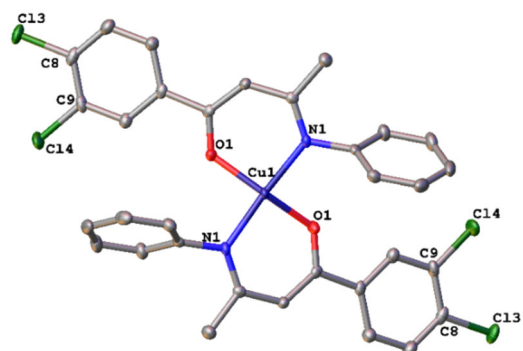
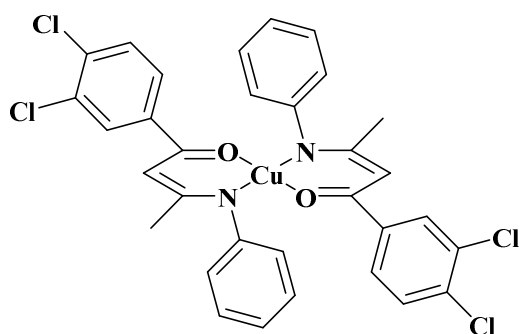
C22, X = F



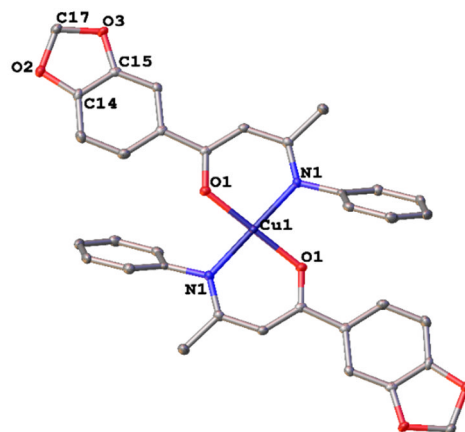
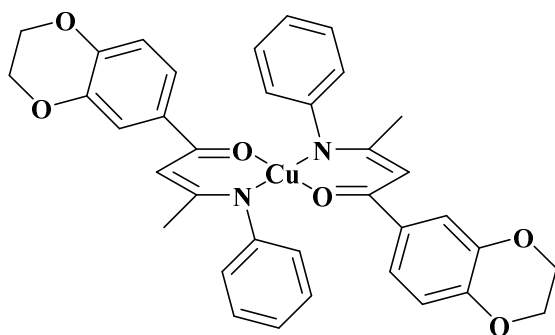
C28



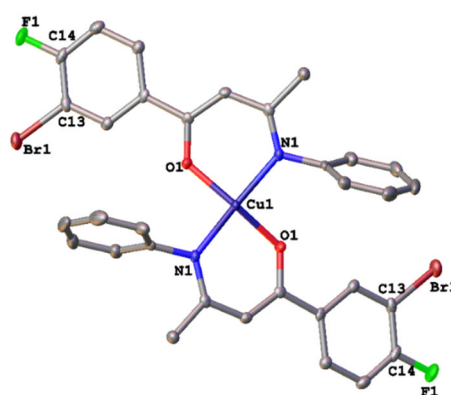
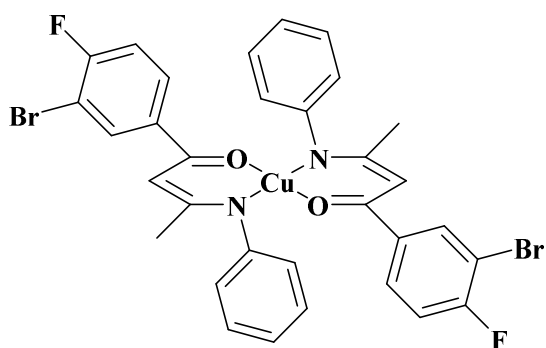
C29



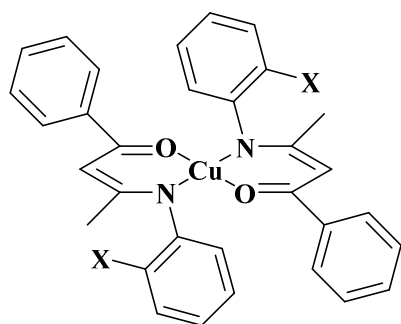
C30



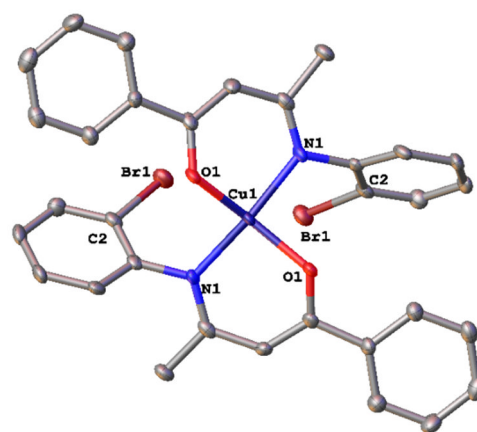
C31



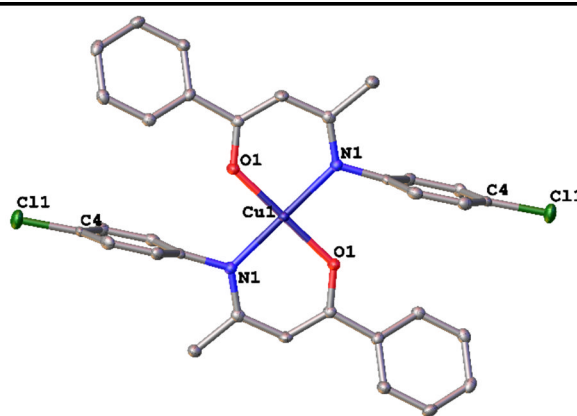
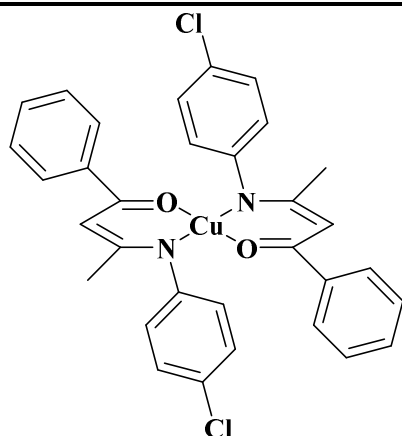
C32



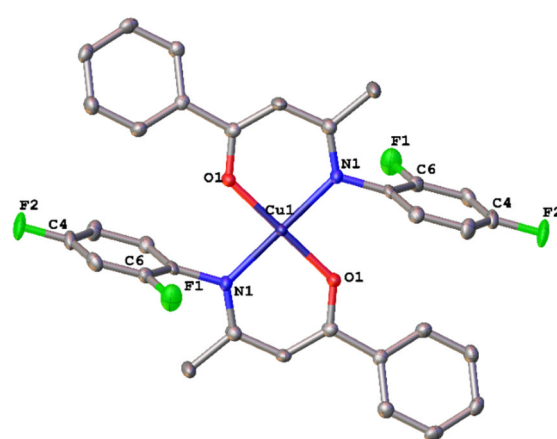
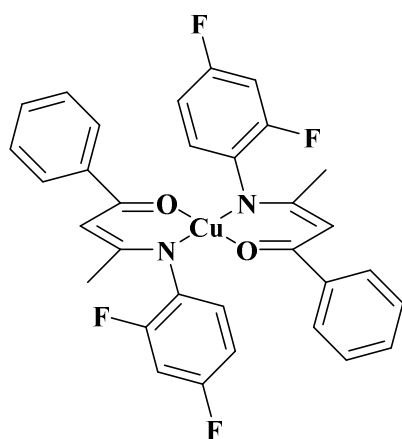
C36, X = Br; C37, X = F



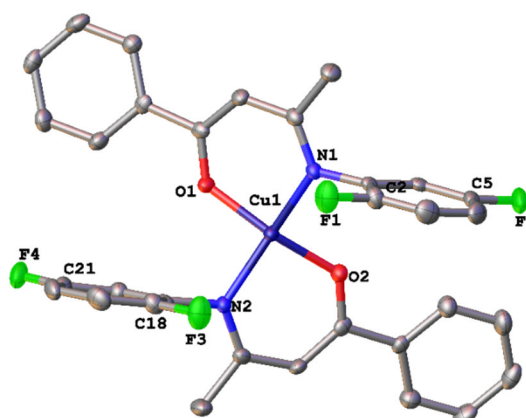
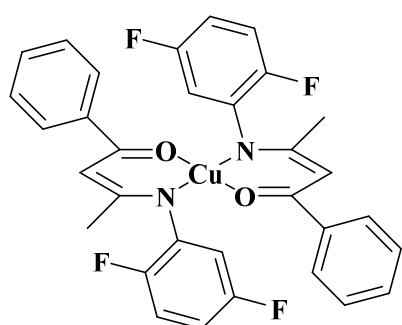
C36, X = Br



C40



C41



C42

Figure 3.3.1: Molecular structures of complexes C17-C32 and C36-C42. Displacement ellipsoids are at the 50 % probability level. Hydrogen atoms and co-crystallising solvent molecules are omitted for clarity. For C19, C26 and C27 only one part of major disordered components is shown

The copper-phenolate oxygen and copper-imine nitrogen bonds lengths are in the ranges 1.89 – 1.91 Å and 1.96 – 2.03 Å respectively (**Table 3.3.2**). This is consistent with related copper(II) ketoiminate complexes found in the literature.¹⁷ Relative bond angles are in the range 88.8 – 94.5°, deviating from the expected 90°, in agreement with the distorted square planar geometry prediction.

Table 3.3.2: Selected bond lengths Cu(II)(acnac)₂ complexes

	Bond Length / Å				
	Cu(1)-N(1)	Cu(1)-N(2)	Cu(1)-O(1)	Cu(1)-O(2)	C-Halogen
C17	1.991(4)	1.987(4)	1.909(4)	1.913(3)	-
C18^a	1.989(3)	1.989(3)	1.899(2)	1.899(2)	1.898(4)
C19^a	1.969(4)	1.969(4)	1.910(3)	1.910(3)	1.737(6)
C20	1.997(4)	1.989(4)	1.904(3)	1.902(3)	1.900(5)
C21^a	1.9773(15)	1.9773(15)	1.8983(13)	1.8983(13)	1.7459(19)
C22^a	2.0042(14)	2.0042(14)	1.8935(12)	1.8935(12)	1.354(2)
C23	1.994(5)	2.002(4)	1.908(4)	1.902(4)	2.108(5)
C24^a	1.9751(18)	1.9751(18)	1.9009(14)	1.9009(14)	-
C25^a	1.998(2)	1.998(2)	1.9054(19)	1.9054(19)	1.294(3)
C26	1.976(2)	1.9745(19)	1.8984(16)	1.8922(17)	1.370(3)
C27^a	2.004(4)	2.004(4)	1.910(3)	1.910(3)	1.368(10)
C28	1.9558(19)	1.9652(18)	1.9021(16)	1.9169(16)	-
C29	1.973(4)	1.974(4)	1.907(4)	1.892(3)	-
C30^a	1.986(2)	1.986(2)	1.8966(19)	1.8965(19)	1.735(3)
C31^a	2.014(2)	2.014(2)	1.9172(17)	1.9172(17)	1.383(3)
C32^a	1.977(2)	1.977(2)	1.9053(17)	1.9053(17)	1.886(3)
C36^a	1.979(3)	1.979(3)	1.906(3)	1.906(3)	1.896(5)
C37^a	1.966(2)	1.966(2)	1.9071(19)	1.9071(19)	1.345(4)
C40^a	1.9945(19)	1.9945(19)	1.8978(17)	1.8978(17)	1.750(2)
C41^a	1.998(2)	1.998(2)	1.8965(19)	1.8965(19)	1.340(4)
C42	1.968(2)	1.966(2)	1.9080(18)	1.9148(18)	1.360(3)

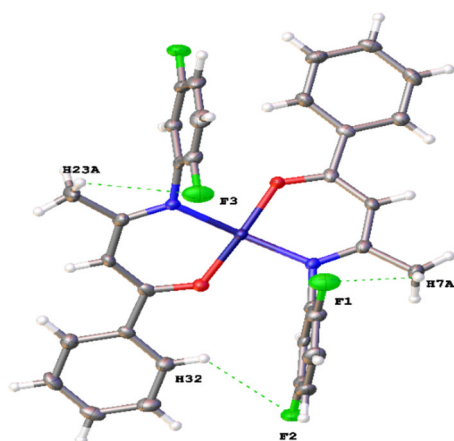
^a = half molecule in asymmetric unit

Table 3.3.3: Selected bond angles Cu(II)(acnac)₂ complexes

	Angles / °			
	O(1)-Cu(1)-N(1)	O(1)-Cu(1)-N(2)	O(1)-Cu(1)-O(2)	N(1)-Cu(1)-N(2)
C17	91.78(16)	87.92(16)	172.93(18)	175.6(2)
C18^a	91.98(11)	88.02(11)	180.0	180.00(17)
C19^a	93.83(15)	89.77(15)	155.7(2)	162.8(2)
C20	92.22(15)	89.23(15)	174.25(17)	175.06(18)
C21^a	93.85(6)	92.54(6)	148.92(9)	155.98(9)
C22^a	91.51(6)	88.49(6)	180.0	180.0
C23	91.62(17)	87.66(17)	174.53(19)	174.3(2)
C24^a	94.20(7)	92.43(7)	148.84(9)	155.15(10)
C25^a	90.86(8)	89.14(8)	180.0	180.0
C26	93.65(8)	92.43(7)	148.77(7)	155.05(8)
C27^a	90.97(14)	89.03(14)	180.00(18)	180.0
C28	94.07(7)	92.16(7)	149.64(7)	155.87(8)
C29	93.69(17)	92.33(17)	153.50(17)	154.49(19)
C30^a	93.83(9)	93.83(9)	152.00(15)	158.11(15)
C31^a	90.86(8)	89.14(8)	180.0	180.00(11)
C32^a	93.03(8)	91.18(8)	155.46(11)	160.09(12)
C36^a	94.59(13)	94.59(13)	146.2(2)	158.2(2)
C37^a	93.92(9)	92.05(9)	149.73(13)	156.98(14)
C40^a	92.03(7)	87.97(7)	180.0	180.0
C41^a	91.46(9)	88.54(9)	180.0	180.0
C42	92.86(8)	92.69(8)	148.90(9)	153.38(10)

^a = half molecule in asymmetric unit

For this series of complexes, intramolecular hydrogen bonding is absent in all complexes with the exception of complex **C42**. Complex **C42**, shows intramolecular hydrogen bonding between the fluorine substituents in the *aniline* ring and the C-H in the *phenolate* ring (**Figure 3.3.2**).



Atom (A...D)	Bond length / Å
C(23)-H...F(3)	3.757(4)
C(7)-H...F(1)	3.366(4)
C(32)-H...F(2)	3.533(3)

Figure 3.3.2: Intramolecular hydrogen bonding seen in complex **C42**

Non-classical intermolecular hydrogen bonds between the *phenolate* oxygen atom and methyl protons on carbon atom C7 (shown in **Figure 3.3.3**) are common for all complexes. Typical bond lengths for such interactions are in the range of 3.40- 3.85 Å. Selected examples, complexes **C20** and **C25** are shown in **Figure 3.3.3**.

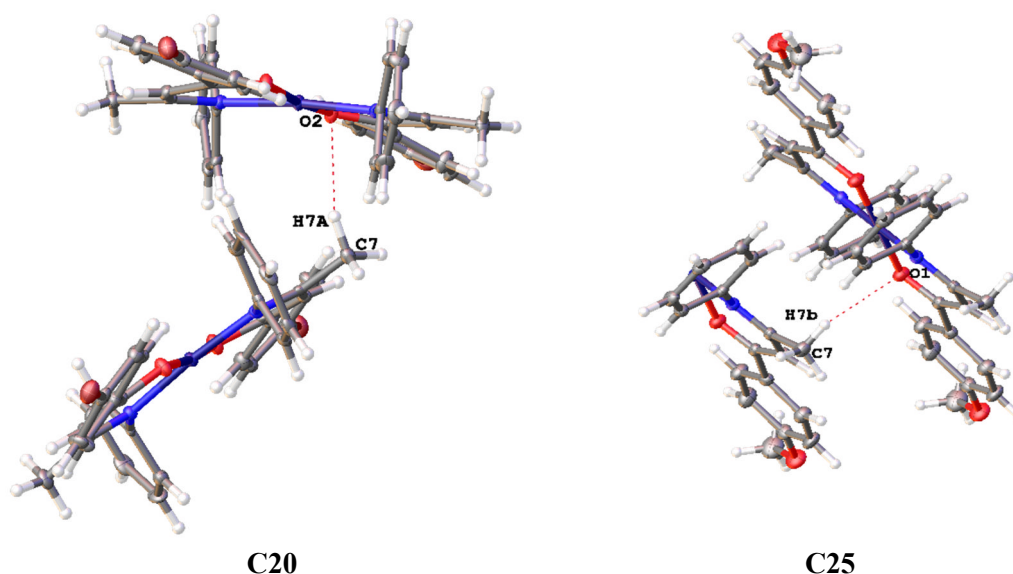
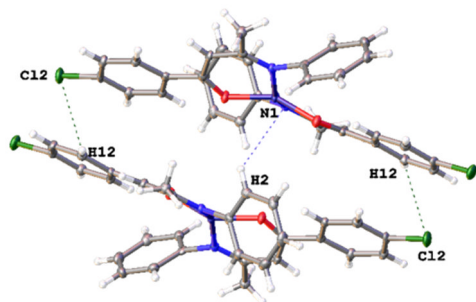


Figure 3.3.3: Intermolecular hydrogen bonding

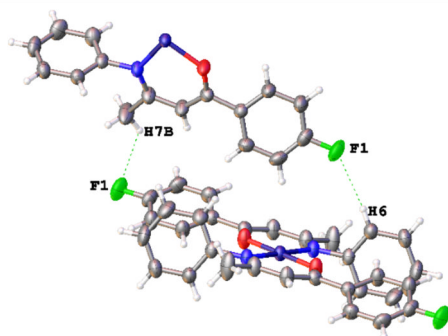
Other non-classical hydrogen bonds as a result of the substituents on the *phenolate* or *aniline* phenyl rings are observed. In many cases the molecules are predominantly linked together through this type of hydrogen bonds. These substituents form hydrogen bonds with C(H) hydrogen atoms in the phenyl rings (**Figure 3.3.4**) or with the C(H) hydrogen atoms of carbon atom C7 (**C22** in **Figure 3.3.4**). Selected non-classical hydrogen bond lengths are given in **Figure 3.3.4**. Although other

authors have reported coupling of similar complexes through weak $\text{Cu}\cdots\text{H}$ contacts,¹ no such interactions were observed for this particular series of complexes.



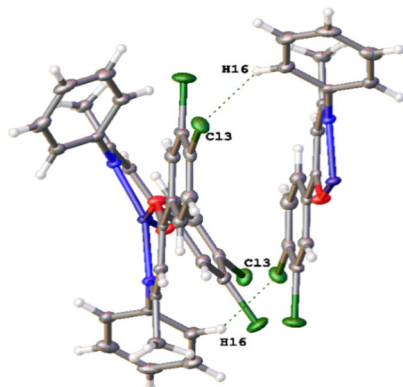
C21

Atom (A...D)	Bond length / Å
C(12)-H \cdots Cl(2)	3.806(3)
C(2)-H \cdots N(1)	3.691(3)



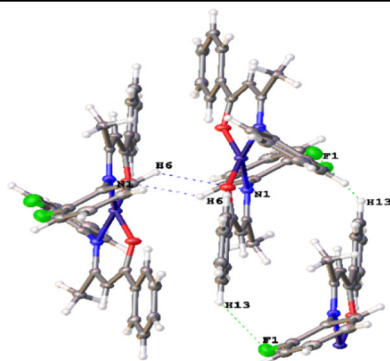
C22

Atom (A...D)	Bond length / Å
C(6)-H \cdots F(1)	3.538(2)
C(7B)-H \cdots F(1)	3.605(3)



C30

Atom (A...D)	Bond length / Å
C(13)-H \cdots Cl(3)	3.645(3)



C37

Atom (A...D)	Bond length / Å
C(13)-H \cdots F(1)	3.344(4)
C(6)-H \cdots N(1)	3.679(4)

Figure 3.3.4: Intermolecular hydrogen bonding with substituents

All the complexes show close packing crystal arrangement, with selected examples shown in **Figure 3.3.5**. There is no evidence of π - π interactions and some complexes showing herringbone arrangement along the c-axis, **Figure 3.3.6**.

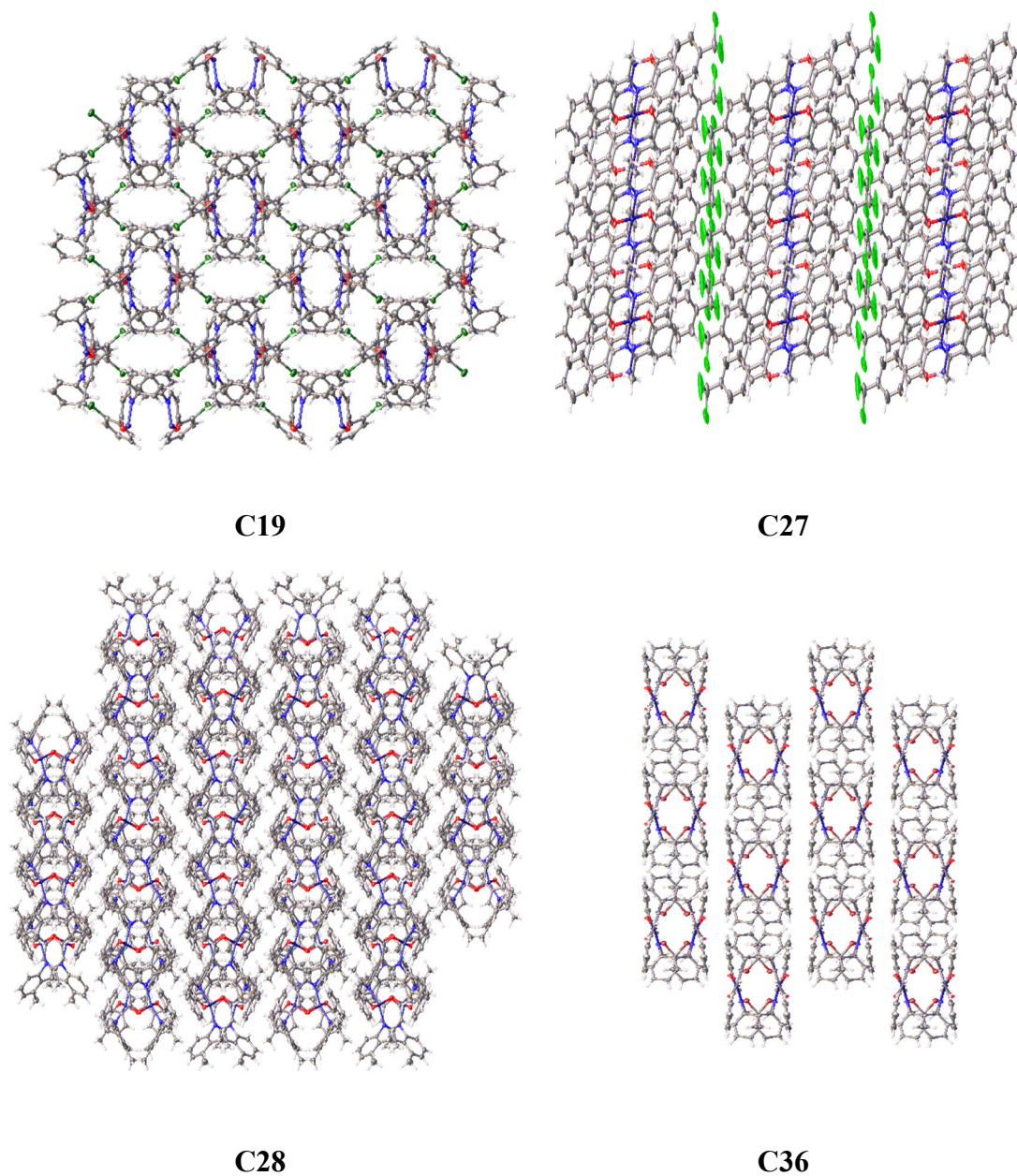
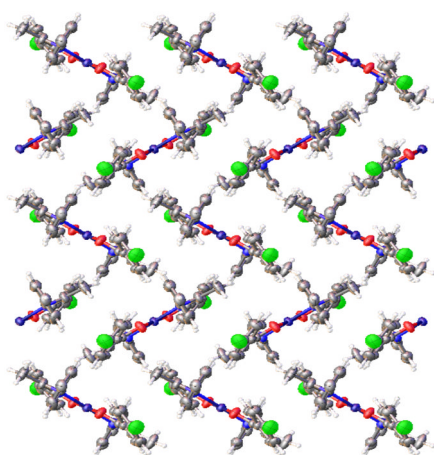
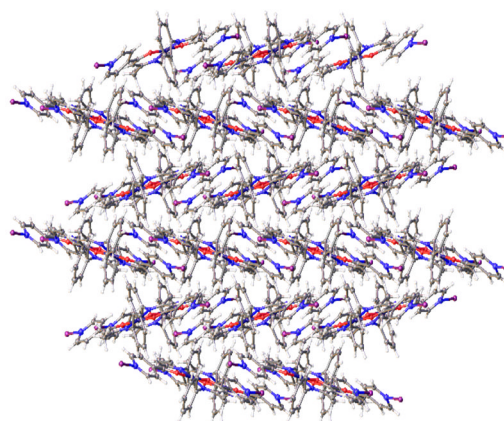
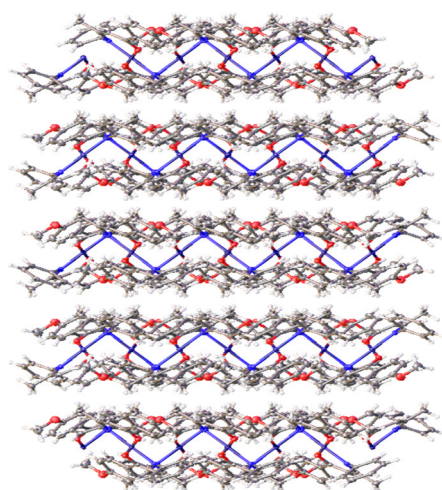
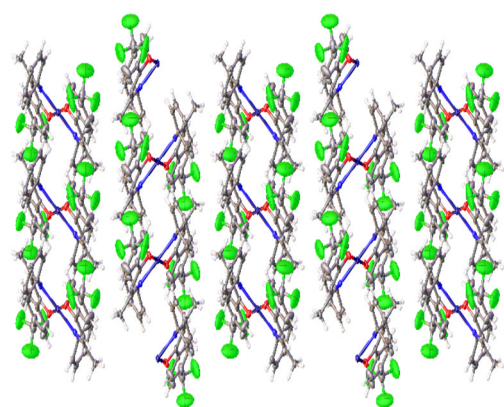
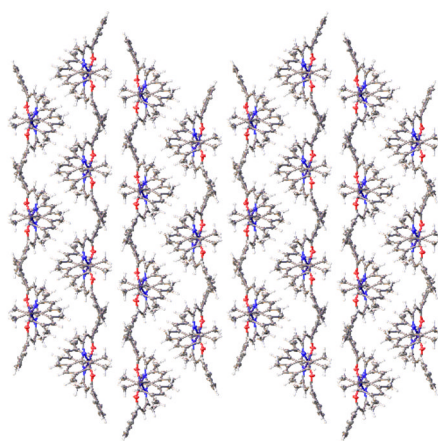
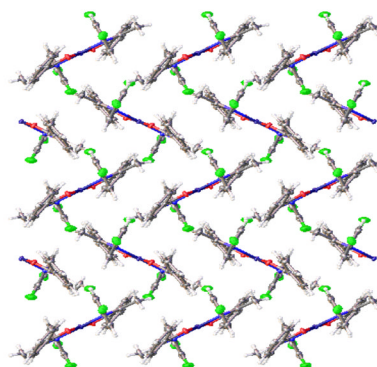


Figure 3.3.5: Selected examples of crystal close packing arrangement

**C22****C23****C25****C27****C29****C41****Figure 3.3.6:** Herringbone crystal packing arrangement observed in some complexes

3.4 Conclusion

This chapter presents the synthesis and characterisation of a range of novel functionalised β -bis-ketoiminate copper(II) *pseudo* square planar complexes, with X-ray crystallographic analysis obtained for all complexes. Synthesis of the complexes is possible under both aerobic or inert conditions; reactions under inert atmosphere allowed for reproducible synthesis and was adopted for all complexes. This range of complexes show bidentate (N,O) coordination around the copper(II) centre with the ligands *trans* to each other. Crystallographic data shows that these complexes have close packing crystal arrangement with some complexes showing interesting herringbone packing, as well as intermolecular hydrogen bonding between molecules. The efficacy of these complexes as anti-cancer agents and catalysts is discussed in **Chapter 4** and **Chapter 6** respectively.

3.5 References

1. I. A. Baidina, P. A. Stabnikov, A. D. Vasiliev, S. A. Gromilov and I. K. Igumenov, *Journal of Structural Chemistry*, 2004, **45**, 671-677.
2. G. W. Everett and R. H. Holm, *Proceedings of the Chemical Society*, 1964, 238-239.
3. X. He, Y. Yao, X. Luo, J. Zhang, Y. Liu, L. Zhang and Q. Wu, *Organometallics*, 2003, **22**, 4952-4957.
4. X.-F. Li, K. Dai, W.-P. Ye, L. Pan and Y.-S. Li, *Organometallics*, 2004, **23**, 1223-1230.
5. S.-M. Yu and S. Mecking, *Journal of the American Chemical Society*, 2008, **130**, 13204-13205.
6. G. W. Everett and R. H. Holm, *Journal of the American Chemical Society*, 1966, **88**, 2442-2451.
7. R. E. Ernst, M. J. O'Connor and R. H. Holm, *Journal of the American Chemical Society*, 1967, **89**, 6104-6113.
8. G. W. Everett and R. H. Holm, *Journal of the American Chemical Society*, 1965, **87**, 2117-2127.
9. R. A. Maya, A. Maity and T. S. Teets, *Organometallics*, 2016, **35**, 2890-2899.
10. R. M. Lord, A. J. Hebden, C. M. Pask, I. R. Henderson, S. J. Allison, S. L. Shepherd, R. M. Phillips and P. C. McGowan, *Journal of Medicinal Chemistry*, 2015, **58**, 4940-4953.
11. X. Xiao, Y. C. Wen, X. J. Wang, L. Lei, P. Xia, T. C. Li, A. Q. Zhang and G. Y. Xie, *Russian Journal of Coordination Chemistry*, 2015, **41**, 543-548.
12. G. Xie, W. Song, T. Li, X. Xu, Z. Lan, Y. Li and A. Zhang, *Journal of Applied Polymer Science*, 2014, **131**.
13. K. C. Joshi and B. S. Joshi, *Synthesis and Reactivity in Inorganic and Metal-Organic Chemistry*, 1986, **16**, 1009-1024.

14. A. Kumar, R. Pandey, R. K. Gupta, M. Dubey and D. S. Pandey, *Dalton Transactions*, 2014, **43**, 13169-13173.
15. B. Vidjayacoumar, D. J. H. Emslie, S. B. Clendenning, J. M. Blackwell, J. F. Britten and A. Rheingold, *Chemistry of Materials*, 2010, **22**, 4844-4853.
16. S. Saha, S. Jana, S. Gupta, A. Ghosh and H. P. Nayek, *Polyhedron*, 2016, **107**, 183-189.
17. G. Grivani, M. Vakili, A. D. Khalaji, G. Bruno, H. A. Rudbari and M. Taghavi, *Journal of Molecular Structure*, 2016, **1116**, 333-339.
18. P. A. Stabnikov, I. A. Baidina, S. V. Sysoev, N. S. Vanina, N. B. Morozova and I. K. Igumenov, *Journal of Structural Chemistry*, 2003, **44**, 1054-1061.
19. R. D. Archer, *Inorganic Chemistry*, 1963, **2**, 292-294.
20. R. Knoch, A. Wilk, K. J. Wannowius, D. Reinen and H. Elias, *Inorganic Chemistry*, 1990, **29**, 3799-3805.

Chapter 4

Biological investigations on β -*bis*-Ketoiminate analogue Complexes of Ruthenium and Copper

4.1 Introduction to biological studies

The discovery of new anti-cancer drugs generally follows conventional well known stages in the drug discovery and development process. The preliminary non-clinical stages are not limited to, but include, identification and validation of a drug target, assay development and identification of lead compounds and their optimisation. The lead compounds, defined as molecules that show efficacy towards the biological target are identified by screening a large library of compounds against functional assays or known biological targets. The lead compounds are then modified to produce other compounds with a better profile of desirable properties compared to unwanted properties. Such properties include water solubility, potency and stability. Successful candidates are then taken further into clinical trials, where properties such as pharmacokinetics, pharmacodynamics and toxicity are evaluated.¹⁻⁵

4.2 Cytotoxicity

Biological assays such as *in vitro* cytotoxicity screening are widely used to measure the effectiveness of drug candidates against a variety of human cancer cell lines and to identify potential drugs for further analysis. Drug candidates can be classified as inactive, moderately active or highly active based on their IC₅₀ values. The IC₅₀ value is defined as the concentration of the drug required to inhibit 50% of cell proliferation. The cytotoxicity of the drug candidates can be monitored using the MTT⁶ or SRB⁷ assays.

This chapter briefly describes the theory behind the MTT assay followed by an evaluation of the potency of novel ruthenium carbonyl and copper ketoiminate complexes synthesised by the author, under both normoxic and hypoxic conditions.

4.2.1 MTT Assay

The well know, rapid colorimetric tetrazolium salt based MTT assay was developed in 1983 by Mosmann.⁶ It is used to measure mammalian cytotoxicity, cell survival and proliferation by the use of a yellow water soluble 3-(4,5-dimethylthiazol-2-yl)-2,5-diphenyltetrazoliumbromide (MTT) salt which is reduced in living cells to purple or dark blue formazan crystals that are water insoluble. This reduction involves the

pyridine nucleotide cofactors, NADP and NADPH, which appears as the basis of established *in vitro* cell viability assays (**Figure 4.2.1**). The formazan crystals formed are solubilised and the colour quantified using a scanning multiwell spectrophotometer (TECAN) reader. The amount of formazan formed is directly proportional to the number of metabolically viable cells present after the MTT exposure.⁸

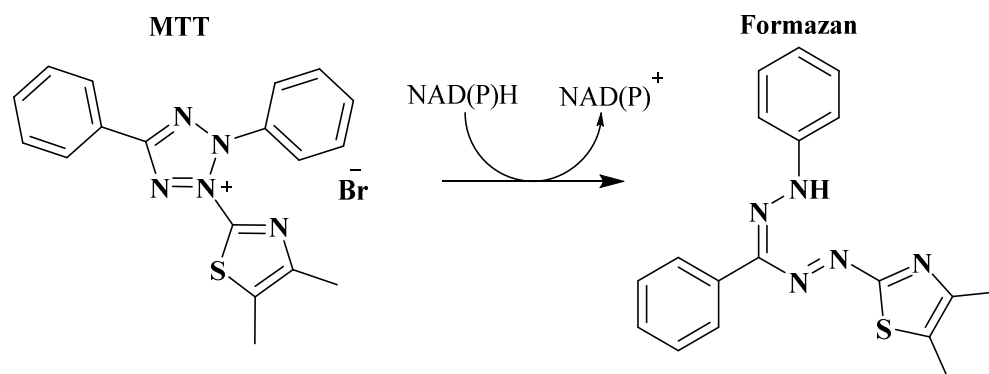


Figure 4.2.1: Reduction of yellow MTT salt to purple formazan

Mitochondrial succinate dehydrogenase in living cells have been implicated in the reduction of MTT, as a result the sites for reduction and formation of the formazan were thought to be the mitochondria. However recent studies show that the non-mitochondria, cytosolic enzymes which utilise NADH/NADPH are also responsible for MTT reduction.⁹

4.3 Results and Discussion

4.3.1 Cytotoxicity of β -bis-Ketoiminate Ru(II) Dicarbonyl Complexes

The cytotoxicity of β -bis-ketoiminate ruthenium(II) dicarbonyl complexes described in **Chapter 2** with the general structure shown in **Figure 4.3.1** were evaluated on two cancerous cell lines, MIA PaCa-2 (human pancreatic carcinoma) and HCT116++ (human colon carcinoma) and on one non-cancerous cell line, ARPE19 (human retinal pigment epithelial cell). All the biological work was done at The University of Huddersfield by Pablo Carames-Mendez in collaboration with Professor Roger Phillips.

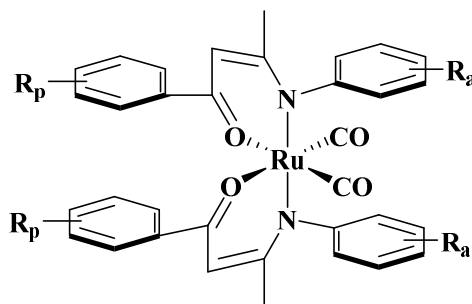


Figure 4.3.1: β -Bis-ketoiminate Ru(II) dicarbonyl complexes under investigation

A 96 hour MTT assay at 37°C in an atmosphere of 5% CO₂ was carried out on the ruthenium carbonyl complexes at various concentrations, ranging from 100 μ M to 0.046 μ M. After incubation and addition of MTT, cell survival was determined by measuring the absorbance at 540 nm. All cytotoxicity assays were performed in triplicate. The IC₅₀ values of the complexes were obtained from plotting graphs of % cell survival against drug concentration (μ M).

The results for the cytotoxicity evaluation of β -bis-ketoiminate Ru(II) dicarbonyl complexes, **C1-C16**, are summarised in **Table 4.3.1** and **Figure 4.3.2**. The complexes vary in their cytotoxicity, with active complexes highlighted in red (IC₅₀ = < 25 μ M) and moderately active complexes in green (IC₅₀ = 25-60 μ M) (**Table 4.3.1**). In all assays, values are compared to the values of cisplatin and oxaliplatin.

The ruthenium(II) dicarbonyl complexes display a wide range of potency against all three cell lines. These complexes are generally inactive against the Mia PaCa-2 cell line, with a decrease in IC₅₀ values observed for HCT116++ cell lines. This is most evident with complexes **C3** and **C4** in which the IC₅₀ values are 96.05 μ M (for **C3**) and > 100 μ M (for **C4**) for Mia PaCa-2 cell line compared to 43.40 μ M (for **C3**) and 21.61 μ M (for **C4**) for HCT116++ cell line. This is true for all for complexes except **C7**, **C14** and **C16** which are inactive against both cell lines. The most active complexes, **C3**, **C4**, **C8** and **C12** (highlighted in **Table 4.3.1**) show poor selectivity towards ARPE19 cell line and are as cytotoxic as they are toxic.

Table 4.3.1: IC₅₀ values of Ru(II) dicarbonyl complexes

Complex	Substituent (R _p /R _a)	IC ₅₀ /μM		
		Mia PaCa-2	HCT116++	ARPE19
C1	H(p)	89.37±9.31	85.96±22.07	92.01±13.84
C2	4'Br(p)	92.89±12.31	68.21±11.04	82.40±21.32
C3	4'Cl(p)	96.05±6.84	43.40±5.67	50.98±2.54
C4	4'F(p)	>100	21.61±3.55	37.74±8.59
C5	3'F(p)	>100	65.29±19.49	>100
C6	3'Br(p)	>100	96.01±6.91	>100
C7	3',4' diCl(p)	>100	>100	>100
C8	4'Me(p)	>100	54.20±14.00	51.62±12.28
C9	3'Me(a)	>100	64.80±16.19	>100
C10	4'F(a)	91.80±14.20	66.79±6.84	88.59±19.76
C11	4'Cl(a)	>100	71.90±5.62	>100
C12	2'F(a)	61.49±9.64	59.50±6.53	77.50±20.17
C13	3'Br(a)	84.02±19.23	81.61±8.07	90.18±17.01
C14	2',4' diCl(a)	>100	>100	>100
C15	2',4' diF(a)	80.90±11.82	63.31±7.84	78.61±25.15
C16	2',3' diMe(a)	>100	>100	>100
cisplatin		3.62±0.74	3.26±0.38	6.41±0.95
oxaliplatin		6.44±1.05	0.93±0.12	6.15±2.68

(p) = substituent on *phenolate* ring; (a) = substituent on *aniline* ring

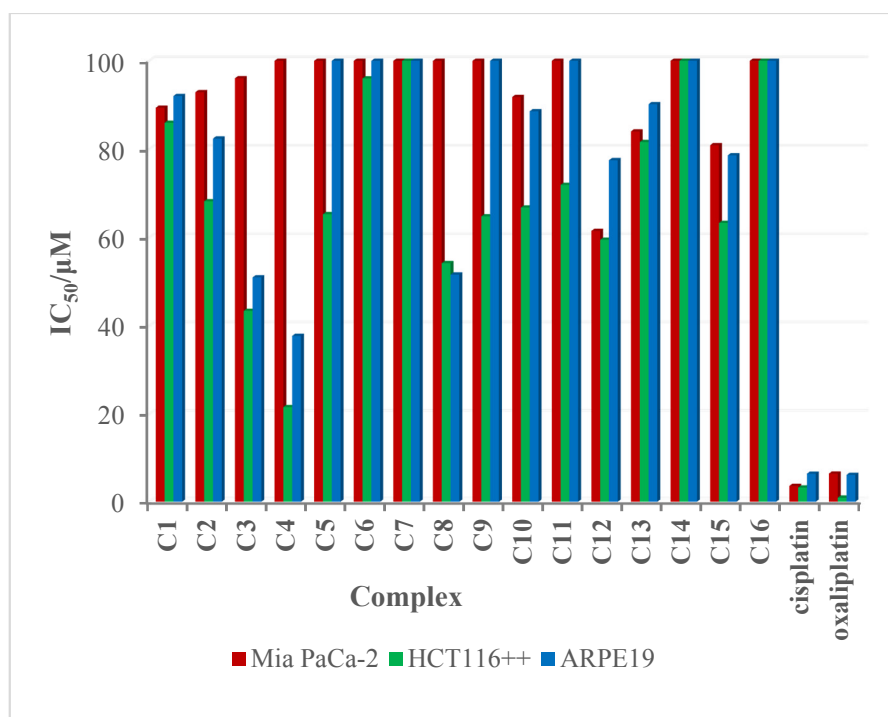


Figure 4.3.2: IC₅₀ values of Ru(II) dicarbonyl complexes (C1-C16)

Previous work within the McGowan research group on β -diketonate complexes of titanium have shown the *para* fluoro substituted diketonate titanium complex as the lead complex.^{10,11} Thus, the activities of the *para* substituted complexes with differing electronic and steric effects (C2 = 4'Br, C3 = 4'Cl and C8 = 4'Me) was compared for this class of complexes. The *para* iodo complex is not included as it was not fully characterised due to purification difficulties. From the IC₅₀ values shown in **Table 4.3.1**, the most active complex is the *para* fluoro substituted complex, C4. These results are consistent with those previously highlighted within our research group. Furthermore the *para* substituted complex C4 (IC₅₀ = 21.61 μ M) shows higher efficacy when compared to its *meta* substituted analogue C5 (IC₅₀ = 65.29 μ M).

Although further investigative experiments are needed to ascertain the effect of fluorine on the cytotoxicity of drug candidates, literature review shows that the introduction of fluorine into a drug candidate, in drug design and development is of critical importance.¹² The incorporation of fluorine can affect properties such as pK_a, conformation, intrinsic potency, metabolic pathways, membrane permeability, bioavailability and pharmacokinetics.¹³ These properties have significant effects in the overall potency of a drug molecule.

A rather unusual result is the potency of complex **C8** ($IC_{50} = 54.20 \mu\text{M}$), the electron donating methyl group results in enhanced cytotoxicity when compared to the *para* bromo substituted complex, **C2** ($IC_{50} = 68.21 \mu\text{M}$). This result potentially implies that with complexes of the type β -bis-ketoiminate Ru(II) dicarbonyl, electronics (electron donating or electron withdrawing ability) have a minor effect on the resultant potency of the complexes.

Incorporation of halide substituents in either of the phenyl rings (*aniline* (R_a) or *phenolate* (R_p)) of the ketoiminate ligands results in significant effects on the potency of the complexes. The unsubstituted complex **C1** has an IC_{50} value of $85.96 \mu\text{M}$ and is classed as inactive, addition of halide substituents going from the most electronegative to the least electronegative results in an increase in the potency of the complexes. This is shown by complexes **C4** (4'F, $IC_{50} = 21.60 \mu\text{M}$), **C3** (4'Cl, $IC_{50} = 43.40 \mu\text{M}$) and **C2** (4'Br, $IC_{50} = 68.21 \mu\text{M}$). Overall we can conclude that the electronegativity of halide substituents can influence the anticancer activity of these complexes.

The cytotoxicity of the lead complex **C4** is significantly reduced when the phenyl ring carrying the substituted halide is changed, such as in its analogue **C10** (**Figure 4.3.3**). A similar result is observed for the *para* chloro substituted complexes, **C3** (4'Cl, $IC_{50} = 43.40 \mu\text{M}$) and **C11** (4'Cl, $IC_{50} = 71.90 \mu\text{M}$). However, in order to justify this as a trend the library of β -bis-ketoiminate Ru(II) dicarbonyl complexes must be extended and fully investigated.

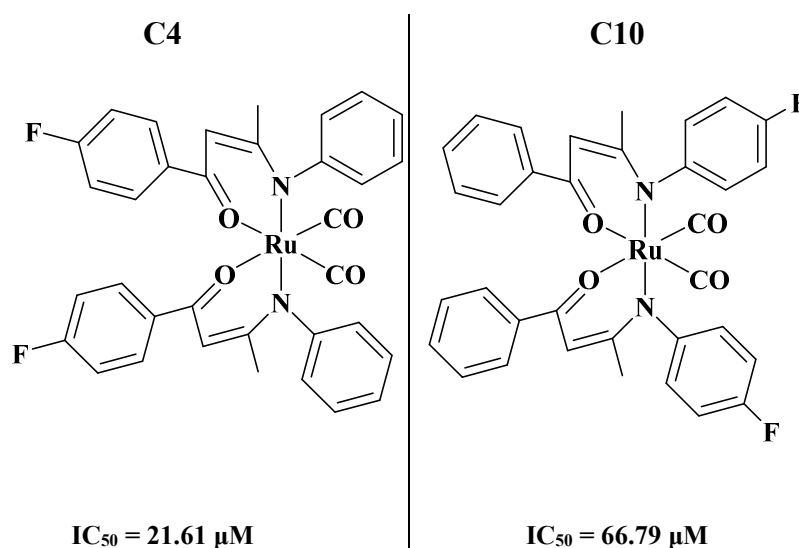


Figure 4.3.3: Representation of phenyl ring effect on anti-cancer activity

4.3.2 Hypoxia

Molecular oxygen, O₂, required by many organic and inorganic reactions as an electron receptor is also required for aerobic metabolism to maintain intracellular bioenergetics.¹⁴ The pioneering work by Peter Vaupel *et al.* has shown that solid tumours that have reached 2-3 mm in diameter are usually characterised by areas of low oxygen levels, characterised by a reducing environment in comparison to surrounding normal tissues. Such under-perfused regions, referred to as hypoxic regions, are used to selectively distinguish between healthy and cancerous cells.¹⁵ Hypoxia can also be found in a number of conditions such as tissue ischaemia, stroke and inflammation. Healthy mammalian organs typically exist at 2-9% O₂ (40mmHg) (normoxia), hypoxic regions exist at $\leq 2\%$ O₂, while severe hypoxia (anoxia) is defined as $\leq 0.02\%$.^{14 16} It is also important to note that although it a common feature in solid tumours, the incidence, extent and severity of hypoxia varies between and within individual tumours.^{17, 18}

Solid tumours are known to have fundamentally different vascular networks in comparison to normal tissues. In order to metastasize and obtain the necessary nutrients to facilitate their rapid and uncontrolled growth, cancer cells use host cell vessels to create new vessels (angiogenesis). The result is the tumour vasculature being structurally and functionally abnormal. In addition to the solid pressure from proliferating cancer cells, typical cancer cell blood vessels are dilated, hyper-permeable, tortuous, saccular with a random pattern of interconnection. All these factors result in heterogeneous blood flow leading to abnormal microenvironments within the tumour (**Figure 4.3.4**). Typically oxygen can diffuse 170 μm through tissue cells but cells located at a distance greater than this from a functioning blood vessel will have impaired blood supply.¹⁹⁻²¹

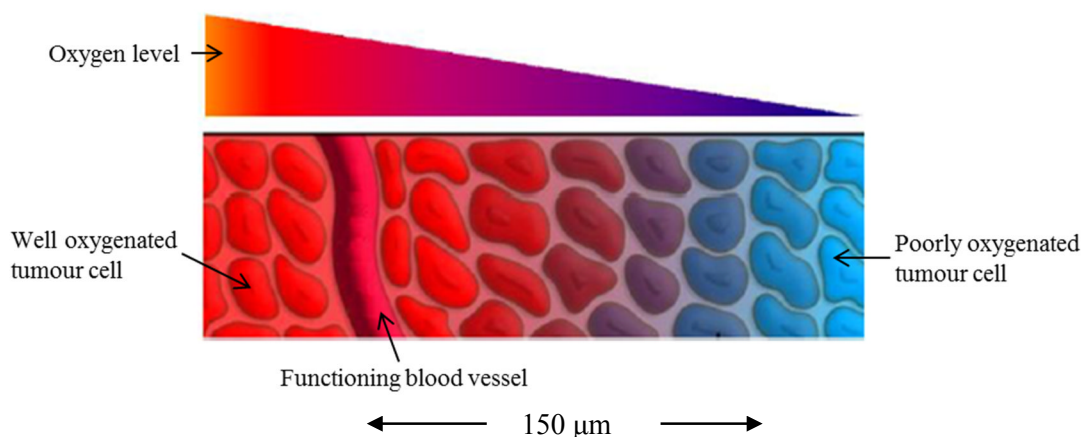


Figure 4.3.4: Schematic representation of the effect impaired blood supply in tumour cells.²¹

The abnormal vasculature and microenvironment of solid tumours present difficulties in chemotherapy and radiation cancer treatments. Although cancer cells are able to survive in hypoxic environments, drug delivery and efficacy are greatly compromised; most cytotoxic agents are highly dependent on normal blood circulation and delivery at correct concentrations.^{20, 22} The ultimate result is compromised clinical outcomes such as poor prognosis, treatment failure, recurrence and ultimately patient mortality.²¹

Hypoxia has been pursued as a therapeutic target through the development of bio-reductive (hypoxia activated) prodrugs, which are activated when they reach the hypoxic regions with reducing environments. Nitro groups, quinones, aliphatic and aromatic N-oxides and transition metals are some of the chemical moieties that can be enzymatically reduced under hypoxic conditions.¹⁶⁻¹⁸ The proposed molecular pharmacology (**Figure 4.3.5**) of these hypoxia activated prodrugs is initiated by one-electron enzymatic reduction to give a radical anion of the prodrug. In normoxia, this radical anion is quickly taken up by molecular oxygen, resulting in a failed redox process. However, in hypoxic environments the radical anion spontaneously fragments or is further reduced to produce a cytotoxic species. The cytotoxic species can then target biological agents through processes such as oxidation or poisoning of topoisomerase II, DNA alkylation and kinase inhibition.^{17, 23}

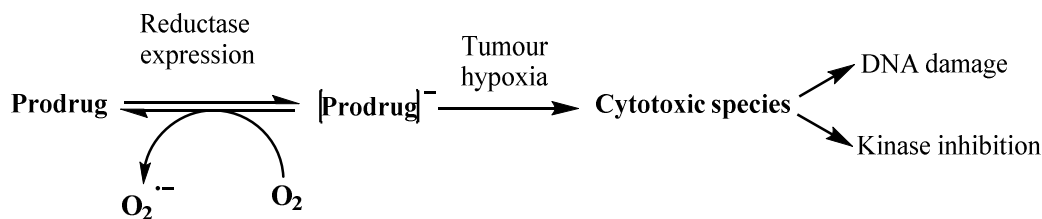


Figure 4.3.5: Mechanism for activation of bio-reductive prodrugs

Transition metal complexes have been exploited as potential bio-reductive prodrugs due to their ability to vary their coordination number, geometry and redox states making them accessible in the reducing biological surroundings. They can possibly be transported to the targeted environment as inert prodrugs, becoming reduced metabolically into their active form.²⁴ Transition metals such as platinum(IV),²⁵ ruthenium(III),^{26, 27} chromium²⁸ and iron(III)²⁹ have been investigated as hypoxia activated prodrugs; the author will give a brief overview on copper and cobalt.

Cobalt: Polyazamacrocyclic nitrogen mustards are a well-known class of potent but non-selective cytotoxins. Their selectivity has been shown to improve when they are deactivated through coordination to an inert metal centre. Denny *et al.*^{28, 30, 31} have synthesised a number of inert cobalt complexes (**Figure 4.3.6**), that are activated in hypoxic medium.

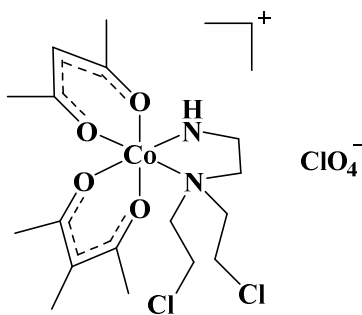


Figure 4.3.6: Hypoxia selective Co(III) acetylacetonate complex

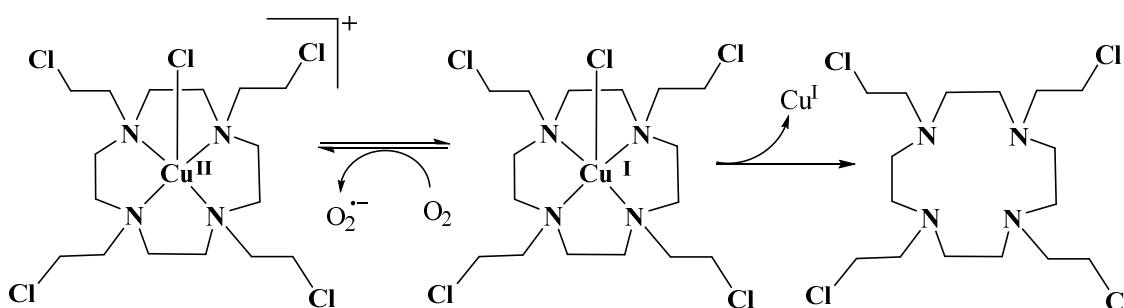
The cobalt centre inhibits early hydrolysis of the mustard ligand, allowing the inert complex to be taken up by the cells. Once taken up the Co(III) complex is then reduced to the labile Co(II) which subsequently undergoes slow decomposition to free the active cytotoxin nitrogen mustard ligand. The mustard alkylating agents can then covalently interact with cellular components such as DNA and enzymes.³²⁻³⁵

Copper: Copper has two oxidation states, +2 and +1, which are accessible within the physiological cellular potential range. This ability makes copper an attractive metal for hypoxic activated prodrugs.³⁶ Parker *et al.* have synthesised Cu(II) complexes with polyazamacrocyclic N-mustard ligands and evaluated their potential as hypoxia activated prodrugs on lung derived human tumour cell line A549.³⁷

The cyclen-based mustard complex shown in

Scheme 4.3.1 was the most selective, with a 24 fold increase in its cytotoxicity under hypoxia compared to normoxia.

Scheme 4.3.1 shows the proposed bio-reduction mechanism; the Cu(II) complex acts as a prodrug, becoming reduced to Cu(I) in the hypoxic region, releasing the cytotoxic cyclen ligand to its target cell.



Scheme 4.3.1: Hypoxia selective Cu(II) cyclen-based mustard complex

4.3.2.1 MTT assay under hypoxic conditions

In order to determine the hypoxia-selective potential activity of the ruthenium dicarbonyl complexes, the efficacy of the lead complex, **C4**, with an IC₅₀ value of 21.61 μM under normoxic conditions was further evaluated under hypoxia. The HCT116++ colon cancer cell line was selected for this assay as the ruthenium dicarbonyl complexes were previously found to be more potent and selective towards this cell line compared to the Mia PaCa-2 pancreatic cancer cell line.

Hypoxia cytotoxicity studies were carried out in a Whitley hypoxia-station with the oxygen level at 0.1%, a physiologically relevant hypoxic level that has been associated with drug resistance in chemotherapy and radiotherapy.³⁸ In order to remove oxygen

from the media, the media used for this study was conditioned for at least 24 hours in the hypoxic chamber. The MTT assay procedure described in 4.3.1 was followed, with the cells being exposed to the lead complex after 24 hours of seeding.

The results for hypoxia studies on complex **C4** are shown in **Table 4.3.2** and **Figure 4.3.7**. Although the complex retains its potency, the two fold increase in its IC_{50} value indicates that the complex is less active under hypoxia compared to normoxia, however, is still significantly more active than cisplatin.

Table 4.3.2: IC_{50} values of complex **C4** under normoxia and hypoxia

	Hypoxia	Normoxia
C4	50.5	21.61±3.55
cisplatin	95.49	3.26±0.38

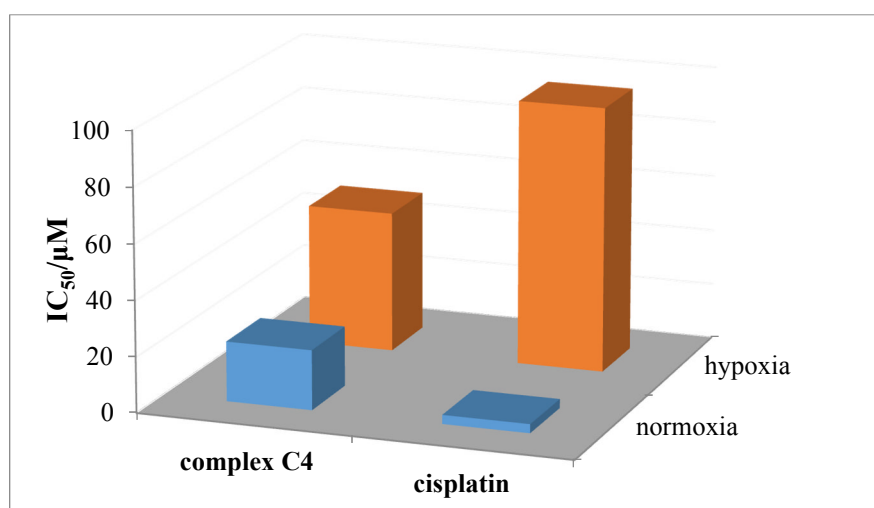


Figure 4.3.7: IC_{50} values for complex **C4** under normoxia and hypoxia

4.3.3 Cytotoxicity of β -bis-Ketoiminate Copper(II) Complexes

The β -bis-ketoiminate copper(II) complexes, **C17-C42**, discussed in **Chapter 3** and shown in **Figure 4.3.8** were evaluated for their cytotoxicity against two cancerous cell lines, Mia PaCa-2 (human pancreatic carcinoma) and HCT116++ (human colon carcinoma) and on one non-cancerous cell line, ARPE19 (human retinal pigment

epithelial cell). Similar to the ruthenium(II) dicarbonyl complexes previously discussed (4.3.1), all the biological work was done at The University of Huddersfield by Pablo Carames-Mendez in collaboration with Professor Roger Phillips.

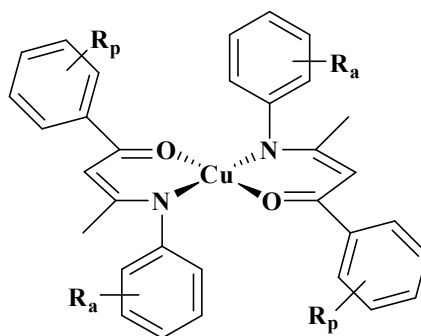


Figure 4.3.8: β -Bis-ketoiminate copper(II) complexes under investigation

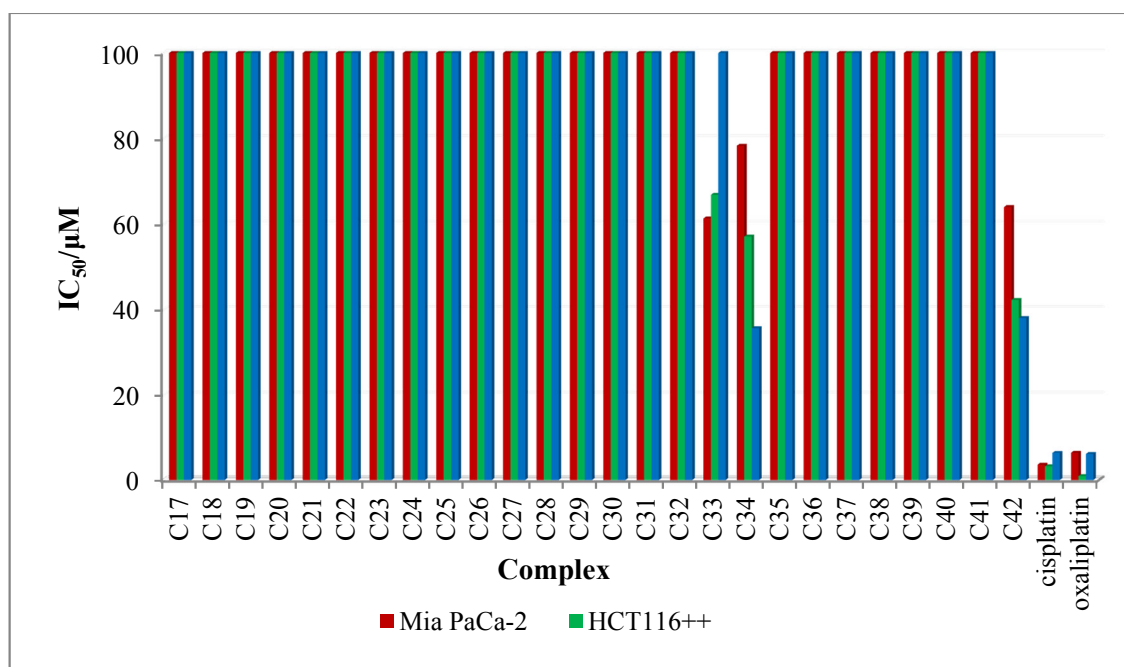


Figure 4.3.9: IC₅₀ values of ketoiminate copper(II) complexes C17-C42

The results for the cytotoxicity evaluation of β -bis-ketoiminate copper(II) complexes, C17-C42, are summarised in **Table 4.3.3** and **Figure 4.3.9**. The copper(II)acnac complexes were inactive against the two cancerous cell lines, with only complexes C33, C34 and C42 displaying moderate activity (highlighted in green in **Table 4.3.3**). The moderately active complexes did not show any selectivity between the colon and pancreatic cancer cell lines. Complex C34 and C42 were as toxic as they were

cytotoxic, however complex **C33** was selective towards the healthy cells. The results suggest that there is no correlation between the electronic and steric properties of the complex and the potency of the compound. No further cytotoxicity studies were carried out on these complexes.

Table 4.3.3: IC₅₀ values of ketoiminate copper(II) complexes **C17-C42**

Complex	Substituent (R _p /R _a)	IC ₅₀ /μM		
		MiaPaca	HCT116++	ARPE19
C17	H(p)	>100	>100	>100
C18	2'Br(p)	>100	>100	>100
C19	2'Cl(p)	>100	>100	>100
C20	4'Br(p)	>100	>100	>100
C21	4'Cl(p)	>100	>100	>100
C22	4'F(p)	>100	>100	>100
C23	4'I(p)	>100	>100	>100
C24	4'Me(p)	>100	>100	>100
C25	4'OMe(p)	>100	>100	>100
C26	4'OEt(p)	>100	>100	>100
C27	4'CF ₃ (p)	>100	>100	>100
C28	2',3'diMe(p)	>100	>100	>100
C29	2',4',6'triMe(p)	>100	>100	>100
C30	3',4'diCl(p)	>100	>100	>100
C31	3',4' methylene(p)	>100	>100	>100
C32	3'Br,4'F(p)	>100	>100	>100
C33	2'OMe(p)	61.36±2.87	66.87±14.55	>100
C34	3'F(p)	78.33±12.48	57.14±11.41	35.73±3.26
C35	2'OEt,4'F(p)	>100	>100	>100
C36	2'Br(a)	>100	>100	>100
C37	2'F(a)	>100	>100	>100
C38	3'Br(a)	>100	>100	>100
C39	3'Cl(a)	>100	>100	>100
C40	4'Cl(a)	>100	>100	>100
C41	2',4' diF(a)	>100	>100	>100
C42	2',5' diF(a)	64.02±10.35	42.35±12.88	38.11±8.84
Cisplatin		3.62±0.74	3.26±0.38	6.41±0.95
Oxaliplatin		6.44±1.05	0.93±0.12	6.15±2.68

(p) = substituent on *phenolate* ring; (a) = substituent on *aniline* ring

4.4 Anti-bacterial Studies

One of the major advances in the medical field has been the development and widespread use of antimicrobials. However, this was followed by the unfortunate rapid and ever increasing emergence of antimicrobial resistance (AMR) which has become a global pandemic, placing a significant amount of burden on public health systems and global economic finance. AMR threatens the effective prevention and treatment of a range of infections caused by bacteria, fungi, parasites and viruses by reducing clinical efficacy while increasing diagnostic uncertainties, treatment costs, mortality and morbidity.³⁹⁻⁴²

In recent years, a group of the most antimicrobial resistant bacteria referred to as “ESKAPE pathogens” have been associated with nosocomial infections among severely ill and immune-compromised individuals. ESKAPE pathogens include both Gram-(+ve) and Gram-(-ve) bacteria, and is made up of *Enterococcus faecium*, *Staphylococcus aureus*, *Klebsiella pneumoniae*, *Acinetobacter baumannii*, *Pseudomonas aeruginosa* and *Enterobacter* species.^{41, 43, 44}

Antimicrobial resistance can be active or passive. Active resistance results when the bacteria, over a period of time, adopts a counter-attack mechanism against an individual antibiotic or a family of antibiotics. An example of passive resistance is when bacteria, for example Gram-negative bacteria develop resistance due to the non-specific barrier in their outer membrane.⁴⁵ Bacteria are able to acquire their resistance through several categories such as drug inactivation, mutation and modification of drug binding target/site, reduced intracellular drug accumulation due to changes in cell permeability and biofilm formation.⁴⁵⁻⁴⁷ It is anticipated that development of bacterial resistance to a given antibiotic evolves within an average of 50 years from initial use.⁴⁸

Old targets, new drugs is one of the several strategies that are being exploited in an attempt to develop improved antimicrobial agents. In this approach the functional lifetime of existing antimicrobials is extended by generations of synthetic tailoring, leading to “new”, improved antimicrobials. In addition to a higher affinity for mutated targets, these modified scaffolds have better solubility, drug uptake and are less prone

to efflux.^{42, 46, 49} Although effective, this strategy delays the problem of resistance rather than offer a solution. *New targets, new drugs* as the phrase suggests seeks to eliminate the problem of antimicrobial resistance through the development of novel and effective antimicrobial agents, with new targets, modes of actions and mechanisms.⁴⁶

As research into new organic based antimicrobial agents continues, transition metals have received remarkable interest for the development of metal based antimicrobial agents.⁴² The antimicrobial activity of metal complexes has been known since antiquity when the antimicrobial properties of the organic molecule oxine were proposed to rise from its chelation with copper and iron ions available in the medium.^{50, 51} The antimicrobial efficacy of bioinorganic complexes can be modified by tuning the coordination sphere around the metal, as well as the metal's oxidation state. The possibility of simultaneous multiple mechanisms of action from these complexes makes the notion of overcoming the drug resistance of micro-organisms using metal based complexes feasible.⁵²

Over the years there has been a growing interest in ruthenium based compounds as alternatives to platinum based complexes for biological applications. As such, considerable focus has been on developing ruthenium(II) complexes as antimicrobial agents.⁴² Dwyer *et al.* have synthesised polypyridylruthenium(II) complexes and evaluated their efficacy on Gram-positive, Gram-negative and acid fast bacteria. They proposed that the complexes were well suited for topical application for surface infection rather than injection routes.⁵³⁻⁵⁵

4.4.1 Ruthenium CORMs in anti-bacterial studies

CORMs, are known to have a different mode of action in their biological and therapeutic applications when compared to other transition metal based molecules. This has prompted investigations into their potential application for treatment of antibiotic resistant bacteria.⁵⁶ Control experiments such as depleting the carbonyl group in CORMs and cell growth experiments with CORMs in the presence of Hb, a high-affinity CO scavenger, have led to the conclusion that the bactericidal effect of CORMs is due to the CO and not the metal ion.^{56, 57}

The well-known CORMs, the lipid soluble CORM-2 [Figure 4.4.1 (a)] and the water soluble CORM-3 [Figure 4.4.1 (b)] have been shown to reduce the viability of Gram-positive and Gram-negative bacterial species such as *Staphylococcus aureus*, *Pseudomonas aeruginosa* and *Escherichia coli*.⁵⁷⁻⁵⁹ In a recent study on *E. coli*, Saraiva *et al.* have investigated the antimicrobial activity, the amount of ROS species released into bacterial cells, toxicity to eukaryotic cells as well as the ability of CORMs to deliver carbon monoxide to bacterial cells and eukaryotic cells. This was done using a range of CO-releasing molecules with different chemical and biocompatibility profiles, coordination sphere type and metal centre. Their results show that CORMs have a viable potential application as antimicrobial drugs as (i) their activity can be modified through manipulation of their coordination spheres, (ii) their toxicity to eukaryotic cells is innocuous or relatively low even at their bactericidal concentrations and (iii) they exhibit opposite toxicity profiles towards bacteria and eukaryotic cells.^{60,}

61

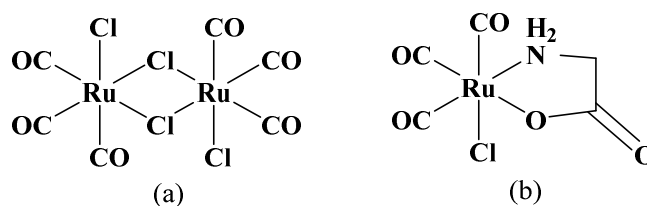


Figure 4.4.1: (a) CORM-2 and (b) CORM-3

The novel β -bis-ketoiminate ruthenium(II) dicarbonyl complexes Figure 4.4.2 were screened for their anti-bacterial activity by measuring the inhibition growth against Gram-positive *Staphylococcus aureus* (*S. aureus*) and Gram-negative *Escherichia coli* (*E. coli*), *Klebsiella pneumoniae* (*K. pneumoniae*), *Pseudomonas aeruginosa* (*P. aeruginosa*) and *Acinetobacter baumannii* (*A. baumannii*) by CO-ADD, The Community for Antimicrobial Drug Discovery at The University of Queensland, Australia. For all the complexes, assays were carried out in duplicate at a single concentration of 32 $\mu\text{g/mL}$ by incubating with the bacterial strains at 37 °C for 18 hours without shaking. Inhibition of bacterial growth was determined by measuring the absorbance at 600 nm (OD_{600}), using a Tecan Pro monochromator plate reader. Complexes with growth inhibition values above 80% are classed as active, while complexes with growth inhibition values between 50 - 80% are classed as partial active.

Vancomycin and colistin were used as positive bacterial inhibitor standards for Gram-(-) and Gram-(+) bacteria, respectively.

The anti-bacterial screening assay results for the ruthenium(II) carbonyl complexes are summarised in **Table 4.4.1**. The results show that the complexes are generally inactive, except for complex **C12** which is partially active against Gram-positive *S. aureus* species, with a growth inhibition of 58%. Partially active complexes are highlighted in purple. Negative growth inhibition values indicate that the growth rate for the complexes in question are higher than the negative control. These complexes could be causing cell proliferation than growth inhibition.

	Complex	Substituent (R_p/R_a)
	C1	H(p)
C2	4'Br(p)	
C3	4'Cl(p)	
C4	4'F(p)	
C5	3'F(p)	
C6	3'Br(p)	
C7	3',4' diCl(p)	
C8	4'Me(p)	
C9	3'Me(a)	
C10	4'F(a)	
C11	4'Cl(a)	
C12	2'F(a)	
C13	3'Br(a)	
C14	2',4' diCl(a)	
C15	2',4' di F(a)	
C16	2',3' diMe(a)	

(p) = substituent on *phenolate* ring; (a) = substituent on *aniline* ring

Figure 4.4.2: β -Bis-ketoiminato Ru(II) dicarbonyl complexes under investigation

Complex, **C12** (with an *ortho*-fluoro substituent on the aniline ring) shows selectivity against the Gram-positive *S. aureus* and is inactive against the other four Gram-negative bacterial species, a trend observed for all the complexes. Bolhuis *et al.* who observed similar selectivity with their Ru(II) complexes suggested that this selectivity against Gram-positive bacteria may be due to the inability of the complexes to cross the outer membrane characteristic of Gram-negative bacterial species.⁶² This outer membrane is known to decrease the permeability of anti-bacterials and is regarded as one of the major mechanisms of resistance to drugs for many pathogenic Gram-negative bacteria.⁴²

Table 4.4.1: Growth inhibition of Ru(II) dicarbonyl complexes against bacterial strains

Complex	Inhibition (%)				
	<i>S. aureus</i>	<i>E. coli</i>	<i>K. pneumoniae</i>	<i>P.aeruginosa</i>	<i>A.baumannii</i>
C1	18.24	1.92	6.31	20.87	4.02
C2	7.82	4.03	-2.85	20.71	-2.52
C3	20.52	4.83	5.43	22.73	12.98
C4	-12.85	-25.79	-31.78	13.86	-37.98
C5	21.58	-2.18	6.55	18.83	3.63
C6	21.36	3.09	10.12	20.96	16.45
C7	13.12	-5.76	-8.64	20.38	-2.04
C8	-9.81	-18.19	-22.32	12.31	-18.13
C9	20.17	-9.26	-2.28	5.07	-12.95
C10	6.95	-27.37	-16.83	14.29	-26.80
C11	8.37	-17.07	-23.92	15.15	-16.54
C12	58.29	-35.64	-31.94	12.73	-48.41
C13	12.52	-11.13	-10.57	16.08	-9.17
C14	20.94	-10.25	-3.27	10.01	-8.62
C15	-6.49	-27.95	-37.23	0.48	-42.00
C16	9.93	-15.75	-5.72	-3.00	-7.06

Although further investigative work needs to be done, some structure-activity relationship can be observed from the results. Moving the fluoro substituent from an *ortho* position to a *para* position results in a tenfold decrease in the activity of the complex (Table 4.4.1, C10 and C12). Similarly addition of another fluorine moiety on the same phenyl ring results in inactivity of the complex (Table 4.4.1, C12 and C15). The addition of electron donating and electron withdrawing groups on either of the phenyl rings of the ligands has no noticeable effect on the activity or selectivity of the complexes against *S. aureus*.

Comparison of the anti-bacterial results of the β -bis-ketoiminate ruthenium(II) dicarbonyl complexes (Table 4.4.1) shows there is no overall selectivity for neither Gram-negative nor Gram-positive bacterial species (except for C12). This result is consistent with the results of Nobre *et al.* who concluded that CORMs have the potential to be used as bactericides against a wide range of microorganisms regardless of the type of bacterial cell wall and the oxygen requirements, aerobic and anaerobic conditions.⁶⁰

4.4.2 Copper complexes in anti-bacterial studies

Although transition metals such as copper, zinc and iron are essential for the growth and development of organisms from bacteria to mammals, free copper ions are known to be toxic to numerous bacteria and fungi. To increase its antimicrobial efficacy several compounds have been synthesised through the coordination of organic moieties to copper.^{52, 63} For thousands of years the antimicrobial benefits of copper have been well known and researched, dating as far back as the ancient Egyptian times when copper was first reported for its water and wound sterilisation properties.⁶⁴ With increasing transmission from pathogens on various surfaces, evolving research and development has seen the establishment of metallic copper surfaces as antimicrobial surfaces that rapidly kill bacteria, yeast and viruses. “Contact killing” as it termed is largely used in hospitals and other health care settings to curb nosocomial infections.^{65, 66}

Several copper complexes with ligands such as Schiff bases, heteroatomic thiophene/furan carboxamides and perimidine derivatives, with the general compositions $[ML_2]$ have been synthesised and their antimicrobial activities against a range of Gram-negative and Gram-positive pathogens investigated. A trend common to these complexes is that the complexes showed enhanced inhibitory activity than the free parent ligands.⁶⁷⁻⁷¹ The copper(II) Schiff base complexes were more potent against Gram-positive bacteria than Gram-negative bacteria. This result, consistent with the antimicrobial activity results of complexes and compounds of Schiff bases with amino acids was ascribed to the presence of the outer membrane cell wall present in Gram-positive bacteria which acts a barrier, interacting with the complexes and reducing their permeability.^{67, 68} Copper sulfonamide complexes synthesised by Karacan *et al.* however displayed no antimicrobial activity when tested against a range of bacterial pathogens.⁶⁹

The β -bis-ketoiminate copper(II) complexes, **C17-C42 (Figure 4.4.3)**, discussed in **Chapter 3** were screened for their anti-bacterial activity by measuring the inhibition growth against Gram-positive *Staphylococcus aureus* (*S. aureus*) and Gram-negative *Escherichia coli* (*E. coli*), *Klebsiella pneumoniae* (*K. pneumoniae*), *Pseudomonas*

aeruginosa (*P. aeruginosa*) and *Acinetobacter baumannii* (*A. baumannii*) by CO-ADD, The Community for Antimicrobial Drug Discovery at The University of Queensland, Australia. The same procedure as that previously outlined (for β -bis-Ketoiminate ruthenium(II) dicarbonyl complexes was followed.

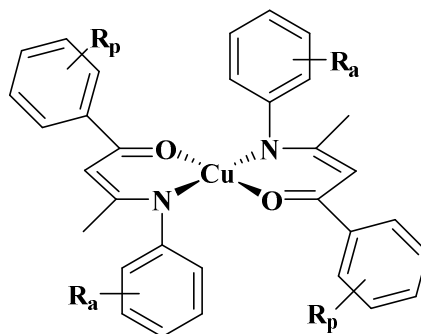


Figure 4.4.3: Copper(II) acnac complexes under anti-bacterial and anti-fungal studies

Table 4.4.2: Growth inhibition of copper(II)acnac complexes against bacterial strains

Complex	Inhibition (%)				
	<i>S. aureus</i>	<i>E. coli</i>	<i>K. pneumoniae</i>	<i>P.aeruginosa</i>	<i>A.baumannii</i>
C17	-14.67	-21.81	-7.38	27.86	25.34
C18	17.37	-10.42	-4.27	24.85	-30.96
C19	24.13	-4.45	-11.59	23.02	-28.87
C20	24.89	-10.39	-13.08	25.28	-29.87
C21	19.90	-11.95	-10.79	17.18	-29.91
C22	21.10	-9.02	-10.73	23.80	-32.74
C23	7.04	-14.83	-24.09	12.55	-35.24
C24	23.14	-3.20	-5.78	18.40	-9.30
C25	11.01	-0.44	-9.15	29.07	-26.58
C26	16.82	-6.49	3.89	17.10	-27.00
C27	23.60	-4.40	-2.08	18.4	-8.60
C28	17.34	-6.62	5.52	15.13	-33.38
C29	16.62	-12.20	-7.07	19.49	-7.09
C30	5.98	-15.15	-4.85	16.49	-42.98
C31	10.72	-13.30	-17.20	15.66	-2.66
C32	-0.26	14.61	-15.97	11.72	-40.89
C33	15.24	-5.43	-19.04	29.45	-24.35
C34	19.63	-4.92	-4.42	22.5	-14.45
C35	23.67	-6.39	-10.62	16.19	-23.85
C36	3.51	-20.57	-5.58	29.38	-3.92
C37	-0.48	-13.32	-29.78	24.65	-41.98
C38	2.63	-15.21	-16.89	16.21	-37.78
C39	2.21	-16.07	-3.12	23.53	-10.67
C40	1.75	-14.12	-9.03	9.76	-18.61
C41	3.76	-15.22	-14.53	17.49	-22.09

C42	-9.99	-18.64	-14.35	21.79	-43.57
------------	-------	--------	--------	-------	--------

The results for the screening assays are summarised in **Table 4.4.2**. Complexes, **C17-C42** were generally classed as inactive against all the different strains of Gram-negative and Gram-positive bacteria. Contrary to the results discussed earlier on other copper(II) complexes found in the literature, Gram-negative *P. aeruginosa* bacteria showed the most positive response towards the copper(II)acnac complexes, as seen from the positive inhibition values. Although further investigative work needs to be done, the results indicate that these novel copper(II) are able to a certain extent, interact with the outer membrane cell wall present in Gram-negative *P. aeruginosa* bacteria. The negative inhibitory growth results shown for the other three Gram-negative bacteria, *E. coli*, *K. pneumoniae* and *A. baumannii* suggest that the complexes initiated cell proliferation rather than growth inhibition. The positive response, although poor, of the complexes to Gram-positive bacteria, *S. aureus*, implies that the complexes have the potential to be used as bactericidal agents for both Gram-negative and Gram-positive bacteria.

4.5 Anti-fungal Studies

Fungi are eukaryotic cells that closely resemble mammalian eukaryotic cells. They are more complex than bacterial pathogens; universally found in the environment they are more difficult to treat than bacterial infections.⁷² The past decades have seen an increase in the rate of fungal infections. A study by the National Institute of Health, United States, showed that the rate of fungal infections was directly proportional to the number of immune-compromised individuals, carcinoma, autoimmune disorders and organ transplants and this has resulted in high mortality and morbidity. Drug resistance, lack of effective anti-fungal therapy and poor diagnosis are some of the leading contributors to high morbidity and mortality.^{73, 74}

Although significant, advances in medical and surgical therapy such as the discovery of chemotherapeutic agents, bone marrow or solid-organ transplants, broad spectrum antimicrobial agents, use of invasive monitoring devices, assisted ventilation and parenteral nutrition have resulted in an appreciable increase in the number of immune-compromised individuals susceptible to mycosis infections.⁷⁴⁻⁷⁶ Immune-compromised patients suffering from diseases like HIV-AIDS, cancer, diabetes and cystic fibrosis are

particularly prone to infections from opportunistic mycoses, *Candida albicans*, *Cryptococcus neoformans*, and *Aspergillus fumigatus*, resulting in life threatening infections.⁷⁷⁻⁷⁹ Currently they are five main classes of anti-fungals in use, (i) azoles, (ii) polyenes, (iii) allylmines, (iv) echinocandins and (v) pyrimidine analogues, based on their site of action.^{80, 81} The efficacy of these anti-fungals is limited by the development of anti-fungal resistance, fungi-static activity and host toxicity.⁴⁵

4.5.1 Ruthenium complexes in anti-fungal studies

Despite the remarkable increase in the application of coordination and organometallic compounds of ruthenium in medicine and biology, very little has been reported on their application as anti-fungal agents. Schiff base complexes of bases were the first known ruthenium anti-fungals.⁸² Since then the activity against fungi, namely, *Aspergillus flavus* and *fusarium* species, of a number of ruthenium Schiff base complexes has been evaluated. Under identical experimental conditions and the same microorganisms, the vast majority of these complexes exhibited higher cytotoxicity when compared to the free or parent Schiff base ligand(s). This increase in anti-fungal activity is likely due to the effect of chelation on the normal cell process, as explained by Tweedy's theory.⁸³⁻⁸⁶ The activity of the complexes was both dependent and independent of the concentration of the complexes, with some of the complexes showing a direct proportional between complex concentration and anti-fungal activity.⁸⁵ The anti-fungal activity of other ruthenium complexes with perimidine derivatives⁷⁰, β -diketones⁸⁷ and catecholamine⁸⁸ ligands have also been evaluated on a range of fungi, for example, *Candida albicans*, *Candida glabrata* and *A. niger*. It is interesting to note that free catecholamine ligands did not show any anti-fungal activity, whilst the catecholamine complexes showed strong inhibitory activity against pathogenic yeast fungus.⁸⁸

β -Bis-ketoiminate ruthenium(II) dicarbonyl complexes, **C1-C16 (Figure 4.4.2)**, were screened for their anti-fungal activity on two fungi, *Candida albicans* (*C. albicans*) and *Cryptococcus neoformans* var. *grubii* (*C. neoformans*), by CO-ADD, The Community for Antimicrobial Drug Discovery at The University of Queensland, Australia. Assays were carried out in duplicate at a single concentration of 32 μ g/mL by incubating with the fungal strains at 35 °C for 24 hours without shaking. Growth inhibition of *C. albicans* was determined by measuring absorbance at 530 nm (OD₅₃₀),

while growth inhibition of *C. neoformans* was determined measuring the difference in absorbance between 600 and 570 nm ($OD_{600-570}$), using a Biotek Synergy HTX plate reader. Fluconazole was used as a positive fungal inhibitor standard for *C. albicans* and *C. neoformans*. Complexes with growth inhibition values above 80% are classed as actives, while complexes with growth inhibition values between 50-80% are classed as partial actives.

The anti-fungal screening assay results for complexes **C1-C16** are summarised in **Table 4.5.1**. Although not significantly active, the complexes showed selectivity towards *C. albicans* fungal strain as shown by the positive growth inhibition values when compared to the negative values obtained for *C. neoformans*.

Table 4.5.1: Growth inhibition of Ru(II) dicarbonyl complexes against fungal strains

Complex	Substituent (R _p /R _a)	Inhibition (%)	
		<i>C. albicans</i>	<i>C. neoformans</i>
C1	H(p)	14.47	-11.64
C2	4'Br(p)	34.89	-5.14
C3	4'Cl(p)	26.74	-16.64
C4	4'F(p)	10.02	-9.24
C5	3'F(p)	25.93	-17.85
C6	3'Br(p)	44.1	2.38
C7	3,4'diCl(p)	5.93	9.24
C8	4'Me(p)	7.03	-15.43
C9	3'Me(a)	12.23	-23.9
C10	4'F(a)	-0.23	-16.79
C11	4'Cl(a)	8.44	-8.92
C12	2'F(a)	-2.67	-18.6
C13	3'Br(a)	6.47	-22.69
C14	2,4'diCl(a)	0.37	-15.27
C15	2,4'diF(a)	5.93	-24.81
C16	2,3'diMe(a)	7.69	-18.3

(p) = substituent on *phenolate* ring; (a) = substituent on *aniline* ring

Complex **C6** showed the highest activity against *C. albicans* with a growth inhibition of 44.1%. Tuning the electronic and steric properties of the complexes *via* the substituents, R_a and R_p on the ketoiminate ligands had a negligible effect on the activity of the complexes. This is highlighted by the broad spectrum activity of complexes **C2**–

C16 when compared to that of **C1**. The position of the substituent R_1 and R_2 seemingly have an effect on the activity of the complexes. The anti-fungal activity of the complexes decreases when similar substituents are on the *aniline* phenyl ring as compared to the *phenolate* phenyl ring, for example, **C6** (44.1%) compared to **C13** (6.47%); **C3** (26.74%) compared to **C11** (8.44%) and **C4** (10.02%) compared to **C10** (-0.23%). Direct comparison of the anti-fungal activity of these complexes with other carbon monoxide releasing molecules is not possible as these complexes are novel and the few CORMs that have been tested have been on different fungi strains and use different methods to quantify anti-fungal activity.

4.5.2 Copper complexes in anti-fungal studies

Similar to its anti-bacterial activities discussed above, copper, as metallic Cu, Cu salts and Cu complexes have been investigated as an anti-fungal agent. Schiff base complexes of copper have been evaluated by several researchers for their anti-fungal activity on *Candida albicans*, *Aspergillus fumigatus* and *Aspergillus niger*.^{67-69, 71} These complexes displayed broad spectrum anti-fungal activity when compared to that of the free ligand. Sevgi *et al.*, on studying the Schiff base complexes of copper, iron and cobalt found that the Cu complexes were less active than the Fe and Co complexes. Contrary to the trend observed in their anti-bacterial activity, the complexes were less active than the free ligand.⁶⁸ Orojloo *et al.* also observed that Schiff base complexes of copper showed no anti-bacterial activity but were significantly active against *C. albicans* fungi.⁶⁷

Amphotericin B (AmB) is a polyene anti-fungal antibiotic extracted from *Streptomyces nodosus*, used as anti-fungal medication against acute systemic fungal infections for more than 50 years.⁸⁹ In an attempt to enhance the activity of AmB at lower dose concentrations, Chudzik *et al.* synthesised AmB-Cu²⁺ complexes and evaluated the fungicidal activity against *C. albicans*. As expected the AmB-Cu²⁺ complex had higher anti-fungal activity compared to the conventional amphotericin. The unique structure of this molecule also contributed to the increase in toxicity of the copper complex.⁹⁰ Recently metal organic frameworks based on copper have been investigated as anti-fungals. The copper based benzenetricarboxylate MOF (Cu-BTC MOF) was shown to inhibit the growth rate of *C. albicans*, while inhibiting the spore growth rate of *A. niger*,

A. oryzae and *F. oxysporum*.⁹¹ These results support the potential application of copper complexes as anti-fungals.

Copper complexes, **C17–C42** (**Figure 4.4.3**) were evaluated as anti-fungal agents against *Candida albicans* (*C. albicans*) and *Cryptococcus neoformans* var. *grubii* (*C. neoformans*), by CO-ADD, The Community for Antimicrobial Drug Discovery at The University of Queensland, Australia. A similar procedure as that outlined for the β -bis-ketoiminate ruthenium(II) dicarbonyl complexes was followed. The results for complexes **C17–C42** are summarised in **Table 4.5.2**.

Table 4.5.2: Growth inhibition of copper(II)acnac complexes against fungal strains

Complex	Substituent (R _p /R _a)	Inhibition (%)	
		<i>C. albicans</i>	<i>C. neoformans</i>
C17	H(p)	11.2	-16.64
C18	2'Br(p)	9.11	-22.39
C19	2'Cl(p)	3.73	-14.06
C20	4'Br(p)	7.08	-20.87
C21	4'Cl(p)	7.83	-22.99
C22	4'F(p)	4.1	-21.33
C23	4'I(p)	7.36	-16.79
C24	4'Me(p)	6.96	-21.78
C25	4'OMe(p)	4.6	-13.01
C26	4'OEt(p)	15.01	-20.27
C27	4'CF ₃ (p)	6.88	-21.33
C28	2',3'diMe(p)	8.30	-15.88
C29	2',4',6'triMe(p)	-0.23	-19.81
C30	3',4'diCl(p)	2.59	-22.23
C31	3',4' methylene(p)	7.15	-23.75
C32	3'Br,4'F(p)	5.21	-19.66
C33	2'OMe(p)	2.27	-20.12
C34	3'F(p)	9.85	-22.69
C35	2'OEt,4'F(p)	4.27	-19.21
C36	2'Br(a)	5.11	-17.54
C37	2'F(a)	5.52	-13.46
C38	3'Br(a)	5.32	-17.7
C39	3'Cl(a)	7.43	-25.71
C40	4'Cl(a)	8.71	-15.88
C41	2',4' diF(a)	9.93	-12.85
C42	2',5' diF(a)	3.06	-20.57

(p) = substituent on *phenolate* ring; (a) = substituent on *aniline* ring

Complexes **C17–C42** had a positive response towards *C. albicans* compared to *C. neoformans*. Focusing on *C. albicans*, ligand tuning of steric and electronic properties had no significant effect on the fungicidal efficacy of the copper complexes. No further work was done on these complexes as they did not show sufficient activity to undergo hit confirmation to determine their MIC (minimum inhibitory concentration).

4.6 Conclusions

Anti-cancer activity screening using the MTT assay were carried out on novel β -bis-ketoiminate analogue complexes of ruthenium(II) and copper(II), on three cell lines, pancreatic carcinoma, colon carcinoma and retinal epithelial cells. Ruthenium(II) dicarbonyl complexes were the most active showing significant selectivity towards colon cancer cell line. This work presents the first time that ruthenium(II) dicarbonyl complexes with ketoiminate (*N,O*) ligands, potentially acting as carbon monoxide releasing molecules have shown high potency as anti-cancer agents. The complexes showed a broad spectrum activity; high, moderate and poor activity. The most active was complex **C4**, with the fluoro substituent in the *para* position of the ligands' *phenolate* phenyl ring. Although expansion of the library of complexes is necessary, some structure-activity relationships (SARs) were deduced from the lack of or activity of the complexes. The most intriguing being the pronounced activity as a result of the presence of either electron donating or electron withdrawing groups. In addition the complexes were as cytotoxic as they were toxic. Copper(II) ketoiminate complexes were generally inactive against the cancerous cell lines with IC₅₀ values greater than 100, with the exception of complexes. Complexes **C34** and **C42** were more potent than cytotoxic while complex **C33** showed high selectivity towards the healthy cell line, ARPE19. In further investigative assays, the lead complex **C4** was found to be less active in reducing (hypoxic) environments compared to normal oxygen (normoxic) environments.

Anti-bacterial and anti-fungal activity studies were also carried out on β -bis-ketoiminate ruthenium(II) dicarbonyl complexes and β -bis-ketoiminate copper(II) complexes. Both complexes showed poor activity as anti-bacterial or anti-fungal agents, with only complex **C12** showing moderate anti-bacterial activity.

4.7 References

1. E. L. Andrade, A. F. Bento, J. Cavalli, S. K. Oliveira, C. S. Freitas, R. Marcon, R. C. Schwanke, J. M. Siqueira and J. B. Calixto, *Brazilian Journal of Medical and Biological Research*, 2016, **49**, e5644.
2. E. L. Andrade, A. F. Bento, J. Cavalli, S. K. Oliveira, R. C. Schwanke, J. M. Siqueira, C. S. Freitas, R. Marcon and J. B. Calixto, *Brazilian Journal of Medical and Biological Research*, 2016, **49**, e5646.
3. D. A. Erlanson, R. S. McDowell and T. O'Brien, *Journal of Medicinal Chemistry*, 2004, **47**, 3463-3482.
4. J. A. Harrington, T. C. Hernandez-Guerrero and B. Basu, *Clinical Oncology*, 2017, **29**, 770-777.
5. I. Kola and J. Landis, *Nature Reviews Drug Discovery*, 2004, **3**, 711.
6. T. Mosmann, *Journal of Immunological Methods*, 1983, **65**, 55-63.
7. P. Skehan, R. Storeng, D. Scudiero, A. Monks, J. McMahon, D. Vistica, J. T. Warren, H. Bokesch, S. Kenney and M. R. Boyd, *JNCI: Journal of the National Cancer Institute*, 1990, **82**, 1107-1112.
8. A. A. Stepanenko and V. V. Dmitrenko, *Gene*, 2015, **574**, 193-203.
9. J. C. Stockert, A. Blázquez-Castro, M. Cañete, R. W. Horobin and Á. Villanueva, *Acta Histochemica*, 2012, **114**, 785-796.
10. B. D. Crossley, PhD, University of Leeds, 2011.
11. J. J. Mannion, PhD, University of Leeds, 2008.
12. J. Wang, M. Sánchez-Roselló, J. L. Aceña, C. del Pozo, A. E. Sorochinsky, S. Fustero, V. A. Soloshonok and H. Liu, *Chemical Reviews*, 2013, **114**, 2432-2506.
13. E. P. Gillis, K. J. Eastman, M. D. Hill, D. J. Donnelly and N. A. Meanwell, *Journal of Medicinal Chemistry*, 2015, **58**, 8315-8359.

14. J. A. Bertout, S. A. Patel and M. C. Simon, *Nature Reviews Cancer*, 2008, **8**, 967.
15. P. Vaupel and A. Mayer, *Cancer and Metastasis Reviews*, 2007, **26**, 225-239.
16. J. J. Yeh and W. Y. Kim, *Journal of Clinical Oncology*, 2015, **33**, 1505-1508.
17. W. R. Wilson and M. P. Hay, *Nature Reviews Cancer*, 2011, **11**, 393.
18. F. W. Hunter, B. G. Wouters and W. R. Wilson, *British Journal of Cancer*, 2016, **114**, 1071-1077.
19. A. R. Pries, A. J. M. Cornelissen, A. A. Sloot, M. Hinkeldey, M. R. Dreher, M. Hopfner, M. W. Dewhirst and T. W. Secomb, *Plos Computational Biology*, 2009, **5**.
20. R. K. Jain, *Science*, 2005, **307**, 58-62.
21. G. L. Semenza, *The Journal of Clinical Investigation*, 2008, **118**, 3835-3837.
22. R. K. Jain, *Nature medicine*, 2001, **7**, 987-989.
23. S. P. Fricker, *Dalton Transactions*, 2007, 4903-4917.
24. N. Graf and S. J. Lippard, *Advanced Drug Delivery Reviews*, 2012, **64**, 993-1004.
25. M. D. Hall and T. W. Hambley, *Coordination Chemistry Reviews*, 2002, **232**, 49-67.
26. C. G. Hartinger, M. A. Jakupec, S. Zorbas-Seifried, M. Groessl, A. Egger, W. Berger, H. Zorbas, P. J. Dyson and B. K. Keppler, *Chemistry & Biodiversity*, 2008, **5**, 2140-2155.
27. A. Levina, A. Mitra and P. A. Lay, *Metallomics*, 2009, **1**, 458-470.
28. D. C. Ware, B. G. Siim, K. G. Robinson, W. A. Denny, P. J. Brothers and G. R. Clark, *Inorganic Chemistry*, 1991, **30**, 3750-3757.
29. T. W. Failes and T. W. Hambley, *Journal of Inorganic Biochemistry*, 2007, **101**, 396-403.

30. D. C. Ware, B. D. Palmer, W. R. Wilson and W. A. Denny, *Journal of Medicinal Chemistry*, 1993, **36**, 1839-1846.
31. D. C. Ware, W. R. Wilson, W. A. Denny and C. E. F. Rickard, *Journal of the Chemical Society, Chemical Communications*, 1991, 1171-1173.
32. C. A. Rabik and M. E. Dolan, *Cancer Treatment Reviews*, **33**, 9-23.
33. C. S. Allardyce, P. J. Dyson, D. J. Ellis and S. L. Heath, *Chemical Communications*, 2001, 1396-1397.
34. K. C. Reed and F. L. Bygrave, *Biochemical Journal*, 1974, **140**, 143-155.
35. J. Durig, J. Danneman, W. Behnke and E. Mercer, *Chemico-biological Interactions*, 1976, **13**, 287-294.
36. P. J. Blower, J. R. Dilworth, R. I. Maurer, G. D. Mullen, C. A. Reynolds and Y. Zheng, *Journal of Inorganic Biochemistry*, 2001, **85**, 15-22.
37. L. L. Parker, S. M. Lacy, L. J. Farrugia, C. Evans, D. J. Robins, C. C. O'Hare, J. A. Hartley, M. Jaffar and I. J. Stratford, *Journal of Medicinal Chemistry*, 2004, **47**, 5683-5689.
38. S. Faivre, D. Chan, R. Salinas, B. Woynarowska and J. M. Woynarowski, *Biochemical Pharmacology*, 2003, **66**, 225-237.
39. C. L. Ventola, *Pharmacy and Therapeutics*, 2015, **40**, 277.
40. C. J. von Wintersdorff, J. Penders, J. M. van Niekerk, N. D. Mills, S. Majumder, L. B. van Alphen, P. H. Savelkoul and P. F. Wolfs, *Frontiers in Microbiology*, 2016, **7**.
41. S. Santajit and N. Indrawattana, *BioMed Research International*, 2016, **2016**.
42. F. F. Li, J. G. Collins and F. R. Keene, *Chemical Society Reviews*, 2015, **44**, 2529-2542.
43. L. B. Rice, *Infection Control & Hospital Epidemiology*, 2010, **31**, S7-S10.

44. H. W. Boucher, G. H. Talbot, J. S. Bradley, J. E. Edwards, D. Gilbert, L. B. Rice, M. Scheld, B. Spellberg and J. Bartlett, *Clinical Infectious Diseases*, 2009, **48**, 1-12.
45. G. D. Wright, *Advanced Drug Delivery Reviews*, 2005, **57**, 1451-1470.
46. D. N. Wilson, *Nature Reviews Microbiology*, 2014, **12**, 35-48.
47. X.-Z. Li and H. Nikaido, *Drugs*, 2004, **64**, 159-204.
48. B. D. Brooks and A. E. Brooks, *Advanced Drug Delivery Reviews*, 2014, **78**, 14-27.
49. M. A. Fischbach and C. T. Walsh, *Science*, 2009, **325**, 1089-1093.
50. A. Albert, M. Gibson and S. Rubbo, *British Journal of Experimental Pathology*, 1953, **34**, 119.
51. S. Rubbo, A. Albert and M. I. Gibson, *British Journal of Experimental Pathology*, 1950, **31**, 425.
52. A. Regiel-Futyra, J. M. Dąbrowski, O. Mazuryk, K. Śpiewak, A. Kyzioł, B. Pucelik, M. Brindell and G. Stochel, *Coordination Chemistry Reviews*, 2017.
53. F. Dwyer and D. Mellor, *New York and London*, 1964, 118.
54. F. Dwyer, I. Reid, A. Shulman, G. M. Laycock and S. Dixon, *Immunology and Cell Biology*, 1969, **47**, 203.
55. F. Dwyer, E. C. Gyarfás, W. Rogers and J. H. KOCH, *Nature*, 1952, **170**, 190-191.
56. J. L. Wilson, H. E. Jesse, B. Hughes, V. Lund, K. Naylor, K. S. Davidge, G. M. Cook, B. E. Mann and R. K. Poole, *Antioxidants & Redox Signaling*, 2013, **19**, 497-509.
57. L. S. Nobre, J. D. Seixas, C. C. Romão and L. M. Saraiva, *Antimicrobial Agents and Chemotherapy*, 2007, **51**, 4303-4307.

58. C. S. Bang, R. Kruse, I. Demirel, A. Önnberg, B. Söderquist and K. Persson, *Microbial Pathogenesis*, 2014, **66**, 29-35.
59. M. Desmard, K. S. Davidge, O. Bouvet, D. Morin, D. Roux, R. Foresti, J. D. Ricard, E. Denamur, R. K. Poole and P. Montravers, *The FASEB Journal*, 2009, **23**, 1023-1031.
60. L. S. Nobre, H. Jeremias, C. C. Romão and L. M. Saraiva, *Dalton Transactions*, 2016, **45**, 1455-1466.
61. J. S. Ward, J. M. Lynam, J. Moir and I. J. Fairlamb, *Chemistry-A European Journal*, 2014, **20**, 15061-15068.
62. A. Bolhuis, L. Hand, J. E. Marshall, A. D. Richards, A. Rodger and J. Aldrich-Wright, *European Journal of Pharmaceutical Sciences*, 2011, **42**, 313-317.
63. M. I. Samanovic, C. Ding, D. J. Thiele and K. H. Darwin, *Cell Host & Microbe*, 2012, **11**, 106-115.
64. H. Dollwet and J. Sorenson, *Trace elements in Medicine*, 1985, **2**, 80-87.
65. G. Grass, C. Rensing and M. Solioz, *Applied and Environmental Microbiology*, 2011, **77**, 1541-1547.
66. R. J. Turner, *Microbial Biotechnology*, 2017, **10**, 1062-1065.
67. M. Orojloo, P. Zolgharnein, M. Solimannejad and S. Amani, *Inorganica Chimica Acta*, 2017, **467**, 227-237.
68. F. Sevgi, U. Bagkesici, A. N. Kursunlu and E. Guler, *Journal of Molecular Structure*, 2018, **1154**, 256-260.
69. H. G. Aslan, S. Özcan and N. Karacan, *Inorganic Chemistry Communications*, 2011, **14**, 1550-1553.
70. F. A. Bassyouni, S. M. Abu-Bakr, K. H. Hegab, W. El-Eraky, A. A. El Beih and M. E. A. Rehim, *Research on Chemical Intermediates*, 2012, **38**, 1527-1550.

71. M. S. Aljhdali, A. T. Abdelkarim, A. A. El-Sherif and M. M. Ahmed, *Journal of Coordination Chemistry*, 2014, **67**, 870-890.
72. J. E. Edwards Jr, Mass Medical Soc, Editon edn., 1991.
73. M. M. McNeil, S. L. Nash, R. A. Hajjeh, M. A. Phelan, L. A. Conn, B. D. Plikaytis and D. W. Warnock, *Clinical Infectious Diseases*, 2001, **33**, 641-647.
74. A. Srinivasan, J. L. Lopez-Ribot and A. K. Ramasubramanian, *Drug Discovery Today. Technologies*, 2014, **11**, 65-71.
75. S. K. Fridkin and W. R. Jarvis, *Clinical Microbiology Reviews*, 1996, **9**, 499-511.
76. G. P. Bodey, *Journal of Hospital Infection*, 1988, **11**, 411-426.
77. N. Robbins, G. D. Wright and L. E. Cowen, *Microbiology Spectrum*, 2016, **4**.
78. T. Walsh and A. Groll, *Transplant Infectious Disease*, 1999, **1**, 247-261.
79. S. Ascioğlu, J. Rex, B. De Pauw, J. Bennett, J. Bille, F. Crokaert, D. Denning, J. Donnelly, J. Edwards and Z. Erjavec, *Clinical Infectious Diseases*, 2002, **34**, 7-14.
80. M. M. Balkis, S. D. Leidich, P. K. Mukherjee and M. A. Ghannoum, *Drugs*, 2002, **62**, 1025-1040.
81. A. M. Fuentefria, B. Pippi, D. F. Dalla Lana, K. K. Donato and S. F. de Andrade, *Letters in Applied Microbiology*, 2018, **66**, 2-13.
82. A. I Ramos, T. M Braga and S. S Braga, *Mini Reviews in Medicinal Chemistry*, 2012, **12**, 227-235.
83. N. Dharmaraj, P. Viswanathamurthi and K. Natarajan, *Transition Metal Chemistry*, 2001, **26**, 105-109.
84. R. Ramesh and S. Maheswaran, *Journal of Inorganic Biochemistry*, 2003, **96**, 457-462.
85. R. Ramesh and M. Sivagamasundari, *Synthesis and Reactivity in Inorganic and Metal-Organic Chemistry*, 2003, **33**, 899-910.

86. P. Viswanathamurthi, N. Dharmaraj and K. Natarajan, *Synthesis and Reactivity in Inorganic and Metal-Organic Chemistry*, 2000, **30**, 1273-1285.
87. N. P. Priya, S. V. Arunachalam, N. Sathya, V. Chinnusamy and C. Jayabalakrishnan, *Transition Metal Chemistry*, 2009, **34**, 437-445.
88. R. G. de Lima, A. Lever, I. Y. Ito and R. S. da Silva, *Transition Metal Chemistry*, 2003, **28**, 272-275.
89. S. Medici, M. Peana, V. M. Nurchi, J. I. Lachowicz, G. Crisponi and M. A. Zoroddu, *Coordination Chemistry Reviews*, 2015, **284**, 329-350.
90. B. Chudzik, I. B. Tracz, G. Czernel, M. J. Fiołka, G. Borsuk and M. Gagoś, *European Journal of Pharmaceutical Sciences*, 2013, **49**, 850-857.
91. S. Bouson, A. Krittayavathananon, N. Phattharasupakun, P. Siwayaprahm and M. Sawangphruk, *Open Science*, 2017, **4**, 170654.

Chapter 5

Biological Relevance Studies on β -*bis*-Ketoiminate Complexes of Ruthenium and Copper

5.1 Introduction to biological relevance

This chapter discusses further biological assays and experiments conducted on the β -bis-ketoiminate ruthenium(II) dicarbonyl and β -bis-ketoiminate copper(II) family of complexes synthesised within this thesis and discussed in **Chapter 2** and **3** respectively.

The major drawback for potential organometallic drug candidates is the subsequent failure of these molecules in early stage clinical trials or late development stages, mainly due to poor pharmacokinetic properties. In depth analysis of structure-activity relationships (SARs) that can be related to the molecular structure of the drug candidate allow for further rationale of synthesis and modification leading to new drug candidates with better efficacy, bio-chemical reactivity and physicochemical properties. These SARs assist the medicinal chemist with the fundamental challenge of turning a structural lead into a “drug like” molecule.^{1,2}

5.2 Hydrolysis Studies

5.2.1 Introduction to hydrolysis

In the application of metal based drugs such as cisplatin in cancer treatment, it is assumed that the form of the complex that binds to biomolecules, such as DNA, inside the cell is quite different from the complex initially introduced into the organism.³ In many cases the original metal complex is treated as a prodrug that is inert which later becomes activated through various metabolic pathways. Activation by hydrolysis is a mechanism known to be important for metal based complexes such as cisplatin,⁴⁻⁶ and the ruthenium complexes, NAMI-A and KP1019,⁷⁻¹⁰ and aquation has been proved to be the crucial step in these mechanisms.³ The steps leading to complex activation include ligand substitution, a change in oxidation state, a photochemical process, or in some cases a combination of these. These reactions can be a result of enzyme catalyzed chemical transformation or more commonly internal stimulus such as physiological difference in the environment (pH, salt concentration and redox potential).¹¹ Sadler *et al.*¹¹ have proposed that generally, with few exceptions, the rate of hydrolysis is directly proportional to the cytotoxicity of the complex. This hypothesis has been

observed with ruthenium(III) *bis*-picolinamide complexes previously synthesised within our research group.¹²

5.2.2 Hydrolysis of β -*bis*-Ketoiminate Ru(II) Dicarbonyl Complexes

Hydrolysis studies were not investigated for all complexes, a range of complexes from the least active to the most active were selected, for both classes of complexes. ¹H NMR samples were prepared in 9:1 *d*₃-acetonitrile/D₂O to give a final concentration of 8 mg ml⁻¹, and run every 24 hours over a 4 day period. UV/vis samples were prepared in 9:1 acetonitrile/water to give a final concentration of 50 μ M. The concentration of the complexes could not be increased due to poor solubility in water. The solutions were scanned using UV/vis spectrophotometry every 24 hours, over a period of 4 days, to correlate with the MTT assay, and after the final analyses, the UV/vis samples were analysed by ESI-MS.

For β -*bis*-ketoiminate Ru(II) dicarbonyl complexes, the most active or partially active complexes (**C3**, **C4** and **C8**), and their inactive closest analogies (**C10** and **C11**) were analysed (**Figure 5.2.1**). In addition, the unsubstituted complex **C1**, was also analysed for comparison purposes. Changes in the UV/vis spectra of the complexes are displayed in **Figure 5.2.2** and the changes in wavelengths of absorption bands are summarised in **Table 5.2.1**. The arrows on the graphs in **Figure 5.2.2**, in either up or down direction, indicate changes in absorption intensities upon hydrolysis, from day 0 to day 4. Slow darkening of the initial colour, from yellow to brown, was observed for all complexes, from day 0 to day 4, with **C3** giving the least colour change.

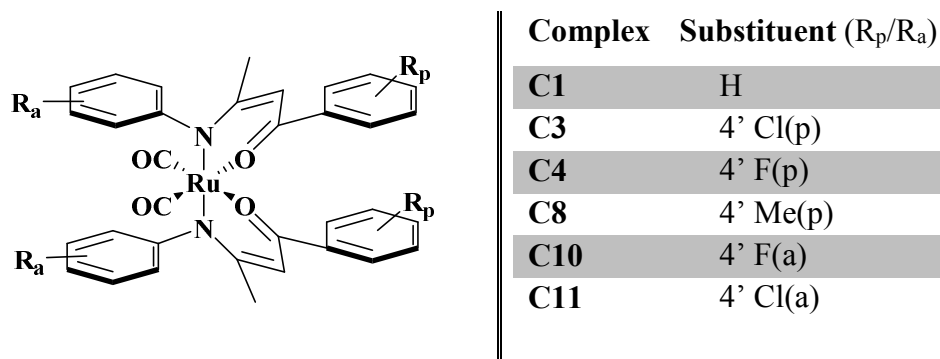
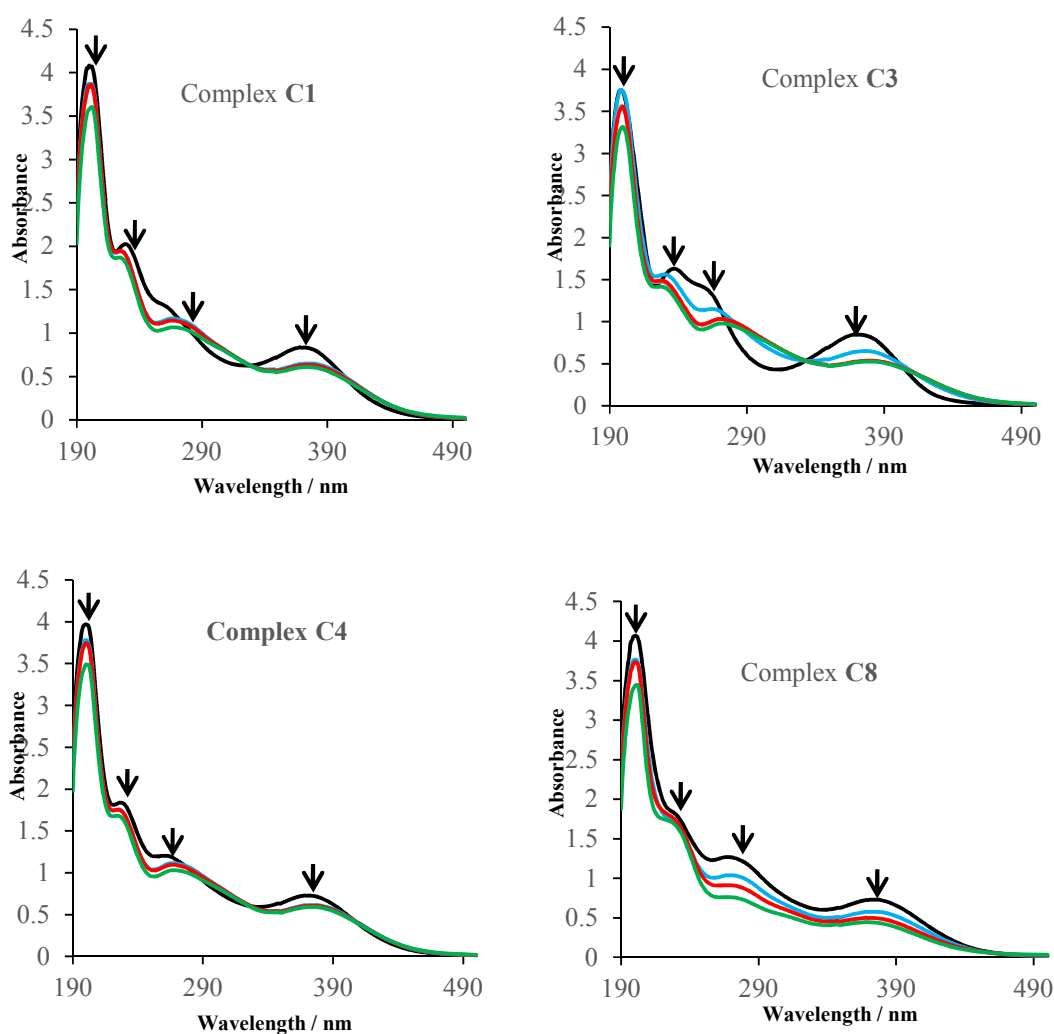


Figure 5.2.1: Ru(II) dicarbonyl complexes under hydrolysis studies

Distinctive changes in the UV/vis spectra were observed for the Ru(II) dicarbonyl complexes under study over the 4 day period. Absorption peaks in the ultraviolet region (190 – 350 nm) were observed for all the complexes. The most intense and evident ultraviolet region absorption within the range 198 - 202 nm, are due to ligand based $\pi - \pi^*$ transitions. Furthermore, at least one (complexes **C1** and **C4** have two) relatively weak peak due to ligand based charge-transfer was observed for all the complexes in the ultraviolet region. The visible light region (350 – 750 nm) of the complexes is characterised by an intense absorption peak at approximately 368 nm, characteristic of metal to ligand charge transfer (MLCT) transitions.^{13, 14}



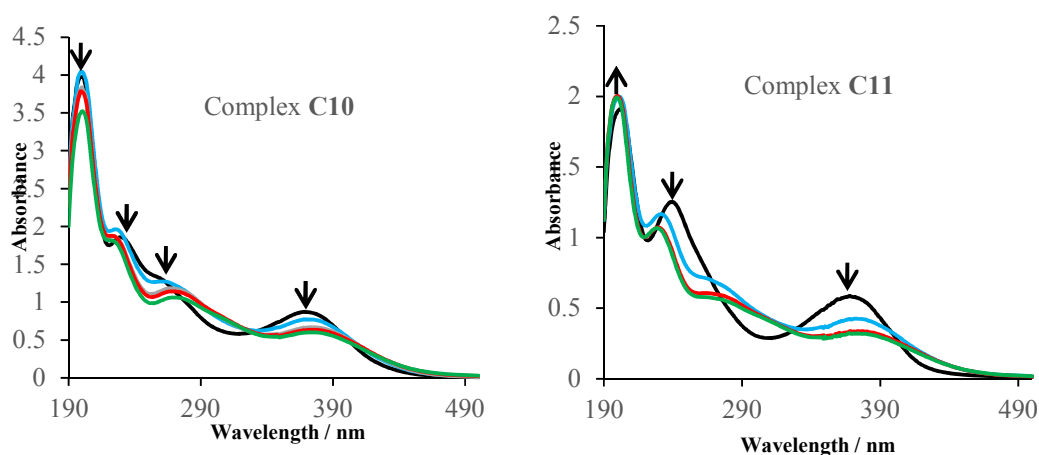


Figure 5.2.2: UV/vis spectra for the hydrolysis of Ru(II) dicarbonyl complexes
Key: day 0 = Black, day 1 = blue, day 2 = grey, day 3 = red, day 4 = green

Table 5.2.1: UV/vis absorption bands for complexes **C1**, **C3**, **C4**, **C8**, **C10** and **C11**

Complex	Substituent (R_p/R_a)	Wavelength / nm	
		Day 0	Day 4
C1	H	200, 229, 261, 368	202, 224, 267, 368
C3	4' Cl(p)	198, 237, 368	201, 228, 272, 368
C4	4' F(p)	200, 227, 261, 368	200, 224, 268, 368
C8	4' Me(p)	200, 267, 368	201, 266, 368
C10	4' F(a)	200, 231, 368	200, 270, 368
C11	4' Cl(a)	202, 239, 368	199, 228, 368

(p) = substituent on *phenolate* ring; (a) = substituent on *aniline* ring

As seen from **Figure 5.2.2**, all the complexes under study, active (**C4** ($IC_{50} = 21.61 \mu\text{M}$)), moderately active (**C3** ($IC_{50} = 43.40 \mu\text{M}$), **C8** ($IC_{50} = 54.20 \mu\text{M}$)) and inactive (**C1** ($IC_{50} = 85.96 \mu\text{M}$), **C10** ($IC_{50} = 66.79 \mu\text{M}$), **C11** ($IC_{50} = 71.90 \mu\text{M}$)), undergo hydrolysis to a greater or lesser degree. A similar trend is observed for all complexes from day 0 to day 4, with changes in the absorption bands indicating that there are ligand substitution reactions occurring when the complexes are in aqueous solution.¹⁵ A decrease in the intensity of the absorption peaks is seen from day 0 to day 4, with the most significant decrease being observed between day 0 and day 1.

However, the rate of hydrolysis differs, and the proposed rate of hydrolysis as seen from the UV/vis absorption spectra is as follows; **C4** > **C1** > **C3** > **C10** > **C11** > **C8**. Complex **C4** is completely hydrolysed by day 1, complex **C1** is completely hydrolysed by day 2, complex **C3** is completely hydrolysed by day 3 and **C10** and **C11** are completely hydrolysed by day 4, while **C8** is still undergoing hydrolysis by day 4. The relatively similar hydrolysis rates of the unsubstituted complex **C1** and the electron withdrawing substituted complex **C4** suggest that addition of the electron withdrawing substituents on the ligand has no significant effect on the rate of hydrolysis. Contrary to this, electron donating substituents such as the *para* methyl group significantly lower the rate of hydrolysis as seen when comparing the spectra of complex **C1** and **C11**.

In addition, the nature of the phenyl ring (*phenolate* or *aniline* phenyl ring) carrying the substituents affects the rate of hydrolysis. This can be seen by comparing the spectra of complexes **C4** and **C10**. Complex **C4**, with a *para* fluoro substituent on the *phenolate* phenyl ring is completely hydrolysed by day 1, while **C10**, with a *para* fluoro substituent on the *aniline* phenyl ring is only completely hydrolysed by day 4. Analogue complexes, **C3** and **C11** also show comparable results. These results suggest that complexes with substituents on the *phenolate* phenyl ring undergo hydrolysis faster than their *aniline* phenyl ring substituted analogues. These differences in the rate of hydrolysis for complexes **C4**, **C3**, **C10** and **C11** are consistent with their observed anti-cancer activities discussed in **Chapter 4**. The anti-cancer activity of complexes **C3** and **C4** with substituents on the *phenolate* phenyl ring is higher than that of their analogue complexes **C10** and **C11** where similar substituents are on the *aniline* phenyl ring, **Figure 5.2.3**.

	Complex	IC ₅₀ / μM
Rate of hydrolysis ↓	C4	21.61±3.55
	C3	43.40±5.67
	C10	66.79±6.84
	C11	71.90±5.62

Figure 5.2.3: Rate of hydrolysis and anti-cancer activity of some complexes

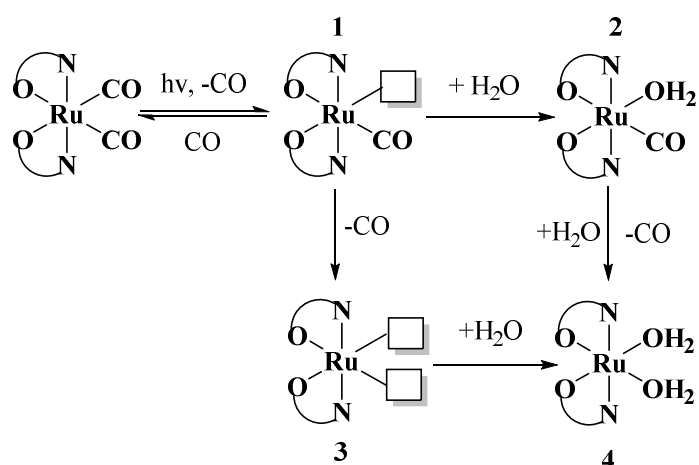
However, the overall proposed rate of hydrolysis; **C4** > **C1** > **C3** > **C10** > **C11** > **C8**, does not correlate with the observed anti-cancer activities of these complexes. The unsubstituted, inactive complex **C1** has a higher hydrolysis rate compared to other moderately active complexes (**C3** and **C8**). This is in contrast with most metal based anti-cancer complexes whose mode of activation is based on “activation by reduction”. For these complexes, inactive complexes are known not to undergo hydrolysis. The contrasting patterns highlight that for this series of complexes hydrolysis plays a role in the resultant anti-cancer activities of the complexes but is not the only influential factor.

Under physiological conditions, β -bis-ketoiminate Ru(II) dicarbonyl complexes are likely to undergo hydrolysis reactions similar to that of cisplatin, NAMI-A, KP1019 and Ru(II)-arene complexes. However, the presence of the carbonyl ligand as the labile group further implicates the use of this class of compounds as CORMs, allowing for different pathways to the conventional ones. A proposed hydrolysis pathway for the neutral Ru(II) dicarbonyl complexes is shown in **Scheme 5.2.1**.^{13, 16}

In this mechanism, hydrolysis of the complexes begins with dissociation of the carbonyl labile ligand to create intermediate **1** with a vacant site. The intermediate can then react with water to form **2**, or undergo further dissociation of the second carbonyl ligand to give intermediate **3**. The latter route is highly unlikely due to the instability of intermediate **3**, which if formed is likely to decompose. The most probable route is that in which intermediate **3** loses the second carbonyl ligand and is further hydrolysed to **4**.

Hydrolysis or ligand exchange mechanisms can thus act as CO release triggers¹⁷ and Mortellini *et al.*¹⁶ have proposed the dissociation of CO as the rate determining step. Even with water adducts likely to form, the intermediates in this mechanism can be toxic and are likely to be reactive, particularly intermediate **1**, with a vacant site. These reactive intermediates can potentially explain the toxicity observed in anti-cancer cell line studies of β -bis-ketoiminate Ru(II) dicarbonyl complexes (**Chapter 4**). Loss of the labile carbonyl group can lead to a number of possibilities for the complexes:

- i. Decomposition of the Ru-ligand intermediate after carbonyl ligand loss due to instability. For this class of complexes this could explain why hydrolysis is observed even for the inactive complexes.^{14, 18}
- ii. The intermediates may be able to react with off-target biomolecules before reaching the target site, resulting in toxicity to healthy cells and decrease in cytotoxicity.
- iii. The rapid and premature release of CO may increase the toxicity while decreasing the selectivity of the active complexes.



Scheme 5.2.1: Proposed hydrolysis mechanism for Ru(II) dicarbonyl complexes

Hydrolysis studies done through observing changes in the 1H NMR spectra are shown in **Figure 5.2.4**. Only the spectra of complexes **C4** and **C8** are given. Complex **C4** showed the highest rate of hydrolysis according to UV/vis spectra while complex **C8** had the least rate (**Figure 5.2.2**). Minor changes in the 1H NMR spectra are observed from day 0 to day 4. Overall the spectra of the selected complexes show changes in the intensity of the peaks particularly in the aromatic region (7-8 ppm) and for the characteristic methine β -ketoiminate proton peak (5.7-5.9 ppm). In both complexes the peak due to the methine proton disappears by day 4. There is no obvious broadening of peaks suggesting that no paramagnetic or charged species are being formed in solution.

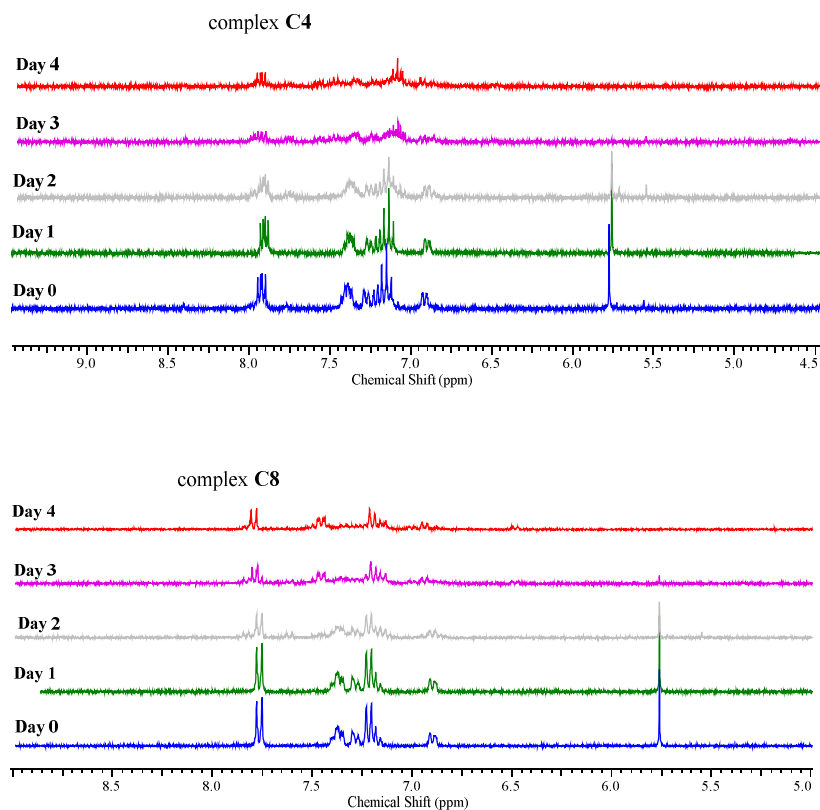


Figure 5.2.4: ^1H NMR of complexes C4 and C8 over 4 days

The loss of the methine proton peak potentially indicates the dissociation and degradation of the ketoiminate ligand from the complex. This is supported by mass spectrometry data obtained for the complexes at the end of day 4, in which no peaks can be assigned to the free ligand. The mass spectra of the complexes are characterised by various peaks each with the ruthenium metal isotope pattern. This suggests that these complexes undergo hydrolysis in which the carbonyl ligand is substituted or released. However, the by-products of hydrolysis differ for each individual complex. Major peaks found in both spectra have been assigned to the complexes shown in **Figure 5.2.5**.

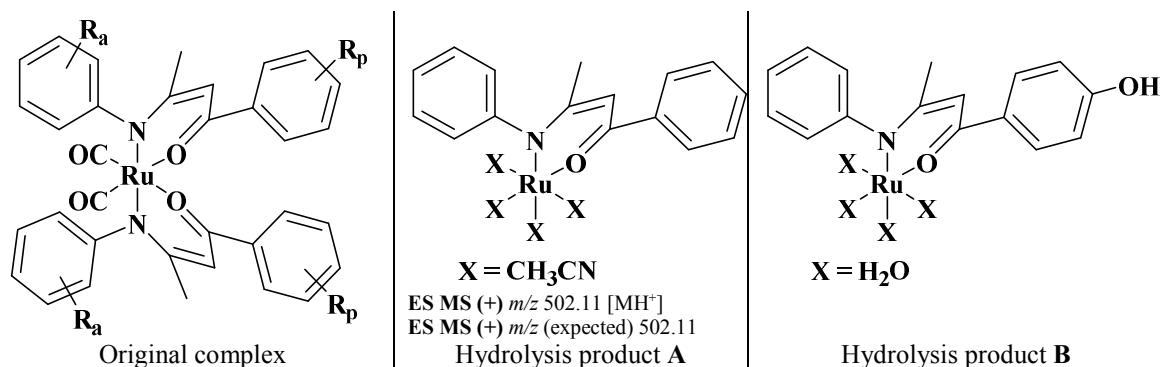


Figure 5.2.5: Possible hydrolysis products (from mass spectrometry)

Although a ruthenium aqua species can be identified from mass spectra, the presence of other various peaks suggests that the complexes also undergo degradation over time.

5.2.3 Hydrolysis of β -bis-Ketoiminate Cu(II) Complexes

Hydrolysis studies were also carried out on β -bis-ketoiminate copper(II) complexes, **C22** ($\text{IC}_{50} > 100 \mu\text{M}$) and **C42** ($\text{IC}_{50} = 42.35 \mu\text{M}$) which are inactive and moderately active, respectively, against HCT116++ cell line. UV/vis samples were prepared in 9:1 acetonitrile/water to give a final concentration of $50 \mu\text{M}$. The concentration of the complexes could not be increased due to poor solubility in water. The solutions were scanned using UV/vis spectrophotometry every 24 hours, over a period of 4 days, to correlate with the MTT assay.

Changes in the UV/vis spectra of the complexes are displayed in **Figure 5.2.6** and the arrows on the graphs indicate changes in absorption intensities upon hydrolysis, from day 0 to day 4. Both complexes, **C22** and **C42** show similar changes in the UV/vis spectra indicating that the resultant anti-cancer activity of this family of complexes is independent of hydrolysis. At day 0, the complexes show intense ligand based absorbance (π - π^*) at approximately 200nm and 360 nm with additional less intense ligand based charge transfer bands (n - π^*) at 245 nm for complex **C22** and 255 nm and 285 nm for complex **C42**. By day 4 the distinct peaks are still present at approximately the same wavelength, with no significant changes in the intensity. No quantitative information could be inferred from the mass spectrometry data of these complexes

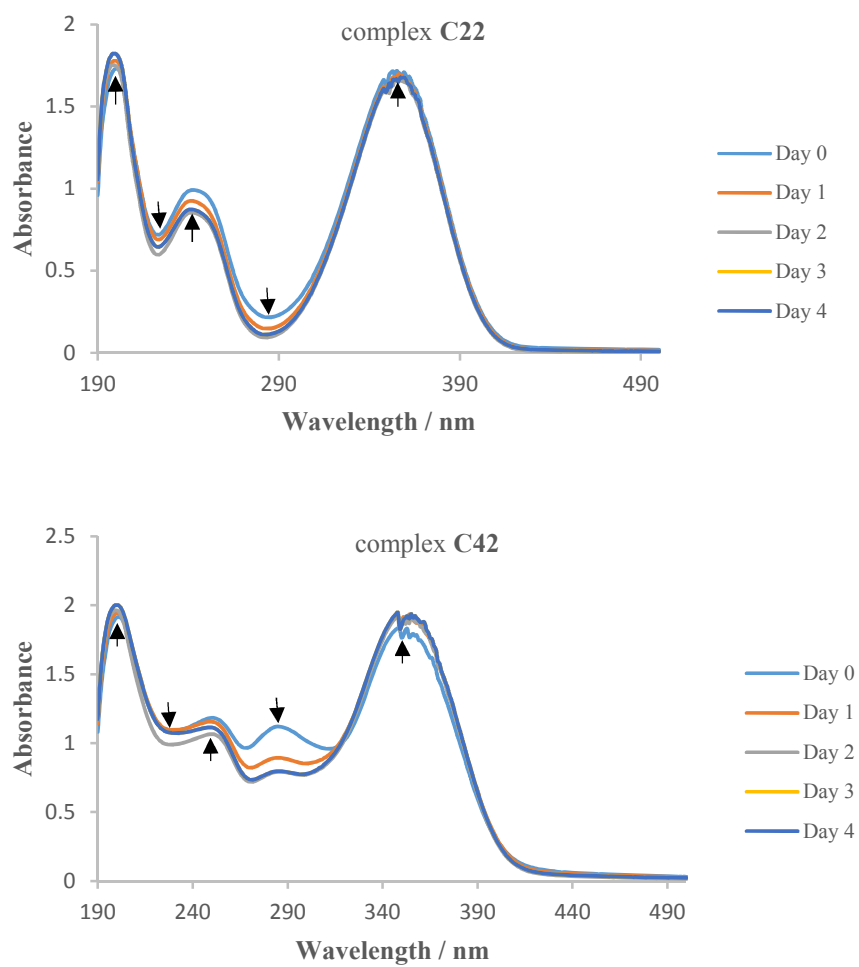


Figure 5.2.6: UV/vis spectra for the hydrolysis of copper complexes **C22** and **C42**

5.3 Biomembrane Studies

5.3.1 Introduction to biomembrane studies

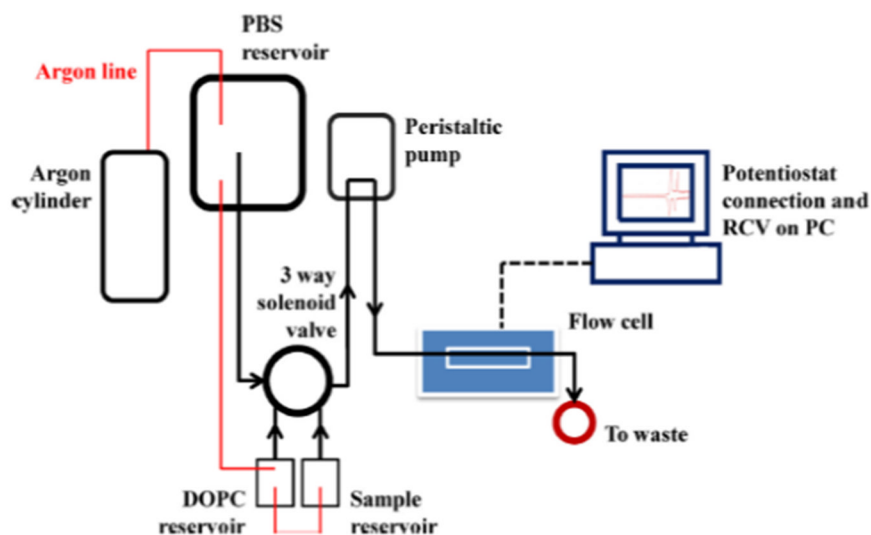
Organisms, including the human body, have a number of biological membranes whose functions range from protecting cells from foreign molecules, hosting bioactive molecules to regulating traffic between the inside of the cell and the extracellular medium. Post administration, a drug molecule encounters one or more of these biomembranes, from simple ones such as blood vessel endothelium to circulating macrophages to the more complex ones such as blood-brain or blood-retinal barriers. Therefore, its interaction with a biomembrane physically or chemically is unique.¹⁹

Biological membranes acting either as a barrier to drug permeation or the site of action of a drug molecule can act as the final step. However, in many cases drug-membrane interactions are the start of a series of chemical and physical processes that affect the rate of penetration and partitioning of the drug molecule into the cell and ultimately its specific site of action. As such drug distribution, in terms of both concentration and rate is highly dependent on the interactions of a drug molecule with various biomembranes.²⁰

The study of drug-membrane interactions during the preclinical phase is a powerful tool as it can be used to design and optimise the activity and tolerability profiles of new drug candidates, and also to allow compatible drugs to enter clinical trials. Simplified artificial models of biological membranes, still under intensive development, have been used to study and better understand drug-membrane interactions such as cellular uptake, drug transport, drug activity and toxicity.¹⁹⁻²² Four types of lipid membrane models have been identified and are commonly used: monolayers (Langmuir monolayers), vesicle forming bilayers (liposomes), supported bilayers and tethered bilayer lipid membranes.²²

Phospholipid monolayers on the surface of a mercury electrode have received widespread interest and application as biological membrane models.^{23, 24} Over the last decade, Nelson *et al.* have developed a unique membrane based sensing device. In this model shown in **Scheme 5.3.1** a phospholipid monolayer is

deposited on a mercury electrode strongly bound to a platinum contact. This sensing electrode is connected to a high throughput flow system which uses rapid cyclic voltammetry (RCV) to monitor changes in capacitance current with voltage and allows rapid screening of large numbers of compounds. The monolayer is selectively damaged, through interaction with biomembrane active compounds in the sample.^{21, 25-29}



Scheme 5.3.1: Schematic representation of model biomembrane system²⁸

Compared to other supported membrane techniques, the smooth mercury support surface is complimentary to the fluidity and hydrophobic nature of the phospholipids forming defect-free, self-renewing phospholipid monolayers. Monolayers made from phospholipid dioleoyl phosphatidylcholine (DOPC) act as the model biomembrane.²⁸ The model has been used for analysing ion channel function and co-enzyme electron transfer.^{30, 31} However its main application is as a sensor for biological membrane active compounds. The fluid and highly ordered phospholipid monolayers allow for easy detection of any alterations arising from the active compounds.^{21, 32} The model has been applied on biomembrane studies with peptides,³³⁻³⁶ nanoparticles^{37, 38} and organic molecules such as steroids, flavonoids, polycyclic aromatic hydrocarbons, tricyclic anti-depressants and tricyclic phenothiazines.^{28, 39} In line with the widespread interest in the application of organometallic compounds in the medical and biological fields, this model was

recently applied and reported for a series of silver(I) non-heterocyclic carbene (NHC) complexes.⁴⁰

Monolayers of DOPC are known to undergo various phase transitions in response to changes in potential. These phase transitions are visualised as sharp peaks in the capacitance current [Figure 5.3.1 (a)]. The capacitance peaks correspond to the entrance of electrolytes into the layer leading to a mixed electrolyte phospholipid and the re-organisation of the layer to form bilayer areas [Figure 5.3.1 (b)]. In an experimental flow system, such as the one used in this study, a typical RCV plot with two capacitance peaks such as that shown in Figure 5.3.2 is observed.^{25, 26, 41-43} The capacitance peaks have been intensely investigated and characterised, undisputedly their formation is dependent on the interaction of the lipid monolayer with biological membrane active species in solution.^{42, 44}

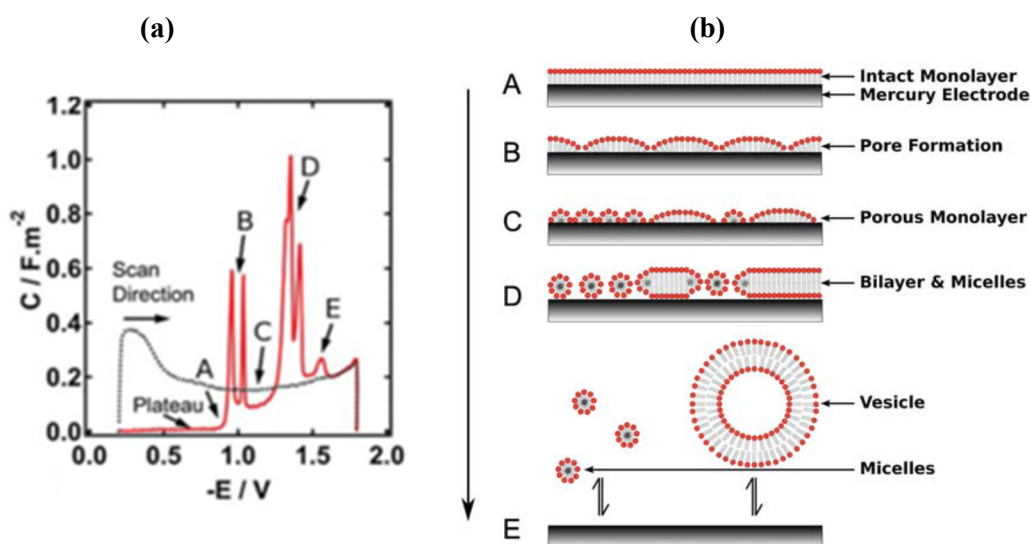


Figure 5.3.1: (a) Typical RCV plot of DOPC monolayer with (b) associated phase transitions⁴³

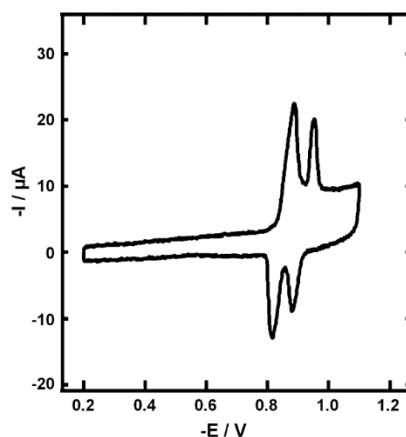


Figure 5.3.2: Typical RCV plot of DOPC monolayer in a flow cell ²⁵

As the biomembrane active species in solution interact with the monolayer, any modifications in its organisation and fluidity results in alterations in the characteristic peak shapes, heights and/or positions in the RCV plot. Increase in capacitance current; with subsequent reduction in the peak heights indicate disruption of the monolayer due to penetration of the DOPC layer. In cases where the active species adsorb to the monolayer, changes such as reduction in peak height and broadening of peaks with no changes in capacitance current are seen on the RCV plot.⁴⁵

5.3.2 Biomembrane Studies of β -bis-Ketoiminate Ru(II) Dicarbonyl Complexes

In collaboration with the Nelson Research Group at The University of Leeds, β -bis-ketoiminate ruthenium(II) dicarbonyl complexes were tested for their potential to interact with the artificial biomembrane by Danielle Marriott and Dr. Shahrzad Mohamadi. Deposition of dioleoyl phosphatidylcholine (DOPC) on the Pt/Hg electrode is performed before introduction of a complex. A potential excursion from -0.4 to -3.0 V at 100 V s⁻¹ scan rate is applied, and 100-200 μ L of DOPC introduced into the flow cell. The potential excursion is then altered to -0.4 to -1.2 V. By repetitive cycling, the characteristic RCV plots of DOPC are obtained. The complex is introduced into the flow cell and the RCV plot monitored while varying the electrode potential from -0.4 to -3.0 V. Recovery, or failure to recover, of the characteristic RCV peaks after complex exposure, indicate that the interaction leads to a permanent damage of the membrane.

Biomembrane studies were not conducted on the entire series of β -bis-ketoiminate Ru(II) dicarbonyl complexes, only complexes **C1**, **C4**, **C7**, **C8**, **C9** and **C11** were analysed. The selected complexes include active **C1** ($IC_{50} = 21.61 \mu\text{M}$), partially active **C8** ($IC_{50} = 54.20 \mu\text{M}$) and **C9** ($IC_{50} = 64.80 \mu\text{M}$), as well as inactive complexes **C1** ($IC_{50} = 85.96 \mu\text{M}$) and **C11** ($IC_{50} = 71.90 \mu\text{M}$), with varying electronic and steric properties. The RCV plots of the interaction of the complexes with the artificial biomembrane are shown in **Figure 5.3.3**.

The complexes show varying degrees of changes from the typical DOPC RCV membrane plots, with complex **C9** showing the most pronounced distortions. The RCV plots show changes mainly in peak height and breath, with no changes in baseline current. This indicates that the complexes are able to adsorb and to some extent interact with the DOPC monolayer. Thus, the implication is that, unlike cisplatin, the complexes are able to enter the cell membrane *via* passive diffusion. This is in agreement with literature reports in which passive diffusion has been implicated as the fundamental mode of entry into cell membranes for carbon monoxide delivery from CORMs.⁴⁶⁻⁴⁸

There is no distinct correlation between biomembrane interaction and neither electronic nor steric properties of the complexes. Complexes **C4**, **C7** and **C11** have electronegative substituents that can provide an area of negative surface charge. Thus, compared to complexes **C8** and **C9** with electropositive substituents, they can potentially interact to a greater extent with the positively charged DOPC monolayer head group. However, the RCV plots show no such differences. Comparing the RCV plot for the unsubstituted complex **C1** with all the other complexes, the author can conclude that addition of either electron donating or withdrawing groups has negligible effect on the degree of interaction of the complexes with the monolayer. Although complexes **C9** and **C11** are structurally similar, the distinctively different RCV plots show that structural properties such as steric have no effect on the membrane interactions.

Complex **C11** is inactive with an IC_{50} value of $71.90 \mu\text{M}$, however, it shows changes in the RCV DOPC plot consistent with interactions with the monolayer. Complex **C9** which shows the most pronounced changes in the RCV DOPC plot is

moderately active, less active than **C4** and **C8**. Complex **C4**, the most cytotoxic of this series of complexes shows a similar DOPC RCV plot to all the other complexes. These comparisons show that there is no direct correlation between cytotoxicity and membrane interactions. Thus, for this class of complexes the ability to passively diffuse through the cell membrane has no relation to the resultant potency of the complex. This conclusion is in-line with the findings by Stamellou *et al.*⁴⁷ who concluded that for enzyme triggered CORMS, it is unclear how factors such as structural differences influence cellular uptake, which in turn influences the biological activity.

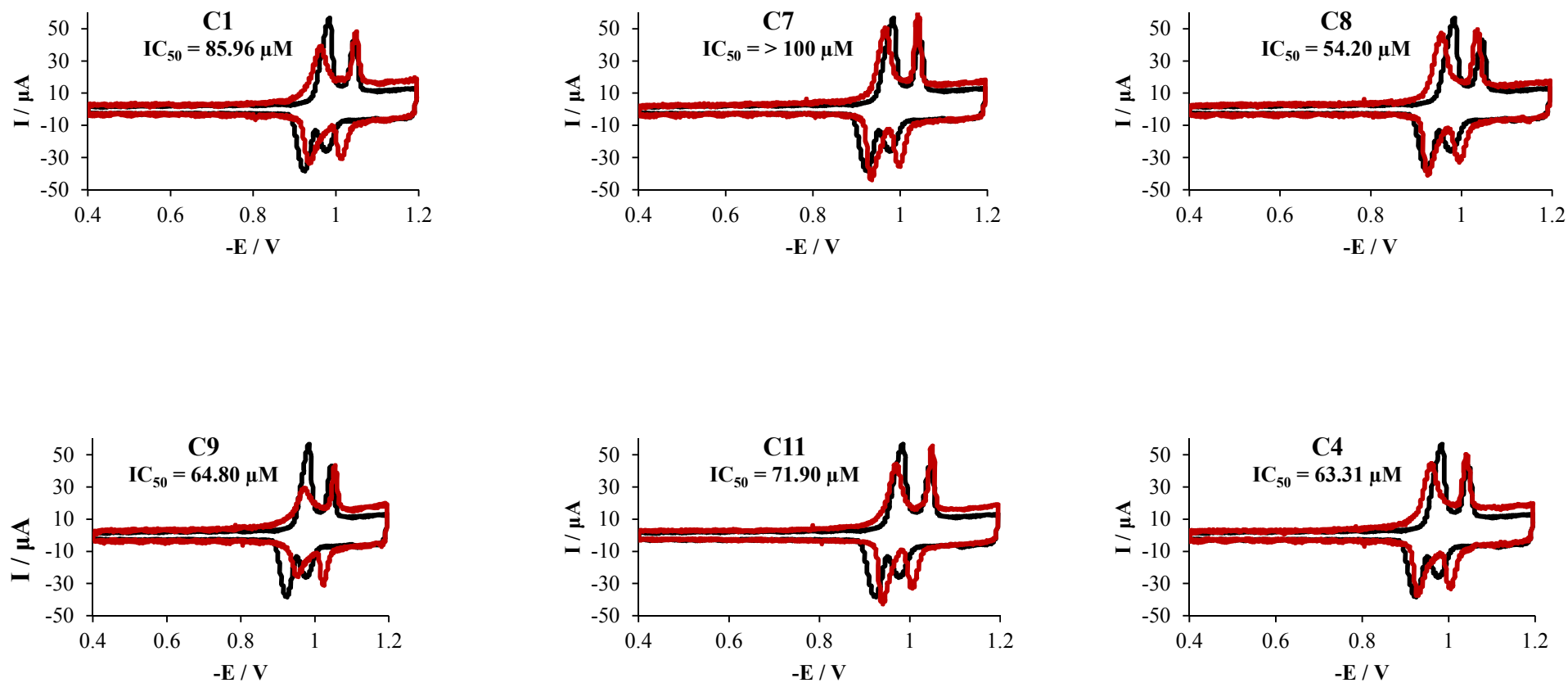


Figure 5.3.3: RCV plots for the interaction of complexes with the DOPC artificial biomembrane: **Key:** **Black** = DOPC membrane in the absence of complex, **Red** = DOPC membrane in the presence of complex

5.4 Conclusion

Two complexes **C22** and **C42** taken as representatives from the β -*bis*-ketoiminate copper(II) family of complexes showed changes in their respective UV/vis spectra upon hydrolysis over four days. These results from the moderately active complex **C42** ($IC_{50} = 42.35 \mu\text{M}$) and the inactive complex **C22** ($IC_{50} > 100 \mu\text{M}$) show that the cytotoxicity of this family is independent on the ability of these complexes to hydrolyse. In a similar way, complexes from the β -*bis*-ketoiminate ruthenium(II) dicarbonyl family displayed distinct changes in the UV/vis spectra, showing that these complexes also undergo hydrolysis. The presence of the carbonyl groups, as labile ligands is thought to promote decomposition of the initial complex into various products as seen from the mass spectrometry. The rate of hydrolysis was found to be dependent on the nature of the substituent present on the *phenolate* or *aniline* phenyl rings of the ketoiminate ligands. Complexes with electron withdrawing groups resulted in faster hydrolysis compared to complexes with electron donating groups. In addition, the complexes with substituents on the *phenolate* phenyl ring had a higher hydrolysis rates than their analogue complexes with substituents on the *aniline* phenyl ring. However, for this family of complexes, the rate of hydrolysis did not correlate to the anti-cancer activity for all complexes.

Although to varying degrees, selected β -*bis*-ketoiminate ruthenium(II) dicarbonyl complexes were able to adsorb and interact with the artificial biomembrane. This suggests that passive diffusion is a potential mode of entry into the cell for this family of complexes. Interestingly, the RCV plot of the inactive complex, **C9** showed the most pronounced distortions, prompting the conclusion that the anti-cancer activities of this series of complexes is not dependent on the ability of the complex to passively diffuse through the cell membrane.

5.5 References

1. S. P. Fricker, *Dalton Transactions*, 2007, 4903-4917.
2. S. Gupta, *Chemical Reviews*, 1994, **94**, 1507-1551.
3. A. Küng, T. Pieper, R. Wissiack, E. Rosenberg and B. K. Keppler, *JBIC Journal of Biological Inorganic Chemistry*, 2001, **6**, 292-299.
4. B. Lippert, *Cisplatin: Chemistry and Biochemistry of a leading anticancer drug*, John Wiley & Sons, 1999.
5. S. Aggarwal, *Journal of Histochemistry & Cytochemistry*, 1993, **41**, 1053-1073.
6. J. K.-C. Lau and B. Ensing, *Physical Chemistry Chemical Physics*, 2010, **12**, 10348-10355.
7. M. Bouma, B. Nuijen, M. T. Jansen, G. Sava, A. Flaibani, A. Bult and J. H. Beijnen, *International Journal of Pharmaceutics*, 2002, **248**, 239-246.
8. V. Brabec and J. Kasparkova, *Drug Resistance Updates*, 2005, **8**, 131-146.
9. G. Mestroni, E. Alessio, G. Sava, S. Pacor, M. Coluccia and A. Boccarelli, *Metal-Based Drugs*, 1994, **1**, 41-63.
10. M. Bacac, A. C. Hotze, K. van der Schilden, J. G. Haasnoot, S. Pacor, E. Alessio, G. Sava and J. Reedijk, *Journal of Inorganic Biochemistry*, 2004, **98**, 402-412.
11. P. C. Bruijninx and P. J. Sadler, *Advances in Inorganic Chemistry*, 2009, **61**, 1-62.
12. A. M. Basri, R. M. Lord, S. J. Allison, A. Rodríguez-Bárzano, S. J. Lucas, F. D. Janeway, H. J. Shepherd, C. M. Pask, R. M. Phillips and P. C. McGowan, *Chemistry-A European Journal*, 2017, **23**, 6341-6356.
13. M. A. Wright and J. A. Wright, *Dalton Transactions*, 2016, **45**, 6801-6811.

14. I. Chakraborty, S. J. Carrington and P. K. Mascharak, *Accounts of Chemical Research*, 2014, **47**, 2603-2611.
15. S. Betanzos-Lara, A. Habtemariam, G. J. Clarkson and P. J. Sadler, *European Journal of Inorganic Chemistry*, 2011, **2011**, 3257-3264.
16. R. Alberto and R. Motterlini, *Dalton Transactions*, 2007, 1651-1660.
17. S. García-Gallego and G. J. Bernardes, *Angewandte Chemie International Edition*, 2014, **53**, 9712-9721.
18. J. Marhenke, K. Trevino and C. Works, *Coordination Chemistry Reviews*, 2016, **306**, 533-543.
19. R. Pignatello, *Drug-biomembrane Interaction Studies: The Application of Calorimetric Techniques*, Elsevier, 2013.
20. R. Pignatello, T. Musumeci, L. Basile, C. Carbone and G. Puglisi, *Journal of Pharmacy and Bioallied Sciences*, 2011, **3**, 4.
21. Z. Coldrick, A. Penezić, B. Gašparović, P. Steenson, J. Merrifield and L. A. Nelson, *Journal of Applied Electrochemistry*, 2011, **41**, 939-949.
22. J. Knobloch, D. K. Suhendro, J. L. Zieleniecki, J. G. Shapter and I. Köper, *Saudi Journal of Biological Sciences*, 2015, **22**, 714-718.
23. L. A. Nelson and A. Benton, *Journal of Electroanalytical Chemistry and Interfacial Electrochemistry*, 1986, **202**, 253-270.
24. I. Miller, J. Rishpon and A. Tenenbaum, *Bioelectrochemistry and Bioenergetics*, 1976, **3**, 528-542.
25. Z. Coldrick, P. Steenson, P. Millner, M. Davies and L. A. Nelson, *Electrochimica Acta*, 2009, **54**, 4954-4962.
26. L. A. Nelson, *Journal of Electroanalytical Chemistry*, 2007, **601**, 83-93.
27. L. A. Nelson, *Current Opinion in Colloid & Interface Science*, 2010, **15**, 455-466.

28. S. Mohamadi, D. J. Tate, A. Vakurov and L. A. Nelson, *Analytica Chimica Acta*, 2014, **813**, 83-89.
29. A. Vakurov, M. Galluzzi, A. Podesta, N. Gamper, A. L. Nelson and S. D. Connell, *ACS nano*, 2014, **8**, 3242-3250.
30. L. A. Nelson, *Biophysical Journal*, 2001, **80**, 2694-2703.
31. M. R. Moncelli, L. Becucci, L. A. Nelson and R. Guidelli, *Biophysical Journal*, 1996, **70**, 2716-2726.
32. L. A. Nelson, *Analytica Chimica Acta*, 1987, **194**, 139-149.
33. F. Neville, D. Gidalevitz, G. Kale and L. A. Nelson, *Bioelectrochemistry*, 2007, **70**, 205-213.
34. E. Protopapa, S. Maude, A. Aggeli and L. A. Nelson, *Langmuir*, 2009, **25**, 3289-3296.
35. E. Protopapa, L. Ringstad, A. Aggeli and L. A. Nelson, *Electrochimica Acta*, 2010, **55**, 3368-3375.
36. L. Ringstad, E. Protopapa, B. Lindholm-Sethson, A. Schmidtchen, L. A. Nelson and M. Malmsten, *Langmuir*, 2008, **24**, 208-216.
37. N. Ormategui, S. W. Zhang, I. Loinaz, R. Brydson, L. A. Nelson and A. Vakurov, *Bioelectrochemistry*, 2012, **87**, 211-219.
38. A. Vakurov, R. Brydson and L. A. Nelson, *Langmuir*, 2012, **28**, 1246-1255.
39. D. Sanver, B. S. Murray, A. Sadeghpour, M. Rappolt and A. L. Nelson, *Langmuir*, 2016, **32**, 13234-13243.
40. H. A. M. A. Abdelgawad, PhD, University of Leeds, 2016.
41. L. A. Nelson and F. Leermakers, *Journal of Electroanalytical Chemistry and Interfacial Electrochemistry*, 1990, **278**, 73-83.
42. D. Bizzotto and L. A. Nelson, *Langmuir*, 1998, **14**, 6269-6273.

43. A. V. Brukhno, A. Akinshina, Z. Coldrick, L. A. Nelson and S. Auer, *Soft Matter*, 2011, **7**, 1006-1017.
44. L. A. Nelson, N. Auffret and J. Borlakoglu, *Biochimica et Biophysica Acta (BBA)-Biomembranes*, 1990, **1021**, 205-216.
45. A. Vakurov, R. Brydson and L. A. Nelson, *Langmuir*, 2011, **28**, 1246-1255.
46. R. Mede, P. Hoffmann, M. Klein, H. Görls, M. Schmitt, U. Neugebauer, G. Gessner, S. H. Heinemann, J. Popp and M. Westerhausen, *Zeitschrift für anorganische und allgemeine Chemie*, 2017, **643**, 2057-2062.
47. E. Stamellou, D. Storz, S. Botov, E. Ntasis, J. Wedel, S. Sollazzo, B. Krämer, W. van Son, M. Seelen and H. Schmalz, *Redox Biology*, 2014, **2**, 739-748.
48. M. Westerhausen, P. Hoffmann, H. Görls, M. Schmitt, J. Popp, U. Neugebauer and R. Mede, *Chemistry-A European Journal*, 2018.

Chapter 6
Catalytic Investigations on β -*bis*-Ketoiminate
Complexes of Ruthenium and Copper

6.1 Transition metals in catalysis

The use of transition metals in catalysis is well studied and established dating back to the 20th century when Fischer and Tropsch used Fe and Co in the synthesis of hydrocarbons.^{1, 2} Their ability to catalyse and accelerate important chemical transformations without being consumed is due to a number of reasons.³⁻⁵

1. Bonding ability: Transition metals are able to coordinate to any functional groups; once coordinated the reactivity of the functional group can be tuned to enhance catalytic activity. More importantly, highly reactive species can coordinate to the metal and be stabilised enough to react in a controlled and productive way, evading degradation.
2. Ligand effects: Transition metal catalysts are able to accommodate a number of ligands, participative and non-participative, in their coordination sphere. These ligands can influence the behaviour of the catalyst through modification of electronic and steric properties.
3. Variable oxidation states: A common feature of transition metals is the ability to form stable compounds with variable oxidation states. As such, organometallic compounds used in catalysis readily interchange between oxidation states during the course of a catalytic reaction, an inherent property that purely organic catalysts lack.
4. Variable coordination numbers: Organometallic compounds acting as catalysts have variable coordination numbers, and are able to accommodate several different ligands in the coordination sphere. This feature is of importance as it allows these compounds to catalyse and tolerate reactions with a broad range of substrates.

Of primary importance in catalysis is selectivity, and organometallic compounds have been shown to enhance selectivity through modulation and fine tuning of the ligand, its chirality and metal centre.⁵⁻⁷

6.2 Catalytic transfer hydrogenation

6.2.1 Introduction to transfer hydrogenation

Hydrogenation, with industrial applications ranging from fine chemicals to pharmaceutical synthesis, is one of the most important and extensively investigated reactions in catalysis.⁸⁻¹⁰ Hydrogenation of organic unsaturated substrates can be achieved *via* direct hydrogenation using pressurised H₂ gas or transfer hydrogenation. According to Braude and Linstead, hydrogen transfer reactions can be sub divided into three classes, (i) hydrogen migration within one molecule, (ii) hydrogen transfer disproportionation between identical donor and acceptor substrates and (iii) transfer hydrogenation-dehydrogenation, with different donor and acceptor units.^{11, 12}

Of the three subdivisions, transfer hydrogenation-dehydrogenation, simply known as transfer hydrogenation (TH) is the most important and widely applied. In transfer hydrogenation, hydrogen is abstracted from molecules such as alcohols or amines acting as hydrogen donors, and unsaturated compounds such as aldehydes or ketones, imines or alkenes acting as hydrogen acceptors.¹²

Hydrogenation using molecular hydrogen involves the use of high temperatures and pressure, therefore transfer hydrogenation is an attractive alternative as it only requires mild temperature and pressure conditions, suitable for both laboratory and industrial applications. More importantly, molecules acting as hydrogen donors are readily available, easy to handle and inexpensive.¹³⁻¹⁵ In transfer hydrogenation reactions, several catalysts can be employed; enzyme-, thermal-, transition metal-, base- and organo catalysts. Of particular importance to the author are transition metal catalysts, mainly those of ruthenium which will be briefly discussed.¹²

The use of transition metals in transfer hydrogenation dates as far back as the 1960s when Henbest and colleagues showed that an iridium hydride complex could catalyse the reduction of ketones to alcohols with isopropanol.¹⁶⁻¹⁸ The most common and frequently employed catalysts for TH are platinum group metal (Ru, Ir and Rh) complexes with N, O, P and C element based ligands, such as multidentate complexes, half sandwich complexes and metal-N-heterocyclic carbenes.¹² Within this group ruthenium based catalysts have proved to be the most widely used.

Figure 6.2.1 shows the first ruthenium complex used in the transfer hydrogenation of acetophenone with isopropanol.¹⁹⁻²¹ Chowdhury *et al.* later improved on the efficiency of the reaction using the same ruthenium complex as a catalyst, but with addition of catalytic amounts of a base.²² Since then remarkable improvements on ruthenium catalysed TH reactions have been reported. Of particular significance are expansions on the library of applicable ligands, the application of economical and “greener” catalytic processes, the practical application of such systems in fine chemicals and pharmaceuticals and the intensive investigations into the mechanisms of the catalytic processes.¹²

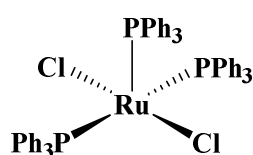


Figure 6.2.1: First ruthenium complex used in transfer hydrogenation

Asymmetric transfer hydrogenation (ATH), a sub class of transfer hydrogenation is an important process in pharmaceutical and fragrance industries.^{23, 24} Noyori, who received a Nobel Prize in 2001 for his outstanding contribution in the field of ATH, has developed a series of highly efficient Ru-arene complexes (**1** in **Figure 6.2.2**) as catalysts (Noyori catalysts) for the stereo-selective transfer hydrogenation of ketones^{25, 26} and imines²⁷ in the presence of a base (**Figure 6.2.2**).

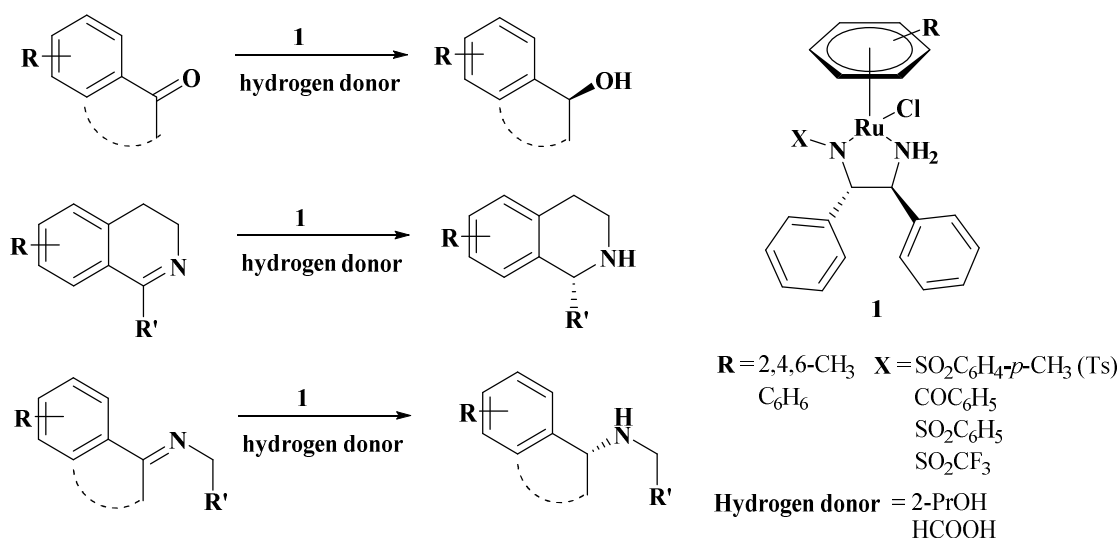
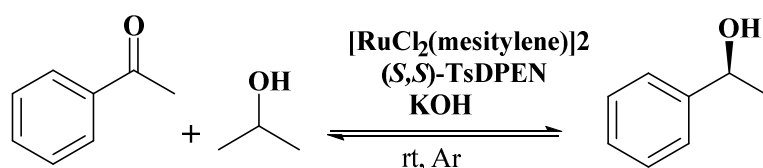


Figure 6.2.2: Noyori catalysts for stereo-selective ATH

Scheme 6.2.1 shows one of the best performing catalysts from the 1st generation Noyori catalysts for the transfer hydrogenation of acetophenone. In this reaction, the Ru catalyst was prepared *in situ* from the reaction of $[\text{RuCl}_2(\eta^6\text{-mesitylene})]_2$ and (*S,S*)-*N*-(*p*-toluenesulfonyl)-1,2-diphenylethylenediamine ((*S,S*)-Ts-DPEN), in isopropanol with KOH as the base, at room temperature. The reaction gave a 95% conversion of acetophenone to (*S*)-1-phenylethanol with 97% ee in 15 hours. Reaction under similar conditions, without Ts-DPEN resulted in < 8% of 1-phenylethanol.²⁶



Scheme 6.2.1: ATH of acetophenone using $[\text{RuCl}_2(\text{mesitylene})]_2$ and (*S,S*)-TsDPEN

Over the years, the Noyori catalysts' family has been extensively investigated, well established and widely applied for TH and ATH using either isopropanol or formic acid as hydrogen sources.²⁸ In an effort to increase the activity and efficiency of this robust family of catalysts several structural variations have been explored and reported. Interestingly, the catalytic efficiency and coordination behaviour of the Ru-arene complexes could be fine tuned through minute modifications in the ligand system.^{24, 29-31}

Of notable interest in the various alternatives to monotosylated diamines in Noyori catalysts was the discovery that replacing the (*N,N*) DPEN ligands with (*N,O*) amino-alcohol ligands significantly increased the catalytic activity when an appropriate arene and chiral amino-alcohol auxiliary are combined.³¹

Figure 6.2.3 shows the 2nd generation Ru-arene catalyst generated *in situ* from the reaction of Ru-arene dimer and *N*-substituted amino-alcohol in isopropanol with KOH at room temperature. Substitution of the chiral diamines, whose synthesis is lengthy and complicated, with chiral β -amino alcohols that are readily available and variable has greatly improved the industrial applications of Noyori catalysts.¹²

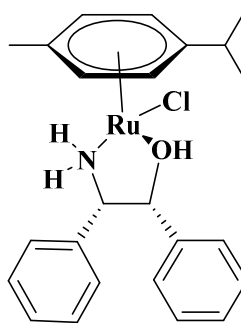


Figure 6.2.3: An example of 2nd generation Noyori half sandwich Ru- η^6 -arene TH catalysts with (*N,O*) ligands

Investigative reactions on the Ru- η^6 -arene amino-alcohol complexes have shown that the N-H proximity in the ligand is important for catalytic activity, a trend common to other Ru-catalysed reactions.^{26, 32} Catalytic activity was also shown to be highly dependent on the steric and electronic properties of the ligand, increase in steric bulk of the arene ring resulted in a decrease in catalytic activity.³¹

In catalysis, the activity and selectivity of the complex is highly dependent on the ligand of choice. *N*-heterocyclic carbenes (NHCs) are another class of ligands that have been widely explored in transfer hydrogenation reactions. Ruthenium NHCs complexes in variable oxidation states and coordination geometries have shown good selectivity and catalytic activity in TH.³³⁻³⁶

Within the McGowan research group, a series of Ru-*p*-cymene complexes containing diphosphine ligands³⁷ and Ir-Cp* picolinamide complexes³⁸ (**Figure 6.2.4**) were synthesised for application in the ATH reaction of benzaldehyde. Picolinamide ligands can bind (*N,N*) or (*N,O*) to the metal centre. For ATH of benzaldehyde with ^tBuOK in isopropanol at 60°C, higher catalytic activity was observed for (*N,O*) ligand coordination to the Ir metal centre with 97% conversion compared to 26% for (*N,N*) ligand coordination, after 24 hours.

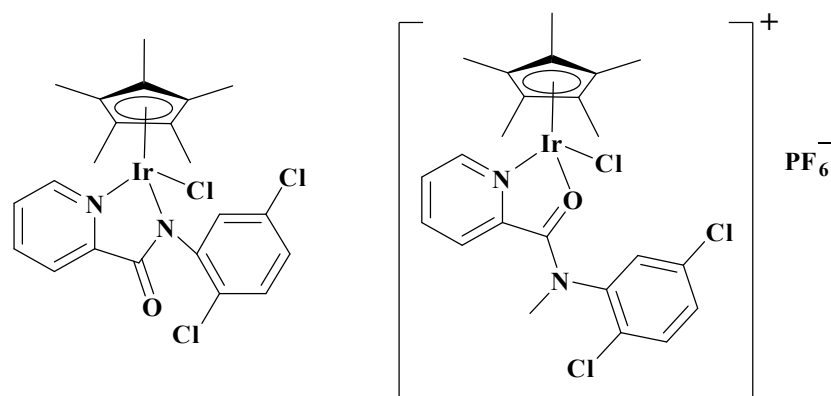


Figure 6.2.4: Ir-Cp* picolinamide complexes for ATH by McGowan *et al.*

6.2.2 Catalytic Mechanisms

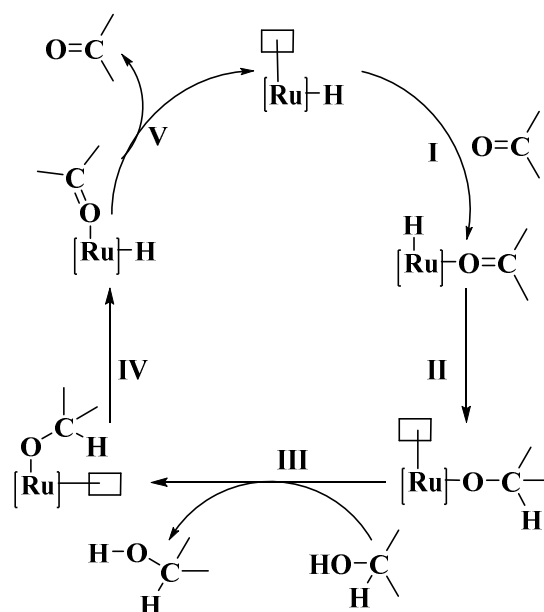
Hydrogen transfer reactions can occur in different pathways. Two mechanistic pathways have been proposed by Brandt *et al.*, direct hydrogen transfer, most prevalent with main group metals and the hydridic route, most common with transition metals.³⁹

6.2.2.1 Hydridic Route

Direct hydrogen transfer and transfer hydrogenation are closely related mechanistically. Both reactions have been shown to proceed through formation of a metal hydride species, a key intermediate, acting as a catalyst or pre-catalyst in the catalytic cycle.⁴⁰ This mechanism is known as the hydridic route, which is further classified into the monohydride and dihydride routes. In transfer hydrogenation reactions, hydrogen transfer reagents such as isopropanol/base or formic acid/base provide hydrides, through β -elimination reactions, for the formation of the highly active metal hydride species. As such, catalytic reactions in the presence of a base are highly efficient compared to reactions in the absence of a base.^{22, 41, 42}

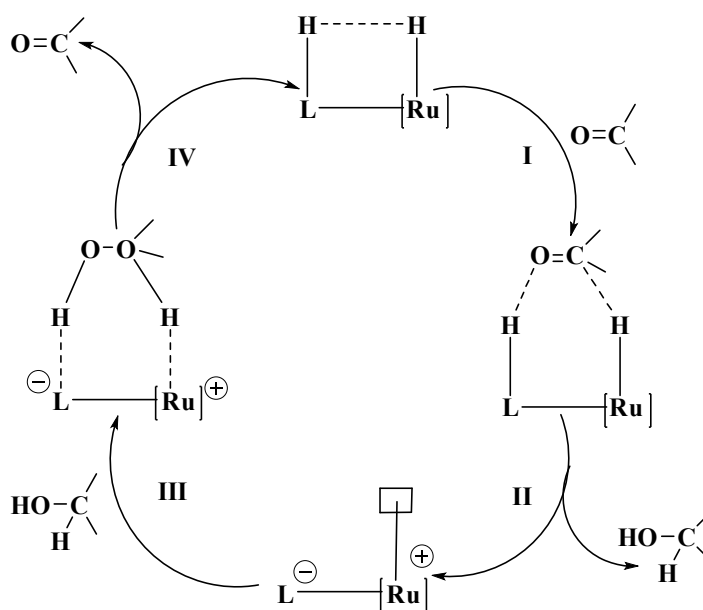
The monohydride route can occur in the inner or outer coordination sphere of the catalyst's metal centre. In the inner sphere mechanism (**Scheme 6.2.2**) the substrate, for example a ketone or imine, coordinates to a vacant site on the metal centre allowing product formation through bonding to the metal centre. This allows the electrophilic activation of the carbon of the ketone or imine group. Ancillary ligands with acidic hydrogen bond donor groups on the metal centre are known to promote hydride transfer to the substrate.⁴² Catalysts that favour inner sphere mechanism

show poor selectivity for C=O over C=C bonds in the reduction of α , β unsaturated ketones and aldehydes.^{43, 44}



Scheme 6.2.2: Inner sphere transfer hydrogenation mechanism

Contrary to inner sphere coordination, in the outer sphere coordination mechanism, catalytic activity proceeds without coordination of the substrate to the metal centre. The substrate is usually in the 2nd coordination sphere of the catalyst complex (**Scheme 6.2.3**). In this mechanism C=O or C=N bonds are selected over C=C bonds. The ancillary ligands are pivotal in activating the carbon of the substrate towards nucleophilic hydride attack.⁴² This mechanism was further proposed by Noyori *et al.* for the ruthenium complex, Ru^{II}-TsDPEN, as catalyst for ATH of ketones.^{26, 45}



Scheme 6.2.3: Outer sphere transfer hydrogenation mechanism

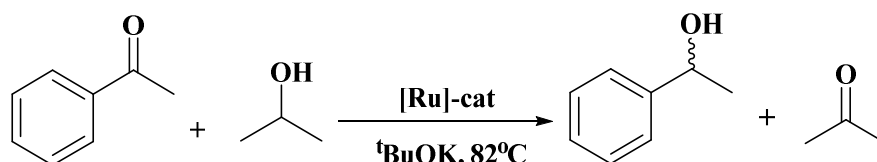
6.2.3 Catalytic viability of β -bis-Ketoiminate Ru(II) Dicarbonyl Complexes

Transfer hydrogenation studies on the β -bis-ketoiminate ruthenium(II) dicarbonyl complexes described in **Chapter 2** with the general structure shown in **Figure 6.2.5** were investigated. Complexes with various electronic and steric properties were chosen in an attempt to investigate structure-activity relationships.

	Complex	Substituent (R_p/R_a)
	C1	H(p)
C2	4'Br(p)	
C3	4'Cl(p)	
C4	4'F(p)	
C5	3'F(p)	
C7	3',4' diCl(p)	
C8	4'Me(p)	
C10	4'F(a)	
C15	2',4' di F(a)	
C16	2',3' diMe(a)	

Figure 6.2.5: β -bis-ketoiminate Ru(II) dicarbonyl complexes under TH catalytic investigations

The reduction of acetophenone with isopropanol to 1-phenylethanol shown in **Scheme 6.2.4** was chosen as the model reaction. The use of isopropanol as the hydrogen donor is common in transfer hydrogenation reactions, isopropanol is easy to handle, inexpensive, abundant, environmentally friendly and non-toxic. The by-product of the reaction, acetone, is volatile and can be easily removed.



Scheme 6.2.4: Model reaction for TH catalytic investigations

Catalytic control experiments were carried out at 82 °C with acetophenone (1 mmol), Ru(II) dicarbonyl complexes (0.01 mmol) as catalysts, potassium tert-butoxide (0.1 mmol) in isopropanol (30 mmol). Excess isopropanol was used to minimise the occurrence of the reverse reaction. Conversions were calculated using ^1H NMR spectroscopy by comparing the integration of the methyl resonance of the product 1-phenylethanol with the internal standard 1,3,5-trimethoxybenzene (0.33 mmol).⁴⁶ Control reactions were carried out using no catalyst (entry 1), ruthenium(III) chloride trihydrate (entry 2) and dichloro(*p*-cymene)ruthenium(II) dimer (entry 3).

Table 6.2.1: Investigation of a range of Ru(II) dicarbonyl catalysts in the transfer hydrogenation of acetophenone to 1-phenylethanol

Entry	Catalyst	Conversion (%)
1	No catalyst	13
2	$\text{RuCl}_3 \cdot 3\text{H}_2\text{O}$	19
3	$[\text{Ru}(p\text{-cymene})_2\text{Cl}_2]_2$	100
4	C1	50
5	C2	55
6	C3	63
7	C4	93
8	C5	92
9	C7	83
10	C8	28
11	C10	92
12	C15	32
13	C16	37
14 ^a	C4	0

^a - no base added in reaction

Table 6.2.1 shows the results obtained for a range of the Ru(II) dicarbonyl complexes. The conversion values are an average of two separate runs. Comparison of the results for the starting material (entry 2) to the complexes (entries 4–13) show that coordination of bidentate ketoiminate ligands as well as carbonyl ligands greatly improves the catalytic activity of the complexes.

The Ru(II) dicarbonyl complexes only differ through the functionalisation on the ketoiminate ligands, specifically on the *aniline* (R_a) or *phenolate* (R_p) phenyl ring (**Figure 6.2.5**). Functionalisation with electron withdrawing substituents on either of the phenyl rings generally results in an increase in the catalytic efficacy of the complexes, except for **C15**. This is seen when comparing entry 4 to entries 5–9, 11 and 12. The highest catalytic conversions (> 90%) are obtained when the substituent on the complexes is fluorine, entries 7 (4'F(p): 93%), 8 (3'F(p): 92%) and 11 (4'F(a): 92%). As seen from these entries, the position of the fluoro substituent (*meta* or *para*) and the ring substituted (*aniline* or *phenolate*) seemingly has no effect on the overall catalytic activity of the complexes. However, the type of halogen present as a substituent has an effect on the efficacy of the complex. The catalytic activity increases with increase in electronegativity, entry 5 (4'Br: 55%), entry 6 (4'Cl: 63%) and entry 7 (4'F: 93%).

Electron donating substituents on either of the phenyl rings results in an overall decrease in the catalytic activity of the complexes. Comparison of catalytic conversions for entry 4 with entries 10 and 13 clearly shows that addition of the methyl substituents lowers the yield from 50% to 28% and 37% respectively. When no base is added in the reaction, entry 14, no product is formed (0% conversion). This suggests that the base plays a crucial role in the catalytic mechanism.

Further catalytic experiments to monitor the rate of catalytic activity were done with the best performing Ru(II) dicarbonyl catalyst, complex **C4**. For comparison, dichloro(*p*-cymene)ruthenium(II) dimer was chosen as it is the “gold standard” for transfer hydrogenation and the ruthenium centre is in the same oxidation state as the catalyst **C4**. The same reaction conditions as stated above were used, with samples taken at 1, 2, 3, 6, 10 and 24 hour intervals. The results are displayed in **Figure 6.2.6**.

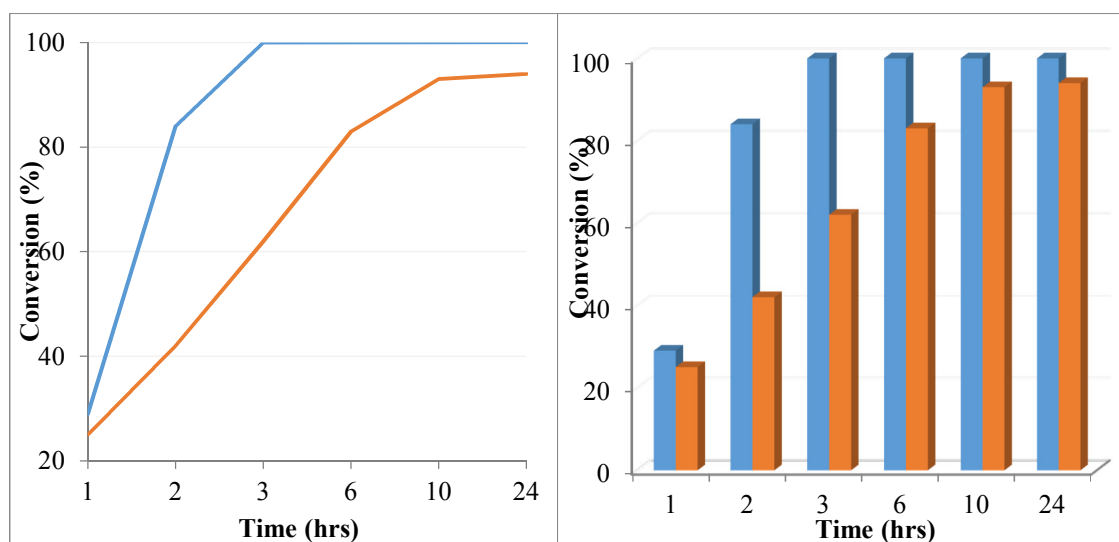


Figure 6.2.6: Comparison of catalytic conversion rates of Ru(*p*-cymene) dimer and complex **C4**; Key: Blue = Ru(*p*-cymene) and Orange = complex **C4**

Both catalysts are active within the 1st hour, reaching nearly the same conversion at the end of the first hour, 29% for Ru(*p*-cymene) dimer and 25% for **C4**. However, in the first 3 hours, the catalytic activity of the Ru(*p*-cymene) dimer exponentially increases reaching 100% conversion, while that of **C4** gradually increases to reaching only 62% conversion. Maximum conversion for complex **C4** (93%) is reached after 10 hours. From these results, the catalytic activity of complex **C4** is comparable to that of the dimer although its catalytic rate is much slower.

6.3 Catalytic Ullmann reactions

6.3.1 Copper in catalysis

The application of late transition metals such as Ru and Pd in catalysis is well understood and established. However with economic and environmental concerns to go green and cut costs a quest in developing alternative catalysts is being pursued. As such, first row transition metals such as copper are being exploited, being more abundant, versatile and cheaper.⁴⁷ Another advantage is that in catalysis copper can easily access four of its five oxidation states (0 to +3).⁴⁸

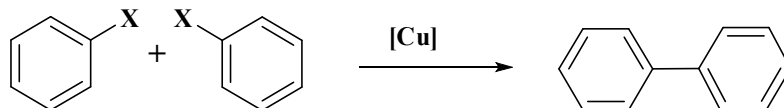
Copper is known to catalyse similar sets of reactions to that of palladium, one of the most common modern day catalysts.^{49, 50} Examples of such reactions include the Heck reaction, cyclo-addition with azide (click chemistry) and Sonogashira

coupling.⁴⁷ These reactions are common tools for synthetic organic chemists, with applications in the pharmaceutical, fine chemicals, polymer and agricultural sectors. However, one of the major drawbacks is the use of the expensive palladium catalyst; as such copper is a better economic alternative.⁵¹⁻⁵³

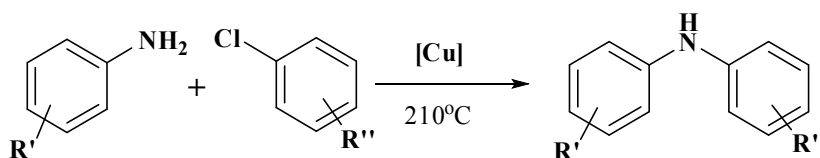
6.3.2 Introduction to Ullmann reaction

The pioneering works of Ullmann and Gordberg more than a century ago formed the basis of cross coupling reactions and the subsequent use of copper in catalysis.⁵⁴ In 1901 Fritz Ullmann reported the first copper catalysed cross coupling in which biaryl moieties were formed through coupling of two molecules of aryl halides. This is now referred to as the “classical Ullmann reaction”.⁵⁵ The reaction has been used to synthesise symmetric and asymmetric biaryls and to activate ring closure at an aryl-aryl bond.⁵⁶ Over the years “Ullmann reactions” have evolved to “Ullman condensation reactions” as shown in **Scheme 6.3.1**. Examples of the latter include copper catalysed formation of aryl amines from an aryl halide and an amine and/or aryl ether from an aryl halide and a phenol.⁵⁷⁻⁶⁰ In 1906, Irma Goldberg reported the copper mediated synthesis of aryl amides from an aryl halide and an amide.⁵⁹

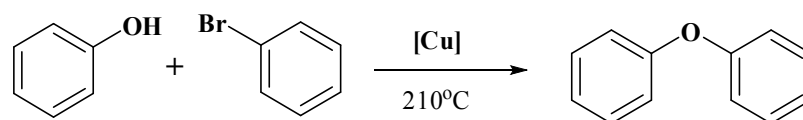
Ullmann, 1901



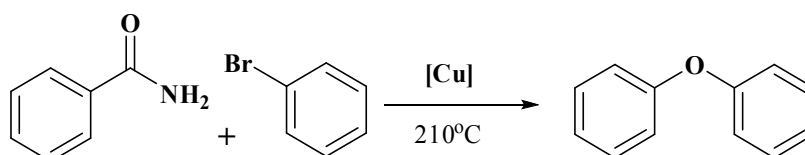
Ullmann, 1903



Ullmann, 1905



Ullmann, 1905

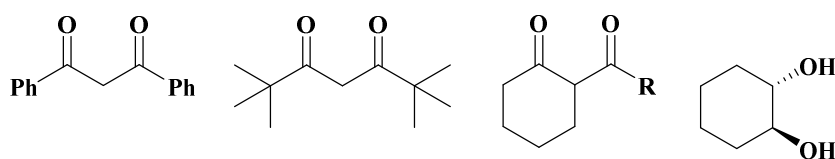
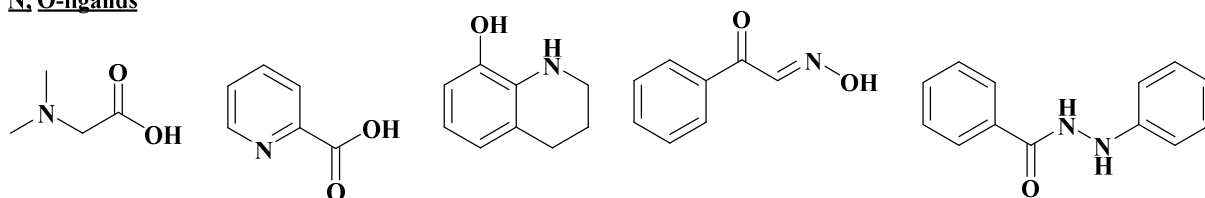
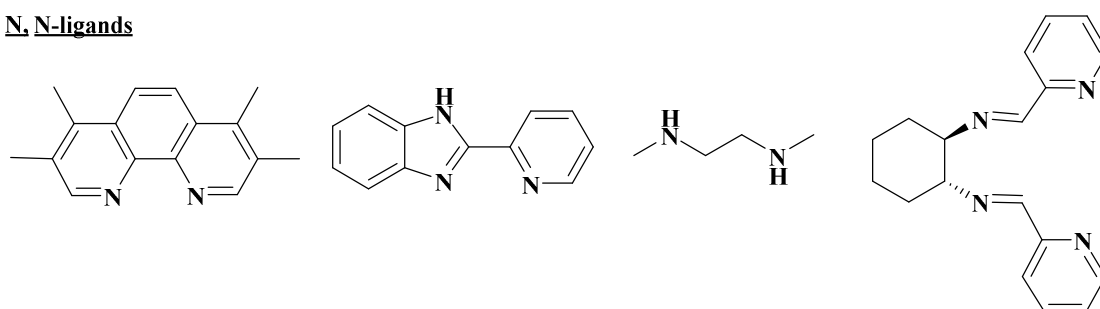


Scheme 6.3.1: Ullmann reaction progression from 1900s

Despite the impressive start, these reactions were characterised by high temperatures ($> 200^{\circ}\text{C}$), long reaction times, high catalyst loading, poor functional group tolerance and use of strong bases. Gradually, in an effort to improve the efficiency of the reaction palladium replaced copper as the catalyst of choice.^{47, 53} As highlighted earlier, economic and environmental concerns have forced researchers to revisit the application of copper in catalysis. Improved versions of the “classical Ullmann reactions” have emerged. Termed “modified Ullmann reactions” these procedures have addressed and improved on the efficiency of the initial Ullmann reactions. In “modified Ullmann reaction”, the addition of ligands to the copper catalyst is highly credited for the reactions proceeding under milder conditions.⁶⁰

6.3.2.1 Ligand effect

Coordination of ligands to copper salts dramatically improves the efficiency of the copper catalyst, making it chemo-, enantio- and regio-selective. Their role was mostly linked to the increased solubility and reduced aggregation of Cu salts, rather than to other effects. This subsequently led to reactions occurring under milder conditions such as lower temperatures (usually $80\text{-}100^{\circ}\text{C}$) and catalytic loading (5-20%). **Figure 6.3.1** shows some of the first ligands to be used in copper mediated catalytic reactions. The ligands can be classed as (*O,O*)-, (*N,O*)- or (*N,N*)- according to their chemical structure.^{53, 60} Bidentate ligands have been shown to be more efficient than monodentate ones.^{54, 61} A potential explanation is that the bidentate ligands block the two adjacent coordination sites, forcing close proximity of the aryl donor and the nucleophile and ensuring easier coupling.⁴⁷

O, O-ligands**N, O-ligands****N, N-ligands****Figure 6.3.1:** Historic ligands in copper mediated catalytic reactions

In the McGowan Research group, Dr Carlo Sambigiio has extensively investigated a range of N-phenylpicolinamide ligands as catalysts for Cu-catalysed aryl ether formation. His work highlighted that electron withdrawing substituents on the phenyl ring of the ligand increased the catalytic activity of the active species. The picolinamide ligands showed high catalytic conversions, even for the sterically hindered phenols, *ortho*-substituted phenols, *tert*-butyl and *tert*-amyl substituents, some of which are known to be challenging coupling partners in Cu-catalysed reaction.⁶² The geometrical and electronic similarities between N-phenylpicolinamide copper(II) complexes [Figure 6.3.2(a)] and the authors' β -bis-ketoiminate copper(II) complexes [Figure 6.3.2(b)] prompted catalytic investigations on the β -bis-ketoiminate copper(II) complexes

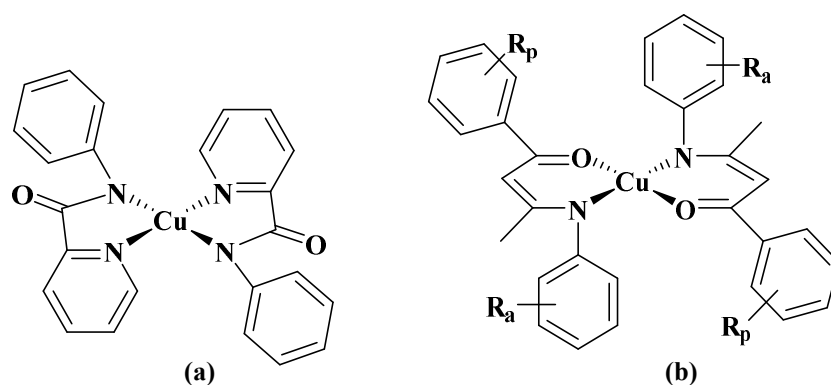
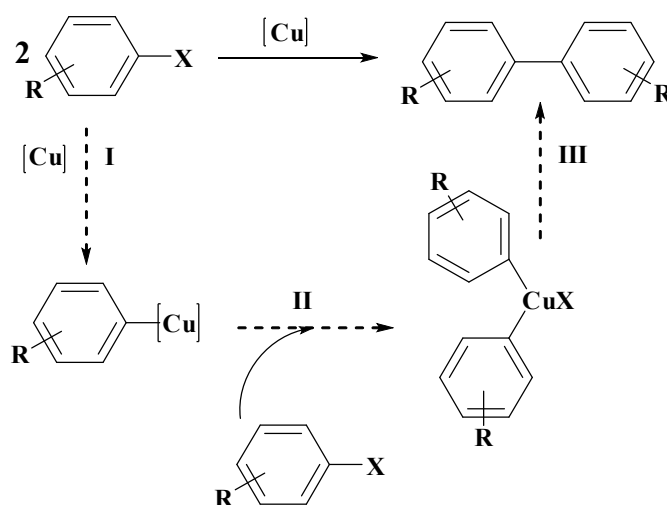


Figure 6.3.2: (a) Dr Sambiagio's picolinamide copper (II) complexes,⁶² (b) the author's ketoiminate copper(II) complexes

6.3.3 The mechanism of the Ullmann reaction

Various copper sources ranging from Cu(I) to Cu(II) salts and metallic copper are effective catalysts in Ullmann reactions, although Cu(I) salts result in higher activities. It is generally accepted that a single catalytic active species, most likely Cu(I) species, is produced from all these precursors and is the primary catalytic species.^{58, 59, 63-65}



Scheme 6.3.2: General mechanism for Ullmann cross coupling reactions

Scheme 6.3.2 shows the mechanism generally accepted for Ullmann cross coupling reactions. However, some of the catalytic steps have generated controversy over the years and are still under debate.⁶⁰ In step **I** an organo-cuprate intermediate is formed from the reaction of a molecule of the aryl halide with the copper complex precursor. Step **II** is oxidative addition of the second aryl halide molecule, followed by reductive elimination to give the final product (step **III**).⁴⁷

Other proposed mechanisms within the literature differ on the activation of the aryl halide, a rate determining step. The mechanisms can be classed into four main categories:

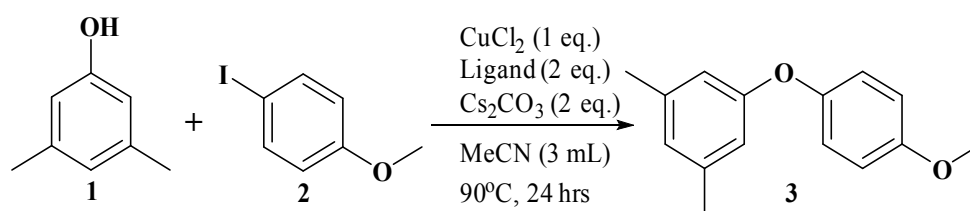
- i. Mechanistic pathways involving oxidative addition/reductive elimination
- ii. Mechanistic pathways involving single electron transfer (SET) or Halogen Atom Transfer (HAT).
- iii. Mechanistic pathways involving π -complexation of the Cu(I) active species to the aromatic ring.
- iv. Mechanistic pathways involving σ -bond metathesis

In mechanisms i and ii the copper species changes its oxidation state during the catalytic cycle, whilst in iii and iv the copper species maintain the same oxidation state throughout.^{47, 60}

Based on the literature it is clear that there is no single mechanism for all the copper catalysed Ullmann reactions. However, for the modified Ullmann reaction most researchers agree that the reaction between the copper complex and the nucleophile precedes the activation of the aryl halide species. Overall the mechanism varies depending on factors such as the substrates of choice, ligands, side reactions and reaction conditions.^{47, 60}

6.3.4 Catalytic viability of β -bis-Ketoiminate Copper(II) Complexes

The model reaction chosen to investigate the catalytic activity of the β -bis-ketoiminate copper(II) complexes was the coupling between 3,5-dimethylphenol **1** and 4-iodoanisole **2**, leading to the biaryl ether **3**, **Scheme 6.3.3**.



Scheme 6.3.3: Ullmann reaction for the synthesis of aryl ethers

Electron donating substituents on the aryl halide, **2**, make the substrate less reactive through deactivation, hence the reaction shown in **Scheme 6.3.3** would be relatively challenging. More importantly the deactivated substrate can clearly highlight the

differences in the versatility and efficacy of the ligand and metal complexes, an observation that may be less obvious with a more reactive substrate. Caesium carbonate and acetonitrile were chosen as the base and solvent of choice respectively based on previous literature reports.⁶² All catalytic reactions were done under nitrogen using un-purified reagents, reactions with anhydrous reagents did not improve the catalytic efficiency.

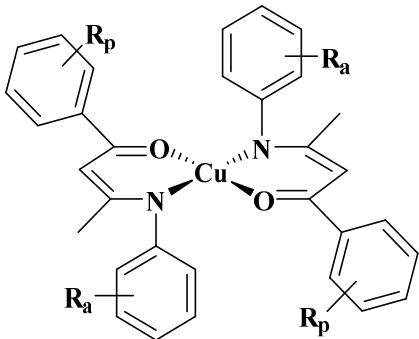
	H(p)	C17	2',3' diMe(p)	C28
	2'Br(p)	C18	2',4',6' triMe(p)	C29
	2'Cl(p)	C19	3',4' diCl(p)	C30
	4'Br(p)	C20	3',4' methylene(p)	C31
	4'Cl(p)	C21	3'Br, 4'F(p)	C32
	4'F(p)	C22	2'OMe(p)	C33
	4'I(p)	C23	2'OEt, 4'F(p)	C35
	4'Me(p)	C24	2' Br (a)	C36
	4'OMe(p)	C25	3'Cl(a)	C39
	4'OEt(p)	C26	4'Cl(a)	C40
	4'CF ₃ (p)	C27		

Figure 6.3.3: β -Bis-ketoiminato copper(II) complexes under study

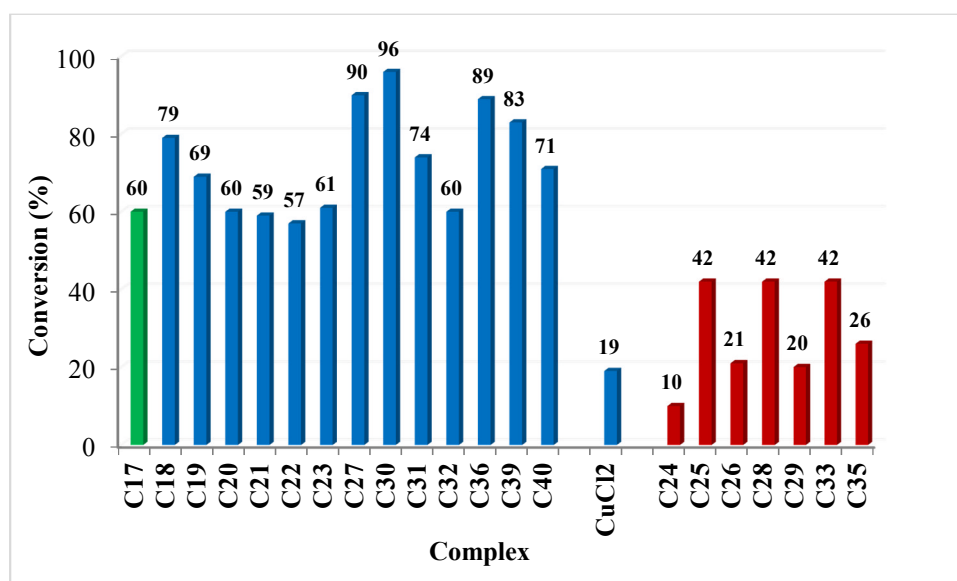


Figure 6.3.4: Catalytic results for β -bis-ketoiminato copper(II) complexes (GC yields):
Key blue bars – complexes with EWG, red bars – complexes with EDG

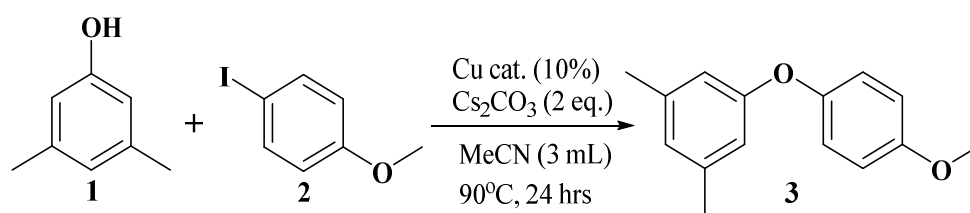
To investigate the effect of electronic and steric properties of the copper(II) complexes, a range of complexes with different substituents on the ketoiminate ligand were studied (**Figure 6.3.3**). Reactions with the alternative copper source, copper(II) chloride, were also evaluated for comparison purposes. **Figure 6.3.4** shows the results obtained for the various complexes. With the exception of **C24**, the presence of the ketoiminate ligand with either EDG (electron donating groups) or EWG (electron withdrawing groups) improved the catalytic activity of the copper complexes when compared to the copper salt, CuCl₂. Complex **C17** with the parent unsubstituted ligand was a competitive catalyst, with a conversion of 60%.

The presence of electron donating groups on the complexes [**Figure 6.3.4** (red)] resulted in poor conversions. Complexes **C25** (4' Me), **C28** (2',3' diMe) and **C33** (2' OMe) gave the same conversion (42%) regardless of the differences in the extent of the electron donating properties. Complexes with electron withdrawing groups on the ligand phenyl rings gave high catalytic conversions (**Figure 6.3.4** (blue), particularly **C27** (4' CF₃) and **C30** (3',4' diCl) with conversions of 90% and 96% respectively. The effect of EDG and EWG were further displayed by the differences in catalytic conversions of complexes **C22** (4' F), **C32** (3' Br, 4' F) and **C35** (2' OEt, 4' F). Complex **C22** has the fluoro substituent in the *para* position, addition of a bromo substituent in the *meta* position (**C32**) results in negligible increase in catalytic conversion. However, addition of the electron donating ethoxy-substituent in the *ortho* position (**C35**) results in a two-fold decrease in catalytic conversion.

The effect of halogenated substituents in catalysis is of particular interest; the position and type of halogen can drastically change the catalytic activity of the ligand or complex. Complexes, **C22** (4' F: 57%), **C21** (4' Cl: 59%), **C20** (4' Br: 60%) and **C23** (4' I: 61%) show a slight decrease in catalytic efficacy going from the most to the least electronegative halogen. Although not conclusive, these results imply that the electronegative strength of the halogen has little effect on the overall efficacy of the resultant complex. However, the position of the halogen substituent on the ligand in the complex has a significant effect on the catalytic activity of the complex. Complexes with *ortho* substituents resulted in higher conversions compared to their *para* analogues, shown by **C18** (2' Br: 79%) and **C20** (4' Br: 60%) as well as **C19** (2' Cl: 69%) and **C21** (4' Cl: 59%). In β -bis-ketoiminate copper(II) complexes the substituent can either be on the *aniline* ring or the *phenolate* ring,

shown as R_a and R_p respectively in **Figure 6.3.3**. Interestingly substitution on the *aniline* ring resulted in an increase in the catalytic efficacy of the complexes when compared to *phenolate* substituted analogues. These results are highlighted by complexes **C18** (2'Br(p): 79%) and its analogue **C36** (2'Br(a): 89%) as well as **C21** (4'Cl(p): 59%) and its analogue **C40** (4'Cl(a): 71%).

For comparison purposes further investigations in catalytic efficacy when complexes are formed *in situ* were carried out. The same model reaction as above was chosen, **Scheme 6.3.4**. Copper(II) chloride was chosen as the copper source, similar to the conditions in the actual copper complex synthesis.



Scheme 6.3.4: Model Ullmann reaction under investigation

The results for catalytic conversions when complexes are made *in situ* are shown in **Figure 6.3.5** and summarised in **Table 6.3.1**. These results show that for both EDG and EWG the catalytic efficacy was higher when pre-synthesised complexes were used compared to when the complexes were made *in situ*. This decrease in catalytic activity can be explained by the high probability of the occurrence of side reactions when the complexes are formed *in situ*. In the synthesis of the complexes side reactions were avoided or minimised by carrying out the reaction under nitrogen and further purification *via* recrystallization of the bulk product.

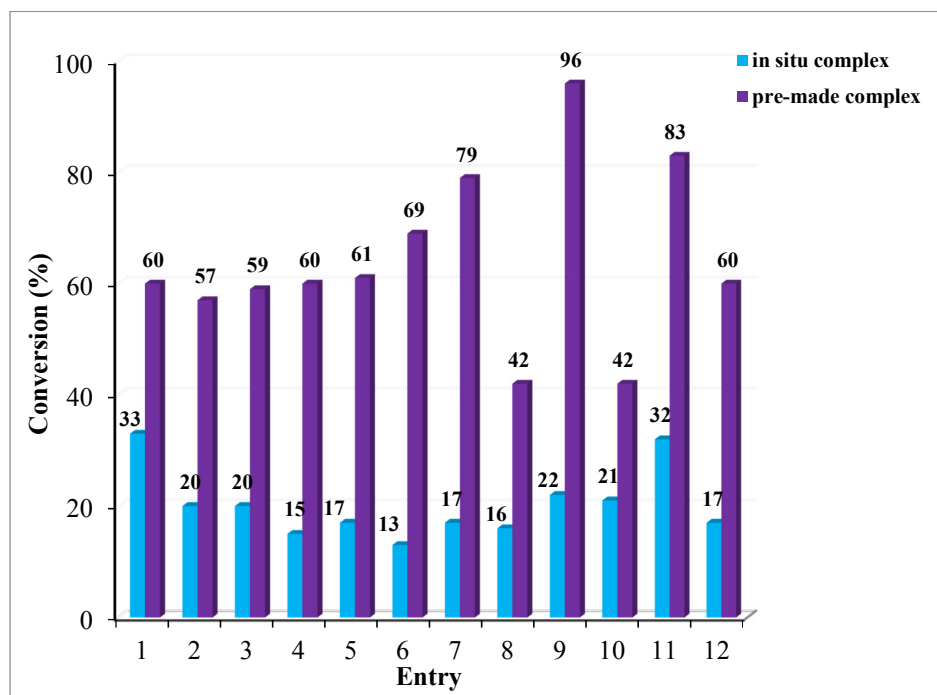


Figure 6.3.5: Catalytic results for acnac ligands and Cu(acnac)₂ complexes (GC yields)

Table 6.3.1: Catalytic results for acnac ligands and Cu(acnac)₂ complexes (GC yields)

Entry	Substituent (R _p /R _a)	Complex	Catalytic conversion (%)	
			Complex made in situ	Pre- synthesised complex
1	H(p)	C17	33	60
2	4'F(p)	C22	6	57
3	4'Cl(p)	C21	6	59
4	4'Br(p)	C20	5	60
5	4'I(p)	C23	17	61
6	2'Cl(p)	C19	13	69
7	2'Br(p)	C18	7	79
8	4'OMe(p)	C25	16	42
9	3',4' diCl(p)	C30	22	96
10	2',3' diMe(p)	C28	21	42
11	3'Cl(a)	C39	32	83
12	3'Br, 4'F(a)	C32	7	60

(p) = substituent on *phenolate* ring; (a) = substituent on *aniline* ring

Having identified that pre-synthesised complexes result in higher catalytic efficacy, with complex **C30** giving the best conversion, solvents and bases were screened in an effort to analyse their effect on the reaction.

Table 6.3.2: Screening results for solvents and bases for Ullmann reaction

Entry	Solvent	Base	Yield (%)
1	DMSO	Cs ₂ CO ₃	23
2	DMF	Cs ₂ CO ₃	29
3	Toluene	Cs ₂ CO ₃	32
4	MeCN	Cs ₂ CO ₃	90
5	MeCN	K ₂ CO ₃	17
6	MeCN	Na ₂ CO ₃	11
7	MeCN	^t BuOK	34
8	MeCN	K ₃ PO ₄	70

The results in **Table 6.3.2** were compared to entry 4 as it gave the highest catalytic conversion yield. The use of other polar solvents in the reaction resulted in poor yield, entries 1-3, 23-32%. The substitution of caesium carbonate with other bases resulted in relatively poor yields (entries 5-7). However K₃PO₄ (entry 8) gave a competitive yield of 70%.

6.4 Conclusion

Several β -*bis*-ketoiminate ruthenium(II) dicarbonyl complexes have been studied as catalysts in the reduction of acetophenone. The complexes tested were functionalised in an effort to incorporate different steric and electronic properties in order to investigate and deduce any structural-activity relationships. The coordination of the ligands, mono- or bidentate, to the metal centre results in an increase in catalytic efficiency. This can be seen when comparing the results of the starting material (RuCl₃.3H₂O) and of the complexes. Electron donating substituents resulted in low catalytic conversions, while an overall increase was observed when electron withdrawing substituents were present on either of the phenyl rings. Catalytic efficiency increased with increase in electronegativity with fluoro substituents giving the highest conversions irrespective of their position on the phenyl rings (i.e. *meta*, *ortho* or *para*). Complex **C4**, with a fluoro substituent in the *para* position of the *aniline* phenyl ring gave the highest catalytic conversion of 94%. Interesting complex **C4** was also the most cytotoxic in anti-cancer studies against colon cancer cell lines (see **Chapter 4**). Further catalytic experiments with complex **C4** and dichloro(*p*-cymene)ruthenium(II) dimer, the “gold standard”, showed that the rate of catalytic activity of the dimer exponentially increases while that of **C4** gradually increases reaching maximum conversion after 6 hours. In conclusion, β -*bis*-

ketoiminate ruthenium(II) dicarbonyl complexes have shown viable activity as catalysts in the transfer hydrogenation of acetophenone using isopropanol.

This chapter also presents results for the catalytic activity of ketoiminate ligands and β -bis-ketoiminate copper(II) complexes for the bi-aryl ether formation in Ullmann type reactions. Comparison of catalytic activities with complexes made *in situ* and pre-synthesised complexes showed higher conversions with pre-synthesised complexes. The significant decrease in catalytic activity is likely due to the presence of side reactions. The wide range of complexes tested with different electronic and steric properties allowed for evaluation of structure-activity relationships. As seen with copper(II) picolinamide complexes previously investigated in our group, the presence of electron donating substituents on the phenyl rings resulted in poor conversions, while electron withdrawing substituents gave high conversions. Furthermore the effect of halogenated substituents was also considered; the extent of electronegativity, electronegative strength, had no significant effect on the catalytic activity of the complexes, while the position of the halogen substituent greatly influenced the catalytic efficiency. The most active catalyst were complexes **C27** (4'CF₃) and **C30** (3',4' diCl) with percentage conversions of 90 and 96 respectively. Investigative reactions with different bases and solvent have shown that the best combination for this type of Ullmann reaction is with acetonitrile as the solvent and caesium carbonate as the base.

6.5 References

1. J. Tsuji, John Wiley & Sons, Chichester, Editon edn., 1985.
2. K. Fagnou and M. Lautens, *Chemical Reviews*, 2003, **103**, 169-196.
3. C. Masters, *Homogeneous Transition-metal Catalysis: A gentle art*, Springer Science & Business Media, 2012.
4. W. Keim, *Journal of Molecular Catalysis*, 1989, **52**, 19-25.
5. H.-U. Blaser, A. Indolese and A. Schnyder, *Current Science*, 2000, 1336-1344.
6. S. Das, G. W. Brudvig and R. H. Crabtree, *Chemical Communications*, 2008, 413-424.
7. A. L. Noffke, A. Habtemariam, A. M. Pizarro and P. J. Sadler, *Chemical Communications*, 2012, **48**, 5219-5246.
8. A. J. Blacker, *Enantioselective Transfer Hydrogenation*, Wiley Online Library, 2007.
9. L. Cervený, *Catalytic Hydrogenation*, Elsevier, 1986.
10. H. U. Blaser, C. Malan, B. Pugin, F. Spindler, H. Steiner and M. Studer, *Advanced Synthesis & Catalysis*, 2003, **345**, 103-151.
11. E. Braude and R. Linstead, *Journal of the Chemical Society (Resumed)*, 1954, 3544-3547.
12. D. Wang and D. Astruc, *Chemical Reviews*, 2015, **115**, 6621-6686.
13. G. Brieger and T. J. Nestruck, *Chemical Reviews*, 1974, **74**, 567-580.
14. R. A. Johnstone, A. H. Wilby and I. D. Entwistle, *Chemical Reviews*, 1985, **85**, 129-170.
15. G. Zassinovich, G. Mestroni and S. Gladiali, *Chemical Reviews*, 1992, **92**, 1051-1069.

16. M. McPartlin and R. Mason, *Chemical Communications (London)*, 1967, 545-546.
17. J. Trocha-Grimshaw and H. Henbest, *Chemical Communications (London)*, 1967, 544-544.
18. Y. Haddad, J. Husbands, H. Henbest and T. Mitchell, Royal Soc Chemistry, Editon edn., 1964, pp. 361-&.
19. J. Blum, Y. Sasson and S. Iflah, *Tetrahedron Letters*, 1972, **13**, 1015-1018.
20. Y. Sasson and J. Blum, *Tetrahedron Letters*, 1971, **12**, 2167-2170.
21. Y. Sasson and J. Blum, *The Journal of Organic Chemistry*, 1975, **40**, 1887-1896.
22. R. L. Chowdhury and J.-E. Bäckvall, *Journal of the Chemical Society, Chemical Communications*, 1991, 1063-1064.
23. B. Pugin and H.-U. Blaser, *Topics in Catalysis*, 2010, **53**, 953-962.
24. J. Václavík, P. Šot, B. Vilhanová, J. Pecháček, M. Kuzma and P. Kačer, *Molecules*, 2013, **18**, 6804-6828.
25. A. Fujii, S. Hashiguchi, N. Uematsu, T. Ikariya and R. Noyori, *Journal of the American Chemical Society*, 1996, **118**, 2521-2522.
26. S. Hashiguchi, A. Fujii, J. Takehara, T. Ikariya and R. Noyori, *Journal of the American Chemical Society*, 1995, **117**, 7562-7563.
27. N. Uematsu, A. Fujii, S. Hashiguchi, T. Ikariya and R. Noyori, *Journal of the American Chemical Society*, 1996, **118**, 4916-4917.
28. T. Ohkuma, N. Utsumi, K. Tsutsumi, K. Murata, C. Sandoval and R. Noyori, *Journal of the American Chemical Society*, 2006, **128**, 8724-8725.
29. J. Václavík, P. Šot, J. Pecháček, B. Vilhanová, O. Matuška, M. Kuzma and P. Kačer, *Molecules*, 2014, **19**, 6987-7007.
30. K. Murata, K. Okano, M. Miyagi, H. Iwane, R. Noyori and T. Ikariya, *Organic Letters*, 1999, **1**, 1119-1121.

31. J. Takehara, S. Hashiguchi, A. Fujii, S.-i. Inoue, T. Ikariya and R. Noyori, *Chemical Communications*, 1996, 233-234.
32. T. Ohkuma, H. Ooka, S. Hashiguchi, T. Ikariya and R. Noyori, *Journal of the American Chemical Society*, 1995, **117**, 2675-2676.
33. Z. Strassberger, M. Mooijman, E. Ruijter, A. H. Alberts, C. de Graaff, R. V. Orru and G. Rothenberg, *Applied Organometallic Chemistry*, 2010, **24**, 142-146.
34. A. Aktaş and Y. Gök, *Transition Metal Chemistry*, 2014, **39**, 925-931.
35. A. Aktaş and Y. Gök, *Catalysis Letters*, 2015, **145**, 631-639.
36. X.-W. Li, G.-F. Wang, F. Chen, Y.-Z. Li, X.-T. Chen and Z.-L. Xue, *Inorganica Chimica Acta*, 2011, **378**, 280-287.
37. A. Rodriguez Barzano, *Novel ruthenium complexes and their applications as catalysts and anticancer agents*, University of Leeds, 2013.
38. S. J. Lucas, *The synthesis of group 9 complexes for use as transfer hydrogenation catalysts and anti-cancer agents*, PhD, University of Leeds, 2013.
39. J. S. Samec, J.-E. Bäckvall, P. G. Andersson and P. Brandt, *Chemical Society Reviews*, 2006, **35**, 237-248.
40. J.-E. Bäckvall, *Journal of Organometallic Chemistry*, 2002, **652**, 105-111.
41. A. Aranyos, G. Csornyik, K. J. Szabó and J.-E. Bäckvall, *Chemical Communications*, 1999, 351-352.
42. S. E. Clapham, A. Hadzovic and R. H. Morris, *Coordination Chemistry Reviews*, 2004, **248**, 2201-2237.
43. A. Salvini, P. Frediani and S. Gallerini, *Applied organometallic chemistry*, 2000, **14**, 570-580.
44. F. Joó, J. Kovács, A. C. Bényei and Á. Kathó, *Catalysis Today*, 1998, **42**, 441-448.
45. K. J. Haack, S. Hashiguchi, A. Fujii, T. Ikariya and R. Noyori, *Angewandte Chemie International Edition*, 1997, **36**, 285-288.

46. J. Holmes, C. M. Pask and C. E. Willans, *Dalton Transactions*, 2016, **45**, 15818-15827.
47. C. Sambiago, S. P. Marsden, A. J. Blacker and P. C. McGowan, *Chemical Society Reviews*, 2014, **43**, 3525-3550.
48. I. P. Beletskaya and A. V. Cheprakov, *Coordination Chemistry Reviews*, 2004, **248**, 2337-2364.
49. C. Fischer and B. Koenig, *Beilstein Journal of Organic Chemistry*, 2011, **7**, 59.
50. J. D Senra, L. CS Aguiar and A. BC Simas, *Current Organic Synthesis*, 2011, **8**, 53-78.
51. I. P. Beletskaya and A. V. Cheprakov, *Chemical Reviews*, 2000, **100**, 3009-3066.
52. S.-i. Kuwabe, K. E. Torraca and S. L. Buchwald, *Journal of the American Chemical Society*, 2001, **123**, 12202-12206.
53. H. Lin and D. Sun, *Organic preparations and procedures international*, 2013, **45**, 341-394.
54. E. R. Strieter, B. Bhayana and S. L. Buchwald, *Journal of the American Chemical Society*, 2008, **131**, 78-88.
55. F. Ullmann and J. Bielecki, *European Journal of Inorganic Chemistry*, 1901, **34**, 2174-2185.
56. P. E. Fanta, *Synthesis*, 1974, **1974**, 9-21.
57. F. Ullmann and P. Sponagel, *European Journal of Organic Chemistry*, 1906, **350**, 83-107.
58. F. Ullmann, *European Journal of Inorganic Chemistry*, 1903, **36**, 2382-2384.
59. I. Goldberg, *European Journal of Inorganic Chemistry*, 1906, **39**, 1691-1692.
60. E. Sperotto, G. P. van Klink, G. van Koten and J. G. de Vries, *Dalton Transactions*, 2010, **39**, 10338-10351.

61. A. A. Kelkar, N. M. Patil and R. V. Chaudhari, *Tetrahedron letters*, 2002, **43**, 7143-7146.
62. C. Sambigiato, R. H. Munday, S. P. Marsden, A. J. Blacker and P. C. McGowan, *Chemistry-A European Journal*, 2014, **20**, 17606-17615.
63. F. Ullmann, *European Journal of Inorganic Chemistry*, 1904, **37**, 853-854.
64. P. E. Weston and H. Adkins, *Journal of the American Chemical Society*, 1928, **50**, 859-866.
65. A. J. Paine, *Journal of the American Chemical Society*, 1987, **109**, 1496-1502.

Chapter 7 Experimental

7.1 General Experimental Procedure

All novel β -bis-ketoiminate copper(II) complexes were synthesised using standard Schlenk line techniques, under an atmosphere of dry dinitrogen with a dual vacuum/dinitrogen line to perform the synthesis. All β -bis-ketoiminate ruthenium(II) dicarbonyl complexes were synthesised under aerobic conditions.

All chemicals were supplied by Sigma-Aldrich Chemical Co., Acros Organics, Alfa Aesar and BOC gases. Deuterated NMR solvents were purchased from Sigma-Aldrich Chemical Co. or Acros Organics. Functionalised β -diketonate and β -ketoiminate ligands were prepared by adaptations of literature methods.^{1,2}

7.2 Instrumentation

All NMR spectra were recorded by the author on a Bruker DPX 300 or DRX 500 spectrometer. Chemical shifts (δ) are expressed in parts per million (ppm) and referenced to the solvent signal, used as an internal reference. Microanalyses were acquired by Mr. Stephen Boyer at the London Metropolitan University Elemental Analysis Service. Mass Spectra were recorded by the author or Dr Stuart Warriner on a Bruker Daltonics MicroTOF instrument with electrospray ionisation (ESI) and a photodiode array analyser at the University of Leeds Mass Spectrometry Service. UV/vis absorption spectra were acquired on a Cary Series UV-Vis spectrophotometer using 1 cm path length quartz cuvettes. Infrared spectra were obtained using a Platinum ATR Spectrometer on a crystal plate with samples analysed using OPUS software.

For catalytic studies reported in this thesis, the same commercial sources of chemicals and solvents were used. Reactions were routinely performed in carousel tubes of the same size and shape, using the same type of stirrer bars at a stirring rate of 500 rpm. Reactions were analysed using a HP6890 series GC-MS with a split/splitless injector system and FID was used. Chromatographic separation was performed by using a 30 m X 0.32 m HP-5MS column ($d_f = 0.25\mu\text{m}$) and helium used as a carrier gas at a flow rate of $97.4\text{ mL}\cdot\text{min}^{-1}$. All $1\mu\text{L}$ injections were carried out in a split flow mode with split ratio of 50:1. The injector was initially ramped to 60°C for 2 minutes, followed by an increase to 300°C at a rate of $20^\circ\text{C}\cdot\text{min}^{-1}$.

7.3 X-ray crystallography

Single crystal X-ray diffraction data were collected either by the author or Dr. Christopher Pask using an Agilent (Rigaku) SuperNova X-ray diffractometer fitted with an Atlas area detector using mirror monochromated Mo-K α ($\lambda = 0.71073 \text{ \AA}$) or Cu-K α ($\lambda = 1.54184 \text{ \AA}$) radiation. The crystal was cooled to 120 K using an Oxford Cryosystem low temperature device.³ The full dataset was collected and the images processed using CrysAlisPro program.⁴ Structure solution by direct methods was achieved through the use of SHELXS86,⁵ SHELXL-2014⁶ or SHELXT,⁷ and the structural model refined by full matrix least squares on F² using SHELX97⁸ interfaced through the program Olex2.⁹ Molecular graphics were plotted, editing of CIFs and construction of tables of bond lengths and angles were achieved using Olex2. Unless otherwise stated, hydrogen atoms were placed using idealised geometric positions (with free rotation for methyl groups), allowed to move in a “riding model” along with the atoms to which they were attached, and refined isotropically. The SQUEEZE routine of Platon was used to refine structures where diffuse electron density could not be adequately modelled as solvent of crystallisation.¹⁰

7.4 Synthesis of functionalised β -diketonate ligands

β -Diketonate ligands, precursors to β -bis-ketoiminate ligands, have been previously synthesised and fully characterised within the McGowan research group by Dr. Felix Janeway, Dr. Andrew Hebden and Dr Rianne Lord (University of Leeds), as such no characterisation data is given herein.

7.4.1 General synthetic procedure for β -diketonate ligands

Ligands were synthesised *via* modified literature methods.^{11, 12} Sodium ethoxide (1 equivalent) was added to a solution of the required acetophenone (1.2 equivalents) in ethyl acetate and refluxed for 2 hours, followed by stirring at room temperature for a further 16 hours. The solvent was removed under reduced pressure and washed with petrol (60-80°C) (3 x 10 mL). The suspension was then dissolved in water (40-100 mL) and sulfuric acid (1 molar) was added until just acidic to litmus. The crude product was extracted into diethyl ether (3 x 10 mL) and dried over MgSO₄. After cooling to room temperature, ice cold sulfuric acid was added dropwise until the

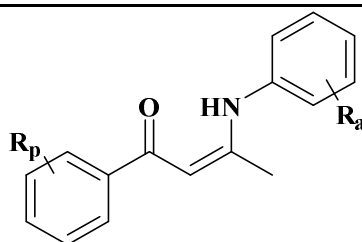
mixture was just acidic. Solvent was removed under reduced pressure and the residue recrystallised from hot ethanol.

7.5 Synthesis of functionalised β -bis-ketoiminate ligands

β -bis-ketoiminate ligands have been previously synthesised and fully characterised by Dr Rianne Lord (University of Leeds).¹³ As such no characterisation data for ligands **L1-L32** are given herein.

7.5.1 General synthetic procedure for β -bis-ketoiminate ligands

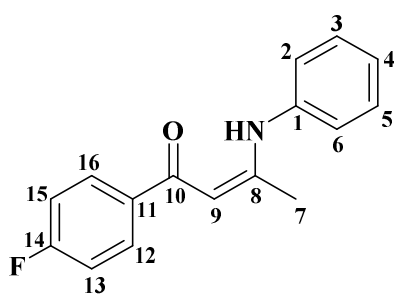
Ligands **L1-L32** were synthesised using a modified synthetic route based on work by Tang *et al.*¹⁴ In this synthesis the functionalised diketonate was dissolved in toluene, and aniline and dilute HCl added. This was allowed to stir at room temperature for 16 hours, after which the precipitate was filtered off and the solvent removed under reduced pressure. The crude products were recrystallised from hot ethanol. The synthesis of ligand **L2** is given as an example.



$R_a = H, R_p = H$	L1	2',4',6' triMe	L16
4'F	L2	3',4' methylene	L17
4'Cl	L3	3'Br, 4'F	L18
4'Br	L4	$R_p = H, R_a = 4'Cl$	L21
3'F	L5	4'F	L22
3'Br	L6	4'Me	L23
4'I	L7	3'Br	L24
4'Me	L8	3'Me	L25
2'Cl	L9	2'F	L26
2'Br	L10	2',4' diCl	L27
4'OMe	L11	2',4' diF	L28
4'CF ₃	L12	2',3' diMe	L29
4'OEt	L13	2'Br	L30
2'OMe	L14	3'Cl	L31
3',4' diCl	L15	2',5' diF	L32

7.5.2 Synthesis of L2

4'-Fluoro- β -diketonate (750 mg, 4.20 mmol) was dissolved in toluene (10 mL), aniline (1.5 mL) and HCl (0.75 mL) were then added. This was stirred for 16 hours, after which the precipitate was filtered and the solvent removed under reduced pressure. The crude product was recrystallised from hot ethanol (10 mL), yielding yellow crystals of **L2** (890 mg, 3.49 mmol, 83%).



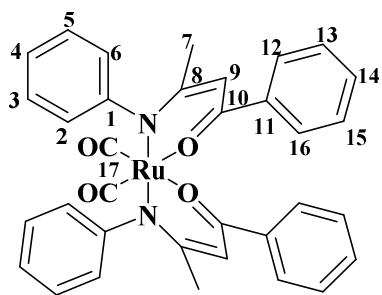
$^1\text{H NMR}$ (CDCl_3 , 500.23 MHz, 299.9 K) δ 13.06 (br. s, 1H, NH), 7.94 (br. dd, 2H, H_{12} and H_{16} , 3J ($^1\text{H}-^1\text{H}$) = 8.7, 4J ($^1\text{H}-^{19}\text{F}$) = 5.5), 7.38 (br. t, 2H, H_3 and H_5 , 3J ($^1\text{H}-^1\text{H}$) = 8.0, 3J ($^1\text{H}-^1\text{H}$) = 7.8), 7.24 (br. t, 1H, H_4 , 3J ($^1\text{H}-^1\text{H}$) = 7.4), 7.19 (d, 2H, H_2 and H_6 , 3J ($^1\text{H}-^1\text{H}$) = 7.5), 7.11 (br. t, 2H, H_{13} and H_{15} , 3J ($^1\text{H}-^1\text{H}$) = 8.7, 3J ($^1\text{H}-^{19}\text{F}$) = 8.7), 5.85 (s, 1H, H_9), 2.16 (s, 3H, H_7).

7.6 Synthesis of β -bis-ketoiminate Ru(II) dicarbonyl complexes

All β -bis-ketoiminate ruthenium(II) dicarbonyl complexes were synthesised as follows. Ruthenium(III) chloride trihydrate (1 equivalent) was dissolved in 2-ethoxyethanol (10 mL) and the solution warmed up to reflux temperature. In a separate flask the ketoiminate ligand (2.2 equivalents) and triethylamine (4 equivalents) were dissolved in 2-ethoxyethanol (5-10 mL) and stirred for 20-30 minutes. The ligand and base solution was then added to the metal solution dropwise and the dark coloured solution stirred under reflux for 6 hours. After cooling to room temperature the product was filtered off and solvent removed under reduced pressure. The product was purified by column chromatography using dichloromethane/hexane as the eluant.

7.6.1 Synthesis of C1 ($\text{C}_{34}\text{H}_{28}\text{N}_2\text{O}_4\text{Ru}$)

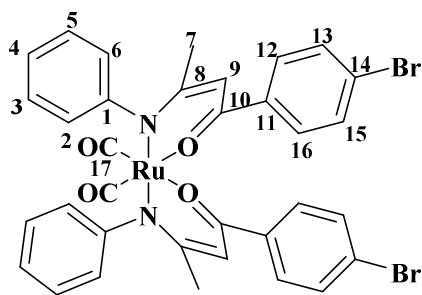
Complex **C1** was purified by column chromatography (DCM/hexane, 1:1) and further recrystallised from hot acetonitrile to give a green solid (510 mg, 0.80 mmol, 35 %). Single crystals suitable for X-ray diffraction were obtained from vapour diffusion of hexane into a saturated solution of the complex in DCM, at room temperature.



^1H NMR (CDCl_3 , 500.23 MHz, 299.9 K) δ , 7.93-7.87 (m, 2H, H_{12} and H_{16}), 7.31-7.27 (br. t, 3H, H_{13} , H_{14} and H_{15} , $^3J(^1\text{H}-^1\text{H}) = 6.5$ Hz), 7.26-7.21 (br. m, 3H, H_3 , H_5 and H_2 or H_6), 7.05 (br. t, 1H, H_4 , $^3J(^1\text{H}-^1\text{H}) = 7.2$ Hz), 6.77 (br. d, 1H, H_2 or H_6 , $^3J(^1\text{H}-^1\text{H}) = 8.3$ Hz), 5.60 (s, 1H, H_9), 1.83 (s, 3H, H_7). **$^{13}\text{C}\{^1\text{H}\}$ NMR** (CDCl_3 , 300 MHz, 299.9 K) δ 197.1 ($\underline{\text{C}}\text{O}$), 173.3 (quaternary $\underline{\text{C}}$, C_{10}), 166.7 (quaternary $\underline{\text{C}}$, C_8), 157.9 (quaternary $\underline{\text{C}}$, C_1), 140.5 (quaternary $\underline{\text{C}}$, C_{11}), 129.3 (aniline $\underline{\text{C}}\text{H}$, C_3 or C_5), 129.2 (aniline $\underline{\text{C}}\text{H}$, C_3 or C_5), 128.8 (aromatic $\underline{\text{C}}\text{H}$, C_{14}), 128.0 (aromatic $\underline{\text{C}}\text{H}$, C_{13} and C_{15}), 127.0 (aromatic $\underline{\text{C}}\text{H}$, C_{12} and C_{16}), 125.1 (aniline $\underline{\text{C}}\text{H}$, C_4), 124.6 (aniline $\underline{\text{C}}\text{H}$, C_2 or C_6), 122.4 (aniline $\underline{\text{C}}\text{H}$, C_2 or C_6), 95.2 (acnac $\underline{\text{C}}\text{H}$, C_9), 24.3 (acnac $\underline{\text{C}}\text{H}_3$, C_7). **IR** (cm^{-1}), 2039 (s, CO), 1964 (s, CO). **Analysis calculated:** C, 64.85, H, 4.48, N, 4.45 % **Analysis found:** C, 64.89, H, 4.79, N, 4.50 %. **ES MS** (+) m/z 631.12 [M^+].

7.6.2 Synthesis of **C2** ($\text{C}_{34}\text{H}_{26}\text{Br}_2\text{N}_2\text{O}_4\text{Ru}$)

Complex **C2** was purified using column chromatography (DCM/hexane, 3:2). Further purification through vapour diffusion of hexane into a solution of the complex in DCM gave **C2** as yellow single crystals suitable for X-ray diffraction (210 mg, 0.27 mmol, 34 %).

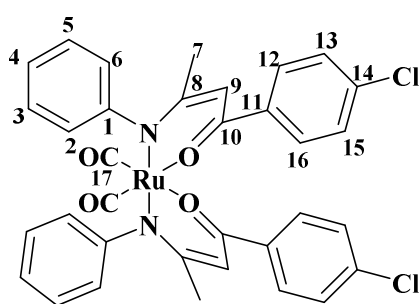


^1H NMR (CDCl_3 , 500.23 MHz, 299.9 K) δ 7.71 (br. d, 2H, H_{12} and H_{16} , $^3J(^1\text{H}-^1\text{H}) = 8.6$ Hz), 7.50 (br. d, 2H, H_{13} and H_{15} , $^3J(^1\text{H}-^1\text{H}) = 8.4$ Hz), 7.37-7.31 (m, 2H, H_3 and H_5), 7.24 (br. d, 1H, H_2 or H_6 , $^3J(^1\text{H}-^1\text{H}) = 7.3$ Hz), 7.16 (br. t, 1H, H_4 , $^3J(^1\text{H}-^1\text{H}) = 7.5$ Hz), 6.85 (d, 1H, H_2 or H_6 , $^3J(^1\text{H}-^1\text{H}) = 7.6$ Hz), 5.62 (s, 1H, H_9), 1.91 (s, 3H, H_7). **$^{13}\text{C}\{^1\text{H}\}$ NMR** (CDCl_3 , 300 MHz, 299.9 K) δ 196.9 ($\underline{\text{C}}\text{O}$), 172.0 (quaternary $\underline{\text{C}}$, C_{10}), 167.0 (quaternary $\underline{\text{C}}$, C_8), 157.6 (quaternary $\underline{\text{C}}$, C_1), 139.3 (quaternary $\underline{\text{C}}$, C_{11}), 131.1 (quaternary $\underline{\text{C}}-\text{Br}$, C_{14}), 129.3 (aniline $\underline{\text{C}}\text{H}$, C_3 or C_5), 129.0 (aniline $\underline{\text{C}}\text{H}$, C_3 or C_5), 128.6 (aromatic $\underline{\text{C}}\text{H}$, C_{13} and C_{15}), 125.3 (aromatic $\underline{\text{C}}\text{H}$, C_{12} and C_{16}), 124.3 (aniline $\underline{\text{C}}\text{H}$, C_2 or C_6), 123.7 (aniline $\underline{\text{C}}\text{H}$, C_4), 122.3 (aniline $\underline{\text{C}}\text{H}$, C_2 or C_6), 95.2 (acnac $\underline{\text{C}}\text{H}$, C_9), 24.3 (acnac $\underline{\text{C}}\text{H}_3$, C_7).

IR (cm^{-1}), 2037 (s, CO), 1963 (s, CO). **Analysis calculated:** C, 51.86, H, 3.33, N, 3.56 % **Analysis found:** C, 52.05, H, 3.70, N, 3.25 %. **ES MS (+)** m/z 788.94 [M^+].

7.6.3 Synthesis of C3 ($\text{C}_{34}\text{H}_{26}\text{Cl}_2\text{N}_2\text{O}_4\text{Ru}$)

The crude product was purified using column chromatography (DCM/hexane, 1:1), to give complex **C3** as a yellow-green solid (490 mg, 0.70 mmol, 36 %).

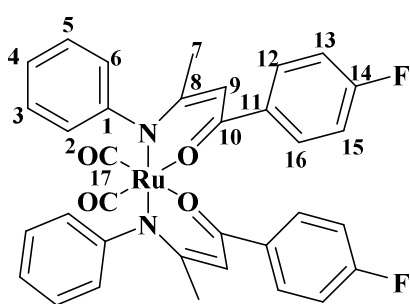


^1H NMR (CDCl_3 , 500.23 MHz, 299.9 K) δ , 7.70 (d, 2H, H_{12} and H_{16} , 3J ($^1\text{H}-^1\text{H}$) = 8.55 Hz), 7.29-7.22 (m, 4H, H_3 , H_5 , H_{13} and H_{15}), 7.16 (d, 1H, H_2 or H_6 , 3J ($^1\text{H}-^1\text{H}$) = 7.7 Hz), 7.07 (t, 1H, H_4 , 3J ($^1\text{H}-^1\text{H}$) = 7.5 Hz), 6.76 (d, 1H, H_2 or H_6 , 3J ($^1\text{H}-^1\text{H}$) = 7.7 Hz), 5.56 (s, 1H, H_9), 1.82 (s, 3H, H_7).

$^{13}\text{C}\{^1\text{H}\}$ NMR (CDCl_3 , 300 MHz, 299.9 K) δ 196.9 (C=O), 172.0 (quaternary C , C_{10}), 167.0 (quaternary C , C_8), 157.7 (quaternary C , C_1), 138.9 (quaternary C , C_{11}), 135.3 (quaternary C-Cl , C_{14}), 129.3 (aniline CH , C_3 or C_5), 129.0 (aniline CH , C_3 or C_5), 128.3 (aromatic CH , C_{13} and C_{15}), 128.2 (aromatic CH , C_{12} and C_{16}), 125.4 (aniline CH , C_4), 124.4 (aniline CH , C_2 or C_6), 122.3 (aniline CH , C_2 or C_6), 95.2 (acnac CH , C_9), 24.3 (acnac CH_3 , C_7). **IR** (cm^{-1}), 2039 (s, CO), 1969 (s, CO). **Analysis calculated:** C, 58.46, H, 3.75, N, 4.01 % **Analysis found:** C, 58.57, H, 3.80, N, 4.15 %. **ES MS (+)** m/z 699.04 [M^+].

7.6.4 Synthesis of C4 ($\text{C}_{34}\text{H}_{26}\text{F}_2\text{N}_2\text{O}_4\text{Ru}$)

Complex **C4** was purified using column chromatography (DCM/hexane, 1:1). Further purification through vapour diffusion of hexane into a solution of the complex in DCM gave **C4** as single crystals suitable for X-ray diffraction (170 mg, 0.26 mmol, 39 %).

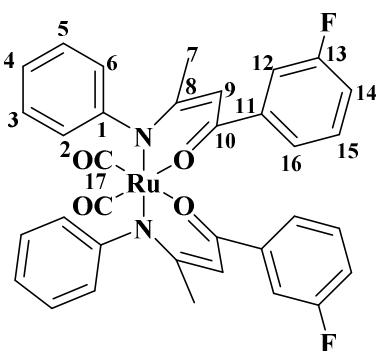


^1H NMR (CDCl_3 , 500.23 MHz, 299.9 K) δ , 7.85 (br. dd, 2H, H_{12} and H_{16} , 3J ($^1\text{H}-^1\text{H}$) = 8.4 Hz, 4J ($^1\text{H}-^{19}\text{F}$) = 5.7 Hz), 7.4 (br. dd, 2H, H_{13} and H_{15} , 3J ($^1\text{H}-^1\text{H}$) = 8.0 Hz, 3J ($^1\text{H}-^{19}\text{F}$) = 8.8 Hz), 7.26 (br. d, 1H, H_2 or H_6 , 3J ($^1\text{H}-^1\text{H}$) = 8.3 Hz), 7.15 (t, 1H, H_4 , 3J ($^1\text{H}-^1\text{H}$) = 7.5 Hz), 7.05 (br. t, 2H, H_3 and H_5 , 3J

(^1H - ^1H) = 8.5 Hz), 6.85 (d, 1H, H_2 or H_6 , 3J (^1H - ^1H) = 8.0 Hz), 5.62 (s, 1H, H_9), 1.92 (s, 3H, H_7). $^{13}\text{C}\{^1\text{H}\}$ NMR (CDCl_3 , 300 MHz, 299.9 K) δ 197.0 (CO), 172.2 (quaternary $\underline{\text{C}}$, C_{10}), 166.8 (quaternary $\underline{\text{C}}$, C_8), 163.7 (quaternary $\underline{\text{C}}$ -F, C_{14} , 1J (^{13}C - ^{19}F) = 248.8 Hz), 157.7 (quaternary $\underline{\text{C}}$, C_1), 136.4 (quaternary $\underline{\text{C}}$, C_{11} , 4J (^{13}C - ^{19}F) = 3.1 Hz), 129.2 (aniline $\underline{\text{C}}\text{H}$, C_3 or C_5), 128.9 (aniline $\underline{\text{C}}\text{H}$, C_3 or C_5), 128.9 (aromatic $\underline{\text{C}}\text{H}$, C_{12} and C_{16} , 3J (^{13}C - ^{19}F) = 8.30 Hz), 125.3 (aniline $\underline{\text{C}}\text{H}$, C_4), 124.4 (aniline $\underline{\text{C}}\text{H}$, C_2 or C_6), 122.3 (aniline $\underline{\text{C}}\text{H}$, C_2 or C_6), 114.8 (aromatic $\underline{\text{C}}\text{H}$, C_{13} and C_{15} , 2J (^{13}C - ^{19}F) = 21.8 Hz), 94.9 (acnac $\underline{\text{C}}\text{H}$, C_9), 24.3 (acnac $\underline{\text{C}}\text{H}_3$, C_7). IR (cm^{-1}), 2033 (s, CO), 1963 (s, CO). **Analysis calculated:** C, 61.35, H, 3.94, N, 4.21 % **Analysis found:** C, 61.35, H, 4.14, N, 4.29 %. **ES MS (+) m/z 667.10 [M^+].**

7.6.5 Synthesis of C5 ($\text{C}_{34}\text{H}_{26}\text{F}_2\text{N}_2\text{O}_4\text{Ru}$)

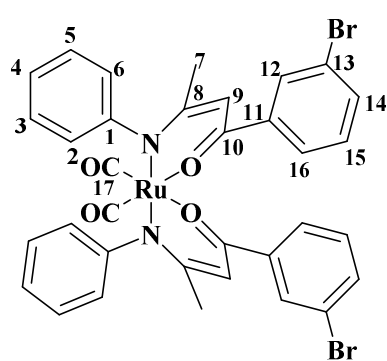
The crude product was purified using column chromatography (DCM/hexane; 1:1) to give complex, **C5** as a yellow solid, which was further purified through recrystallisation with hot acetonitrile, (420 mg, 0.64 mmol, 30 %).



^1H NMR (CDCl_3 , 500.23 MHz, 299.9 K) δ , 7.62 (d, 1H, H_{16} , 3J (^1H - ^1H) = 7.8 Hz), 7.57 (dt, 1H, 3J (^1H - ^{19}F) = 10.4 Hz), 7.39-7.31 (m, 3H, H_3 , H_5 and H_{15}), 7.28 (d, 1H, H_2 or H_6 , 3J (^1H - ^1H) = 8.1 Hz), 7.17 (t, 1H, H_4 , 3J (^1H - ^1H) = 7.4 Hz), 6.86 (d, 1H, H_2 or H_6 , 3J (^1H - ^1H) = 7.9 Hz), 5.66 (s, 1H, H_9), 1.93 (s, 3H, H_7). $^{13}\text{C}\{^1\text{H}\}$ NMR (CDCl_3 , 300 MHz, 299.9 K) δ 196.9 (CO), 171.6 (d, quaternary $\underline{\text{C}}$, C_{10} , 4J (^{13}C - ^{19}F) = 1.9 Hz), 167.1 (quaternary $\underline{\text{C}}$, C_8), 164.4 (quaternary $\underline{\text{C}}$ -F, C_{14} , 1J (^{13}C - ^{19}F) = 243.9 Hz), 157.6 (quaternary $\underline{\text{C}}$, C_1), 142.8 (d, quaternary $\underline{\text{C}}$, C_{11} , 3J (^{13}C - ^{19}F) = 7.1 Hz), 129.3 (d, aromatic $\underline{\text{C}}\text{H}$, C_{15} , 3J (^{13}C - ^{19}F) = 7.4 Hz), 129.3 (aniline $\underline{\text{C}}\text{H}$, C_3 or C_5), 129.0 (aniline $\underline{\text{C}}\text{H}$, C_3 or C_5), 125.4 (aniline $\underline{\text{C}}\text{H}$, C_4), 124.4 (aniline $\underline{\text{C}}\text{H}$, C_2 or C_6), 122.4 (d, aromatic $\underline{\text{C}}\text{H}$, C_{16} , 4J (^{13}C - ^{19}F) = 2.6 Hz), 122.2 (aniline $\underline{\text{C}}\text{H}$, C_2 or C_6), 116.1 (d, aromatic $\underline{\text{C}}\text{H}$, C_{14} , 2J (^{13}C - ^{19}F) = 22.5 Hz), 114.1 (d, aromatic $\underline{\text{C}}\text{H}$, C_{12} , 2J (^{13}C - ^{19}F) = 22.9 Hz), 95.5 (acnac $\underline{\text{C}}\text{H}$, C_9), 24.3 (acnac $\underline{\text{C}}\text{H}_3$, C_7). IR (cm^{-1}), 2039 (s, CO), 1963 (s, CO). **Analysis calculated:** C, 61.35, H, 3.94, N, 4.21 % **Analysis found:** C, 61.42, H, 3.84, N, 4.29 %. **ES MS (+) m/z 667.10 [M^+].**

7.6.6 Synthesis of C6 (C₃₄H₂₆Br₂N₂O₄Ru)

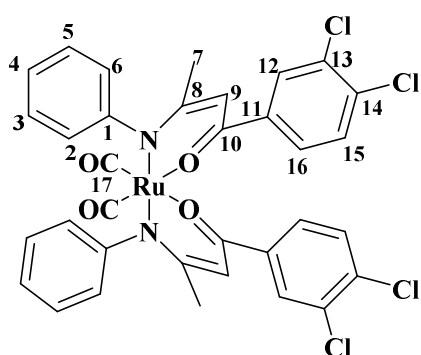
The crude product was purified using column chromatography (DCM/hexane, 3:2) to give complex **C6** as a yellow solid (430 mg, 0.53 mmol, 33 %). Single crystals suitable for X-ray diffraction were obtained from slow vapour diffusion of pentane into a solution of the complex in DCM.



¹H NMR (CDCl₃, 500.23 MHz, 299.9 K) δ, 8.02 (t, 1H, H₁₂, ⁴*J* (¹H-¹H) = 1.8 Hz), 7.76 (d, 1H, H₁₆, ³*J* (¹H-¹H) = 7.8 Hz), 7.49 (dt, 1H, H₁₄, ³*J* (¹H-¹H) = 7.9 Hz, ⁴*J* (¹H-¹H) = 0.9 Hz), 7.42-7.38 (m, 1H, H₃ or H₅), 7.37-7.33 (m, 1H, H₃ or H₅), 7.28 (d, 1H, H₂ or H₆, ³*J* (¹H-¹H) = 8.4 Hz), 7.24 (t, 1H, H₁₅, ³*J* (¹H-¹H) = 7.8 Hz), 7.17 (br. t, 1H, H₄, ³*J* (¹H-¹H) = 7.5 Hz), 6.86 (d, 1H, H₂ or H₆, ³*J* (¹H-¹H) = 7.1 Hz), 5.63 (s, 1H, H₉), 1.93 (s, 3H, H₇). **¹³C{¹H} NMR** (CDCl₃, 300 MHz, 299.9 K) δ 196.8 (C=O), 171.6 (quaternary C, C₁₀), 167.3 (quaternary C, C₈), 157.4 (quaternary C, C₁), 142.5 (quaternary C-Br, C₁₃), 132.10 (quaternary C, C₁₁), 130.3 (aromatic CH, C₁₂ or C₁₄), 129.6 (aromatic CH, C₁₂ or C₁₄), 129.3 (aniline CH, C₃ or C₅), 129.0 (aniline CH, C₃ or C₅), 128.0 (aromatic CH, C₁₅), 127.0 (aromatic CH, C₁₆), 125.4 (aniline CH, C₂ or C₆), 124.4 (aniline CH, C₄), 122.2 (aniline CH, C₂ or C₆), 95.8 (acnac CH, C₉), 24.3 (acnac CH₃, C₇). **IR** (cm⁻¹), 2039 (s, CO), 1962 (s, CO). **Analysis calculated** (+ 0.5 pentane): C, 53.20, H, 3.57, N, 3.40 % **Analysis found**: C, 53.23, H, 3.92, N, 3.40 %. **ES MS** (+) *m/z* 788.94 [M⁺].

7.6.7 Synthesis of C7 (C₃₄H₂₄Cl₄N₂O₄Ru)

The crude product was purified using column chromatography (DCM/hexane, 1:1) to give complex **C7** as a green solid (360 mg, 0.47 mmol, 31 %).

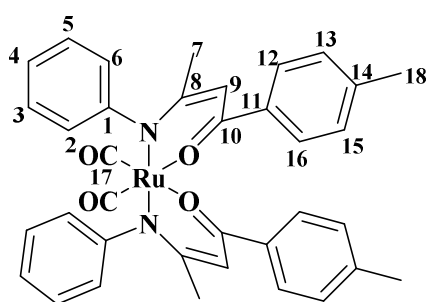


¹H NMR (CDCl₃, 500.23 MHz, 299.9 K) δ, 7.94 (d, 1H, H₁₂, ⁴*J* (¹H-¹H) = 1.9 Hz), 7.65 (dd, 1H, H₁₆, ³*J* (¹H-¹H) = 8.5 Hz, ⁴*J* (¹H-¹H) = 1.9 Hz), 7.43 (d, 1H, H₁₅, ³*J* (¹H-¹H) = 8.3 Hz), 7.39 (t, 1H, H₃ or H₅, ³*J* (¹H-¹H) = 7.7 Hz), 7.35 (t, 1H, H₃ or H₅, ³*J* (¹H-¹H) = 7.7 Hz), 7.23 (d, 1H, H₂ or

H₆, $^3J(^1\text{H}-^1\text{H}) = 7.7$ Hz), 7.18 (t, 1H, H₄, $^3J(^1\text{H}-^1\text{H}) = 7.5$ Hz), 6.85 (d, 1H, H₂ or H₆, $^3J(^1\text{H}-^1\text{H}) = 7.5$ Hz), 5.61 (s, 1H, H₉), 1.92 (s, 3H, H₇). **$^{13}\text{C}\{^1\text{H}\}$ NMR** (CDCl₃, 300 MHz, 299.9 K) δ 196.7 (C=O), 170.5 (quaternary C, C₁₀), 167.4 (quaternary C, C₈), 157.3 (quaternary C, C₁), 140.3 (quaternary C-Cl, C₁₃ and C₁₄), 133.2 (quaternary C, C₁₁), 132.2 (aromatic CH, C₁₅), 130.0 (aromatic CH, C₁₂), 129.3 (aniline CH, C₃ or C₅), 129.1 (aniline CH, C₃ or C₅), 126.0 (aromatic CH, C₁₆), 125.5 (aniline CH, C₂ or C₆), 124.2 (aniline CH, C₄), 122.2 (aniline CH, C₂ or C₆), 95.7 (acnac CH, C₉), 24.3 (acnac CH₃, C₇). **IR** (cm⁻¹), 2043 (s, CO), 1975 (s, CO). **Analysis calculated:** C, 53.21, H, 3.51, N, 3.65 % **Analysis found:** C, 53.35, H, 3.39, N, 3.76 %.

7.6.8 Synthesis of C8 (C₃₆H₃₂N₂O₄Ru)

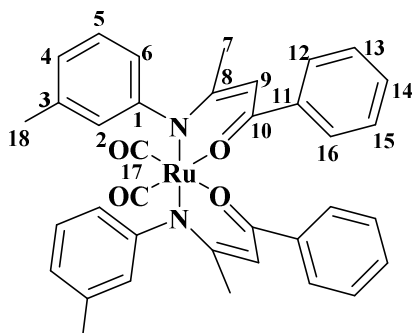
Complex **C8** was purified by column chromatography (DCM/hexane, 7:3) and further recrystallised from hot acetonitrile to give a yellow solid (220 mg, 0.33 mmol, 42 %).



^1H NMR (CDCl₃, 500.23 MHz, 299.9 K) δ , 7.78 (d, 2H, H₁₂ and H₁₆, $^3J(^1\text{H}-^1\text{H}) = 8.1$ Hz), 7.36-7.31 (m, 2H, H₃, and H₅), 7.28 (d, 1H, H₂ or H₆, $^3J(^1\text{H}-^1\text{H}) = 7.1$ Hz), 7.18 (d, 1H, H₁₃ and H₁₅, $^3J(^1\text{H}-^1\text{H}) = 8.1$ Hz), 7.15-7.11 (m, 1H, H₄), 6.86 (d, 1H, H₂ or H₆, $^3J(^1\text{H}-^1\text{H}) = 8.3$ Hz), 5.66 (s, 1H, H₉), 2.38 (s, 3H, H₁₈), 1.83 (s, 3H, H₇). **$^{13}\text{C}\{^1\text{H}\}$ NMR** (CDCl₃, 300 MHz, 299.9 K) δ 197.2 (C=O), 173.4 (quaternary C, C₁₀), 166.4 (quaternary C, C₈), 158.0 (quaternary C, C₁), 139.3 (quaternary C, C₁₁), 137.7 (quaternary C, C₁₄), 129.1 (aniline CH, C₃ or C₅), 128.8 (aniline CH, C₃ or C₅), 128.6 (aromatic CH, C₁₃ and C₁₅), 127.0 (aromatic CH, C₁₂ and C₁₆), 125.0 (aniline CH, C₂ or C₆), 124.7 (aniline CH, C₄), 122.5 (aniline CH, C₂ or C₆), 94.8 (acnac CH, C₉), 24.2 (acnac CH₃, C₇), 21.3 (aromatic CH₃, C₁₈). **IR** (cm⁻¹), 2033 (s, CO), 1964 (s, CO). **Analysis calculated:** C, 65.74, H, 4.90, N, 4.26 % **Analysis found:** C, 65.85, H, 4.98, N, 4.31 %. **ES MS (+)** m/z 659.13 [M⁺].

7.6.9 Synthesis of C9 (C₃₆H₃₂N₂O₄Ru)

The crude product was purified by column chromatography (DCM/hexane, 4:1) and further recrystallised from hot acetonitrile to give a yellow solid of complex **C9** (530 mg, 0.81 mmol, 37 %).

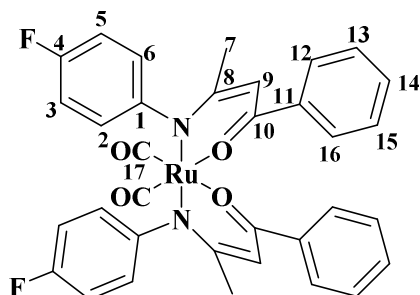


¹H NMR (CDCl₃, 500.23 MHz, 299.9 K) δ, 7.92-7.86 (m, 2H, H₁₂ and H₁₆), 7.41-7.35 (m, 3H, H₁₃, H₁₄ and H₁₅), 7.26-7.16 (br. m, 1H, H₅), 7.15-7.11 (m, 1H, H₂), 6.96 (d, 1H, H₄, ³J (¹H-¹H) = 7.6 Hz), 6.67 (d, 1H, H₆, ³J (¹H-¹H) = 7.4 Hz), 5.67 (s, 1H, H₉), 2.33 (d, 3H, H₁₈, ⁴J (¹H-¹H) = 4.9 Hz), 1.93 (d, 3H, H₇, ⁴J (¹H-¹H) = 1.9 Hz).

¹³C{¹H} NMR (CDCl₃, 300 MHz, 299.9 K) δ 197.4 (C=O), 173.7 (quaternary C, C₁₀), 166.7 (quaternary C, C₈), 157.5 (quaternary C, C₁), 140.5 (quaternary C, C₁₁), 138.8 (quaternary C, C₃), 129.2 (aniline CH, C₅), 128.8 (aromatic CH, C₁₄), 127.9 (aromatic CH, C₁₃ or C₁₅), 127.9 (aromatic CH, C₁₃ or C₁₅), 127.0 (aromatic CH, C₁₂ and C₁₆), 125.8 (aniline CH, C₄), 122.9 (aniline CH, C₂ or C₆), 121.6 (aniline CH, C₂ or C₆), 95.4 (acnac CH, C₉), 24.2 (acnac CH₃, C₇), 21.4 (aromatic CH₃, C₁₈). IR (cm⁻¹), 2037 (s, CO), 1964 (s, CO). Analysis calculated: C, 65.74, H, 4.90, N, 4.26 % Analysis found: C, 65.85, H, 4.79, N, 4.31 %. ES MS (+) m/z 659.11 [M⁺].

7.6.10 Synthesis of C10 (C₃₄H₂₆F₂N₂O₄Ru)

Complex **C10** was purified by column chromatography (DCM/hexane, 7:3) and further recrystallised from hot acetonitrile to give a yellow solid (560 mg, 0.85 mmol, 42 %).

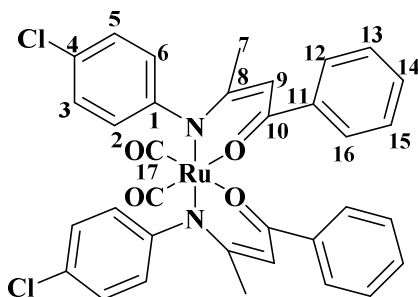


¹H NMR (CDCl₃, 500.23 MHz, 299.9 K) δ, 7.86-7.81 (m, 2H, H₁₂ and H₁₆), 7.41-7.35 (m, 3H, H₁₃, H₁₄ and H₁₅), 7.30 (br. d, 2H, H₃ and H₅, ³J (¹H-¹H) = 8.6 Hz), 7.25-7.21 (m, 1H, H₂ or H₆), 6.82-6.78 (m, 1H, H₂ or H₆), 5.68 (s, 1H, H₉), 1.91 (s, 3H, H₇). ¹³C{¹H} NMR (CDCl₃, 300 MHz, 299.9 K) δ 197.0 (C=O), 173.7 (quaternary C, C₁₀), 167.3 (quaternary C, C₈), 161.6 (quaternary C-F, C₄, ¹J (¹³C-¹⁹F) = 244.4 Hz), 154.0 (d, quaternary C, C₁, ⁴J (¹³C-

^{19}F) = 3.1 Hz), 140.4 (quaternary $\underline{\text{C}}$, C_{11}), 129.4 (aromatic $\underline{\text{C}}\text{H}$, C_{14}), 128.0 (aromatic $\underline{\text{C}}\text{H}$, C_{13} and C_{15}), 126.9 (aromatic $\underline{\text{C}}\text{H}$, C_{12} and C_{16}), 126.1 (d, aniline $\underline{\text{C}}\text{H}$, C_2 or C_6 , $^3J(^{13}\text{C}-^{19}\text{F}) = 8.1$ Hz) 123.7 (aniline $\underline{\text{C}}\text{H}$, C_2 or C_6 , $^3J(^{13}\text{C}-^{19}\text{F}) = 8.1$ Hz), 116.1 (aromatic $\underline{\text{C}}\text{H}$, C_3 or C_5 , $^2J(^{13}\text{C}-^{19}\text{F}) = 22.4$ Hz), 115.5 (aromatic $\underline{\text{C}}\text{H}$, C_3 or C_5 , $^2J(^{13}\text{C}-^{19}\text{F}) = 22.4$ Hz), 94.9 (acnac $\underline{\text{C}}\text{H}$, C_9), 24.3 (acnac $\underline{\text{C}}\text{H}_3$, C_7). **IR** (cm^{-1}), 2036 (s, CO), 1964 (s, CO). **Analysis calculated:** C, 61.35, H, 3.94, N, 4.21 % **Analysis found:** C, 61.43, H, 3.81, N, 4.38 %. **ES MS (+)** m/z 6670.13 [M^+].

7.6.11 Synthesis of C11 ($\text{C}_{34}\text{H}_{26}\text{Cl}_2\text{N}_2\text{O}_4\text{Ru}$)

The crude product was purified using column chromatography (DCM/hexane, 1:1), to give complex **C11** as a green solid (600 mg, 0.86 mmol, 31 %). Single crystals suitable for X-ray diffraction were obtained through vapour diffusion of hexane into a saturated solution of the complex in dichloromethane.

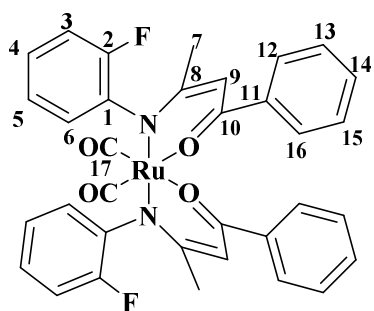


^1H NMR (CDCl_3 , 500.23 MHz, 299.9 K) δ , 7.86-7.81 (m, 2H, H_{12} and H_{16}), 7.41-7.35 (m, 3H, H_{13} , H_{14} and H_{15}), 7.30 (br. d, 2H, H_3 and H_5 , $^3J(^1\text{H}-^1\text{H}) = 8.6$ Hz), 7.25-7.21 (m, 1H, H_2 or H_6), 6.82-6.78 (m, 1H, H_2 or H_6), 5.68 (s, 1H, H_9), 1.91 (s, 3H, H_7) **$^{13}\text{C}\{^1\text{H}\}$ NMR** (CDCl_3 , 300 MHz, 299.9 K) δ 196.9 ($\underline{\text{C}}\text{O}$), 174.0 (quaternary $\underline{\text{C}}$, C_{10}), 167.1

(quaternary $\underline{\text{C}}$, C_8), 158.1 (quaternary $\underline{\text{C}}$, C_1), 140.3 (quaternary $\underline{\text{C}}$, C_{11}), 130.7 (quaternary $\underline{\text{C}}-\text{Cl}$, C_4), 129.5 (aniline $\underline{\text{C}}\text{H}$, C_3 or C_5), 129.4 (aniline $\underline{\text{C}}\text{H}$, C_3 or C_5), 129.0 (aromatic $\underline{\text{C}}\text{H}$, C_{14}), 128.0 (aromatic $\underline{\text{C}}\text{H}$, C_{13} and C_{15}), 127.0 (aromatic $\underline{\text{C}}\text{H}$, C_{12} and C_{16}), 126.2 (aniline $\underline{\text{C}}\text{H}$, C_2 or C_6), 123.8 (aniline $\underline{\text{C}}\text{H}$, C_2 or C_6), 95.5 (acnac $\underline{\text{C}}\text{H}$, C_9), 24.4 (acnac $\underline{\text{C}}\text{H}_3$, C_7). **IR** (cm^{-1}), 2041 (s, CO), 1971 (s, CO). **Analysis calculated:** C, 58.46, H, 3.75, N, 4.01 % **Analysis found:** C, 58.56, H, 3.81, N, 4.10 %. **ES MS (+)** m/z 699.09 [M^+].

7.6.12 Synthesis of C12 (C₃₄H₂₆F₂N₂O₄Ru)

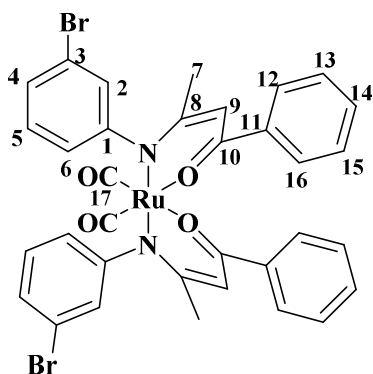
Complex **C12** was purified by column chromatography (DCM/hexane, 1:1) and further recrystallised from hot acetonitrile to give an orange solid (380 mg, 0.57 mmol, 29 %).



¹H NMR (CDCl₃, 500.23 MHz, 299.9 K) δ, 7.99-7.86 (m, 2H, H₁₂ and H₁₆), 7.49-7.34 (m, 4H, H₃, H₁₃, H₁₄ and H₁₅), 7.20-7.08 (m, 3H, H₄, H₅ and H₆), 5.68 (t, 1H, H₉), 1.91 (s, 3H, H₇). **¹³C{¹H} NMR** (CDCl₃, 300 MHz, 299.9 K) δ 196.2 (C=O), 174.6 (quaternary C, C₁₀), 168.1 (quaternary C, C₈), 155.5 (quaternary C-F, C₂, ¹J (¹³C-¹⁹F) = 245.7 Hz), 154.0 (quaternary C, C₁, ²J (¹³C-¹⁹F) = 12.4 Hz), 140.3 (quaternary C, C₁₁), 129.5 (aromatic CH, C₁₄), 128.0 (aromatic CH, C₁₃ and C₁₅), 127.3 (d, aniline CH C₄, ⁴J (¹³C-¹⁹F) = 6.8 Hz), 127.1 (aromatic CH, C₁₂ and C₁₆), 126.8 (d, aniline CH, C₆, ³J (¹³C-¹⁹F) = 7.5 Hz), 124.5 (d, aniline CH, C₅, ⁴J (¹³C-¹⁹F) = 3.7 Hz), 116.0 (aromatic CH, C₃, ²J (¹³C-¹⁹F) = 20.5 Hz), 94.9 (acnac CH, C₉), 24.3 (acnac CH₃, C₇). **IR** (cm⁻¹), 2047 (s, CO), 1972 (s, CO). **Analysis calculated:** C, 61.35, H, 3.94, N, 4.21 % **Analysis found:** C, 61.56, H, 4.05, N, 4.30 %. **ES MS (+)** *m/z* 667.10 [M⁺].

7.6.13 Synthesis of C13 (C₃₄H₂₆Br₂N₂O₄Ru)

The crude product was purified using column chromatography (DCM/hexane; 1:1) to give complex, **C13** as a yellow solid, which was further purified through recrystallisation with hot acetonitrile (680 mg, 0.86 mmol, 37 %).

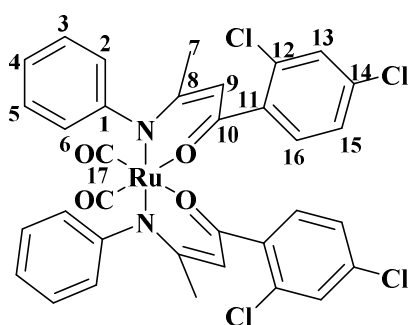


¹H NMR (CDCl₃, 500.23 MHz, 299.9 K) δ, 7.90-7.81 (m, 2H, H₁₂ and H₁₆), 7.41-7.35 (m, 3H, H₁₃, H₁₄ and H₁₅), 7.33-7.28 (m, 1H, H₂), 7.27-7.20 (m, 2H, H₄ and H₅), 6.85 (br. d, 1H, H₆, ³J (¹H-¹H) = 7.7 Hz), 5.72-5.67 (m, 1H, H₉), 1.93 (d, 3H, H₇). **¹³C{¹H} NMR** (CDCl₃, 300 MHz, 299.9 K) δ 196.8 (C=O), 175.1 (quaternary C, C₁₀), 167.1 (quaternary C, C₈), 158.6 (quaternary C, C₁), 140.3 (quaternary C, C₁₁), 130.7 (quaternary C-Br, C₃), 129.6 (aniline CH, C₅), 129.4 (aniline CH, C₃

or C₅), 128.5 (aromatic $\underline{\text{C}}\text{H}$, C₁₄), 128.1 (aromatic $\underline{\text{C}}\text{H}$, C₁₃ or C₁₅), 128.0 (aromatic $\underline{\text{C}}\text{H}$, C₁₃ or C₁₅), 127.1 (aromatic $\underline{\text{C}}\text{H}$, C₁₂ and C₁₆), 125.7 (aniline $\underline{\text{C}}\text{H}$, C₄), 122.6 (aniline $\underline{\text{C}}\text{H}$, C₂ or C₆), 121.4 (aniline $\underline{\text{C}}\text{H}$, C₂ or C₆), 96.1 (acnac $\underline{\text{C}}\text{H}$, C₉), 24.4 (acnac $\underline{\text{C}}\text{H}_3$, C₇). **IR** (cm^{-1}), 2045 (s, CO), 1973 (s, CO). **Analysis calculated:** C, 51.86, H, 3.33, N, 3.56 % **Analysis found:** C, 52.05, H, 3.41, N, 3.68 %. **ES MS (+)** m/z 788.94 [M^+]

7.6.14 Synthesis of C14 (C₃₄H₂₄Cl₄N₂O₄Ru)

Complex **C14** was purified by column chromatography (DCM/hexane, 3:2) and further recrystallised from hot acetonitrile to give a green solid (150 mg, 0.19 mmol, 21 %). Single crystals suitable for X-ray diffraction were obtained from vapour diffusion of hexane into a saturated solution of the complex in DCM, at room temperature.



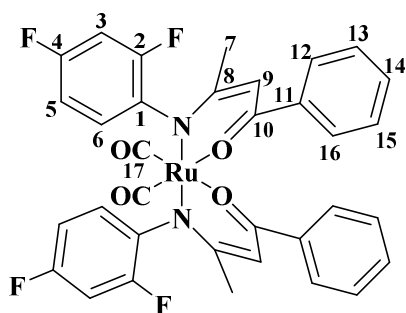
¹H NMR (CDCl₃, 500.23 MHz, 299.9 K) δ , 7.45-7.42 (m, 1H, H₁₆), 7.40 (s, 1H, H₁₃), 7.32 (d, 2H, H₂ or H₆ and H₁₅, ³J (¹H-¹H) = 7.6 Hz), 7.16 (d, 1H, H₂ or H₆, ³J (¹H-¹H) = 7.7 Hz), 7.20-7.20 (br. m. 2H, H₃ and H₅), 7.15 (br. t, 1H, H₄, ³J (¹H-¹H) = 7.2 Hz), 6.82 (d, 1H, H₂ or H₆, ³J (¹H-¹H) = 7.9 Hz), 5.20 (s, 1H, H₉), 1.78 (s, 3H, H₇). **¹³C{¹H}**

NMR (CDCl₃, 300 MHz, 299.9 K) δ 196.6 ($\underline{\text{C}}\text{O}$), 172.9 (quaternary $\underline{\text{C}}$, C₁₀), 167.0 (quaternary $\underline{\text{C}}$, C₈), 157.6 (quaternary $\underline{\text{C}}$, C₁), 139.8 (quaternary $\underline{\text{C}}$, C₁₁), 134.2 (quaternary $\underline{\text{C}}\text{-Cl}$, C₁₂ or C₁₄), 132.8 (quaternary $\underline{\text{C}}\text{-Cl}$, C₁₂ or C₁₄), 130.5 (aromatic $\underline{\text{C}}\text{H}$, C₁₅), 129.7 (aniline $\underline{\text{C}}\text{H}$, C₃ or C₅), 129.2 (aromatic $\underline{\text{C}}\text{H}$, C₁₆), 128.7 (aniline $\underline{\text{C}}\text{H}$, C₃ or C₅), 124.2 (aromatic $\underline{\text{C}}\text{H}$, C₁₃), 125.4 (aniline $\underline{\text{C}}\text{H}$, C₂ or C₆), 124.7 (aniline $\underline{\text{C}}\text{H}$, C₄), 121.9 (aniline $\underline{\text{C}}\text{H}$, C₂ or C₆), 99.2 (acnac $\underline{\text{C}}\text{H}$, C₉), 24.0 (acnac $\underline{\text{C}}\text{H}_3$, C₇). **IR** (cm^{-1}), 2045 (s, CO), 1978 (s, CO). **Analysis calculated:** C, 53.21, H, 3.51, N, 3.65 % **Analysis found:** C, 53.33, H, 3.42, N, 3.74 %.

7.6.15 Synthesis of C15 (C₃₄H₂₄F₄N₂O₄Ru)

The crude product was purified using column chromatography (DCM/hexane, 1:1), to give complex **C15** as a yellow solid (350 mg, 0.50 mmol, 30 %), which was further purified from hot acetonitrile. Complex **C15** crystallised as green plates from

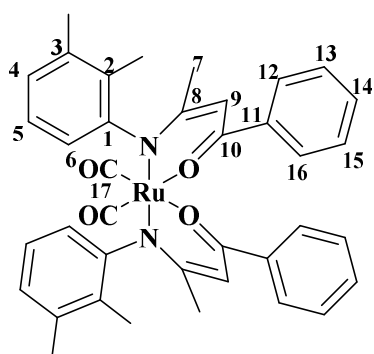
slow vapour diffusion of hexane into a concentrated solution of the complex in dichloromethane



^1H NMR (CDCl_3 , 500.23 MHz, 299.9 K) δ , 7.94-7.83 (m, 2H, H_{12} and H_{16}), 7.41-7.30 (m, 4H, H_6 , H_{13} , H_{14} and H_{15}), 6.92-6.82 (m, 2H, H_3 and H_5), 5.68 (s, 1H, H_9), 1.91 (s, 3H, H_7). **$^{13}\text{C}\{^1\text{H}\}$ NMR** (CDCl_3 , 300 MHz, 299.9 K) δ 196.0 ($\underline{\text{C}}\text{O}$), 175.0 (quaternary $\underline{\text{C}}$, C_{10}), 168.7 (quaternary $\underline{\text{C}}$, C_8), 161.7 (quaternary $\underline{\text{C}}\text{-F}$, C_2 or C_4 , $^1J(^{13}\text{C}\text{-}^{19}\text{F}) = 237.0$ Hz), 155.4 (quaternary $\underline{\text{C}}\text{-F}$, C_2 or C_4 , $^1J(^{13}\text{C}\text{-}^{19}\text{F}) = 247.5$ Hz) 140.9 (quaternary $\underline{\text{C}}$, C_1), 140.2 (quaternary $\underline{\text{C}}$, C_{11}), 129.7 (aromatic $\underline{\text{C}}\text{H}$, C_{14}), 128.1 (aromatic $\underline{\text{C}}\text{H}$, C_{13} and C_{15}), 127.0 (aromatic $\underline{\text{C}}\text{H}$, C_{12} and C_{16}), 111.7 (d, aniline $\underline{\text{C}}\text{H}$, C_6 , $^3J(^{13}\text{C}\text{-}^{19}\text{F}) = 21.8$ Hz), 104.6 (aromatic $\underline{\text{C}}\text{H}$, C_3 and C_5 , $^2J(^{13}\text{C}\text{-}^{19}\text{F}) = 50.4$ Hz), 95.8 (acnac $\underline{\text{C}}\text{H}$, C_9), 24.0 (acnac $\underline{\text{C}}\text{H}_3$, C_7). **IR** (cm^{-1}), 2047 (s, CO), 1971 (s, CO). **Analysis calculated:** C, 58.20, H, 3.45, N, 3.99 % **Analysis found:** C, 58.17, H, 3.47, N, 4.15 %.

7.6.16 Synthesis of C16 ($\text{C}_{38}\text{H}_{36}\text{N}_2\text{O}_4\text{Ru}$)

The crude product was purified using column chromatography (DCM/hexane, 3:2), to give complex **C16** as a yellow solid (530 mg, 0.77 mmol, 37 %). Single crystals suitable for X-ray diffraction were obtained through vapour diffusion of hexane into a saturated solution of the complex in dichloromethane.

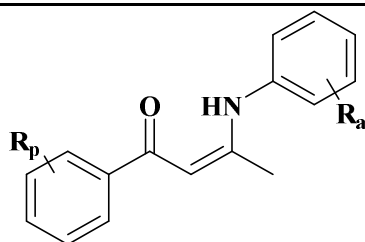


^1H NMR (CDCl_3 , 500.23 MHz, 299.9 K) δ , 7.92-7.86 (m, 2H, H_{12} and H_{16}), 7.41-7.35 (m, 3H, H_{13} , H_{14} and H_{15}), 7.26-7.16 (br. m, 1H, H_5), 7.15-7.11 (m, 1H, H_2), 6.96 (d, 1H, H_4 , $^3J(^1\text{H}\text{-}^1\text{H}) = 7.6$ Hz), 6.67 (d, 1H, H_6 , $^3J(^1\text{H}\text{-}^1\text{H}) = 7.4$ Hz), 5.67 (s, 1H, H_9), 2.33 (d, 3H, H_{18} , $^4J(^1\text{H}\text{-}^1\text{H}) = 4.9$ Hz), 1.93 (d, 3H, H_7 , $^4J(^1\text{H}\text{-}^1\text{H}) = 1.9$ Hz). **$^{13}\text{C}\{^1\text{H}\}$ NMR** (CDCl_3 , 300 MHz, 299.9 K) δ 197.6 ($\underline{\text{C}}\text{O}$), 173.3 (quaternary $\underline{\text{C}}$, C_{10}), 167.1 (quaternary $\underline{\text{C}}$, C_8), 155.9 (quaternary $\underline{\text{C}}$, C_1), 140.7 (quaternary $\underline{\text{C}}$, C_{11}), 138.1 (quaternary $\underline{\text{C}}$, C_2 or C_3), 137.4 (quaternary $\underline{\text{C}}$, C_2 or C_3), 129.4 (aniline $\underline{\text{C}}\text{H}$, C_5), 129.0 (aromatic $\underline{\text{C}}\text{H}$, C_{14}), 128.0 (aromatic $\underline{\text{C}}\text{H}$, C_{13} or C_{15}), 127.8 (aromatic $\underline{\text{C}}\text{H}$, C_{13} or C_{15}), 127.1 (aromatic $\underline{\text{C}}\text{H}$, C_{12} and C_{16}), 123.2 (aniline $\underline{\text{C}}\text{H}$, C_4), 121.1 (aniline $\underline{\text{C}}\text{H}$, C_6), 95.2 (acnac $\underline{\text{C}}\text{H}$, C_9), 23.9

(acnac $\underline{\text{C}}\text{H}_3$, C₇), 20.5 (aromatic $\underline{\text{C}}\text{H}_3$, C₁₈ or C₁₉), 14.4 (aromatic $\underline{\text{C}}\text{H}_3$, C₁₈ or C₁₉).
IR (cm⁻¹), 2036 (s, CO), 1961 (s, CO). **Analysis calculated:** C, 66.55 H, 5.29, N,
4.08 % **Analysis found:** C, 66.44, H, 5.39, N, 4.16 %. **ES MS (+)** *m/z* 687.18 [M⁺]

7.7 Synthesis of β -bis-ketoiminate copper(II) complexes

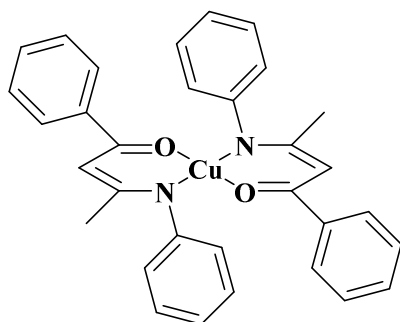
All copper complexes were synthesised at room temperature under nitrogen, using standard Schlenk techniques, on 200 mg of a copper salt, CuCl_2 , unless otherwise stated. The β -bis-ketoiminate ligand (2 eq.) and NaOMe (2 eq.) were dissolved in dry solvent (MeOH or EtOH) (20-40 mL) and stirred for 30 minutes. In a separate schlenk, the copper salt was dissolved in the same solvent as above (10-15 mL). The ligand solution was then slowly added to the metal solution, and stirred at room temperature for 20-24 hours. At the end of the reaction, the solid was filtered off and washed with cold ethanol, dried under vacuum, and recrystallised through slow vapour diffusion of hexane into a solution of the complex in dicholoromethane. All the investigative reactions described in **Chapter 3** were performed in the same way. All yields reported below refer to recrystallised products. All complexes reported are air stable.



$R_a = \text{H}, R_p = \text{H}$	L1	$R_p = \text{H}, R_a = .4'\text{Cl}$	L21
4'F	L2	4'F	L22
4'Cl	L3	4'Me	L23
4'Br	L4	3'Br	L24
3'F	L5	3'Me	L25
3'Br	L6	2'F	L26
4'I	L7	2',4' diCl	L27
4'Me	L8	2',4' diF	L28
2'Cl	L9	2',3' diMe	L29
2'Br	L10	2'Br	L30
4'OMe	L11	3'Cl	L31
4'CF ₃	L12	2',5' diF	L32
4'OEt	L13		
2'OMe	L14		
3',4' diCl	L15		
2',4',6' triMe	L16		
3',4' methylene	L17		
3'Br, 4'F	L18		

7.7.1 Synthesis of C17 (C₃₂H₂₈N₂O₂Cu)

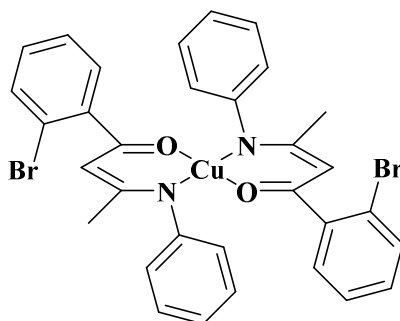
Complex **C17** was obtained from reaction with **L1** as a red solid. Dark crystals were obtained after recrystallisation. Yield: 152.6 mg, 0.28 mmol, 20 %.



Analysis calculated: C, 71.69, H, 5.26, N, 5.23 %, **Analysis found:** C, 71.75, H, 5.36, N, 5.26 %.
ES MS (+) *m/z* 537.13 [MH⁺].

7.7.2 Synthesis of C18 (C₃₂H₂₆N₂O₂Br₂Cu)

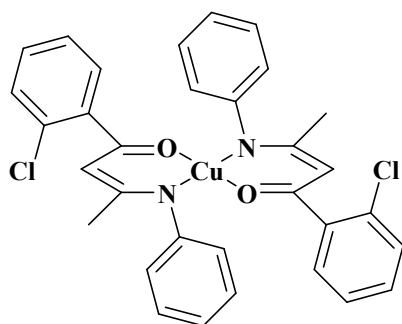
Obtained from reaction with **L10** as a brown solid, upon recrystallization dark brown crystals suitable for X ray crystallography were obtained. Yield: (319.6 mg, 0.46 mmol, 36 %).



Analysis calculated: C, 55.39, H, 3.78, N, 4.04 %
Analysis found: C, 54.60, H, 3.34, N, 4.52 %.

7.7.3 Synthesis of C19 (C₃₂H₂₆N₂O₂Cl₂Cu)

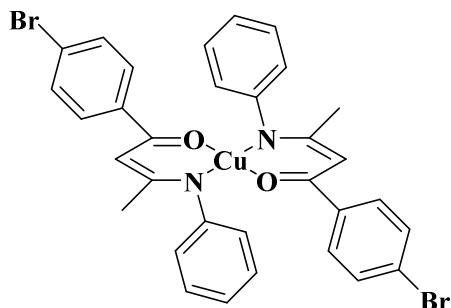
Red solid obtained from reaction with ligand **L9**. Yield: 364.7 mg, 0.60 mmol, 41 %.



Analysis calculated: C 63.53, H 4.33, N, 4.63 %, **Analysis found:** C, 63.64, H, 4.27, N, 4.75 %.
ES MS (+) *m/z* 606.12 [MH⁺].

7.7.4 Synthesis of C20 (C₃₂H₂₆N₂O₂Br₂Cu)

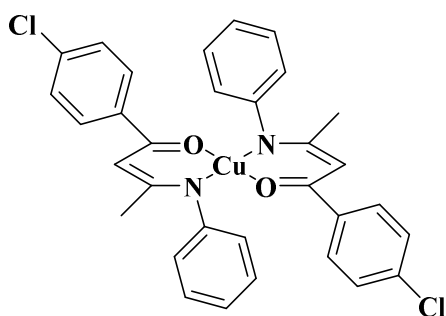
Obtained from reaction with **L4** as an olive green solid. Yield after recrystallization (300.0 mg, 0.43 mmol, 51%).



Analysis calculated: C, 55.39, H, 3.78, N, 4.04 %, **Analysis found:** C, 55.34, H, 3.88, N, 4.11 %; **ES MS (+)** *m/z* 691.97 [MH⁺]

7.7.5 Synthesis of C21 (C₃₂H₂₆N₂O₂Cl₂Cu)

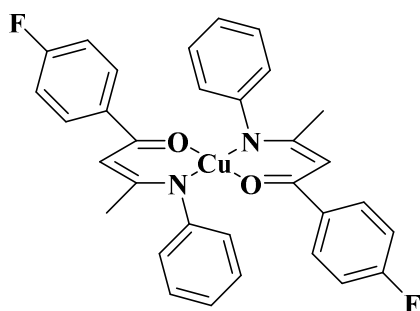
Obtained from reaction with ligand **L3** as a brick red solid. Recrystallisation yield: 428.0 mg, 0.71 mmol, 48 %.



Analysis calculated: C, 63.53, H, 4.58, N, 4.90 %, **Analysis found:** C, 63.42, H, 4.45, N, 4.66 %; **ES MS (+)** *m/z* 623.07 [MNa⁺].

7.7.6 Synthesis of C22 (C₃₂H₂₆N₂O₂F₂Cu)

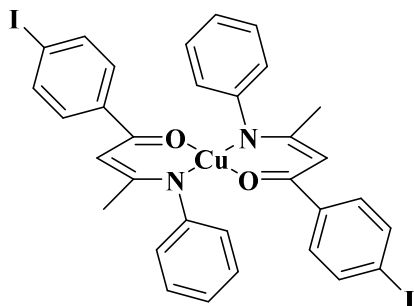
Obtained from reaction with **L2** as an olive green solid. Dark green crystals obtained after recrystallisation (250.0 mg, 0.44 mmol, 52 %).



Analysis calculated: C, 67.18 H, 4.58, N, 4.90 %, **Analysis Found:** C, 67.14, H, 4.66, N, 4.91 %; **ES MS (+)** *m/z* 572.13 [MH⁺].

7.7.7 Synthesis of C23 (C₃₂H₂₆N₂O₂I₂Cu)

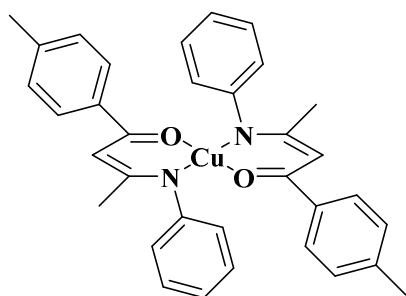
Red solid obtained from reaction with ligand L7. Dark crystals obtained from recrystallisation (637.0 mg, 0.81 mmol, 54 %).



Analysis calculated: C, 48.78, H, 3.38, N, 3.56 %, **Analysis found:** C, 48.83, H, 3.41, N, 3.65 %. **ES MS (+) *m/z*** 810.93 [MNa⁺].

7.7.8 Synthesis of C24 (C₃₄H₃₂N₂O₂Cu)

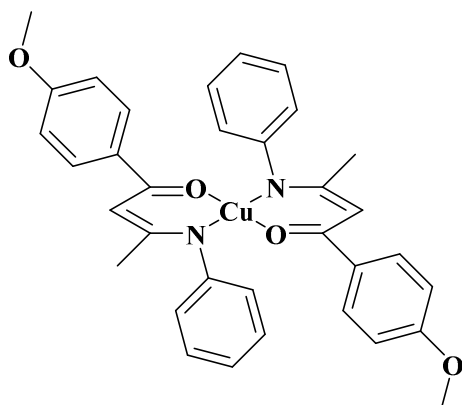
Obtained from reaction with ligand L8 as a brown solid. Yield: 262.0 mg, 0.47 mmol, 63%.



Analysis calculated: C, 72.38, H, 5.72, N, 4.97 %, **Analysis found:** C, 72.21, H, 5.81, N, 4.94 %. **ES MS (+) *m/z*** (565.19) [MH⁺].

7.7.9 Synthesis of C25 (C₃₄H₃₂N₂O₄Cu)

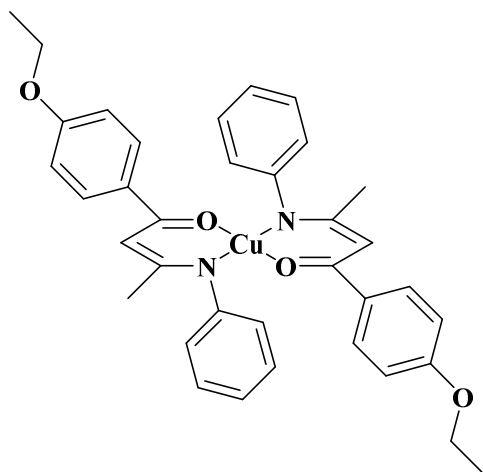
Obtained from reaction with L11 as a dark brown solid. Dark crystals suitable for X ray crystallography obtained at 40% yield (352.0 mg, 0.59 mmol).



Analysis calculated (+0.33 EtOH +0.33 pentane): C, 65.70, H, 5.46, N, 4.38 %, **Analysis found:** C, 65.85, H, 5.46, N, 4.92 %.

7.7.10 Synthesis of C26 (C₃₆H₃₆N₂O₄Cu)

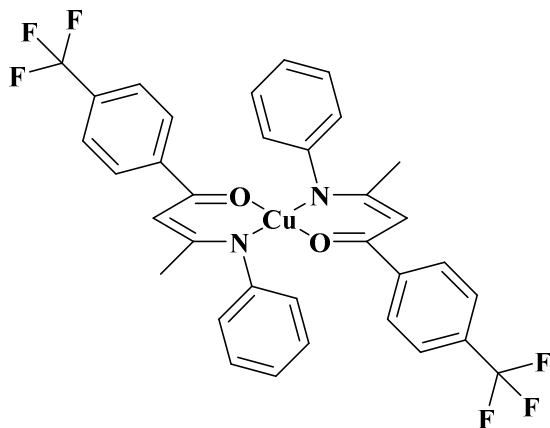
After recrystallisation, dark crystals suitable for X-ray crystallography were obtained as product from reaction with ligand **L13**. Yield: 634.2 mg, 1.02 mmol, 68 %.



Analysis calculated: C, 69.27, H, 5.81, N, 4.49 %, **Analysis found:** C, 69.58, H, 5.90, N, 4.87 %.

7.7.11 Synthesis of C27 (C₃₄H₂₆N₂O₂F₆Cu)

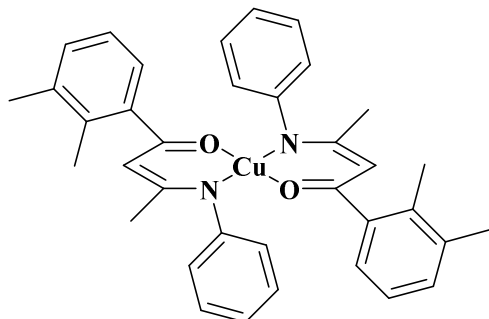
Gold crystalline solid obtained from reaction with ligand **L12**. Recrystallisation yield, 550.0 mg, 0.82 mmol, 72%.



Analysis calculated: C, 60.76, H, 3.90, N, 4.17 %, **Analysis found:** C, 60.85, H, 3.96, N, 4.23 %.

7.7.12 Synthesis of C28 (C₃₆H₃₆N₂O₂Cu)

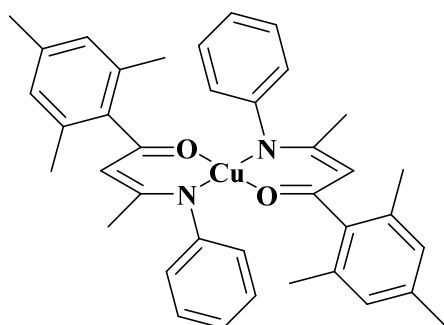
Dark crystals obtained from reaction with ligand **L29**. Yield: 387.5 mg, 0.65 mmol, 44 %.



Analysis calculated: C, 73.01, H, 6.13, N, 4.73 %, **Analysis found:** C, 73.23, H, 6.12, N 4.80 %.

7.7.13 Synthesis of C29 (C₃₈H₄₀N₂O₂Cu)

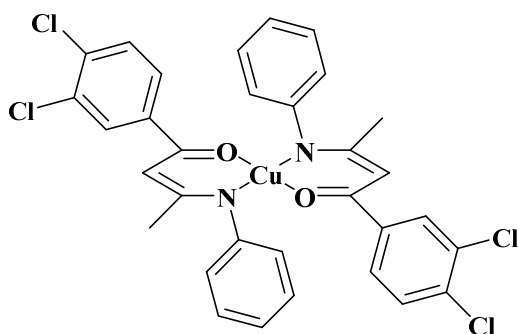
Obtained from reaction with **L16**, and gave dark crystals on recrystallization (263.3 mg, 0.43 mmol, 37%).



Analysis calculated: C, 73.58, H, 6.50, N, 4.52 %, **Analysis found:** C, 73.68, H, 6.60, N, 4.64 %. **ES MS (+) *m/z* 620.25 [MH⁺].**

7.7.14 Synthesis of C30 (C₃₂H₂₄N₂O₂Cl₄Cu)

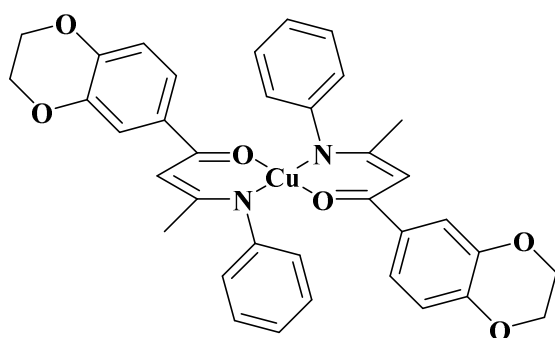
Obtained as a red solid from reaction with ligand **L15**. Yield: 244.1 mg, 0.36 mmol, 46 %.



Analysis calculated: C, 57.03, H, 3.59, N, 4.16 %, **Analysis found:** C, 56.95, H, 3.66, N, 4.25 %. **ES MS (+) *m/z* 674.90 [MH⁺].**

7.7.15 Synthesis of C31 (C₃₄H₃₂N₂O₆Cu)

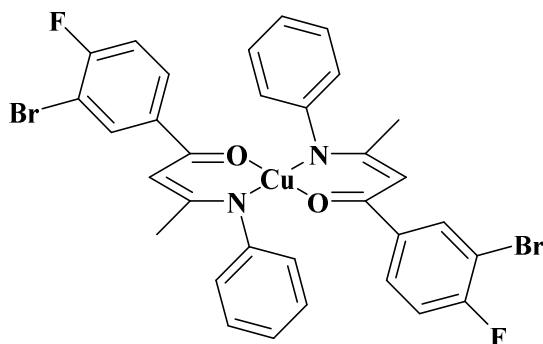
Gold crystalline solid obtained from reaction with **L17**. Recrystallisation yield: 157.4 mg, 0.25 mmol, 28 %.



Analysis calculated (+ EtOH): C, 64.52, H, 5.11, N, 4.18 % **Analysis found**: C, 64.81, H, 5.11, N, 4.18 %.
ES MS (+) *m/z* 624.12 [MH⁺].

7.7.16 Synthesis of C32 (C₃₂H₂₄N₂O₂F₂Br₂Cu)

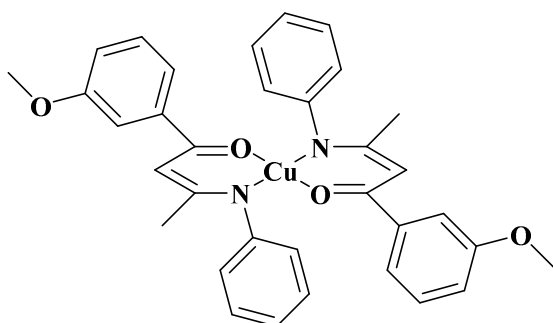
Red solid obtained from reaction with ligand **L18**. Yield: 345.0 mg, 0.47 mmol, 63 %.



Analysis calculated: C, 52.66, H, 3.31, N, 3.84 %, **Analysis found**: C, 52.77, H, 3.20, N, 3.91 %.

7.7.17 Synthesis of C33 (C₃₄H₃₂N₂O₄Cu)

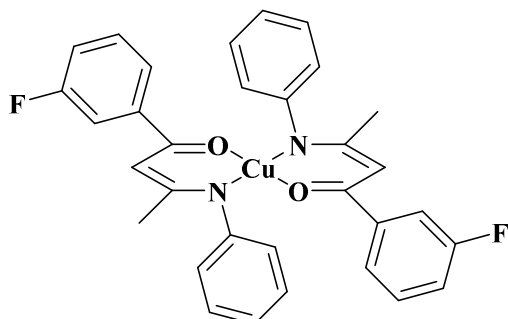
Brown solid obtained from reaction with **L14**. Yield (420.0 mg, 0.70 mmol, 47 %).



Analysis calculated (+1.5 DCM): C, 63.78, H, 4.87, N, 5.05 %, **Analysis found**: C, 63.00, H, 4.87, N, 5.05 %.

7.7.18 Synthesis of C34 (C₃₂H₂₆CuF₂N₂O₂)

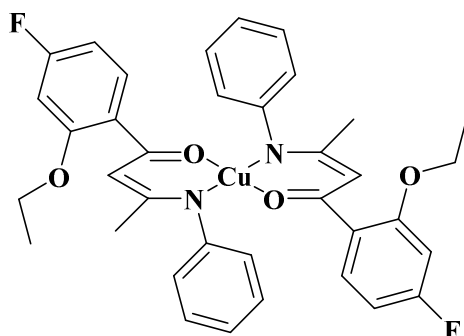
Brown solid obtained from reaction with ligand **L5**. Yield after recrystallisation (409.0 mg, 0.79 mmol, 53 %).



Analysis calculated (+0.5 EtOH): C, 66.79, H, 4.80, N, 4.77 %, **Analysis found:** C, 67.00, H, 4.49, N, 4.97 %.

7.7.19 Synthesis of C35 (C₃₆H₃₄N₂O₄F₂Cu)

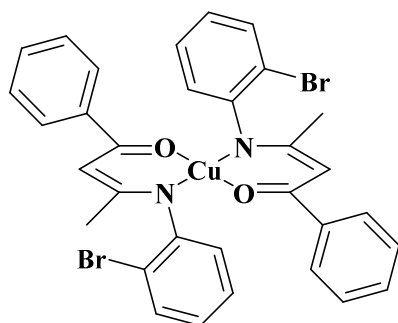
Dark crystals obtained from reaction with ligand **L33**. Yield (387.2 mg, 0.59 mmol, 40 %).



Analysis calculated (+0.5 CH₂Cl₂): C, 62.39, H, 5.02, N, 3.99 %, **Analysis found:** C, 62.16, H, 4.90, N, 4.04 %.

7.7.20 Synthesis of C36 (C₃₂H₂₆N₂O₂Br₂Cu)

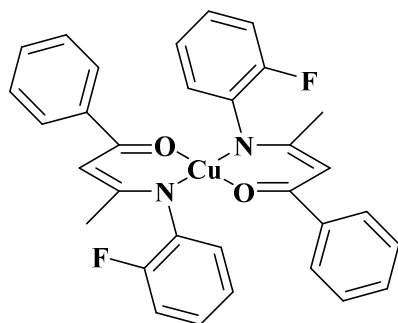
Obtained from reaction with ligand **L30** as a brown solid. Recrystallisation yield, (243.7 mg, 0.35 mmol, 31 %).



Analysis calculated: C, 55.39, H, 3.78, N, 4.04 %, **Analysis found:** C, 55.44, H, 3.86, N, 4.06 %. **ES MS (+) m/z** 691.97 [MH⁺].

7.7.21 Synthesis of C37 (C₃₂H₂₆N₂O₂F₂Cu)

Obtained from reaction with ligand **L26**, and gave dark brown crystals suitable for X ray crystallography. Yield: 441.9 mg, 0.77 mmol, 52 %.

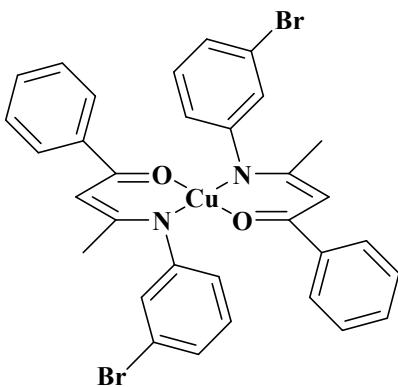


Analysis calculated: C, 67.18, H, 4.58, N, 4.90 %,

Analysis found: C, 67.28, H, 4.67, N, 4.93 %.

7.7.22 Synthesis of C38 (C₃₂H₂₆N₂O₂ Br₂Cu)

Obtained as a brick red solid from reaction with **L24**. Brown blocks obtained from recrystallisation at 401.7 mg, 0.58 mmol, 39 % yield.



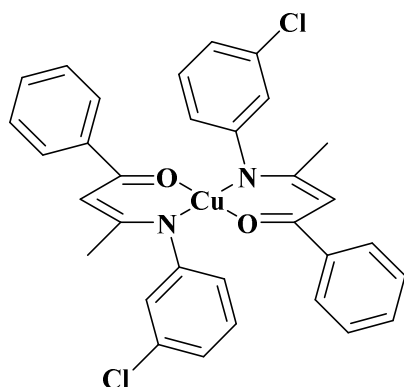
Analysis calculated: C, 55.39, H, 3.78, N, 4.04 %,

Analysis found: C, 55.33, H, 3.83, N, 4.05 %.

ES MS (+) m/z 694.93 [MH⁺].

7.7.23 Synthesis of C39 (C₃₂H₂₆N₂O₂Cl₂Cu)

Obtained from reaction with ligand **L31** as a red solid that gave dark brown crystalline solid on recrystallisation. Yield: 235.5 mg, 0.39 mmol, 26 %.



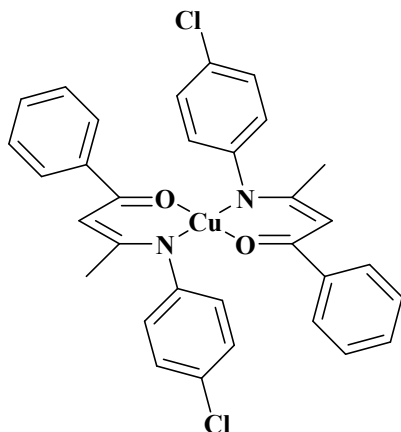
Analysis calculated: C, 63.53, H, 4.33, N, 4.63 %,

Analysis found: C, 63.52, H, 4.39, N, 4.73 %.

ES MS (+) m/z 606.02 [MH⁺].

7.7.24 Synthesis of C40 (C₃₂H₂₆N₂O₂Cl₂Cu)

Dark crystals obtained from brick red product after reaction with ligand **L21**. Yield: 115.5 mg, 0.19 mmol, 33 %.



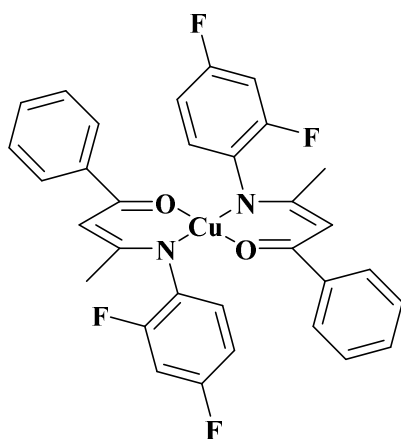
Analysis calculated: C, 63.53, H, 4.58, N, 4.90 %,

Analysis found: C, 63.53, H, 4.29, N, 4.75 %.

ES MS (+) *m/z* 604.07 [MH⁺].

7.7.25 Synthesis of C41 (C₃₂H₂₄N₂O₂F₄Cu)

Olive green solid obtained from reaction with ligand **L27**. Yield: 395.5 mg, 0.65 mmol, 50 %.

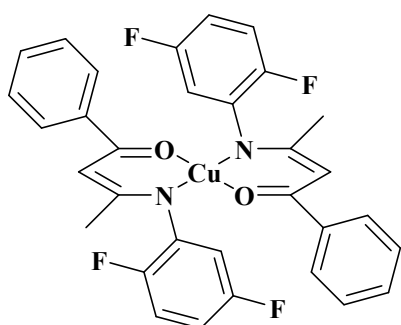


Analysis calculated: C, 63.21, H, 3.98, N, 4.61

%, **Analysis found:** C, 63.25, H, 4.10, N, 4.71 %.

7.7.26 Synthesis of C42 (C₃₂H₂₄N₂O₂F₄Cu)

From the reaction with ligand **L32**, complex **C42** was obtained as a red solid that gave dark crystals on purification. Yield: 233.6 mg, 0.38 mmol, 30 %.



Analysis calculated: C, 63.21, H, 3.98, N, 4.61%, **Analysis found:** C, 63.16, H, 3.99, N, 4.75 %. **ES MS (+) m/z 609.10 [MH⁺].**

7.8 Cytotoxicity Evaluation

7.8.1 General

Sterile techniques were used throughout this work. Unless otherwise stated, chemicals were purchased from Sigma Aldrich, consumables from Sarstedt and were used as supplied MIA PaCa-2 (human pancreatic carcinoma), HCT116 ++ (human colorectal carcinoma p53 upregulated) and ARPE-19 (human retinal epithelium – none cancerous) were the cell lines used. These were purchased from ATCC.

The stock cultures were grown in T-75 flasks containing DMEM and DMEM:F12 complete cell medium (15 mL) for the cancerous and non-cancerous cell lines respectively, and incubated at 37 °C with 5.0% of CO₂. The complete media was prepared from DMEM high glucose without L-glutamine Incomplete Media (450 mL), L-Glutamine 2 mM (5 mL, 200 mM) and foetal bovine serum 10% (50 mL). The complete media was prepared from DMEM:F12 (1:1) (450 mL), L-Glutamine 2 mM (5 mL, 200 mM) and foetal bovine serum 10% (50 mL). Phosphate Buffer Saline (PBS) buffer sterile solution was used to wash the cells, Trypsin-EDTA (1x) was used to detach the cells from the flask. DMEM (complete and incomplete), DMEM:F12 (complete and incomplete), MTT (Alfa Aesar) and MTT stock solutions (5 mg/mL), trypsin-EDTA (1x) were all stored at 4°C. L-Glutamine, foetal bovine serum and trypsin-EDTA stock solutions were stored at -20°C. All chemicals except the MTT solution were incubated in a water bath at 37°C prior to use.

After removing the media from the T-75 flasks, cells were washed with PBS buffer solution (1 x 5 mL) and carefully removed. Trypsin-EDTA (1 x 5 mL) was added and the T-75 flask incubated for 3 min. When the cells were detached from the flask wall, if needed for cell counting, 3 mL were taken and put in a falcon tube (50 mL) and 12 mL of media (different depending on the cell line) added to the falcon tube and 13 mL to the T-75 flask to allow cells to recover and be confluent.

Cells were detached using trypsin as above and centrifuged to 1000 r.p.m. for 3 minutes to form a cell pellet. Media was then carefully removed without disturbing

the pellet, and depending on cell pellet size re-suspended in 1-10 mL of fresh media added to make a homogenous cell suspension. From the suspension 10 μL were taken and carefully placed onto each side of the glass slide of a haemocytometer. Cells were then counted under the microscope in four squares of the haemocytometer and an average taken.

The MTT stock solution (5 mg/mL) was prepared by dissolving MTT (250 mg) in PBS sterile (50 mL), followed by vortexing before passing through a 0.2 μm sterile filter.

The cell suspension was diluted with RPMI-1640 complete media to give a concentration of 5×10^4 cells mL^{-1} . 100 μL of cell media was added to the first lane of the 96-well plate to act as a blank. 100 μL of diluted cell suspension were added to the other wells and the plate incubated at 37 $^{\circ}\text{C}$ for 4 hours. After 4h, the solution was carefully removed from each well and dissolved in 150 μL of DMSO. The plates were read by a Tecan plate reader set at 540 nm. Finally, the mean absorbance was calculated (differing the mean of the blank) for each line and plotted against the cell number, the R value was then calculated in order to quantify the accuracy of the user pipetting technique.

7.8.2 Conducting the 5-Day MTT Assay (Normoxia)

After cell counting, a suspension with a concentration of 2×10^4 cell/mL was prepared. A 96-well plate was used and 200 μL was added to lane 1 to serve as a blank. 200 μL of the diluted cell suspension was then added to lanes 2 to 12, and incubated for 24h at 37 $^{\circ}\text{C}$ in an atmosphere of 5.0% of CO_2 prior to drug exposure. The complexes were dissolved in DMSO and diluted further with media to obtain drug solution concentrations ranging from 100 μM to 0.046 μM . The final DMSO concentration was 0.2% (v/v) which is non-toxic to cells. The second lane was left as a blank. Drug solutions were then added to cells and incubated for 96 hours at 37 $^{\circ}\text{C}$ in an atmosphere of 5% CO_2 . Cell survival was determined using the MTT assay and MTT (20 μL of a 5 mg/mL stock) was added to each well and incubated for 4 hours at 37 $^{\circ}\text{C}$ in an atmosphere of 5.0% of CO_2 . The solutions were then removed and 150 μL of DMSO added to each well plate to dissolve the formazan crystals.

A Tecan plate reader was used to measure the absorbance at 540 nm. Lanes containing medium only and cell suspension (no drug) were used as blanks and 100% cell survival respectively. Cell survival was determined as the absorbance of treated cells divided by the true absorbance of controls and expressed as percentage. The IC₅₀ values were determined from choosing where 50% of cells survive against drug concentration. Each experiment was repeated a minimum of three times, to give the average of IC₅₀ and standard deviations.

7.8.3 Conducting the 5-Day MTT Assay (Hypoxia)

The hypoxic studies were carried out in a Hypoxic chamber (Whitley H35 hypoxystation) with 0.1% of O₂, 5.0% of CO₂, 94.9% of N₂ and 81% of humidity, on HCT116 ++ (human colon carcinoma p53 upregulated) cell lines. DMEM complete media was conditioned for at least 24 hours in the hypoxic chamber prior to start of the experiment in order to purge the oxygen from the media. The cells were seeded as for the 4-day cytotoxic assay above and after 24 hours they were moved to the hypoxic chamber where the cells were exposed to the lead compounds from concentrations starting at 50 µM to 0.048 µM. In this assay, it was seeded one compound per plate in order to decrease the potential cell infection. Cell survival was then determined using the MTT assay described for normoxic conditions.

7.9 Anti-bacterial Evaluation

All anti-bacterial studies were performed by The Community for Antimicrobial Drug Discovery (CO-ADD) at The University of Queensland, funded by The Wellcome Trust.

7.9.1 Anti-bacterial screening procedure

Complexes were prepared in DMSO and water to give a final concentration of 32 µg mL⁻¹ in 384-well non-binding surface (NBS) plate. The final DMSO concentration was at a maximum of 1 % DMSO. All bacteria were cultured in Cation-adjusted Mueller Hinton broth (CAMHB) at 37 °C overnight. A sample of each culture was diluted 40-fold in fresh broth and incubated at 37 °C for 1.5 - 3 hours. The resultant mid-log phase cultures were diluted (CFU mL⁻¹ measured by OD₆₀₀), then added to each well of the compound containing plates, giving a cell

density of 5×10^5 CFU mL⁻¹ and a total volume of 50 μ L. Colistin and vancomycin were used as positive bacterial inhibitor standards for Gram-negative and Gram-positive bacteria, respectively. The antibiotics were provided at four concentrations, with two above and two below the MIC value. All the plates were covered and incubated at 37 °C for 18 hours without shaking.

All experiments were carried out in duplicate. Inhibition of bacterial growth was determined measuring absorbance at 600 nm (OD₆₀₀), using a Tecan M1000 Pro monochromator plate reader. The percentage of growth inhibition was calculated for each well, using the negative control (media only) and positive control (bacteria without inhibitors) on the same plate as references. The significance of the inhibition values was determined by modified Z-scores, calculated using the median and MAD of the samples (no controls) on the same plate. Samples with inhibition value above 80 % and Z-Score above 2.5 for either replicate were classed as actives. Samples with inhibition values in the range 50 to 80 % and Z-Score above 2.5 for either replicate were classed as partial actives.

7.10 Anti-fungal Evaluation

All anti-fungal studies were performed by The Community for Antimicrobial Drug Discovery (CO-ADD) at The University of Queensland, funded by The Wellcome Trust.

7.10.1 Anti-fungal screening procedure

Complexes were prepared in DMSO and water to give a final concentration of 32 μ g mL⁻¹ in 384-well NBS plate. The final DMSO concentration was at a maximum of 1 % DMSO. Fungal strains were cultured for three days on yeast extract-peptone dextrose (YPD) agar at 30 °C. A yeast suspension of 1×10^6 to 5×10^6 CFU mL⁻¹ (as determined by OD₅₃₀) was prepared from five colonies. The suspension was diluted and added to each well of the compound-containing plates giving a final cell density of fungi suspension of 2.5×10^3 CFU mL⁻¹ and a total volume of 50 μ L. Fluconazole was used as a positive fungal inhibitor standard. All the plates were covered and incubated at 35 °C for 24 hours without shaking.

All experiments were carried out in duplicate. Growth inhibition of *C. albicans* was determined measuring absorbance at 530 nm (OD_{530}) and the growth inhibition of *C. neoformans* was determined measuring the difference in absorbance between 600 and 570 nm ($OD_{600-570}$), after the addition of 0.001 % resazurin and incubation at 35 °C for an additional 2 hours. The absorbance was measured using a Biotek Synergy HTX plate reader. The percentage of growth inhibition was calculated for each well, using the negative control (media only) and positive control (fungi without inhibitors) on the same plate. The significance of the inhibition values was determined by modified Z-scores, calculated using the median and MAD of the samples (no controls) on the same plate. Samples with inhibition value above 80 % and Z-Score above 2.5 for either replicate were classed as actives. Samples with inhibition values in the range 50 to 80 % and Z-Score above 2.5 for either replicate were classed as partial actives.

7.11 Hydrolysis

Hydrolysis samples of complexes for investigation by NMR spectroscopy were prepared from a 4:1 mixture of d_3 -acetonitrile/deuterium oxide to give a final concentration of 8 mg mL⁻¹. The NMR spectra of these samples were acquired every 24 hours over a five day period. Hydrolysis samples of complexes for investigation by UV/vis spectroscopy were prepared from a 4:1 mixture of acetonitrile/water to give a final concentration of 50 μM. The UV/vis spectra of these samples were acquired every 24 hours over a five day period. After the five day period investigation period, the mass spectra of the hydrolysis samples were acquired.

7.12 Biomembrane studies

The biomembrane studies were performed by Miss. Danielle Marriott and Dr. Shahrzad Mohamadi (University of Leeds).

The micro fabricated electrode coated with DOPC lipid was contained in a closed flow cell. A constant flow of phosphate-buffered saline (PBS) (pH 7.4) was passed over the electrode using a peristaltic pump at a flow rate of 5 - 10 mL min⁻¹. A constant flow of DOPC dispersion in PBS was deposited on the electrode with the application of a potential excursion from -0.4 to -3.0 V at a scan rate of 100 Vs⁻¹. The electrode in the flow cell was connected to the PGSTAT12 potentiostat

interfaced to a Powerlab signal generator and controlled by Scope software. A flow of argon gas is maintained over the electrolytes and the DOPC layer throughout. RCVs were obtained by applying a saw-tooth waveform from -0.4 to -1.2 V (vs Ag/AgCl) with ramp rate 40 V s^{-1} applied to the electrode surface. In the absence of faradaic reactions, the current on the RCV plot was directly proportional to the capacitance of the surface and is displayed as a function of voltage. All assays were carried out with $15.6 \mu\text{M}$ solutions of each complex in acetone with a constant flow of 0.1 M PBS. The complexes are sampled for 400 seconds followed by PBS for 400 seconds to allow *in situ* cleaning of the electrode.^{15, 16}

7.13 Catalysis

Cleaning procedure for catalysis tubes: Carousel glass tubes used for catalytic reactions were cleaned thoroughly after use. They were initially scrubbed with soapy water, followed by a three-time rinse with acetone, and a soak in a base bath for 10-15 hours (KOH approx. 1 M in water/isopropanol). Following the base bath, the tubes were rinsed multiple times with water and placed in an acid bath for 4-7 hours (HCl 37% approx. 1 L per 8-10 L of water). Finally, the tubes were rinsed thoroughly with water and then with acetone, before being placed to dry in the oven. The same process was followed for the stirrer bars.

7.14 References

1. R. Levine and J. K. Sneed, *Journal of the American Chemical Society*, 1951, **73**, 5614-5616.
2. L.-M. Tang, Y.-Q. Duan, X.-F. Li and Y.-S. Li, *Journal of Organometallic Chemistry*, 2006, **691**, 2023.
3. J. Cosier and A. M. Glazer, *Journal of Applied Crystallography*, 1986, **19**, 105-107.
4. CrysAlisPRO, ed. Oxford Diffraction /Agilent Technologies UK Ltd, Editon edn.
5. G. M. Sheldrick, *Crystallographic Computing 3: Data Collection, Structure Determination, Proteins, and Databases*, Clarendon Press Oxford, 1986.
6. G. M. Sheldrick, SHELXTL Editon edn., 2014.
7. G. M. Sheldrick, *Acta Crystallographica a-Foundation and Advances*, 2015, **71**, 3-8.
8. G. M. Sheldrick, *Acta Crystallographica Section A*, 2008, **64**, 112-122.
9. O. V. Dolomanov, L. J. Bourhis, R. J. Gildea, J. A. K. Howard and H. Puschmann, *Journal of Applied Crystallography*, 2009, **42**, 339-341.
10. A. L. Spek, *Journal of Applied Crystallography*, 2003, **36**, 7-13.
11. J. J. Hollick, B. T. Golding, I. R. Hardcastle, N. Martin, C. Richardson, L. J. M. Rigoreau, G. C. M. Smith and R. J. Griffin, *Bioorganic & Medicinal Chemistry Letters*, 2003, **13**, 3083-3086.
12. R. Levine and J. K. Sneed, *Journal of the American Chemical Society*, 1951, **73**, 5614-5616.
13. R. M. Lord, University of Leeds, 2014.
14. L. M. Tang, Y. Q. Duan, X. F. Li and Y. S. Li, *Journal of Organometallic Chemistry*, 2006, **691**, 2023-2030.

15. Z. Coldrick, P. Steenson, P. Millner, M. Davies and A. Nelson, *Electrochimica Acta*, 2009, **54**, 4954-4962.
16. S. Mohamadi, D. J. Tate, A. Vakurov and A. Nelson, *Analytica Chimica Acta*, 2014, **813**, 83-89.

Appendix

Crystallographic data

Identification code	C1	C2
Empirical formula	C ₃₄ H ₂₈ N ₂ O ₄ Ru	C ₃₅ H ₂₈ Br ₂ Cl ₂ N ₂ O ₄ Ru
Formula weight	629.65	872.38
Temperature/K	120.02(11)	120.01(14)
Crystal system	monoclinic	triclinic
Space group	C2/c	P-1
a/Å	28.1978(15)	10.0294(4)
b/Å	12.4204(4)	11.7480(4)
c/Å	20.7143(11)	17.1687(6)
α/°	90	103.021(3)
β/°	126.304(8)	96.172(3)
γ/°	90	115.014(4)
Volume/Å³	5846.5(7)	1738.29(12)
Z	8	2
ρ_{calc}/cm³	1.431	1.667
μ/mm⁻¹	0.577	2.944
F(000)	2576.0	864.0
Crystal size/mm³	0.16 × 0.12 × 0.09	0.14 × 0.09 × 0.06
Radiation	MoKα (λ = 0.71073)	MoKα (λ = 0.71073)
2Θ range for data collection/°	6.3 to 62.598	4.012 to 62.6
Index ranges	-39 ≤ h ≤ 39, -17 ≤ k ≤ 16, -30 ≤ l ≤ 29	-14 ≤ h ≤ 13, -16 ≤ k ≤ 16, -18 ≤ l ≤ 23
Reflections collected	26638	22298
Independent reflections	8527 [R _{int} = 0.0548, R _{sigma} = 0.0673]	9827 [R _{int} = 0.0444, R _{sigma} = 0.0815]
Data/restraints/parameters	8527/0/372	9827/18/426
Goodness-of-fit on F²	1.023	1.067
Final R indexes [I ≥ 2σ (I)]	R ₁ = 0.0454, wR ₂ = 0.0826	R ₁ = 0.0630, wR ₂ = 0.1377
Final R indexes [all data]	R ₁ = 0.0658, wR ₂ = 0.0903	R ₁ = 0.0942, wR ₂ = 0.1519
Largest diff. peak/hole / e Å⁻³	0.49/-0.73	1.85/-1.36

Identification code	C3	C4
Empirical formula	C ₃₇ H ₃₄ Cl ₂ N ₂ O _{4.5} Ru	C ₃₄ H ₂₆ F ₂ N ₂ O ₄ Ru
Formula weight	750.63	665.64
Temperature/K	293(2)	120.01(13)
Crystal system	triclinic	triclinic
Space group	P-1	P-1
a/Å	11.9078(3)	11.5868(3)
b/Å	16.1911(3)	15.8561(4)
c/Å	19.3368(4)	18.7876(4)
α/°	104.6926(19)	100.9224(19)
β/°	105.485(2)	104.341(2)
γ/°	94.5396(18)	96.7474(19)
Volume/Å³	3431.92(14)	3234.11(13)
Z	4	4
ρ_{calc}/cm³	1.453	1.367
μ/mm⁻¹	0.656	0.534
F(000)	1536.0	1352.0
Crystal size/mm³	0.19 × 0.14 × 0.05	0.34 × 0.19 × 0.14
Radiation	MoKα (λ = 0.71073)	MoKα (λ = 0.71073)
2Θ range for data collection/°	5.9 to 56.566	6.186 to 52.742
Index ranges	-15 ≤ h ≤ 15, -21 ≤ k ≤ 21, -25 ≤ l ≤ 25	-14 ≤ h ≤ 14, -19 ≤ k ≤ 19, -23 ≤ l ≤ 22
Reflections collected	54792	39470
Independent reflections	17018 [R _{int} = 0.0509, R _{sigma} = 0.0570]	13218 [R _{int} = 0.0654, R _{sigma} = 0.0666]
Data/restraints/parameters	17018/0/775	13218/0/788
Goodness-of-fit on F²	1.054	1.053
Final R indexes [I ≥ 2σ (I)]	R ₁ = 0.0804, wR ₂ = 0.2395	R ₁ = 0.0782, wR ₂ = 0.2271
Final R indexes [all data]	R ₁ = 0.1018, wR ₂ = 0.2585	R ₁ = 0.0890, wR ₂ = 0.2395
Largest diff. peak/hole / e Å⁻³	5.94/-0.63	6.03/-1.13

Identification code	C5	C6
Empirical formula	C ₃₄ H ₂₆ F ₂ N ₂ O ₄ Ru	C ₃₄ H ₂₆ Br ₂ N ₂ O ₄ Ru
Formula weight	665.64	787.46
Temperature/K	120.00(10)	120.00(10)
Crystal system	triclinic	triclinic
Space group	P-1	P-1
a/Å	10.6629(6)	11.1240(4)
b/Å	11.4624(4)	11.6007(4)
c/Å	12.7982(7)	12.6400(5)
α/°	79.262(4)	79.330(3)
β/°	71.771(5)	74.574(3)
γ/°	82.312(4)	82.230(3)
Volume/Å³	1454.92(14)	1538.83(10)
Z	2	2
ρ_{calc}/cm³	1.519	1.699
μ/mm⁻¹	0.594	3.147
F(000)	676.0	780.0
Crystal size/mm³	0.24 × 0.15 × 0.12	0.19 × 0.16 × 0.08
Radiation	MoKα (λ = 0.71073)	MoKα (λ = 0.71073)
2Θ range for data collection/°	6.784 to 62.592	6.228 to 62.716
Index ranges	-15 ≤ h ≤ 14, -16 ≤ k ≤ 16, -17 ≤ l ≤ 13	-15 ≤ h ≤ 12, -16 ≤ k ≤ 15, -18 ≤ l ≤ 18
Reflections collected	17327	19384
Independent reflections	8224 [R _{int} = 0.0567, R _{sigma} = 0.0953]	8794 [R _{int} = 0.0384, R _{sigma} = 0.0615]
Data/restraints/parameters	8224/0/390	8794/0/390
Goodness-of-fit on F²	1.046	1.054
Final R indexes [I ≥ 2σ (I)]	R ₁ = 0.0548, wR ₂ = 0.1041	R ₁ = 0.0533, wR ₂ = 0.1305
Final R indexes [all data]	R ₁ = 0.0775, wR ₂ = 0.1207	R ₁ = 0.0699, wR ₂ = 0.1405
Largest diff. peak/hole / e Å⁻³	1.48/-1.34	1.26/-2.20

Identification code	C8	C9
Empirical formula	C ₁₆ H ₁₄ NOFIRu _{0.11}	C ₃₆ H ₃₂ N ₂ O ₄ Ru
Formula weight	292.73	657.70
Temperature/K	250.01(10)	120.01(16)
Crystal system	monoclinic	orthorhombic
Space group	I2/a	Pbcn
a/Å	11.9366(4)	23.6150(7)
b/Å	14.5646(4)	12.7987(4)
c/Å	19.2008(6)	20.7365(7)
α/°	90	90
β/°	104.682(3)	90
γ/°	90	90
Volume/Å³	3229.10(17)	6267.4(3)
Z	9	8
ρ_{calc}/cm³	1.3547	1.394
μ/mm⁻¹	0.526	0.542
F(000)	1351.2	2704.0
Crystal size/mm³	0.13 × 0.15 × 0.06	0.21 × 0.14 × 0.11
Radiation	Mo Kα (λ = 0.71073)	MoKα (λ = 0.71073)
2Θ range for data collection/°	3.56 to 62.62	6.076 to 59.14
Index ranges	-15 ≤ h ≤ 17, -21 ≤ k ≤ 19, -26 ≤ l ≤ 27	-32 ≤ h ≤ 32, -17 ≤ k ≤ 17, -28 ≤ l ≤ 27
Reflections collected	23143	41312
Independent reflections	4877 [R _{int} = 0.0440, R _{sigma} = 0.0400]	7753 [R _{int} = 0.0482, R _{sigma} = 0.0412]
Data/restraints/parameters	4877/12/250	7753/126/444
Goodness-of-fit on F²	1.050	1.088
Final R indexes [I ≥ 2σ (I)]	R ₁ = 0.0406, wR ₂ = 0.0796	R ₁ = 0.0404, wR ₂ = 0.0738
Final R indexes [all data]	R ₁ = 0.0604, wR ₂ = 0.0906	R ₁ = 0.0735, wR ₂ = 0.0878
Largest diff. peak/hole / e Å⁻³	0.50/-0.76	1.04/-0.62

Identification code	C11	C12
Empirical formula	C _{34.75} H _{27.5} Cl _{3.5} N ₂ O ₄ Ru	C ₃₄ H ₂₆ N ₂ O ₄ F ₂ Ru
Formula weight	762.23	665.64
Temperature/K	120.00(10)	119.99(13)
Crystal system	monoclinic	monoclinic
Space group	P2 ₁ /c	P2 ₁ /c
a/Å	16.2848(5)	10.6592(9)
b/Å	11.5529(3)	23.780(2)
c/Å	19.2890(5)	11.8118(12)
α/°	90	90
β/°	109.019(3)	95.473(9)
γ/°	90	90
Volume/Å ³	3430.86(18)	2980.4(5)
Z	4	4
ρ _{calc} /cm ³	1.476	1.483
μ/mm ⁻¹	0.769	0.580
F(000)	1542.0	1352.0
Crystal size/mm ³	0.33 × 0.21 × 0.11	0.26 × 0.18 × 0.12
Radiation	MoKα (λ = 0.71073)	MoKα (λ = 0.71073)
2Θ range for data collection/°	4.174 to 62.588	3.864 to 59.232
Index ranges	-21 ≤ h ≤ 19, -16 ≤ k ≤ 16, -26 ≤ l ≤ 25	-11 ≤ h ≤ 14, -30 ≤ k ≤ 32, -16 ≤ l ≤ 14
Reflections collected	29853	22748
Independent reflections	9916 [R _{int} = 0.0416, R _{sigma} = 0.0550]	7264 [R _{int} = 0.0540, R _{sigma} = 0.0720]
Data/restraints/parameters	9916/22/435	7264/132/462
Goodness-of-fit on F ²	1.055	1.056
Final R indexes [I ≥ 2σ (I)]	R ₁ = 0.0484, wR ₂ = 0.1097	R ₁ = 0.0483, wR ₂ = 0.0716
Final R indexes [all data]	R ₁ = 0.0651, wR ₂ = 0.1207	R ₁ = 0.0788, wR ₂ = 0.0836
Largest diff. peak/hole / e Å ⁻³	1.19/-0.81	0.98/-0.53

Identification code	C14	C15
Empirical formula	C ₃₄ H ₂₄ F ₄ N ₂ O ₄ Ru	C ₃₄ H ₂₄ F ₄ N ₂ O ₄ Ru
Formula weight	701.62	701.62
Temperature/K	120.2(5)	120.2(5)
Crystal system	monoclinic	monoclinic
Space group	I2/a	I2/a
a/Å	20.2349(4)	20.2349(4)
b/Å	9.7851(2)	9.7851(2)
c/Å	31.1016(6)	31.1016(6)
α/°	90	90
β/°	96.5615(18)	96.5615(18)
γ/°	90	90
Volume/Å³	6117.8(2)	6117.8(2)
Z	8	8
ρ_{calc}/cm³	1.524	1.524
μ/mm⁻¹	0.578	0.578
F(000)	2832.0	2832.0
Crystal size/mm³	0.27 × 0.21 × 0.19	0.27 × 0.21 × 0.19
Radiation	MoKα (λ = 0.71073)	MoKα (λ = 0.71073)
2Θ range for data collection/°	6.274 to 59.214	6.274 to 59.214
Index ranges	-28 ≤ h ≤ 27, -13 ≤ k ≤ 13, -42 ≤ l ≤ 39	-28 ≤ h ≤ 27, -13 ≤ k ≤ 13, -42 ≤ l ≤ 39
Reflections collected	53396	53396
Independent reflections	7948 [R _{int} = 0.0349, R _{sigma} = 0.0238]	7948 [R _{int} = 0.0349, R _{sigma} = 0.0238]
Data/restraints/parameters	7948/2/426	7948/2/426
Goodness-of-fit on F²	1.061	1.061
Final R indexes [I ≥ 2σ (I)]	R ₁ = 0.0292, wR ₂ = 0.0636	R ₁ = 0.0292, wR ₂ = 0.0636
Final R indexes [all data]	R ₁ = 0.0365, wR ₂ = 0.0670	R ₁ = 0.0365, wR ₂ = 0.0670
Largest diff. peak/hole / e Å⁻³	0.42/-0.37	0.42/-0.37

Complex	C17	C18
Empirical formula	C ₃₂ H ₂₈ N ₂ O ₂ Cu	C ₃₂ H ₂₆ N ₂ O ₂ CuBr ₂
Formula weight	536.10	693.91
Temperature/K	120.00(11)	120.01(11)
Crystal system	orthorhombic	triclinic
Space group	P2 ₁ 2 ₁ 2 ₁	P-1
a / Å	9.3387(4)	7.9066(3)
b / Å	9.8103(5)	12.0483(6)
c / Å	27.8867(13)	15.8939(6)
α / °	90	102.562(4)
β / °	90	98.748(3)
γ / °	90	105.207(4)
Volume / Å³	2554.8(2)	1390.48(11)
Z	4	2
ρ_{calc} g / cm³	1.394	1.657
μ / mm⁻¹	0.888	3.692
F(000)	1116.0	694.0
Crystal size / mm³	0.32 × 0.21 × 0.09	0.4 × 0.3 × 0.24
Radiation	MoKα (λ = 0.71073)	MoKα (λ = 0.71073)
2θ range for data collection/°	5.844 to 59.448	5.476 to 59.666
Index ranges	-12 ≤ h ≤ 10 -13 ≤ k ≤ 10 -38 ≤ l ≤ 28	-10 ≤ h ≤ 10 -16 ≤ k ≤ 16 -21 ≤ l ≤ 21
Reflections collected	12227	15816
Independent reflections	5879 [R _{int} = 0.0650, R _{sigma} = 0.1173]	6714 [R _{int} = 0.0444, R _{sigma} = 0.0653]
Data/restraints/parameters	5879/0/336	6714/0/357
Goodness of fit on F²	1.057	0.670
Final R indexes [I ≥ 2σ (I)]	R ₁ = 0.0592, wR ₂ = 0.0900	R ₁ = 0.0401, wR ₂ = 0.0879
Final R indexes [all data]	R ₁ = 0.1053, wR ₂ = 0.1074	R ₁ = 0.0574, wR ₂ = 0.1047
Largest diff. / e Å⁻³	0.40/-0.47	0.60/-0.66

Complex	C19	C20
Empirical formula	C ₃₂ H ₂₆ N ₂ O ₂ Cl ₂ Cu	C ₃₂ H ₂₆ N ₂ O ₂ CuBr ₂
Formula weight	604.99	693.91
Temperature/K	120.00(10)	120.0(2)
Crystal system	monoclinic	orthorhombic
Space group	I2/a	P2 ₁ 2 ₁ 2 ₁
a / Å	12.3890(4)	9.7122(6)
b / Å	13.7094(4)	9.8565(4)
c / Å	16.7856(5)	28.6096(17)
α / °	90	90
β / °	108.096(3)	90
γ / °	90	90
Volume / Å³	2709.97(15)	2738.8(3)
Z	4	4
ρ_{calc} g / cm³	1.483	1.683
μ / mm⁻¹	1.037	3.749
F(000)	1244.0	1388.0
Crystal size / mm³	0.3 × 0.22 × 0.21	0.13 × 0.11 × 0.07
Radiation	MoKα (λ = 0.71073)	MoKα (λ = 0.71073)
2θ range for data collection/°	5.944 to 59.356	6.542 to 59.414
Index ranges	-15 ≤ h ≤ 16, -18 ≤ k ≤ 14, -23 ≤ l ≤ 19	-7 ≤ h ≤ 12, -11 ≤ k ≤ 13, -39 ≤ l ≤ 32
Reflections collected	7088	13396
Independent reflections	3239 [R _{int} = 0.0460, R _{sigma} = 0.0649]	6441 [R _{int} = 0.0397, R _{sigma} = 0.0687]
Data/restraints/parameters	3239/0/178	6441/0/354
Goodness of fit on F²	0.819	1.028
Final R indexes [I ≥ 2σ (I)]	R ₁ = 0.0804, wR ₂ = 0.2055	R ₁ = 0.0407, wR ₂ = 0.0642
Final R indexes [all data]	R ₁ = 0.1016, wR ₂ = 0.2346	R ₁ = 0.0569, wR ₂ = 0.0686
Largest diff. / e Å⁻³	1.86/-1.16	0.48/-0.41

Complex	C21	C22
Empirical formula	C ₃₂ H ₂₆ Cl ₂ CuN ₂ O ₂	C ₃₂ H ₂₆ CuF ₂ N ₂ O ₂
Formula weight	604.99	572.09
Temperature/K	120.01(18)	281(3)
Crystal system	monoclinic	monoclinic
Space group	I2/a	P2 ₁ /n
a / Å	11.9816(8)	11.8091(4)
b / Å	13.1682(10)	7.4235(2)
c / Å	17.2486(13)	15.7723(5)
α / °	90	90
β / °	96.162(7)	101.660(3)
γ / °	90	90
Volume / Å³	2705.7(3)	1354.16(8)
Z	4	2
ρ_{calc} g / cm³	1.485	1.403
μ / mm⁻¹	1.038	1.523
F(000)	1244.0	590.0
Crystal size / mm³	0.31 × 0.23 × 0.06	0.2 × 0.18 × 0.12
Radiation	MoKα (λ = 0.71073)	CuKα (λ = 1.54184)
2θ range for data collection/°	6.352 to 59.688	11.458 to 133.118
Index ranges	-13 ≤ h ≤ 16, -18 ≤ k ≤ 18, -23 ≤ l ≤ 22	-14 ≤ h ≤ 13 -7 ≤ k ≤ 8 -18 ≤ l ≤ 18
Reflections collected	14706	4610
Independent reflections	3472 [R _{int} = 0.0524, R _{sigma} = 0.0511]	2378 [R _{int} = 0.0135, R _{sigma} = 0.0164]
Data/restraints/parameters	3472/0/178	2378/0/179
Goodness of fit on F²	1.084	1.076
Final R indexes [I ≥ 2σ (I)]	R ₁ = 0.0370, wR ₂ = 0.0682	R ₁ = 0.0326, wR ₂ = 0.0906
Final R indexes [all data]	R ₁ = 0.0521, wR ₂ = 0.0746	R ₁ = 0.0348, wR ₂ = 0.0926
Largest diff. / e Å⁻³	0.37/-0.38	0.24/-0.40

Complex	C23	C24
Empirical formula	C ₃₂ H ₂₆ N ₂ O ₂ CuI ₂	C ₃₄ H ₃₂ N ₂ O ₂ Cu
Formula weight	787.89	564.19
Temperature/K	120.01(12)	120.2(3)
Crystal system	orthorhombic	monoclinic
Space group	P2 ₁ 2 ₁ 2 ₁	I2/a
a / Å	9.8152(4)	11.9805(4)
b / Å	10.0201(4)	13.1895(4)
c / Å	29.0295(11)	17.2664(5)
α / °	90	90
β / °	90	97.121(3)
γ / °	90	90
Volume / Å³	2855.0(2)	2707.33(15)
Z	4	4
ρ_{calc} g / cm³	1.833	1.3841
μ / mm⁻¹	2.960	0.841
F(000)	1532.0	1181.8
Crystal size / mm³	0.78 × 0.33 × 0.21	0.4 × 0.2 × 0.11
Radiation	MoKα (λ = 0.71073)	Mo Kα (λ = 0.71073)
2θ range for data collection/°	6.454 to 50.052	6.18 to 50.06
Index ranges	-8 ≤ h ≤ 11, -11 ≤ k ≤ 10, -34 ≤ l ≤ 34	-13 ≤ h ≤ 16, -14 ≤ k ≤ 18, -22 ≤ l ≤ 20
Reflections collected	10274	8124
Independent reflections	4929 [R _{int} = 0.0325, R _{sigma} = 0.0473]	2390 [R _{int} = 0.0328, R _{sigma} = 0.0482]
Data/restraints/parameters	4929/0/354	2390/0/178
Goodness of fit on F²	1.039	1.057
Final R indexes [I ≥ 2σ (I)]	R ₁ = 0.0265, wR ₂ = 0.0514	R ₁ = 0.0312, wR ₂ = 0.0729
Final R indexes [all data]	R ₁ = 0.0284, wR ₂ = 0.0523	R ₁ = 0.0374, wR ₂ = 0.0772
Largest diff. / e Å⁻³	0.38/-0.43	0.33/-0.45

Complex	C25	C26
Empirical formula	C ₃₄ H ₃₂ N ₂ O ₄ Cu	C ₃₆ H ₃₆ CuN ₂ O ₄
Formula weight	596.19	624.21
Temperature/K	120.01(12)	120.0(2)
Crystal system	orthorhombic	triclinic
Space group	Pbca	P-1
a / Å	16.2295(8)	11.3623(6)
b / Å	5.7812(3)	12.1200(7)
c / Å	29.7673(12)	12.1712(7)
α / °	90	77.677(5)
β / °	90	66.949(5)
γ / °	90	85.080(5)
Volume / Å³	2792.9(2)	1506.74(16)
Z	4	2
ρ_{calc} g / cm³	1.4177	1.376
μ / mm⁻¹	0.825	0.768
F(000)	1245.9	654.0
Crystal size / mm³	0.82 × 0.33 × 0.18	0.25 × 0.09 × 0.07
Radiation	Mo Kα (λ = 0.71073)	MoKα (λ = 0.71073)
2θ range for data collection/°	5.72 to 50.04	5.896 to 59.422
Index ranges	-17 ≤ h ≤ 22, -8 ≤ k ≤ 7, -41 ≤ l ≤ 32	-14 ≤ h ≤ 14, -13 ≤ k ≤ 16, -16 ≤ l ≤ 16
Reflections collected	11451	14703
Independent reflections	2461 [R _{int} = 0.0454, R _{sigma} = 0.0551]	7090 [R _{int} = 0.0410, R _{sigma} = 0.0721]
Data/restraints/parameters	2461/0/188	7090/121/450
Goodness of fit on F²	1.073	1.060
Final R indexes [I ≥ 2σ (I)]	R ₁ = 0.0405, wR ₂ = 0.0872	R ₁ = 0.0474, wR ₂ = 0.0881
Final R indexes [all data]	R ₁ = 0.0590, wR ₂ = 0.0981	R ₁ = 0.0722, wR ₂ = 0.0993
Largest diff. / e Å⁻³	0.45/-0.45	0.40/-0.47

Complex	C27	C28
Empirical formula	C ₃₄ H ₂₆ N ₂ O ₂ F ₆ Cu	C ₃₆ H ₃₆ N ₂ O ₂ Cu
Formula weight	672.11	592.21
Temperature/K	120.00(13)	120.01(14)
Crystal system	monoclinic	orthorhombic
Space group	P2 ₁ /c	Pbca
a / Å	15.6718(14)	11.18443(18)
b / Å	16.3749(12)	19.8811(4)
c / Å	5.6359(5)	26.6673(5)
α / °	90	90
β / °	91.504(8)	90
γ / °	90	90
Volume / Å³	1445.8(2)	5929.70(19)
Z	2	8
ρ_{calc} g / cm³	1.544	1.327
μ / mm⁻¹	0.830	0.772
F(000)	686.0	2488.0
Crystal size / mm³	0.36 × 0.27 × 0.16	0.3029 × 0.2097 × 0.1545
Radiation	MoKα (λ = 0.71073)	MoKα (λ = 0.71073)
2θ range for data collection/°	5.614 to 50.05	5.692 to 50.05
Index ranges	-18 ≤ h ≤ 18, -19 ≤ k ≤ 19, -6 ≤ l ≤ 6	-13 ≤ h ≤ 12, -21 ≤ k ≤ 23, -31 ≤ l ≤ 29
Reflections collected	6727	32508
Independent reflections	2552 [R _{int} = 0.0686, R _{sigma} = 0.0746]	5232 [R _{int} = 0.0516, R _{sigma} = 0.0350]
Data/restraints/parameters	2552/36/234	5232/0/376
Goodness of fit on F²	1.044	1.055
Final R indexes [I ≥ 2σ (I)]	R ₁ = 0.0672, wR ₂ = 0.1707	R ₁ = 0.0361, wR ₂ = 0.0858
Final R indexes [all data]	R ₁ = 0.0944, wR ₂ = 0.1943	R ₁ = 0.0515, wR ₂ = 0.0948
Largest diff. / e Å⁻³	1.36/-0.82	0.27/-0.46

Complex	C29	C30
Empirical formula	C ₃₈ H ₄₀ N ₂ O ₂ Cu	C ₃₂ H ₂₄ N ₂ O ₂ Cl ₄ Cu
Formula weight	620.26	673.87
Temperature/K	120.02(13)	120.00(13)
Crystal system	monoclinic	monoclinic
Space group	P2 ₁ /n	C2/c
a / Å	11.2401(5)	22.3235(8)
b / Å	22.1858(11)	7.2386(3)
c / Å	13.1955(5)	18.0461(6)
α / °	90	90
β / °	99.985(4)	100.669(3)
γ / °	90	90
Volume / Å³	3240.7(3)	2865.7(2)
Z	4	4
ρ_{calc} g / cm³	1.271	1.562
μ / mm⁻¹	0.709	1.170
F(000)	1308.0	1372.0
Crystal size / mm³	0.41 × 0.2 × 0.14	0.4887 × 0.2088 × 0.0899
Radiation	MoKα (λ = 0.71073)	MoKα (λ = 0.71073)
2θ range for data collection/°	6.27 to 50.054	6.232 to 50.05
Index ranges	-12 ≤ h ≤ 13, -24 ≤ k ≤ 26, -15 ≤ l ≤ 15	-26 ≤ h ≤ 22, -7 ≤ k ≤ 8, -21 ≤ l ≤ 21
Reflections collected	22244	7665
Independent reflections	5727 [R _{int} = 0.0656, R _{sigma} = 0.0598]	2533 [R _{int} = 0.0363, R _{sigma} = 0.0406]
Data/restraints/parameters	5727/0/396	2533/0/187
Goodness of fit on F²	1.162	1.033
Final R indexes [I ≥ 2σ (I)]	R ₁ = 0.0794, wR ₂ = 0.1774	R ₁ = 0.0407, wR ₂ = 0.0960
Final R indexes [all data]	R ₁ = 0.0999, wR ₂ = 0.1869	R ₁ = 0.0475, wR ₂ = 0.1008
Largest diff. / e Å⁻³	1.18/-1.09	1.40/-0.36

Complex	C31	C32
Empirical formula	C ₃₄ H ₃₂ N ₂ O ₆ Cu	C ₃₂ H ₂₄ N ₂ O ₂ F ₂ CuBr ₂
Formula weight	628.15	729.89
Temperature/K	120.01(10)	120.0(2)
Crystal system	monoclinic	monoclinic
Space group	P2 ₁ /n	C2/c
a / Å	8.8326(4)	22.8983(7)
b / Å	7.0294(3)	6.9815(2)
c / Å	22.0248(11)	17.6021(6)
α / °	90	90
β / °	100.425(5)	101.532(3)
γ / °	90	90
Volume / Å³	1344.90(11)	2757.16(16)
Z	2	4
ρ_{calc} g / cm³	1.551	1.758
μ / mm⁻¹	0.866	3.739
F(000)	654.0	1452.0
Crystal size / mm³	0.35 × 0.32 × 0.18	0.28 × 0.16 × 0.11
Radiation	MoKα (λ = 0.71073)	MoKα (λ = 0.71073)
2θ range for data collection/°	6.094 to 50.044	6.112 to 50.046
Index ranges	-10 ≤ h ≤ 10, -7 ≤ k ≤ 8, -23 ≤ l ≤ 26	-21 ≤ h ≤ 27, -8 ≤ k ≤ 8, -20 ≤ l ≤ 17
Reflections collected	6259	7648
Independent reflections	2383 [R _{int} = 0.0395, R _{sigma} = 0.0504]	2439 [R _{int} = 0.0326, R _{sigma} = 0.0334]
Data/restraints/parameters	2383/0/197	2439/0/187
Goodness of fit on F²	1.049	1.063
Final R indexes [I ≥ 2σ (I)]	R ₁ = 0.0380, wR ₂ = 0.0837	R ₁ = 0.0273, wR ₂ = 0.0582
Final R indexes [all data]	R ₁ = 0.0471, wR ₂ = 0.0908	R ₁ = 0.0328, wR ₂ = 0.0604
Largest diff. / e Å⁻³	0.35/-0.41	0.89/-0.27

Complex	C36	C37
Empirical formula	C ₃₂ H ₂₆ N ₂ O ₂ CuBr ₂	C ₃₂ H ₂₆ N ₂ O ₂ F ₂ Cu
Formula weight	693.91	572.09
Temperature/K	120.00(10)	120.2(4)
Crystal system	monoclinic	monoclinic
Space group	I2/a	I2/a
a / Å	12.1403(8)	12.0159(4)
b / Å	14.0634(11)	13.3394(4)
c / Å	16.3054(14)	16.3350(5)
α / °	90	90
β / °	104.212(8)	100.244(3)
γ / °	90	90
Volume / Å³	2698.7(4)	2576.53(14)
Z	4	4
ρ_{calc} g / cm³	1.708	1.475
μ / mm⁻¹	3.805	0.896
F(000)	1388.0	1180.0
Crystal size / mm³	0.17 × 0.15 × 0.123	0.35 × 0.19 × 0.16
Radiation	MoKα (λ = 0.71073)	MoKα (λ = 0.71073)
2θ range for data collection/°	5.794 to 59.744	6.378 to 50.05
Index ranges	-16 ≤ h ≤ 11, -19 ≤ k ≤ 15, -22 ≤ l ≤ 17	-14 ≤ h ≤ 14, -14 ≤ k ≤ 15, - 19 ≤ l ≤ 17
Reflections collected	6804	6238
Independent reflections	3231 [R _{int} = 0.0451, R _{sigma} = 0.0755]	2279 [R _{int} = 0.0265, R _{sigma} = 0.0314]
Data/restraints/parameters	3231/0/178	2279/0/178
Goodness of fit on F²	1.071	1.092
Final R indexes [I ≥ 2σ (I)]	R ₁ = 0.0495, wR ₂ = 0.1049	R ₁ = 0.0417, wR ₂ = 0.1057
Final R indexes [all data]	R ₁ = 0.0892, wR ₂ = 0.1267	R ₁ = 0.0447, wR ₂ = 0.1079
Largest diff. / e Å⁻³	1.46/-1.00	1.89/-0.44

Complex	C40	C41
Empirical formula	C ₃₂ H ₂₆ N ₂ O ₂ Cl ₂ Cu	C ₃₂ H ₂₄ N ₂ O ₂ F ₄ Cu
Formula weight	604.99	608.07
Temperature/K	120.01(10)	120.00(10)
Crystal system	monoclinic	monoclinic
Space group	P2 ₁ /c	P2 ₁ /n
a / Å	9.8810(4)	11.9032(4)
b / Å	9.4847(3)	7.3795(3)
c / Å	14.5268(5)	15.8968(6)
α / °	90	90
β / °	102.242(3)	104.625(4)
γ / °	90	90
Volume / Å³	1330.47(8)	1351.13(9)
Z	2	2
ρ_{calc} g / cm³	1.510	1.495
μ / mm⁻¹	1.056	0.869
F(000)	622.0	622.0
Crystal size / mm³	0.44 × 0.19 × 0.13	0.41 × 0.36 × 0.25
Radiation	MoKα (λ = 0.71073)	MoKα (λ = 0.71073)
2θ range for data collection/°	6.274 to 50.054	6.558 to 50.05
Index ranges	-11 ≤ h ≤ 10, -9 ≤ k ≤ 11, -17 ≤ l ≤ 15	-14 ≤ h ≤ 13, -8 ≤ k ≤ 7, -18 ≤ l ≤ 17
Reflections collected	6802	7459
Independent reflections	2347 [R _{int} = 0.0401, R _{sigma} = 0.0457]	2383 [R _{int} = 0.0376, R _{sigma} = 0.0411]
Data/restraints/parameters	2347/0/179	2383/0/188
Goodness of fit on F²	1.067	1.080
Final R indexes [I ≥ 2σ (I)]	R ₁ = 0.0339, wR ₂ = 0.0837	R ₁ = 0.0423, wR ₂ = 0.1102
Final R indexes [all data]	R ₁ = 0.0413, wR ₂ = 0.0889	R ₁ = 0.0487, wR ₂ = 0.1161
Largest diff. / e Å⁻³	0.26/-0.43	1.57/-0.4

Complex	C42
Empirical formula	C ₃₂ H ₂₄ N ₂ O ₂ F ₄ Cu
Formula weight	608.07
Temperature/K	120.01(10)
Crystal system	monoclinic
Space group	P2 ₁ /c
a / Å	18.5919(9)
b / Å	10.2406(6)
c / Å	14.2061(7)
α / °	90
β / °	95.537(5)
γ / °	90
Volume / Å³	2692.1(2)
Z	4
ρ_{calc} g / cm³	1.500
μ / mm⁻¹	0.873
F(000)	1244.0
Crystal size / mm³	0.2266 × 0.1825 × 0.1373
Radiation	MoKα (λ = 0.71073)
2θ range for data collection/°	5.966 to 50.048
Index ranges	-20 ≤ h ≤ 22, -11 ≤ k ≤ 12, -16 ≤ l ≤ 15
Reflections collected	17355
Independent reflections	4746 [R _{int} = 0.0555, R _{sigma} = 0.0557]
Data/restraints/parameters	4746/0/372
Goodness of fit on F²	1.052
Final R indexes [I ≥ 2σ (I)]	R ₁ = 0.0426, wR ₂ = 0.0882
Final R indexes [all data]	R ₁ = 0.0608, wR ₂ = 0.1000
Largest diff. / e Å⁻³	0.29/-0.39